The figure on the front page shows a part of fig. 7.6c.

Abstract

In this thesis a theory for steady-state squeezing of an abstract collective spin-variable is developed for particles in a Bose-Einstein condensate. Such a theory can be put to direct use in the field of quantum-metrology, since squeezed states can help improve the precision of atomic clocks. In the two-mode approximation it is easy to see that a steady-state Bose-Einstein condensate will be spin-squeezed, since the Hamiltonian describing such a system has the maximally squeezed state as the lowest energy eigenstate.

The calculation central to this thesis is done using a Bogoliubov transformation of perturbations of the quantum-field operator describing the particles in the condensate. This transformation will diagonalize the Hamiltonian, which enables us to find an (almost) complete set of eigenvalues and eigenstates. These states can be used to calculate the expectation values of the angular momentum operators, from which the spin-squeezing can be calculated.

The atoms in the condensate are described using two constants U and U_{ab} proportional to the scattering lengths for atoms of equal and different spin respectively. The result of a numerical implementation of the theory is that for zero temperature the optimal atoms have $U \approx U_{ab} \approx 0$. This is contrary to the case of higher, physical temperatures, where atoms with $U \gg U_{ab}$ and $U + U_{ab} \gg 1$ will maximize the squeezing. Further results are that the most spin-squeezing is produced for as large a particle number and as low a temperature as possible.

Resumé

I dette speciale vil en teori for steady-state squeezing af en abstrakt kollektiv spin-variabel blive udledt for partikler i et Bose-Einsteinkondensat. En sådan teori vil kunne anvendes direkte inden for kvante-metrologi, idet squeezede tilstande kan bruges til at forbedre præcisionen af atomure. I two-mode approksimationen er det let at se, at et steady-state Bose-Einsteinkondensat vil være spin-squeezed, idet den Hamiltonoperator, som beskriver et sådant system, har den maximalt squeezede tilstand som sin laveste energiegentilstand.

Den centrale udregning i specialet er udført ved hjælp af en Bogoliubovtransformation af perturbationer af den kvantefeltoperator, der beskriver partiklerne i kondensatet. Den transformation vil diagonalisere Hamiltonoperatoren, hvilket gør os i stand til at finde et (stort set) fuldstændigt sæt af egenværdier og egentilstande. De tilstande kan bruges til at udregne forventningsværdierne af impulsmomentoperatorerne, hvorfra spin-squeezingen kan udregnes.

Atomerne i kondensatet bliver beskrevet ved to konstanter U og U_{ab}, der er proportionale med spredningslængderne for atomer med henholdsvis ens og modsat spin. Resultatet af en numerisk implementering af teorien er, at ved nul temperatur har de optimale atomer $U \approx U_{ab} \approx 0$, mens grænsen er den modsatte for højere, fysiske temperaturer, hvor atomer med $U \gg U_{ab}$ og $U + U_{ab} \gg 1$ vil maksimere den opnåede squeezing. Andre resultater er, at så stort et partikelantal og så lav en temperatur som mulig vil maksimere spin-squeezingen.

Contents

Chapter 1

Introduction

This document is a master thesis made by Hjalte Axel Frellesvig under the supervision of Anders Søndberg Sørensen, at the Theoretical Quantum Optics Group at the Niels Bohr Institute at the University of Copenhagen.

The title of the thesis is "Spin-squeezing in Bose-Einstein condensates". This subject has been investigated theoretically several times before[1], which is why the title should be seen as nothing but an abbreviation of a more correct title like "Steady-state, non-symmetry-breaking Bogoliubov theory for spin-squeezing of internal states in Bose-Einstein condensates" describing a set of approaches which, to the best of my knowledge, has not been used before in this combination.

The purpose of the thesis is to derive a model of a Bose-Einstein condensate using the above combination of approaches, use the result to calculate the spin-squeezing and investigate the results.

I try to aim this thesis at people at the same academical level as my own, that is people who are about to finish a master's degree in physics. It is possible to advance that far without ever encountering the concept of spin-squeezing, and without having more than a passing encounter with Bose-Einstein condensates. I therefore devote a chapter to introducing each of these subjects. Let me, however, give a very brief introduction here explaining the relation between the two, so the reader knows what he/she is going into.

A spin-squeezed state is a state where the uncertainty of a measurement of one component of the spin ΔJ_i is less than what can be expected[2] from a state equalizing the uncertainty relation $\Delta J_i \Delta J_j \geq \frac{1}{2}|\langle \hat{J}_k \rangle|$, while Bose-Einstein condensates (in the following denoted BEC) can be considered a[3] fourth state of matter, which is formed when a bosonic gas is cooled so much that all the particles have the same, lowest quantum state. In this thesis the spin in question is an abstract spin describing two different electronic states of some atoms, and when those atoms form a BEC

[1] See [1], [3], [4], [5], [6], etc.

[2] What is expected is not necessarily $\sqrt{\frac{1}{2}|\langle \hat{J}_k \rangle|}$. See section 3.2.

[3] It is not THE fourth state of matter. Plasma, glass, the superconducting Ginzburg-Landau phase, and Bose-Einstein condensates are all competitors for that title.

the Hamiltonian describing the condensate will have such spin-squeezed states as the ground state. This bridges the two subjects of spin-squeezing and Bose-Einstein condensates.

Theoretical physicists do occasionally have a hard time answering questions like "what can this work of yours be used for?" The theory described in this thesis does not have that problem, since there is a direct connection from this theory to the theory of atomic clocks. Even though atomic clocks are the most precise type of clock in existence, they do have some uncertainty. Noise from the classical uncertainty of the involved measurements is still the biggest obstacle, but ultimately the precision is limited by the quantum uncertainty, which can be diminished by squeezing the variable in question. Even though other methods are available[4], the use of Bose-Einstein condensates is a promising way to achieve the desired squeezing.

The thesis starts with a chapter on atomic clocks, making the connection to spin-squeezing obvious. Then follows a chapter on squeezing, containing an explanation of squeezing of xp-variables and spin-variables, and a way to find the minimal spin-squeezing is derived. The chapter also contains a discussion of the connection between spin-squeezing and quantum entanglement. The next chapter is about Bose-Einstein condensates, and contains a derivation of the Gross-Pitaevskii equation describing BEC, and some discussion on ways to solve it. The chapters on squeezing and BEC are written so that they can be read independently; no mention of BEC in the chapter on squeezing and vice versa. Then follows a chapter named "Spin-squeezing in Bose-Einstein condensates" which connects the two subjects, and describes some previous theoretical and experimental results on the subject. It also contains an introduction to the Bogoliubov transformations used in the main calculation. The next chapter named "The full Bogoliubov calculation" presents the central calculation of the thesis, where the desired steady-state Bogoliubov theory is derived. It also contains some discussion of an alternate approach, and discussions on how to implement the theory numerically. Finally the chapter named "Results" contains the results from the numerical calculations, and explanations of some of their essential features. After a section on conclusions and outlooks, some appendices follow. First, two appendices containing some theory, which is too basic to be in the main thesis. Then follows four appendices containing some detailed calculations that are too long compared to their importance to be granted space in the main text, followed by an appendix containing the source code to my simulation, an appendix containing some details on the precision of the simulations, and an appendix containing some results in addition to those presented in the results-chapter, and an appendix showing some of our results in higher resolution. A bibliography is added as a final appendix.

Some of the sections in the first chapters in the thesis, are detours on the way towards the desired theory. If one wants to read the thesis by following the most direct route, one should read sections 3.2, 3.4, 4.2, 4.4, 5.1, 5.2, 5.6, 6.1, 6.2, 6.3,

[4]Like the Quantum non-demolition measurement method described in [16].

and chapter 7.

I would like to thank my thesis advisor Anders Søndberg Sørensen, for patiently answering all my questions, and for reading through my calculations and writings at the intermediate stages. Without him there would have been no thesis. It was also Anders who got the idea for the subject matter in the first place, and this thesis builds upon some of his previous work[5]. In addition I would like to thank Kjeld Frellesvig and Jeppe Søgaard Juul for reading through my thesis and pointing out language errors and obscurities.

1.1 Conventions

In this section I will describe some of the conventions used in the thesis. The chapters are referred to with a number each, while appendices have the chapter number replaced with a letter. Most of the chapters are further split into sections, which are denoted with another number separated from the number of the chapter with a decimal point. When referring to an equation, I write the number of the equation in brackets. The number in question is composed of the chapter-number and an equation number separated with a decimal point. Figures are referred to as fig. xa where x is the number of the figure constructed like the number for equations, and a is a letter denoting the sub-figure. Literature is referred to as $[x]$, where x is a number or a letter denoting the source. If x is a number the source is a paper, and if x is a lower case letter the source is a book. The key to decoding the numbering of the literature can be found in the bibliography at the end of the thesis.

When I write a sum or an integral without limits, I mean summation or integration over all possible values. For integrals I write the integration variable $\mathrm{d}x$ right after the integral sign instead of writing it after the integrand. This means that

$$\int \mathrm{d}\mathbf{r} f(\mathbf{r}) \equiv \int_{-\infty}^{\infty}\int_{-\infty}^{\infty}\int_{-\infty}^{\infty} f(x,y,z)\,\mathrm{d}x\,\mathrm{d}y\,\mathrm{d}z \tag{1.1}$$

One should also note the notation $\sum_{i*}$ used in results of Bogoliubov transformations, which is defined as "sum over all modes, except the 0_+ mode". Another unusual notation used in the final parts of the thesis is the operator $\circ$ which is defined as

$$f \circ g \equiv \int \mathrm{d}\mathbf{r} f(\mathbf{r}) g(\mathbf{r}) \tag{1.2}$$

Quantum operators are denoted with a hat, and vectors are written in bold, with the exception of the vectors in the abstract 2×2-space introduced in (6.13) which are denoted by a bar. No special notation is used for matrices.

[5] See [1], [3] and [4].

Most of the variables used in the thesis are defined along the way. But those of them used in more than one section will be listed below as reference.

a	Standard oscillator length, $a \equiv \sqrt{\hbar/(m\omega)}$.
a_0	Bohr radius, $a_0 = 5.29177 \cdot 10^{-11}$ m.
a_{ij}	Scattering length between particles of type i and j.
$\hat{a}_i$	Annihilation operator for the ith mode (for particles of type a).
$A_\pm$	Two matrix elements defined by (6.16).
$\hat{\alpha}$	An annihilation operator (for xp-variables).
$\hat{\alpha}_{i\pm}$	Annihilation operator for the ith $\pm$ Bogoliubov state.
$\hat{b}_i$	Annihilation operator for the ith mode for particles of type b.
$B_\pm$	Two matrix elements defined by (6.16).
β	Inverse unitless temperature, $\beta \equiv 1/\mathcal{T}$.
$\hat{c}_{i\pm}$	Annihilation operator for the ith mode for particles of type $\pm$.
$\hat{c}$	Annihilation operator for the condensate mode, $\hat{c} \equiv \hat{c}_{0+}$.
$C_{i\pm}$	A quantity defined by (7.15).
$\hat{\mathfrak{c}}$	Annihilation operator for a general particle. See (6.7).
χ	A parameter defined by (5.7).
$\delta\hat{\psi}_\pm$	The small parameter in the Bogoliubov transformation. See (6.2).
δ_{ij}	The Kronecker delta. See [f].
$\delta(\mathbf{r})$	The Dirac delta function. See [f].
Δx	The uncertainty on a measurement of x, $(\Delta x)^2 = \langle x^2 \rangle - \langle x \rangle^2$.
dB	Decibel, $x = y$ dB $\Leftrightarrow x = 10^{y/10}$.
E	An energy.
$\mathcal{E}$	The energies given by (7.10).
ϵ	A small parameter.
ϵ_{ijk}	The Levi-Civita symbol. See [f].
$\varepsilon_{i\pm}$	The energy of the ith $\pm$ Bogoliubov state.
f	Short for the fraction U_{ab}/U.
F	The functions defined by (3.31).
$\hbar$	Reduced Planck's constant, $\hbar = 1.05457 \cdot 10^{-34}$ Js.
$\hat{H}$	A Hamiltonian.
H_0	Harmonic oscillator Hamiltonian, $H_0 \equiv -\frac{1}{2}\nabla^2 + \frac{1}{2}r^2$.
$\hat{H}_s$	The Hamiltonian for "one axis twisting", $\hat{H}_s \equiv \chi \hat{J}_z^2$.
$\hat{\mathcal{H}}$	A second quantization Hamiltonian.
$\hat{\mathfrak{H}}_0$	The constant Hamiltonian defined by (6.9).
i	The imaginary unit, $i \equiv \sqrt{-1}$.
I	A unit matrix.
$\hat{I}$	A unit operator.
j	Some angular momentum.
J	Some collective angular momentum.

$\hat{J}_i$	Angular momentum operator in the i-direction.
$\hat{\mathbf{J}}$	The vector $(\hat{J}_x, \hat{J}_y, \hat{J}_z)$.
k	Some momentum quantum number.
k_B	Boltzmann's constant, $1.38065 \cdot 10^{-23}$ J/K.
l	Some orbital angular momentum quantum number.
$\mathcal{L}$	A matrix defined by (6.36).
$\hat{\Lambda}_\pm$	The operator $\hat{\Lambda}_\pm \equiv \hat{c}^\dagger \delta\hat{\psi}_\pm / \sqrt{N}$.
λ	A Lagrange multiplier. Later identified as $\lambda = -\Omega/\chi$.
m	The atomic mass.
m	Some magnetic quantum number.
$\hat{M}$	The operator $\hat{M} \equiv \hat{J}_z^2 - \lambda \hat{J}_x$. See (3.33).
$\mathcal{M}$	A matrix defined by (6.15).
μ	A chemical potential.
$\check{\mu}$	The effective chemical potential, $\check{\mu} \equiv \mu - \frac{1}{2}\Omega$.
$n_{i\pm}$	The number of particles in the ith $\pm$ Bogoliubov state.
$\hat{n}_{i\pm}$	The particle number operator for the ith $\pm$ Bogoliubov state.
N	The total number of particles.
N_0	The number of particles in the condensate mode.
$\hat{N}$	The particle number operator.
ν	The angle in "one axis twisting". See the text to fig. 5.2.
∇	Nabla, $\nabla^2 \equiv \frac{\partial^2}{\partial x^2} + \frac{\partial^2}{\partial y^2} + \frac{\partial^2}{\partial z^2}$.
$\mathcal{O}$	The order parameter.
$\hat{O}$	Some operator.
ω	The trap frequency.
Ω	The Rabi frequency coupling the a and b-modes. See (4.33).
$\hat{p}$	The momentum operator.
ϕ	Some angle.
φ	Wave function for the condensate mode, $\varphi \equiv \varphi_{0+}$.
$\varphi_{i\pm}$	Wave function for the ith $\pm$-mode.
$\Phi_{i\pm}$	The fraction $\Phi_{i\pm} \equiv B_{i\pm}/A_{i\pm}$.
ψ	Some wave function (normalized to N).
$\hat{\Psi}_i$	Quantum field-operator for particles of type i.
$Q(\theta, \phi)$	The Husimi Q-function defined by (3.21).
$\mathfrak{Q}(\theta, \phi)$	The function defined by (3.29).
$\mathcal{Q}$	The function $\mathcal{Q}(\mathbf{r}, \mathbf{r}') \equiv \delta(\mathbf{r} - \mathbf{r}') - \varphi(\mathbf{r})\varphi^*(\mathbf{r}')$.
$\mathcal{Q} \circ f(\mathbf{r})$	The projection operator $\mathcal{Q} \circ f(\mathbf{r}) \equiv \int \mathrm{d}\mathbf{r}' \mathcal{Q}(\mathbf{r}, \mathbf{r}') f(\mathbf{r}')$.
r	A radial variable.
$\mathbf{r}$	The position vector.
ρ	A density matrix.
s	Short for the sum $U + U_{ab}$.
$\hat{S}$	The squeezing operator for xp-squeezing. Defined by (3.11).
σ_i	The Pauli spin-matrix in the i-direction.

t	A time.
t	An imaginary time, $\tau \equiv it$.
T	The temperature.
$\mathcal{T}$	A unitless temperature, $\mathcal{T} \equiv k_B T/(\hbar\omega)$.
θ	Some angle.
u	The atomic mass unit, $u = 1.66034 \cdot 10^{-27}$ kg.
$u_{i\pm}$	A function used in the Bogoliubov transformation. See (6.19).
$\mathbf{u}_i$	The unit vector in the i-direction.
U	An interaction parameter in the GPE, $U \equiv U_{aa} = U_{bb}$.
U_0	The interaction parameter in the one-species GPE.
U_{ij}	The interaction parameter between particles of type i and j.
$v_{i\pm}$	A function used in the Bogoliubov transformation. See (6.19).
$V_\pm$	Two functions defined by (7.13).
$\bar{w}_{i\pm}$	The vector $\left(u_{i\pm}, v^*_{i\pm}\right)$.
W_-	A function defined by (7.13).
$\hat{x}$	The position operator.
ξ	A squeezing parameter.
ξ_Y	Squeezing parameter for xp-squeezing in the Y-direction.
ξ_{J_i}	Squeezing parameter for spin-squeezing in the J_i-direction.
$\hat{Y}$	A rotated xp-operator. See (3.6).

Some abbreviations are used throughout the thesis. Like the variables, they are explained when introduced, but I will list them here as reference.

BEC	Bose-Einstein Condensate
GP	Gross-Pitaevskii
GPE	Gross-Pitaevskii Equation
NOU	Natural Oscillator Units
SCS	Spin-Coherent State
SSS	Squeezed Spin State

Finally some notes on terminology:

I have chosen to write the thesis using the personal pronoun 'we', by which I mean me as the author and you as the reader. We see x and we do y means that you should see x and do y as well. Exceptions from this are the introduction[6] and the conclusion which are more personal in nature, and a few comments for which I take the full responsibility. Personal pronouns will, however, be avoided when possible using passive forms.

That English is not my first language is an unavoidable fact that unfortunately, but most assuredly, will be apparent in the text, in spite of my efforts to the contrary.

[6]Like this section. "We have chosen to write the thesis using the personal pronoun 'we' " is factually wrong.

1.2 The natural oscillator units

This thesis is written using two sets of units. SI-units and the natural oscillator units (NOU) introduced in this section. From section 4.3 and onwards only NOU will be used.

NOU is introduced in order to get rid of some of the constants in the central equations in the thesis by setting them equal to one. Since no variables with electromagnetic units appear in the central equations, we can only remove three[7] constants corresponding to the mechanical units length, time and mass. In the system of natural oscillator units, these constants are the atomic mass m, the trap frequency ω, and $\hbar$, which gives the unit length, unit mass, and unit time as $a \equiv \sqrt{\frac{\hbar}{m\omega}}$, m, and ω^{-1} respectively. The utility of the NOU is shown best by the Gross-Pitaevskii equation (4.16) which is written

$$-\frac{\hbar^2}{2m}\nabla^2\psi(\mathbf{r}) + \frac{1}{2}m\omega^2\mathbf{r}^2\psi(\mathbf{r}) + U_0|\psi(\mathbf{r})|^2\psi(\mathbf{r}) = \mu\psi(\mathbf{r}) \tag{1.3}$$

in SI-units, but reduces to

$$-\frac{1}{2}\tilde{\nabla}^2\tilde{\psi}(\tilde{\mathbf{r}}) + \frac{1}{2}\tilde{\mathbf{r}}^2\tilde{\psi}(\tilde{\mathbf{r}}) + \tilde{U}_0|\tilde{\psi}(\tilde{\mathbf{r}})|^2\tilde{\psi}(\tilde{\mathbf{r}}) = \tilde{\mu}\tilde{\psi}(\tilde{\mathbf{r}}) \tag{1.4}$$

in NOU, where the tilded variables can be expressed

$$\tilde{\mathbf{r}} = \sqrt{\frac{m\omega}{\hbar}}\mathbf{r}\ ,\quad \tilde{\nabla}^2 = \frac{\hbar}{m\omega}\nabla^2\ ,\quad \tilde{\psi} = \left(\frac{\hbar}{m\omega}\right)^{\frac{3}{4}}\psi\ ,\quad \tilde{U}_0 = \sqrt{\frac{m^3\omega}{\hbar^5}}U_0\ ,\quad \tilde{\mu} = \frac{\mu}{\hbar\omega} \tag{1.5}$$

in terms of the original variables. In the main thesis the tildes will not be written.

[7] In fact a fourth unit appearing in the calculations is that of temperature. I have chosen to handle the temperature by introducing a new variable for the unitless temperature $\mathcal{T} \equiv \frac{k_B T}{\hbar\omega}$, thus handling it different from the mechanical units. The temperature will not be considered part of the NOU.

Chapter 2

Atomic clocks

Almost all[1] clocks build throughout history measures time using the frequency of an oscillating or rotating object. For sundials, what rotates is the earth itself. In traditional mechanical clocks like church clocks and grandfather clocks the oscillator is a pendulum. In most modern mechanical clocks it is a balance wheel, and in digital watches and computers the oscillator is a so-called crystal oscillator usually made using a piezoelectric quartz crystal. None of these devices do, however, have the accuracy necessary for precision measurements and modern navigational instruments. The mechanical clocks are sensitive to temperature[2] and are also subjects to air resistance, and quartz clocks suffer from similar limitations. These effects can be avoided by using an atomic clock. In an atomic clock the oscillations in question are the so-called Rabi oscillations, which are the response of an atom to an external electric field. The uncertainties on an atomic clock coming from the experimental setup[3] can be made so small that the real limit on the precision is set by the quantum uncertainties implied by Heisenberg's uncertainty relation[4]. In fact atomic clocks are so precise that they are used to define the SI-unit "second". One second is defined as 9192631770 times the period of the radiation emitted by the transition between the two hyperfine levels of the ground state in Cesium-133. The most precise clock reported of today[5] has an uncertainty of one second over a period of $3.7 \cdot 10^9$ years corresponding to a loss of 3.7 seconds over the lifetime of the universe.

What is done in practice is that one measures the frequency of the relevant transition, often using a crystal oscillator, and then uses the result of that measurement to calibrate the measurement device, which then can be used as a clock. We want to minimize the uncertainty of the frequency measurement since the uncertainty of a time measurement is proportional to the uncertainty of the frequency measure-

[1] Exceptions are hourglasses and some water clocks.

[2] The density is usually a function of temperature, and if the density changes so does the length of the pendulum and the moment of inertia of the balance wheel.

[3] This is the uncertainty on the number of atoms, on the strength of the magnetic field, etc.

[4] See [18].

[5] See [17].

ment[6]. Another name for frequency measurements is "spectroscopy", so in order to understand atomic clocks we must first understand spectroscopy, or rather the specific experimental procedure used for spectroscopy in the case of atomic clocks, a procedure known as Ramsey Spectroscopy.

2.1 Ramsey Spectroscopy

Mathematically, any quantum mechanical two-level system, like the one consisting of the two levels in Cesium-133 mentioned above, is equivalent to a spin-$\frac{1}{2}$ particle. The Rabi oscillation between the two states, which is induced by an external electrical field[7], will be described as an external magnetic field changing the direction of the spin. This spin-picture is the one we will have in mind for the most of the rest of the thesis.

Such an interaction is described as $E = (-\mu_0/\hbar)\boldsymbol{S} \cdot \boldsymbol{B}$ where $\boldsymbol{S}$ is the spin, and μ_0 is defined as $\mu_0 \equiv g\mu_{_B}$ where $\mu_{_B}$ is the Bohr magneton and g is the gyromagnetic ratio. If an external magnetic field of size B_0 is applied in the z-direction, the Hamiltonian becomes

$$\hat{H} = \omega_0 \hat{S}_z \tag{2.1}$$

where $\omega_0 \equiv -\mu_0 B_0/\hbar$. In realistic experimental settings there will be more than one atom present, so if we define the collective spin as $\hat{\mathbf{J}} = \sum \hat{\boldsymbol{S}}$, the total Hamiltonian becomes $\hat{H} = \omega_0 \hat{J}_z$. Using the Heisenberg equation[8] we can calculate the equation of motion for $\hat{\mathbf{J}}$ to be

$$\frac{d\hat{\mathbf{J}}}{dt} = \boldsymbol{\omega}_0 \times \hat{\mathbf{J}} \tag{2.2}$$

where $\boldsymbol{\omega}_0 = \omega_0 \mathbf{u}_z$ with $\mathbf{u}_i$ denoting a unit vector in the i-direction. This indicates that the effect of the magnetic field is to make the angular momentum rotate around the z-axis with angular frequency ω_0. We now try to follow this rotation by adding another magnetic field[9]

$$\boldsymbol{B}_1 = B_1 \left(\cos(\omega t + \theta)\mathbf{u}_x + \sin(\omega t + \theta)\mathbf{u}_y\right) \tag{2.3}$$

where $\omega \approx \omega_0$ and B_1 is the size of the field. Changing to a new coordinate system rotating around the z-axis with angular frequency ω, the z-component of the resulting magnetic field becomes $B_0 - (-\hbar\omega/\mu_0) = -\hbar\omega_\Delta/\mu_0$ where $\omega_\Delta \equiv (\omega_0 - \omega)$

[6] The relation is $\frac{\Delta t}{t} = \frac{\Delta\omega}{\omega}$, which can be calculated using error propagation.

[7] See [2] and [13].

[8] $\frac{d\hat{O}}{dt} = \frac{i}{\hbar}[\hat{H}, \hat{O}]$. We also need the commutation relations $[\hat{J}_i, \hat{J}_j] = i\hbar\epsilon_{ijk}\hat{J}_k$.

[9] This expression can be a result of the so-called "rotating wave approximation". If we (experimentally more realistic) use $\boldsymbol{B}_1 = 2B_1 \cos(\omega t + \theta)\mathbf{u}_x$ the x- and the y-components of the field in the rotating frame becomes $B_1 = B_1((\cos\theta + \cos(2\omega t + \theta))\mathbf{u}_x + (\sin\theta - \sin(2\omega t + \theta)\mathbf{u}_y))$, and if we are close to resonance, the $2\omega t$-terms move too fast to affect the movement significantly.

is known as the detuning. The x- and y-components become $B_1(\cos\theta\mathbf{u}_x + \sin\theta\mathbf{u}_y)$. If we choose $\theta = \pi/2$, the Heisenberg equation gives

$$\frac{d\hat{\mathbf{J}}'}{dt} = \begin{pmatrix} 0 \\ \omega_1 \\ \omega_\Delta \end{pmatrix} \times \hat{\mathbf{J}}' \tag{2.4}$$

where[10] $\omega_1 \equiv -\mu_0 B_1/\hbar$ and $\hat{\mathbf{J}}'$ is $\hat{\mathbf{J}}$ seen from the rotating frame. From here on we will drop the prime.

In order to measure ω_Δ we measure $\langle\hat{J}_z\rangle$, which is known as the population inversion[11]. The exact relation between $\langle\hat{J}_z\rangle$ and ω_Δ depends on the specific procedure. What is described here is known as "the Ramsey method"[12], and it is chosen since it is the method giving the least experimental uncertainty[13]. The Ramsey method applies the magnetic fields in three distinct periods. The first and third period have duration $t_{\pi/2}$ which is chosen so that $\omega_1 t_{\pi/2} = \pi/2$, and the second period have duration T, where $T \gg t_{\pi/2}$. During the second interval $B_1 = 0$. The total time is then $t_f = 2t_{\pi/2} + T$. The movement of $\hat{\mathbf{J}}$ is as follows:

t	0	$t_{\pi/2}$	$t_{\pi/2} + T$	$t_f = 2t_{\pi/2} + T$
$x_t \equiv \langle\hat{J}_x(t)\rangle$	x_0	z_0	$z_0\cos(\omega_\Delta T) - y_0\sin(\omega_\Delta T)$	$-x_0$
$y_t \equiv \langle\hat{J}_y(t)\rangle$	y_0	y_0	$y_0\cos(\omega_\Delta T) + z_0\sin(\omega_\Delta T)$	$y_0\cos(\omega_\Delta T) + z_0\sin(\omega_\Delta T)$
$z_t \equiv \langle\hat{J}_z(t)\rangle$	z_0	$-x_0$	$-x_0$	$-z_0\cos(\omega_\Delta T) + y_0\sin(\omega_\Delta T)$

(2.5)

where the important part is

$$\langle\hat{J}_z(t_f)\rangle = -\langle\hat{J}_z(0)\rangle\cos(\omega_\Delta T) + \langle\hat{J}_y(0)\rangle\sin(\omega_\Delta T) \tag{2.6}$$

since that is what is measured. An illustration of the movement of the expectation value of the collective spin can be seen in fig. 2.1.

The uncertainty on ω_0 can be minimized using error propagation with the result[14]

$$\Delta\omega = \Delta J_z(t_f)/|\partial\langle\hat{J}_z(t_f)\rangle/\partial\omega| = \tag{2.7}$$

$$\frac{\sqrt{\Delta J_z(0)^2\cos^2(\omega_\Delta T) + \Delta J_y(0)^2\sin^2(\omega_\Delta T) + \left(\langle\hat{J}_z\rangle\langle\hat{J}_y\rangle - 1/2\langle\hat{J}_z\hat{J}_y + \hat{J}_y\hat{J}_z\rangle\right)\sin(2\omega_\Delta T)}}{T\left|\langle\hat{J}_z(0)\rangle\sin(\omega_\Delta T) + \langle\hat{J}_y(0)\rangle\cos(\omega_\Delta T)\right|}$$

[10] ω_1 is known as the Rabi frequency and is sometimes denoted Ω.

[11] This name comes from the fact that $\langle\hat{J}_z\rangle = \frac{1}{2}(\langle N_a\rangle - \langle N_b\rangle)$, where N_a and N_b are the populations in $|\uparrow\rangle$ and $|\downarrow\rangle$ respectively.

[12] The Ramsey method is described in further detail in [2].

[13] See [2].

[14] If we were to include the experimental uncertainty on the measurement of $\langle\hat{J}_z\rangle$ it should be added to (2.7) squared inside the square root in the numerator.

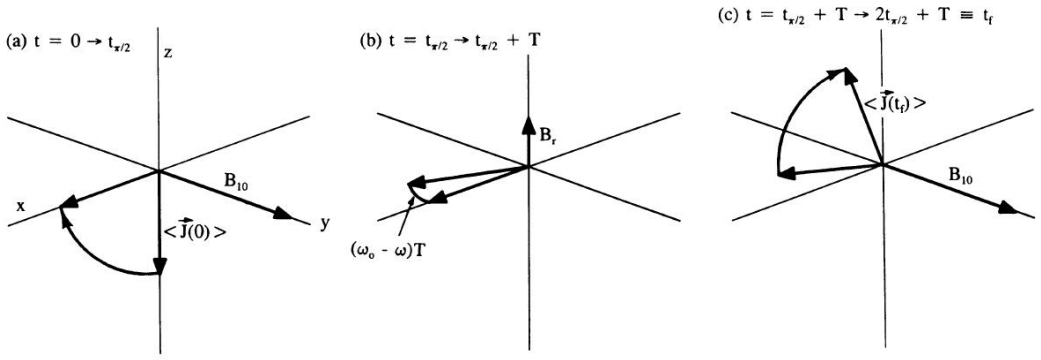

Figure 2.1: The three subplots shows the movement of $\langle \hat{\mathbf{J}} \rangle$ for the initial state $|j, -j\rangle$, in each of the three time intervals making up the procedure of Ramsey spectroscopy. This figure is taken directly from [2] where it is denoted FIG. 2.

If $\langle \hat{J}_z(t_f) \rangle(\omega)$ were symmetric around $\omega = \omega_0$ and thereby an even function of the detuning ω_Δ, we could find the point with $\omega = \omega_0$ by locating it right between two points with the same $\langle \hat{J}_z(t_f) \rangle$ with lower uncertainty on ω, if such points were to exist, given that the expression for $\Delta\omega$ has the same symmetry. These criteria are met by a state with $\langle \hat{J}_y(0) \rangle = \langle \hat{J}_x(0)\hat{J}_y(0) + \hat{J}_y(0)\hat{J}_x(0) \rangle = 0$, which reduces (2.6) and (2.7) to

$$\langle \hat{J}_z(t_f) \rangle = -\langle \hat{J}_z(0) \rangle \cos(\omega_\Delta T) \tag{2.8}$$

$$\Delta\omega = \frac{\sqrt{\Delta J_z(0)^2 \cos^2(\omega_\Delta T) + \Delta J_y(0)^2 \sin^2(\omega_\Delta T)}}{T \left| \langle \hat{J}_z(0) \rangle \sin(\omega_\Delta T) \right|} \tag{2.9}$$

This expression for $\Delta\omega$ is minimized by frequencies with $\omega_\Delta T = \pi/2$, which turns it into

$$\Delta\omega = \frac{\Delta J_y(0)}{T|\langle \hat{J}_z(0) \rangle|} \tag{2.10}$$

Let us compare this general expression for the uncertainty to the uncertainty of a so-called Dicke state, which is a state with $J = N/2$. For the particular Dicke state with $\langle \hat{J}_z \rangle = -J$ we can calculate[15]

$$\Delta J_x = \Delta J_y = \sqrt{J/2}\ ,\ \Delta J_z(0) = 0\ ,\ \langle \hat{J}_x \rangle = \langle \hat{J}_y \rangle = 0\ ,\ \langle \hat{J}_z\hat{J}_y + \hat{J}_y\hat{J}_z \rangle = 0 \tag{2.11}$$

all evaluated at $t = 0$. From this we can find the uncertainty to

$$\Delta\omega_{DS} = \frac{\sqrt{J/2}}{TJ} = \frac{1}{T\sqrt{N}} \tag{2.12}$$

[15]This state is equivalent to what is known as the spin-coherent state in the $-J_z$-direction, see section 3.3. In the $|j, m\rangle$-basis it is given as $|j, -j\rangle$ from which we can calculate the following expressions, using the material in appendix B.

A good measure of the size of $\Delta\omega$, would be to compare it to $\Delta\omega_{DS}$, which gives the result

$$\frac{\Delta\omega}{\Delta\omega_{DS}} = \frac{\sqrt{N}\Delta J_y(0)}{|\langle \hat{J}_z(0)\rangle|} \tag{2.13}$$

For a proper choice of the axis, this expression is similar to the the general expression for the squeezing parameter which is given by (3.18)

$$\xi_{J_i} = \frac{\sqrt{N}\Delta J_i}{\sqrt{\langle \hat{J}_j\rangle^2 + \langle \hat{J}_k\rangle^2}} \tag{2.14}$$

as we will see in section 3.2.

Finally it should be mentioned that there is a parallel between the Mach-Zehnder interferometer known from quantum optics and the procedure of Ramsey spectroscopy. A Mach-Zehnder interferometer is a quantum-optical device consisting of two 50/50 beam-splitters and phase-shifter with phase ϕ, mounted so the first output of the first beam-splitter is the first input of the second beam-splitter, and the second output of the first beam-splitter goes through the phase-shifter and further into the second input of the second beam-splitter. The effect of a Mach-Zehnder interferometer on the input state $|10\rangle$ having one photon in the first input of the first beam-splitter, and zero photons in the second input on the first beam-splitter, is[16]

$$|10\rangle \rightarrow \frac{1}{\sqrt{2}}\left(|10\rangle + |01\rangle\right) \rightarrow \frac{1}{\sqrt{2}}\left(|10\rangle + e^{i\phi}|01\rangle\right) \rightarrow \frac{1+e^{i\phi}}{2}|10\rangle + \frac{1-e^{i\phi}}{2}|01\rangle \tag{2.15}$$

From this we can calculate the $\langle\sigma\rangle_i$s in the final state to be

$$\langle\sigma_x\rangle = 0 \quad , \quad \langle\sigma_y\rangle = \sin(\phi) \quad , \quad \langle\sigma_z\rangle = -\cos(\phi) \tag{2.16}$$

If we identify $\phi = \pi + \omega_\Delta T$, we see from (2.5) that the effect of applying a Mach-Zehnder interferometer to the state $|10\rangle$ is the same as applying the three steps of Ramsey spectroscopy on the initial state $|j = \frac{1}{2}, m = -\frac{1}{2}\rangle$. This correspondence can be extended to more general initial states, and to higher photon numbers / particle numbers, and it is for that reason the word interferometry occasionally appears in articles about spectroscopy[17].

[16] For more information on Mach-Zehnder interferometry including a derivation of the following expression, see [d].

[17] An example is [13].

Chapter 3

Squeezing

To any set of quantum operators $\hat{A}$ and $\hat{B}$ obeying some commutation relation

$$\left[\hat{A}, \hat{B}\right] = \hat{C} \tag{3.1}$$

is associated[1] the uncertainty relation

$$\Delta A \Delta B \geq \frac{1}{2}\left|\langle \hat{C} \rangle\right| \tag{3.2}$$

When the uncertainty of a measurement of one of the variables, say A, is less than what is expected from a state equalizing the uncertainly relation, the state is said to be squeezed in A. This thesis will limit the discussion of squeezing to xp-like operators and to angular momentum-like operators of which the spin-operators are an example. The reason for the word "squeezing" is illustrated by fig. 3.1b for the case of xp-squeezing, where the uncertainty, which for a coherent state forms a circle, is squeezed into an ellipse. A similar example for spin-squeezing can be seen in fig. 3.5c.

3.1 xp-squeezing

$\hat{x}$ and $\hat{p}$-like operators, referred to as xp-operators, are defined as operators obeying the so-called canonical commutation relation

$$[\hat{x}, \hat{p}] = i\hbar \tag{3.3}$$

$\hat{x}$ and $\hat{p}$ can be the usual position and momentum, but there are plenty of other examples, one is the quadrature operators used in the quantization of the electromagnetic field[2]. The canonical commutation relation gives rise to Heisenberg's uncertainty principle

$$\Delta x \Delta p \geq \frac{\hbar}{2} \tag{3.4}$$

[1] See [b].
[2] See [d].

A state squeezed in the x-variable is defined as a state fulfilling $\Delta x < \sqrt{\frac{\hbar}{2m\omega}}$ or in the natural oscillator units

$$\Delta x < \frac{1}{\sqrt{2}} \tag{3.5}$$

indicating that the uncertainty of a measurement of x is less than the uncertainty of a measurement of p. A state having $\Delta x = \Delta p = 1/\sqrt{2}$ is known as a coherent state[3]. As shown in fig. 3.1b[4], a state can be squeezed without being squeezed in either x or p but instead in a new generalized variable

$$\hat{Y}(\theta) = \cos(\theta/2)\hat{x} + \sin(\theta/2)\hat{p} \tag{3.6}$$

where $\hat{Y}(\theta)$ and $\hat{Y}(\theta + \pi)$ is a set of xp-variables. Wee see that $\hat{x} = \hat{Y}(0)$ and $\hat{p} = \hat{Y}(\pi)$, so both x and p squeezing are special cases of squeezing in $Y(\theta)$.

In order to measure the amount of squeezing of a variable, we will define a squeezing parameter ξ. The most obvious definition for xp-operators is

$$\xi_Y \equiv \sqrt{2}\Delta Y \tag{3.7}$$

which is < 1 if the Y-variable is squeezed.

We notice that since squeezing corresponds to $\xi < 1$ more squeezing corresponds to a smaller value of ξ, which means that the point of maximal squeezing is the point of minimal ξ. This terminology is used throughout the thesis.

To any set of $\hat{x}$ and $\hat{p}$-like operators, another set of operators denoted $\hat{\alpha}^\dagger$ and $\hat{\alpha}$ known as creation and annihilation operators can be associated. The relation is

$$\hat{\alpha}^\dagger \equiv \frac{1}{\sqrt{2}}(\hat{x} - i\hat{p}) \qquad \hat{\alpha} \equiv \frac{1}{\sqrt{2}}(\hat{x} + i\hat{p}) \tag{3.8}$$

which can be inverted to

$$\hat{x} = \frac{1}{\sqrt{2}}(\hat{\alpha}^\dagger + \hat{\alpha}) \qquad \hat{p} = \frac{i}{\sqrt{2}}(\hat{\alpha}^\dagger - \hat{\alpha}) \tag{3.9}$$

The rotated operator $\hat{Y}$ can be expressed by the annihilation and creation operators as

$$\hat{Y} \;=\; \frac{\exp(i\theta/2)}{\sqrt{2}}\hat{a}^\dagger + \frac{\exp(-i\theta/2)}{\sqrt{2}}\hat{a} \tag{3.10}$$

[3]Another definition of a coherent state is an eigenstate to the $\hat{\alpha}$-operator having $\hat{\alpha}|\alpha\rangle = \alpha|\alpha\rangle$. One can show that the two definitions are equivalent, see [d].

[4]The figures fig. 3.1b and fig. 3.2 are supposed to show a cross section of the probability distribution of a measurement of x and p. But mathematically, such a collective probability distribution is not well defined due to the non-commuting nature of $\hat{x}$ and $\hat{p}$, so a more stringent plot would have shown one of the well-defined quasi-probability distributions, like the P-function, the Q-function or the Wigner-function instead. See [d]. For a discussion of the Q-function in the context of angular momentum variables, see section 3.3.

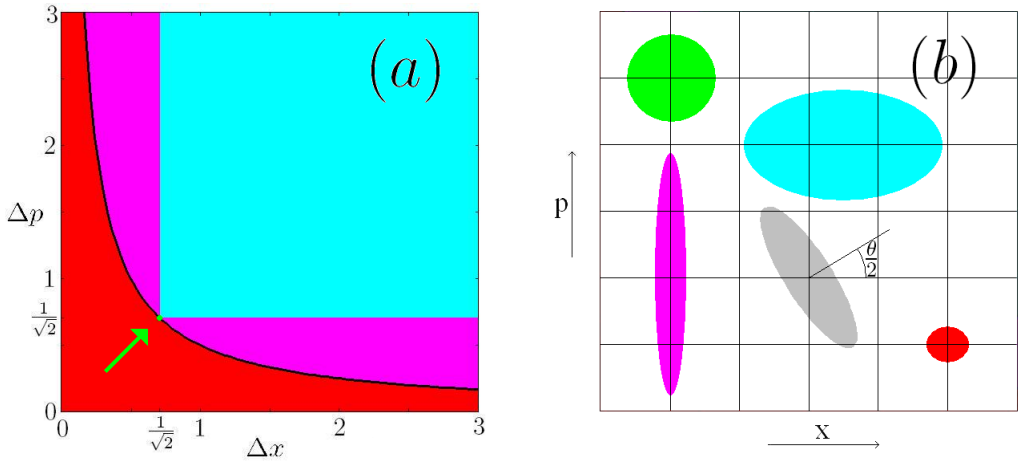

Figure 3.1: A graphical representation of xp-squeezing. (a) shows the quantum uncertainty of a set of conjugate variables x and p. The red area contains the states forbidden by Heisenberg's uncertainty relation (3.4). The bold black curve shows the intelligent states defined as those fulfilling the equality in that relation, and the green dot shows the coherent states with $\Delta x = \Delta p = \frac{1}{\sqrt{2}}$. The pink area contains the states squeezed in x or p, and the light blue area contains the rest of the allowed states. (b) shows the states in phase space. The green, blue, red and pink states belongs to the similar coloured area in figure (a). The light gray state belongs to the blue area, since both Δx and Δp are $> \frac{1}{\sqrt{2}}$. But still the state is squeezed, not in any of the variables x or p, but in the rotated variable Y defined by (3.6), where the angle of rotation $\frac{\theta}{2}$ is indicated on the figure.

which we will use in the following.

A xp-squeezed state can be formed by applying an operator known as the squeeze operator

$$\hat{S}(r,\phi) \equiv \exp\left(\frac{1}{2}r\left(e^{-i\phi}\hat{\alpha}\hat{\alpha} - e^{i\phi}\hat{\alpha}^\dagger\hat{\alpha}^\dagger\right)\right) \tag{3.11}$$

where ϕ is shown in fig. 3.2 and r is a measure of the squeezing. Of course this operator can be used on any state, but let us concentrate on the squeezed vacuum state[5] denoted $|\xi\rangle$ which is the result of applying this operator to the vacuum state. Obviously the result will be a superposition of number states with even numbers

$$|\xi\rangle = \hat{S}(r,\phi)|0\rangle = \sum_m C_{2m}|2m\rangle \tag{3.12}$$

since $\hat{S}$ creates and destroys particles in pairs. The coefficients C_{2m} can be found[6],

[5] According to [d], a squeezed coherent state is made by displacing the squeezed vacuum state, and not by squeezing a coherent state. This is another reason to concentrate on the squeezed vacuum state.

[6] The result is $C_{2m} = (-1)^m \frac{\sqrt{(2m)!}}{2^m m!} \frac{\left(e^{i\theta}\tanh(r)\right)^m}{\sqrt{\cosh(r)}}$. See [d] p. 161.

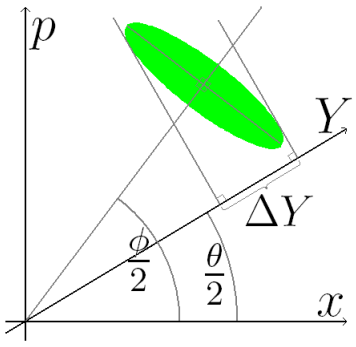

Figure 3.2: Visualization of the angles θ and ϕ. $\theta/2$ is the angle of the axis along which the uncertainty is measured, while $\phi/2$ is the angle of the axis along which the state is squeezed.

but the calculation is tedious and not necessary for our purpose. We want to show that $|\xi\rangle$ indeed is squeezed. This is done by calculating[7] ΔY with the result

$$(\Delta Y)^2 = \frac{1}{2}\Big(\cosh^2(r) + \sinh^2(r) - 2\cosh(r)\sinh(r)\cos(\theta - \phi)\Big) \tag{3.13}$$

where the angles θ and ϕ are shown in fig. 3.2.

This uncertainty is minimized if $\cos(\theta - \phi) = 1$ corresponding to $\theta = \phi$. The result is $\Delta Y = \frac{1}{\sqrt{2}}e^{-r}$ from which we get the expression $r = -\ln(\xi)$ for r in terms of the optimal squeezing parameter ξ. We see that ΔY is a function only of the difference between the rotational angle of the coordinate system θ and the angle of the axis along which we measure the squeezing ϕ. This is not surprising since it tells us that the squeezing is independent of the chosen coordinate system. We also see that the uncertainty when $\theta - \phi = \pi$ is $\Delta Y_\pi = \frac{1}{\sqrt{2}}e^{r}$ from which we see that the squeezed vacuum state is an intelligent state having $\Delta Y_0 \Delta Y_\pi = \frac{1}{2}$.

3.2 Spin-squeezing

The collective spin-operators introduced in section 2.1 are an example of angular momentum operators, which are defined by the commutation relation

$$\left[\hat{J}_i, \hat{J}_j\right] = i\hbar\epsilon_{ijk}\hat{J}_k \tag{3.14}$$

where $i, j, k \in \{x, y, z\}$. Using (3.2), we get the uncertainty relation for angular momentum-like variables to be

$$\Delta J_i \Delta J_j \geq \frac{1}{2}\hbar|\langle \hat{J}_k \rangle| \tag{3.15}$$

[7] To do the calculation we need the Baker-Hausdorff lemma stating $e^{\lambda\hat{A}}\hat{B}e^{-\lambda\hat{A}} = \hat{B} + \lambda\left[\hat{A}, \hat{B}\right] + \frac{\lambda^2}{2!}\left[\hat{A}, \left[\hat{A}, \hat{B}\right]\right] + \ldots$. The calculation is simplified by the fact that $\hat{S}^\dagger\hat{A}\hat{B}\hat{S} = \left(\hat{S}^\dagger\hat{A}\hat{S}\right)\left(\hat{S}^\dagger\hat{B}\hat{S}\right)$ which is true because $\hat{S}$ is unitary.

The most obvious way to define a squeezing parameter for these operators in NOU, is analogous to (3.7)

$$\xi_{J_i}^{(n)} \equiv \Delta J_i / \sqrt{|\langle \hat{J}_k \rangle|/2} \tag{3.16}$$

where the (n) is short for "natural" or "naïve". Another possible definition is the "number squeezing"

$$\xi_{J_i}^{(N)} \equiv \Delta J_i / \sqrt{J/2} \tag{3.17}$$

It does, however, turn out that a third definition

$$\xi_{J_i} \equiv \frac{N^{\frac{1}{2}} \Delta J_i}{\sqrt{\langle \hat{J}_j \rangle^2 + \langle \hat{J}_k \rangle^2}} \tag{3.18}$$

suits our purpose best. The primary reason for this is that (3.18) is the expression that arises naturally in the theory of atomic clocks[8]. We see that for a Dicke state $\xi_{J_i}^{(N)}$ and ξ_{J_i} are related through $\xi_{J_i}^{(N)} = \cos(\phi)\xi_{J_i}$ where ϕ is the angle of $\langle \hat{\mathbf{J}} \rangle$ to the plane perpendicular to J_i.

The essence of the connection between spin-squeezing and atomic clocks, is that ξ_{J_i} can be seen as an indicator for sensitivity to rotations[9], which is shown, in a slightly different way, by the following. Imagine a state with total angular momentum J, with $\langle \hat{J}_x \rangle = J$ and $\langle \hat{J}_y \rangle = \langle \hat{J}_z \rangle = 0$. This state is rotated with an angle θ, so that $\langle \hat{J}_z \rangle = J \sin\theta$, and using error propagation[10] we can calculate $\Delta J_z = J\cos(\theta)\Delta\theta$ or

$$\Delta\theta = \frac{\Delta J_z}{J\cos(\theta)} \tag{3.19}$$

For a Dicke state with[11] $\langle \hat{J}_x \rangle = N/2$, (3.19) gives $\Delta\theta_{DS} = \frac{\sqrt{N/4}}{N/2} = 1/\sqrt{N}$, from which we can calculate the relative uncertainty to be

$$\frac{\Delta\theta}{\Delta\theta_{DS}} = \frac{\Delta J_z \sqrt{N}}{J\cos(\theta)} = \frac{\sqrt{N}\Delta J_z}{\sqrt{\langle \hat{J}_x \rangle^2 + \langle \hat{J}_y \rangle^2}} = \xi_{J_z} \tag{3.20}$$

indicating how the squeezing-parameter, as defined by (3.18), can be used as a measure of sensitivity to rotation. Such a geometrical interpretation cannot be

[8] See (2.13).

[9] Like the rotation made in the second step of the procedure of Ramsey spectroscopy. See section 2.1.

[10] See [c]. The relevant formula states for a function $q(x_1, x_2, \ldots, x_n)$ that $\Delta q = \sqrt{(\Delta x_1 \partial_{x_1} q)^2 + \ldots + (\Delta x_n \partial_{x_n} q)^2}$.

[11] This state in known as a spin-coherent state in the J_x-direction. In the $|j, m\rangle$-basis it is given by (3.24).

made as easily from the alternate definitions (3.16) and (3.17). Another reason to prefer the definition (3.18) is that squeezing by that definition implies entanglement, as we will see in section 3.6 and in appendix C.

Two general methods to generate SSSs independent of the discussions on BEC, are described in [7] and summarized in section 5.3.

3.3 Visualization of spin-squeezing, the Bloch sphere.

For a qubit[12] the density matrix can, in general, be written $\rho = (\frac{1}{2}I + \sum_i P_i\sigma_i)$ where the σ_is are the three Pauli spin matrices. We know that the coefficient on I must be $\frac{1}{2}$ since the trace of ρ should be 1 and the σ_is are traceless. The determinant of ρ must be positive since the two eigenvalues of ρ both are, and this condition can be rewritten to $\boldsymbol{P}^2 \leq \frac{1}{4}$ where $\boldsymbol{P}$ is the vector formed by the three P_is. This means that the allowed values of P_i form a ball with radius $\frac{1}{2}$ known as the Bloch sphere. One can calculate that the states on the surface of Bloch sphere have $\det(\rho) = 0$ corresponding to eigenvalues 0 and 1. Pure states have this characteristic, showing that the surface of the Bloch sphere consists of the pure states. For a qubit described by a vector $\boldsymbol{P}$ we can calculate from $\langle\hat{O}\rangle = \mathrm{Tr}(\rho\hat{O})$ that $\langle\hat{J}_i\rangle = P_i$. This means that there exists a one to one correspondence between the state of the qubit, a point on the Bloch sphere, and the expectation value of the three components of angular momentum.

We want to be able to define a generalized Bloch sphere for states with more internal degrees of freedom (or in our formalism, higher spin) than a qubit. We could use the relation $P_i = \langle\hat{J}_i\rangle$ as definition of our Bloch vector $\boldsymbol{P}$. In this case we can no longer make a one to one correspondence between the state and the value[13] of $\boldsymbol{P}$, nor can we be sure that pure states fulfil $|\boldsymbol{P}| = j$ as was the case for the qubits. We do however get that $|\boldsymbol{P}| \leq j$ like we did for a general state in the qubit case. Fig. 2.1 can be seen as an example of a plot made using this definition.

This description is quite insufficient since we leave out a lot of information about a state, if we depict it as a point only. Any information about $\langle\hat{J}_i^2\rangle$ and thereby about ΔJ_i would be absent in such a visualization. Something like a probability distribution would be better, where the value in a given point in the Bloch sphere corresponds to the probability of measuring the corresponding combination of $\langle\hat{J}\rangle_i$s. But how to define such a distribution mathematically is not clear, due to the impossibility of actually measuring all three angular momentum variables simultaneously. We can, however, obtain something similar. The so-called Husimi Q-function is

[12] A qubit is a system with only two possible quantum states.

[13] This can be seen from the fact that a pure state with total angular momentum j needs $2(2j+1) - 1 = 4j + 1$ real variables for a full description. (The -1 comes from the fact that we can fix an overall phase.) Fixing the three expectation values and requiring normalization gives us four equations, so for $j \geq 1$ we have more variables than equations, indicating that some of them are free.

defined as

$$Q(\theta,\phi) \equiv N_\rho \langle \theta,\phi|\rho|\theta,\phi\rangle \tag{3.21}$$

where $|\theta,\phi\rangle$ is a so-called spin-coherent state (or SCS) and N_ρ is a normalization constant defined so that $\int_0^{2\pi} \mathrm{d}\phi \int_0^{\pi} \mathrm{d}\theta \sin(\theta) Q(\theta,\phi) = 1$. A SCS is defined as an eigenstate to the operator

$$\hat{J}_{\theta,\phi} \equiv \sin(\theta)\cos(\phi)\hat{J}_x + \sin(\theta)\sin(\phi)\hat{J}_y + \cos(\theta)\hat{J}_z \tag{3.22}$$

with eigenvalue j. The SCS can be found by rotating the $|j,j\rangle$-state around the y-axis with an angle θ and then around the z-axis with an angle ϕ. The general expression is[14]

$$|\theta,\phi\rangle = \sum_{m=-j}^{j} \sqrt{\begin{pmatrix} 2j \\ j+m \end{pmatrix}} \cos^{j+m}(\theta/2)\sin^{j-m}(\theta/2) e^{-i(j+m)\phi}|j,m\rangle \tag{3.23}$$

For the special case of $\theta = 0$ corresponding to an eigenstate to $\hat{J}_z$, the above result reduces unsurprisingly to $|z\rangle = |j,j\rangle$, and for $\theta = \pi/2$ and $\phi = 0$ corresponding to an eigenstate to $\hat{J}_x$, the result reduces to

$$|x\rangle = 2^{-j} \sum_{m=-j}^{j} \sqrt{\begin{pmatrix} 2j \\ j+m \end{pmatrix}} |j,m\rangle \tag{3.24}$$

The Husimi Q-function is a quasi probability distribution. It gives the probability of measuring the specific spin-coherent state $|\theta,\phi\rangle$ given that we measure some spin coherent state. For the classical limit $j \to \infty$ where the relative minimal uncertainty goes to 0, the Q-function will go towards the desired probability distribution.

We can illustrate this by calculating the Q-function for the states $|j,j\rangle$ and $|j,0\rangle$. $|j,j\rangle$ is the SCS in the J_z-direction, so the probability of measuring a $J_z \neq j$ should be zero for a true probability distribution. Likewise the state $|j,0\rangle$ must give $J_z = 0$ with no uncertainty. We can find the matrix elements to

$$\begin{aligned} \langle j,j|\theta,\phi\rangle &= \cos^{2j}(\theta/2) e^{-2ij\phi} \\ \langle j,0|\theta,\phi\rangle &= \sqrt{\begin{pmatrix} 2j \\ j+m \end{pmatrix}} \left(\frac{\sin\theta}{2}\right)^j e^{-ij\phi} \end{aligned} \tag{3.25}$$

giving the normalized Q-functions

$$\begin{aligned} Q_{jj}(\theta,\phi) &= \frac{2j+1}{4\pi}\cos^{4j}(\theta/2) \\ Q_{j0}(\theta,\phi) &= \frac{(2j+1)!!}{4\pi\cdot(2j)!!}\sin^{2j}(\theta) \end{aligned} \tag{3.26}$$

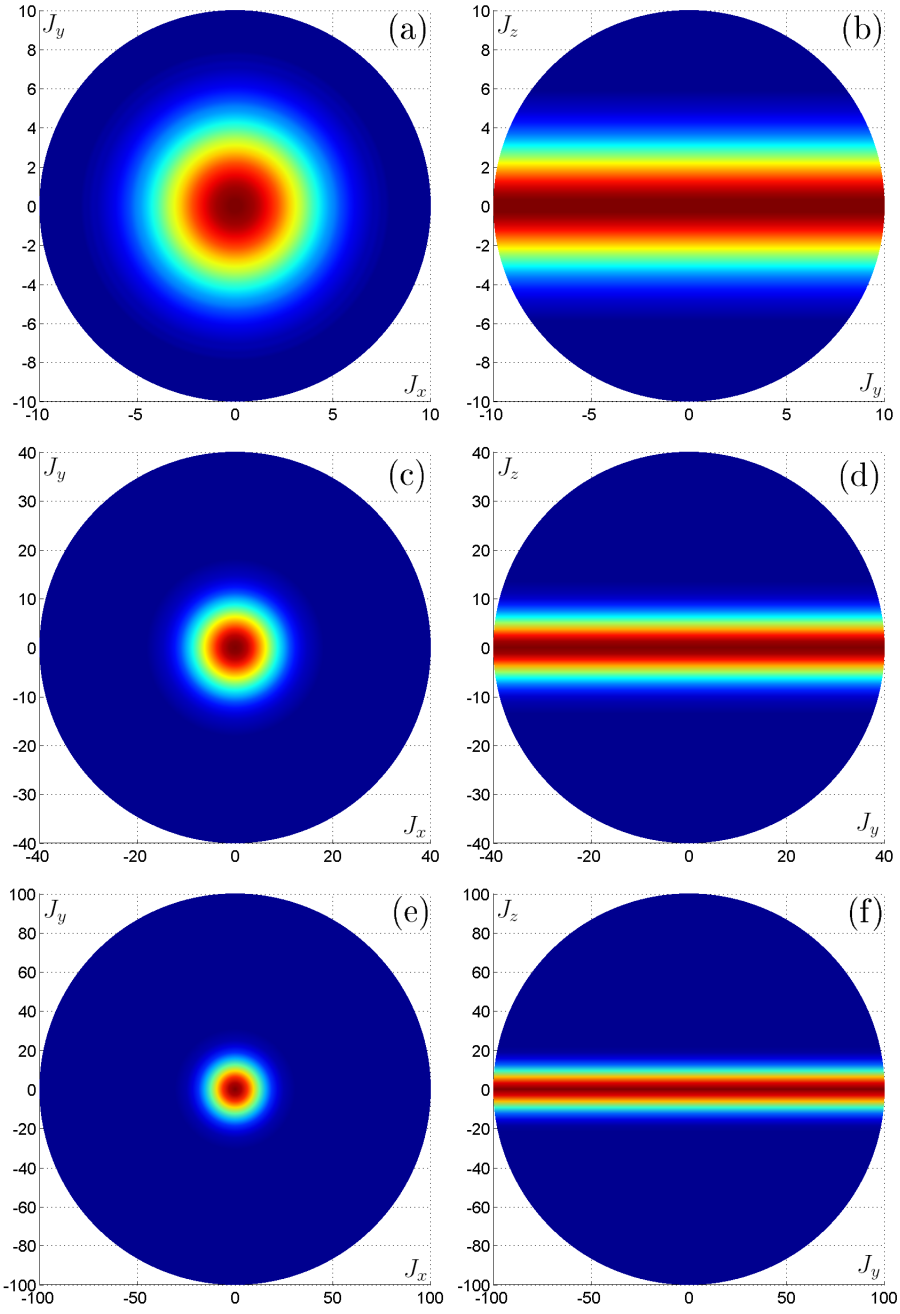

Figure 3.3: This plot shows the Q-functions for the states $|j, j\rangle$ and $|j, 0\rangle$ for various values of j. Exact expressions for these functions are given by (3.26). (a), (c), and (e) shows $Q_{jj}(\theta, \phi)$ and (b), (d), and (f) shows $Q_{j0}(\theta, \phi)$. (a) and (b) are plotted for $j = 10$, (c) and (d) are for $j = 40$ and (e) and (f) are for $j = 100$. We see that the functions become more and more singular as j increases, as postulated in the main text.

where $x!! \equiv x(x-2)(x-4)\cdots$ is the double factorial. We see from (3.26) and from fig 3.3 that as $j \to \infty$ the Q-function becomes more and more singular, indicating that the Q-function goes to a true probability distribution in this limit.

Other kinds of quasi probability distributions can be defined, examples are the P-function and the Wigner function[15], but in this thesis we will stick to using the Q-function as our quasi probability distribution.

We would like to be able to calculate something similar to the Q-function for a state, when we do not have the state expressed in the $|j,m\rangle$-basis. Let us make the assumption[16] that the state can be written as a Gaussian probability distribution in (J'_x, J'_y, J'_z)-space, where J'_x, J'_y, and J'_z are three orthogonal axes. That is

$$\tilde{P}(J'_x, J'_y, J'_x) \quad \propto \quad \exp\left(\frac{-\left(J'_x - \langle J'_x\rangle\right)^2}{2(\Delta J'_x)^2}\right)\exp\left(\frac{-\left(J'_y - \langle J'_y\rangle\right)^2}{2(\Delta J'_y)^2}\right)\exp\left(\frac{-\left(J'_z - \langle J'_z\rangle\right)^2}{2(\Delta J'_z)^2}\right)$$

In order to do that we need to find J'_x, J'_y, and J'_z in terms of our usual J_x, J_y, and J_z coordinates. This can be done[17] by diagonalizing the covariance-matrix, where the eigenvectors will be the J' axes expressed in the J-basis, and the eigenvalues will be the $(\Delta J')^2$s. The covariance matrix can be written as

$$\Sigma \equiv \begin{bmatrix} V_{xx} & V_{xy} & V_{xz} \\ V_{yx} & V_{yy} & V_{yz} \\ V_{zx} & V_{zy} & V_{zz} \end{bmatrix} \tag{3.27}$$

where[18]

$$V_{ij} \quad = \quad \frac{1}{2}\left(\langle \hat{J}_i\hat{J}_j\rangle + \langle \hat{J}_j\hat{J}_i\rangle\right) - \langle \hat{J}_i\rangle\langle \hat{J}_j\rangle \tag{3.28}$$

We see that the diagonal elements reduce to $V_{ii} = \langle \hat{J}_i^2\rangle - \langle \hat{J}_i\rangle^2$, the ordinary expression for the variance.

[14] See [8]. Can be checked by inserting in (3.22).

[15] See [d] for discussions of all three quasi probability distributions in the case of states defined in the xp-basis. The definition of the Wigner function for states in an $|j,m\rangle$-basis is $W_\rho(\theta,\phi) \equiv \sqrt{\frac{2j+1}{4\pi}}\sum_{K=0}^{2j}\left(\sum_{Q=-K}^{K}\varrho_{KQ}Y_{KQ}(\theta,\phi)\right)$ where $\varrho_{KQ} \equiv \mathrm{Tr}(\rho T^\dagger_{KQ})$ where $T_{KQ} \equiv \sum_{m=-j}^{m=j}(-1)^{j-m}\sqrt{2K-1}\times\begin{pmatrix} j & K & j \\ -m & Q & m-Q\end{pmatrix}|j,m\rangle\langle j,m-Q|$. The quantity in the brackets is known as a "Wigner 3j symbol". See [8] and [9]. Like we do for the Q-function, the P-function for $|j,m\rangle$-states can be defined analogous to the xp-case, that is $\rho = \int P(\theta,\phi)|\theta,\phi\rangle\langle\theta,\phi|\sin\theta \mathrm{d}\theta\mathrm{d}\phi$. See [9].

[16] This assumption will always be wrong since we can not measure all three coordinates at the same time. But as $j \to \infty$ the approximation gets better, as we have seen.

[17] See [f].

[18] For ordinary commuting variables, the elements are written $V_{ij} = \langle \hat{J}_i\hat{J}_j\rangle - \langle \hat{J}_i\rangle\langle \hat{J}_j\rangle$, where $V_{ij} = V_{ji}$ which makes Σ Hermitian ensuring real eigenvalues. But when $\left[\hat{J}_i, \hat{J}_j\right] \neq 0$ this is no longer the case, so the generalization to non-commuting variables is the expression (3.28) which preserves $V_{ij} = V_{ji}$.

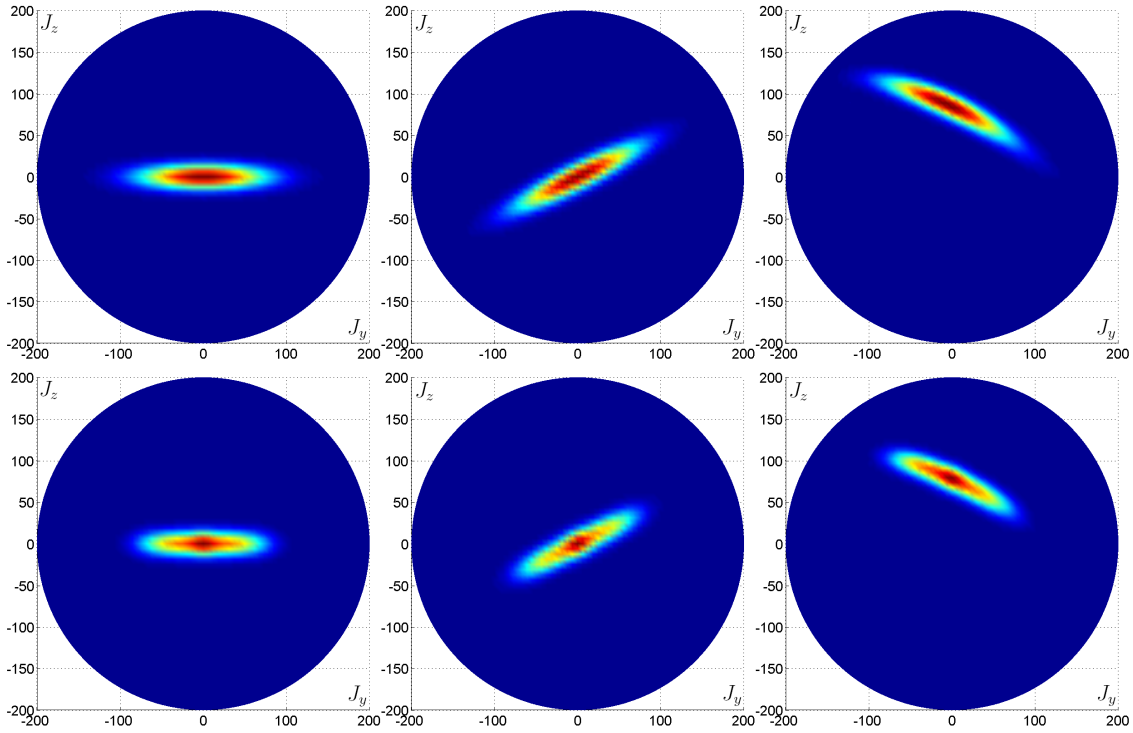

Figure 3.4: This figure compares the functions $Q(\theta,\phi)$ and $\mathfrak{Q}(\theta,\phi)$ for three different states. $Q(\theta,\phi)$ is on the upper row and $\mathfrak{Q}(\theta,\phi)$ is on the lower. We see that $\mathfrak{Q}$ reproduces the essential features of Q.

The 'probability distribution' $\tilde{P}$ can be expressed as a function of j, θ, and ϕ by writing $J'_x = j\sin(\theta)\cos(\phi)$, $J'_y = j\sin(\theta)\sin(\phi)$, and $J'_z = r\cos(\theta)$ where the radial variable has been named j since it has the interpretation as the radius of the Bloch sphere. It is not obvious which way we best define j. One option is to choose $j^2 = \langle \hat{J}'_x\rangle^2 + \langle \hat{J}'_y\rangle^2 + \langle \hat{J}'_z\rangle^2$ which makes the sphere go through the maximum of $\tilde{P}$, and another option is to pick $j = N/2$ which is what we will do in this thesis[19]. The 'probability distribution' $\tilde{P}(\theta,\phi)$ cannot be directly compared to the Q-function since $Q(\theta,\phi)$ has the interpretation as the probability of measuring the SCS in the (θ,ϕ)-direction, given that some SCS is measured. We can however construct a function, which we name the $\mathfrak{Q}$-function, with this interpretation as

$$\mathfrak{Q}(\theta,\phi) \equiv \int \mathrm{d}\theta' \int \mathrm{d}\phi' \sin(\theta')\tilde{P}(\theta',\phi')G_{\theta,\phi}(\theta',\phi') \tag{3.29}$$

where $G_{\theta,\phi}(\theta',\phi')$ is playing the role as the SCS and is modeled as a Gaussian distribution centered in (θ,ϕ) with variance $j/2$ like the ordinary SCS. In fig. 3.4 we see a comparison of Q and $\mathfrak{Q}$ for some states.

[19]The reason for this is that it gives the best correspondence between Q and $\mathfrak{Q}$, which can be seen by a comparison like the one in fig. 3.4.

For the rest of this thesis we will use the $\mathfrak{Q}$-function when we want to plot a state which is not expressed in the $|j,m\rangle$-basis.

3.4 Absolute minimum: the F-functions

When considering[20] spin-squeezing, one has to choose the axes i, j, and k in (3.18). Let us choose the axes so the squeezing parameter becomes

$$\xi^2 \equiv \frac{N(\Delta J_z)^2}{\langle \hat{J}_x \rangle^2} \tag{3.30}$$

where we have abbreviated ξ_{J_z} as ξ. This means that we name the axis, for which we calculate the uncertainty of the collective spin, the z-axis, and that we pick the axes perpendicular to the z-axis so that $\langle \hat{J}_y \rangle = 0$. This choice of axis will be kept for the rest of the thesis. One might think that in order to minimize this squeezing parameter, one just needs to pick a state minimizing ΔJ_z. One such state is $|\uparrow\uparrow \ldots \uparrow\rangle$ which is an eigenstate for the $\hat{J}_z$-operator and has $\Delta J_z = 0$. But this state has $\langle \hat{J}_x \rangle = 0$ as well, so strictly speaking (3.30) is not even defined for that state[21]. If one instead choose a state very close to the above, with $\Delta J_z \approx 0$ and $\langle \hat{J}_x \rangle \approx 0$, it is not clear why that state should result in a smaller ξ_{J_z} than another state having both ΔJ_z and $\langle \hat{J}_x \rangle$ bigger, so we see that there is a trade-off between small ΔJ_z and large $\langle \hat{J}_x \rangle$. Fig. 3.5 shows the two extrema, and a squeezed state as a compromise in between.

Let us investigate the behaviour of ΔJ_z for a fixed value of $\langle \hat{J}_x \rangle$, by defining a family of functions $F_J(x)$, denoted F-functions, with the property that

$$J \cdot F_J\left(\langle \hat{J}_x \rangle / J\right) \tag{3.31}$$

equals the minimal possible value of the variance $(\Delta J_z)^2$. The reason for the Js in this definition, is that we want the F-functions to be easily comparable by making them have the same domain and range for any value of J, and with this definition the domain of $F_J(x)$ is $[-1;1]$ and the range turns out to be $[0;\frac{1}{2}]$ for all values of J. Let us calculate the F-functions for various values of J. Our choice of axis means that we stay in the xz-plane where the states are purely real. For $J = \frac{1}{2}$ this means that we can write a general state vector (c,s) where c and s are short for sine and cosine to some angle. From this we can calculate $(\Delta J_z)^2 = c^2 s^2$ and $\langle \hat{J}_x \rangle = cs$ which gives

$$F_{\frac{1}{2}}(x) = \frac{1}{2}x^2 \tag{3.32}$$

as the expression for the F-function for states with $J = \frac{1}{2}$.

[20] What is done in this section corresponds closely to what is done in [3].

[21] Since it would force us to calculate 0/0.

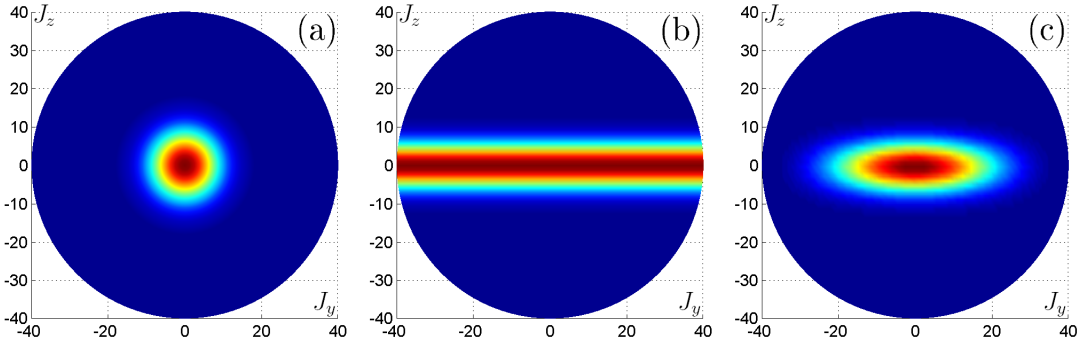

Figure 3.5: (a) shows the Q-function for $|j,j\rangle$, the SCS in the J_x-direction. This is the state that maximizes the denominator of (3.30). (b) shows the same for $|j,0\rangle$ which has $J_z = 0$ and thereby it minimizes the numerator of (3.30). (c) shows a spin-squeezed state found as the lowest eigenvalue eigenstate to (3.33) with $\lambda = \frac{1}{2}$. All states are plotted for $j = 40$. We see that (c) lies in between (a) and (b) showing how a spin-squeezed state (squeezed in the z-direction with $\langle \hat{J}_y \rangle = 0$) is a compromise between low ΔJ_z and high $\langle \hat{J}_x \rangle$.

The state maximizing $\langle \hat{J}_x \rangle$ will always be at the equator of the Bloch sphere. If J is an integer, a state minimizing ΔJ_z will be here as well, namely the state $|J,0\rangle$, which does not exist for half-integer J. This gives us reason to believe that the state minimizing (3.30) will be at the equator as well, at least for integer J which is what we will consider in the following. States on the equator of the Bloch sphere have $\langle \hat{J}_z \rangle = 0$, which means that $(\Delta J_z)^2 = \langle \hat{J}_z^2 \rangle$, so for a fixed value of $\langle \hat{J}_x \rangle$ the minimization of ξ can be done by minimizing $\langle \hat{J}_z^2 \rangle - \lambda \langle \hat{J}_x \rangle$ where λ is a Lagrange multiplier. We know that the state corresponding to this minimization must be an eigenstate to the operator

$$\hat{M} \equiv \hat{J}_z^2 - \lambda \hat{J}_x \tag{3.33}$$

since the eigenstate corresponding to the lowest eigenvalue always gives the lowest possible expectation value. So this means that for integer J, the state minimizing (3.30) will be an eigenstate to $\hat{M}$. For $J = 1$ the state can be calculated analytically. In this case[22]

$$\hat{M}_1 = \begin{pmatrix} 1 & \eta & 0 \\ \eta & 0 & \eta \\ 0 & \eta & 1 \end{pmatrix} \tag{3.34}$$

where $\eta = -\lambda/\sqrt{2}$. $\hat{M}_1$ has the eigenvalues 1 and $\frac{1}{2} \pm \frac{1}{2}\sqrt{1+8\eta^2}$, corresponding to the normalized eigenvectors $\frac{1}{\sqrt{2}}(1,0,-1)$ and $\frac{1}{\sqrt{2+a_\pm^2}}(1,a_\pm,1)$ where $a_\pm \equiv \frac{-1\pm\sqrt{1+8\eta^2}}{2\eta}$. The smallest eigenvalue is the one involving the minus, so now we can

[22] See appendix B.

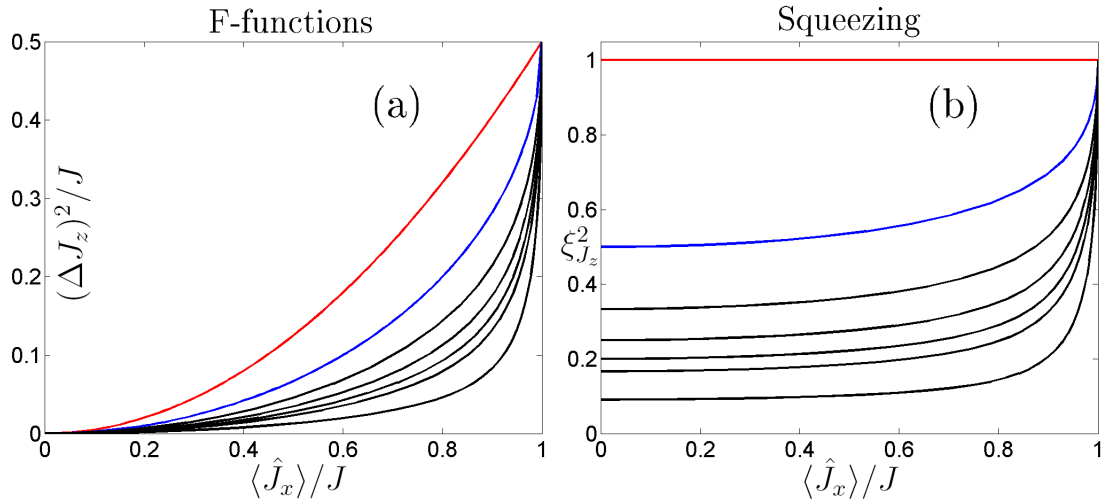

Figure 3.6: (a) shows the F-functions for various values of J. The red curve is the result for $J = \frac{1}{2}$ given by (3.32), and the blue curve is the result for $J = 1$ given by (3.35). The black curves are numerical results for $J = 2$, 3, 4, 5, and 10 starting from above. These numbers are chosen in order to reproduce FIG. 1. in [3]. We see that all the curves are convex, which is shown in the main text. (b) shows the spin-squeezing for the same values of J, with $N = 2J$. We see that the maximal squeezing is obtained at $\langle \hat{J}_x \rangle = 0$, independent of the value of the total angular momentum. The minimal squeezing parameter is given as $\xi^2_{J_z} = 1/(J+1)$ for integer values of J, which is derived in (3.39).

calculate $(\Delta J_z)^2$ and $\langle \hat{J}_x \rangle$ with the results $(\Delta J_z)^2 = \frac{2}{2+a^2}$ and $\langle \hat{J}_x \rangle = \frac{2\sqrt{2}a}{2+a^2}$ giving the F-function

$$F_1(x) = \frac{1}{2}\left(1 - \sqrt{1-x^2}\right) \tag{3.35}$$

For higher values of J the calculation has to be done numerically, and the results for some values are plotted in fig. 3.6a. F-functions for half-integer J or odd N can be calculated using Monte Carlo methods[23], but we will not delve deeper into this here.

We see from fig. 3.6a that all the F-functions are convex, which is a result we will need later. This can be proven[24] for integer J, where the states are eigenstates to (3.33). We can calculate the slope of the F-function to

$$\frac{d\langle \hat{J}_z^2 \rangle}{d\hat{J}_x} = \frac{d\langle \hat{J}_z^2 \rangle}{dt} \Big/ \frac{d\langle \hat{J}_x \rangle}{dt} = \frac{-i\lambda \left[\hat{J}_x, \hat{J}_z^2\right]}{i\left[\hat{J}_z^2, \hat{J}_x\right]} = \lambda \tag{3.36}$$

So if we let λ be an adiabatically increasing function of time starting from $\lambda = 0$, then $\langle \hat{J}_x \rangle$ will increase as well, since a higher λ will give more weight to the $\hat{J}_x$-part

[23] See [3].

[24] This proof is inspired by [3]. I do not know whether a general proof exists.

of (3.33). And since the slope of the F-function equals λ, we have that $\frac{d^2\langle \hat{J}_z^2\rangle}{d\langle \hat{J}_x\rangle^2} > 0$, which is equivalent to $F(x)$ being convex.

The squeezing corresponding to the F-functions can be calculated[25], and the results are potted in fig. 3.6b. We see that a higher J corresponds to more squeezing[26], and therefore the state maximizing the squeezing has as high a J as possible. The highest possible value is $J = N/2$, so therefore the F-function for an ensemble of N spin-$\frac{1}{2}$ particles is the one corresponding to $J = N/2$.

In fig. 3.6b. we have plotted the squeezing as a function of $\langle \hat{J}_x\rangle$. We see that for all values of J, the squeezing parameter has its minimum at $\langle \hat{J}_x\rangle = 0$, where the F-functions tell us that $\langle \hat{J}_z^2\rangle = 0$. This means that the minimizing state must be $|J, 0\rangle$, but as we saw, the squeezing parameter is not defined in that point, so let us instead calculate the squeezing for a perturbation around that state

$$|\psi\rangle = \sqrt{1 - 2|\epsilon|^2}|J, 0\rangle + \epsilon|J, 1\rangle + \epsilon|J, -1\rangle \tag{3.37}$$

where the parameter ϵ is small. From this we can calculate[27]

$$\langle \hat{J}_z^2\rangle = 2|\epsilon|^2 \quad \text{and} \quad \langle \hat{J}_x\rangle = 2\sqrt{1 - 2|\epsilon|^2}\sqrt{j(j+1)}\epsilon \tag{3.38}$$

which gives the squeezing parameter $\xi^2 = \frac{1}{J+1}$ corresponding to

$$\xi^2 = \frac{2}{N+2} \tag{3.39}$$

This result is the absolute maximal squeezing obtainable for a given value of N. The calculation was purely mathematical and, as we will see, realistic physical situations will result in less squeezing than the amount produced by the F-functions.

3.5 Entanglement

Another reason why the definition of the squeezing parameter (3.18) is to be preferred, is that squeezing, according to this parameter, implies quantum entanglement. Quantum entanglement has been the cause of controversy in the history of quantum physics, due to some of the apparent paradoxes it causes[28]. But with the

[25] For $J = \frac{1}{2}$ and $J = 1$ the calculation can be done analytically, and the results are $\xi_{\frac{1}{2}} = 1$ and $\xi_1 = \frac{1}{1+\sqrt{1-\langle \hat{J}_x\rangle^2}}$.

[26] When plotting 3.6b a little cheating was involved, since we already chose $N = 2J$. But choosing a smaller N is impossible, and choosing a bigger N would move the curves upwards and thereby reduce the squeezing.

[27] This is done using $\hat{J}_z|j, m\rangle = m|j, m\rangle$, $\hat{J}_\pm|j, m\rangle = \sqrt{(j \mp m)(j \pm m + 1)}|j, m \pm 1\rangle$ and $\hat{J}_x = \frac{1}{2}\left(\hat{J}_+ + \hat{J}_-\right)$. See appendix B.

[28] These paradoxes were the subject of the famous EPR (Einstein, Podolsky and Rosen) paper [20], and also one of the subjects of the Einstein-Bohr debates. A modern formulation is that entangled states can lead to violations of Bell's inequality, see [10].

emergence of the field of quantum information, ways have been found to utilize this highly non-classical behaviour to produce a theory of a (so far mostly hypothetical) type of computers, called quantum computers, able to do computations faster than what is information-theoretically allowed for classical computers. Another classical limit that quantum entanglement can help to surpass is the limit on the security of cryptographic key distribution[29]. Further discussion of these subjects is beyond the scope of this thesis. In this section only the basic definitions will we presented, enabling us to prove that spin-squeezing implies entanglement in the next section.

The definition of an entangled state of n subsystems is that the density matrix ρ of the state does **not** fulfil

$$\rho = \sum_i p_i \rho_i^{(1)} \otimes \rho_i^{(2)} \otimes \ldots \otimes \rho_i^{(n)} \tag{3.40}$$

where $\rho_i^{(n)}$ is the i'th density matrix for the n'th subsystem. That is, an entangled state can not be written as a sum of products of density matrices for the individual subsystems in any way. A state that does fulfil the above equation is known as a separable state. The definition is inspired by the relation

$$P(x_1, x_2, \ldots, x_n) = \sum_i p_i P_i^{(1)}(x_1) \cdot P_i^{(2)}(x_2) \cdot \ldots \cdot P_i^{(n)}(x_n) \tag{3.41}$$

for the joint probability distribution of n variables x_1 to x_n which holds true for any discrete classical probability distribution.

The general expression for a density matrix is

$$\rho = \sum_i p_i |\psi_i\rangle\langle\psi_i| \tag{3.42}$$

which in the case of a pure state $|\psi\rangle$, reduces to $\rho = |\psi\rangle\langle\psi|$. Since a pure state cannot be made out of a combination of mixed states, (3.40) reduces to $|\psi\rangle\langle\psi| = \sum_i p_i |\psi_i^{(1)}\rangle\langle\psi_i^{(1)}| \otimes \ldots \otimes |\psi_i^{(n)}\rangle\langle\psi_i^{(n)}|$, and we can infer that the only solution making $|\psi\rangle$ pure is

$$|\psi\rangle = |\psi^{(1)}\rangle \otimes \ldots \otimes |\psi^{(n)}\rangle \tag{3.43}$$

which is the separability criterion for pure states.

3.6 Squeezing and entanglement

In this section we will sketch the proof of the fact that spin-squeezing according to (3.18) implies entanglement[30]. The full proof is given in appendix C. For the

[29] For more on the mentioned quantum information procedures, see [10].

[30] Other sketches of this proof can be found in [1] and [3].

variance of a measurement of the z-component of the collective spin, we have

$$(\Delta J_z)^2 = \langle \hat{J}_z^2 \rangle - \langle \hat{J}_z \rangle^2 \tag{3.44}$$

Assuming a separable state, the above expression can be rewritten using (3.40) to

$$(\Delta J_z)^2 \geq \sum_i p_i \sum_k (\Delta j_z^{(k)})_i^2 \tag{3.45}$$

where $j_z^{(k)}$ is the z-component of the angular momentum for the k-th individual subsystem. The expression (3.45) basically states that the the total variance is the sum of the variances of the individual subsystems, just as one would get from error propagation. The '>-part' stems from the fact that the individual subsystems does not need to have their j-vectors pointing in the same direction.

Let us now insert the F-functions found in section 3.4, which were defined so $jF_j\left(\langle \hat{j}_x \rangle / j\right) \leq (\Delta j_z)^2$. This gives

$$(\Delta J_z)^2 \geq \sum_i p_i \sum_k j^{(k)} F_{j^{(k)}}\left(\langle \hat{j}_x^{(k)} \rangle_i / j^{(k)}\right) \tag{3.46}$$

We saw from (3.36) that $F_j(x)$ is convex for all values of j. For all convex functions Jensen's inequality holds, stating that

$$\frac{\sum_k^N a_k F(x_k)}{\sum_k^N a_k} \geq F\left(\frac{\sum_k^N a_k x_k}{\sum_k^N a_k}\right) \tag{3.47}$$

or "the weighted average of a convex function evaluated at some inputs, is greater than or equal to the function evaluated at the weighted average of the same inputs". Using Jensen's inequality on both of the sums in (3.46) gives

$$(\Delta J_z)^2 \geq N j F_j\left(\langle \hat{J}_x \rangle / N j\right) \tag{3.48}$$

where we have used that all the subsystems have the same spin, which is true in the case of an ensemble of spin-$\frac{1}{2}$ particles. Inserting $j = \frac{1}{2}$ corresponding to the F-function $F_{\frac{1}{2}} = \frac{1}{2}x^2$ which is derived in (3.32), gives

$$\begin{aligned} (\Delta J_z)^2 &\geq \frac{\langle \hat{J}_x \rangle^2}{N} \Leftrightarrow \\ \xi_{J_z} &\geq 1 \end{aligned} \tag{3.49}$$

This long calculation started by considering ΔJ_z, but we could have started from ΔJ_i instead where i could be any axis, and we would have got the same result $\xi_{J_i} \geq 1$. This means that, if we start out by a separable state, there will not be squeezing along any axis. This again implies that, if there is squeezing along an axis, then the

state can not be separable and it is therefore entangled. This proves that squeezing implies entanglement. It should be noted that this is a genuine implication. Not all entangled states are squeezed, which should be clear from the facts that most states are entangled and most states are non-squeezed.

We also want to show that the alternate definitions of squeezing given by (3.16) and (3.17) does not imply entanglement. This can be done using a simple example involving two qubits $|\psi\rangle_\pm = \cos(\theta/2)|\uparrow\rangle \pm \sin(\theta/2)|\downarrow\rangle$ combined like $|\psi\rangle = |\psi\rangle_+ \otimes |\psi\rangle_-$ showing that the state is not entangled. In order to calculate the squeezing we must calculate the expectation values of the angular momentum operators[31], giving $\langle \hat{J}_x \rangle = \langle \hat{J}_y \rangle = 0$, $\langle \hat{J}_z \rangle = (c^4 - s^4)$, and $\langle \hat{J}_x^2 \rangle = (c^4 - 2c^2s^2 + s^4)/2$ where c and s are short for $\cos(\theta/2)$ and $\sin(\theta/2)$. This gives $\xi_{J_x}^{(n)} = \sqrt{|\cos(\theta)|}$ and $\xi_{J_x}^{(N)} = |\cos(\theta)|$ which are ≤ 1. If we calculate the squeezing using (3.18), we get $\xi_{J_x} = 1$ i.e. unsqueezed in accordance with what is expected.

The methods used in the first part of this section can be used to prove another interesting result as well. If a state is entangled we saw that it meant that it is could not be written on the form (3.40)

$$\rho = \sum_i p_i \rho_i^{(1)} \otimes \rho_i^{(2)} \otimes \ldots \otimes \rho_i^{(n)} \tag{3.50}$$

where $\rho^{(k)}$ is the density matrix of the kth individual particle. But that does not rule out the possibility that ρ can be written as (3.50) where the $\rho^{(k)}$s are density matrices for subsystems made up of more than one particle. If that is the case, the steps in our "squeezing implies entanglement"-proof will hold up to (3.46), which will have the form

$$(\Delta J_z)^2 \;\geq\; \sum_i p_i \sum_k j_i^{(k)} F_{j_i^{(k)}} \left(\frac{\langle \hat{j}_x^{(k)} \rangle_i}{j_i^{(k)}} \right) \tag{3.51}$$

Using Jensen's inequality enables us to rewrite[32] it to

$$(\Delta J_z)^2 \;\geq\; \tfrac{1}{2} N F_{j_{\max}} \left(\frac{\langle \hat{J}_x \rangle}{\frac{1}{2}N} \right) \tag{3.52}$$

where $j_{\max}$ is the total angular momentum of the subsystem having the largest total angular momentum. This means that if some state has the point $\left(\frac{\langle \hat{J}_x \rangle}{\frac{1}{2}N}, \frac{(\Delta J_z)^2}{\frac{1}{2}N} \right)$ lying below the F-function corresponding to some j we know that the state has $j_{\max} > j$, and therefore the corresponding subsystem is made up of at least $2j$ particles.

[31] For such a combination of qubits, the operators can be calculated as $\hat{J}_i = \hat{j}_i^{(1)} \otimes \hat{I}^{(2)} + \hat{I}^{(1)} \otimes \hat{j}_i^{(2)}$, where the upper index refers to the first and second qubit respectively.

[32] See the final part of appendix C. The calculation uses the relation $f(x) \geq a f(x/a)$ which holds for convex, positive functions, having $f(0) = 0$.

Therefore we have that if we know that a given state corresponds to some point in $\langle \hat{J}_x \rangle$-$(\Delta J_z)^2$-space, we can find a minimum on the number of entangled particles needed in order to produce that state, by finding the F-function with the highest j that lies above the point in question, in which case the minimal number of entangled particles will be $2j$.

Chapter 4

Bose-Einstein condensate

A Bose-Einstein condensate (in the following known as BEC) is a macroscopical state characteristic for bosons. The existence of this macroscopical state stems from the fact that bosons are not subject to the Pauli exclusion principle, and therefore they can assemble in one common quantum state. Identical particles in the same quantum state will have identical behaviour, and this makes a BEC different from an ordinary Bose gas, which is a statistical mixture of particles in many quantum states. The fact that the usual statistical description is insufficient in describing BEC is suggested by the following section.

4.1 The existence of Bose-Einstein condensate

This section describes a crude model of BEC, which is different from the Gross-Pitaevskii model that will be used in the rest of the thesis. The purpose of this section is to show that a gas of bosons forms a condensate at low temperatures.

Usually the energy distribution in a Bose gas is described by the Bose distribution function

$$n_{_B}(E) = \frac{1}{\exp\left(\frac{E-\mu}{k_B T}\right) - 1} \tag{4.1}$$

It can be seen from (4.1) that if $\mu > E$ then $n_{_B} < 0$ which is unphysical, so therefore $\mu \leq 0$ must hold in any case[1], and we also see that $\mu = 0$ will give the highest possible value for $n_{_B}(E)$. In general μ can be found by isolating it in the expression for the total particle number

$$N = \int_0^\infty \mathrm{d}E \; \rho(E) n_{_B}(E) \tag{4.2}$$

[1]This result assumes that the lowest energy state has $E = 0$, which is equivalent to ignoring the zero-point energy. If the zero-point energy is included we find that $\mu = \frac{3}{2}$ in the absence of particle interactions.

where ρ is the density of states.

In this thesis we will only consider the case where the external potential is the isotropic harmonic oscillator[2] given by $V(\mathbf{r}) = \frac{1}{2}m\omega^2\mathbf{r}^2 = \frac{1}{2}m\omega^2(x^2+y^2+z^2)$, and the quantized energy-levels of non-interacting particles in such a potential are $E_{n_x,n_y,n_z} = \hbar\omega\left(n_x+n_y+n_z+\frac{3}{2}\right)$. By integrating up to the plane in n-space made up of states with the same energy, we see that the number of particles with energy less than some energy E is approximately[3] $G(E) = \frac{E^3}{6\hbar^3\omega^3}$, from which we can find the density of states $\rho \equiv \frac{\mathrm{d}G(E)}{\mathrm{d}E}$ to be

$$\rho(E) = \frac{E^2}{2\hbar^3\omega^3} \tag{4.3}$$

Now we may calculate the total particle number from (4.2) using $\mu = 0$, with the result[4]

$$N = 1.2021 \cdot \frac{(k_{_B}T)^3}{\hbar^3\omega^3} \tag{4.4}$$

This means that for values of N bigger than the one found above, the theory for the ordinary Bose gas breaks down, since no value of μ describing the situation can be found. More specifically, the error is that the derivation of (4.3) assumes the existence of a continuum of states. Such a continuum does not exist, since reality is made of a discrete set of quantum states. If we isolate T in (4.4), we get the critical temperature T_c where the transition to BEC happens, to be

$$k_B T_c \;=\; 0.9405 \cdot \hbar\omega N^{1/3} \tag{4.5}$$

For temperatures below T_c we can calculate the number of particles in the condensate N_0 by calculating the number of particles in the Bose gas N_{gas} using (4.4) and finally use conservation of particle number $N = N_{\text{gas}} + N_0$.

All particles in a BEC will be in the same quantum state, as mentioned. Let us in the following name the wave function for this state $\varphi(\mathbf{r})$. For the harmonic trap potential, The Schrödinger equation can be written

$$-\frac{\hbar^2}{2m}\nabla^2\varphi + \frac{1}{2}m\omega^2 r^2\varphi = E\varphi \tag{4.6}$$

[2]For the cases of an anisotropic harmonic oscillator potential or a box-shaped potential, calculations corresponding to those in this section are done in [a] p. 17 ff., which is where the inspiration to the calculations in this section comes from as well.

[3]Here we disregard the vacuum energy $\frac{3}{2}$ and the fact that the levels are discrete.

[4]This is done using the integral $\int_0^\infty \frac{x^{\alpha-1}}{e^x-1}\mathrm{d}x = \Gamma(\alpha)\zeta(\alpha)$ for $\alpha > 1$, where $\Gamma(\alpha)$ and $\zeta(\alpha)$ are the two mathematical functions the gamma function and the Riemann zeta function respectively. The relevant values are $\Gamma(3) = 2$ and $\zeta(3) = 1.20205\ldots$. As we see is $\alpha = 3$ in the case of the isotropic three-dimensional harmonic oscillator, and for a particle in a three-dimensional box we can calculate that $\alpha = \frac{3}{2}$. For $\alpha \leq 1$ as is the case for a particle in a box with dimension ≤ 2, $N(\mu)$ has a singularity in $\mu = 0$, and no condensate will appear.

$\varphi(\mathbf{r})$ will always be the lowest energy state, and by solving (4.6) it can be found[5] to

$$\varphi(\mathbf{r}) = \frac{1}{\pi^{3/4}a^{3/2}} e^{-r^2/2a^2} \tag{4.7}$$

where $a \equiv \sqrt{\hbar/m\omega}$. The associated energy is $E = \frac{3}{2}\hbar\omega$ for each particle.

4.2 The Gross-Pitaevskii equation

The calculation in the previous section is, however, not entirely correct. This is because (4.6) and also the rest of the calculations in the previous section, assumed no interaction between the individual particles in the BEC. In fact the particles will interact electromagnetically, which means that the interaction between two particles i and j should be written $H_{\text{int}} = U(\mathbf{r}_i - \mathbf{r}_j)$.

Let us try to relate this U-function to the better known scattering length denoted a, by considering the scattering of one particle from another. In the first part of this section, we use the assumption that $\omega = 0$ so the particles can move freely. An incoming particle will have a wave function $\varphi(\mathbf{r}) \propto e^{-i\mathbf{k}\cdot\mathbf{r}}$, and under the assumption of so-called s-wave scattering, which means that the outgoing wave-function will be angular dependent, the outgoing wave function will have the form $\zeta(\mathbf{r}) \propto \left(e^{-i\mathbf{k}\cdot\mathbf{r}} + f(\theta,\phi)e^{-ikr}/r\right)$ seen far away from the position of the target particle. For s-wave scattering the definition of a is $a \equiv -f$.

ζ_i for the ith particle is a solution to

$$H_0\zeta_i + \sum_j U_{ij}\zeta_j = E\zeta_i \tag{4.8}$$

where H_0 is short for the operator $-\frac{\hbar^2}{2m}\nabla_i^2 + \frac{1}{2}m\omega^2 r_i^2$. In terms of continuous functions, this becomes $H_0\zeta(\mathbf{r}) + \int \mathrm{d}\mathbf{r}' U(\mathbf{r},\mathbf{r}')\zeta(\mathbf{r}') = E\zeta(\mathbf{r})$ from which we can see that a formal solution for ζ is

$$\zeta(\mathbf{r}) = \varphi(\mathbf{r}) + \int \mathrm{d}\mathbf{r}' \int \mathrm{d}\mathbf{r}'' G(\mathbf{r},\mathbf{r}')U(\mathbf{r}',\mathbf{r}'')\zeta(\mathbf{r}'') \tag{4.9}$$

where $G(\mathbf{r},\mathbf{r}')$ is the Greens function to the operator $(E - H_0)$ with the property $(E - H_0)G(\mathbf{r},\mathbf{r}') = \delta(\mathbf{r} - \mathbf{r}')$ defining for Greens functions. The reason for the φ in (4.9) is that we want $\zeta \to \varphi$ for $U \to 0$. The[6] Greens function can be found[7] to be

$$G(\mathbf{r},\mathbf{r}') = -\frac{2m}{\hbar^2}\frac{1}{4\pi}\frac{e^{ik|\mathbf{r}-\mathbf{r}'|}}{|\mathbf{r}-\mathbf{r}'|} \tag{4.10}$$

[5] See [b].

[6] The solution found here is not THE solution, but a solution known as the retarded Greens function G_R. It corresponds to a ζ being a spherical wave leaving the target particle. Another solution to the same equation is the advanced Greens function G_A corresponding to a spherical wave hitting the target particle at the moment of impact. This is unphysical since it violates causality, so this solution is discarded.

[7] See [b].

Far away from the target particle we have $\mathbf{r} \gg \mathbf{r}'$, so there we can calculate $|\mathbf{r}-\mathbf{r}'| \approx \sqrt{r^2 - 2\mathbf{r}\cdot\mathbf{r}'} \approx r + \frac{\mathbf{r}}{r}\cdot\mathbf{r}'$ which means that $e^{ik|\mathbf{r}-\mathbf{r}'|} \approx e^{ikr}e^{-i\mathbf{k}'\cdot\mathbf{r}'}$ where $\mathbf{k}' \equiv \frac{k\mathbf{r}}{r}$. This allows us to identify

$$f = -\frac{2m}{\hbar^2}\frac{1}{4\pi}\int \mathrm{d}\mathbf{r}' \int \mathrm{d}\mathbf{r}'' e^{-i\mathbf{k}'\cdot\mathbf{r}'} U(\mathbf{r}', \mathbf{r}'')\zeta(\mathbf{r}'') \tag{4.11}$$

If we consider a contact potential with the target particle placed in the origin, we get $U(\mathbf{r}, \mathbf{r}') = U_0\delta(\mathbf{r} - \mathbf{r}')\delta(\mathbf{r})$. Applying the so-called Born approximation[8] which consists of replacing ζ inside the integral with $\varphi \propto e^{i\mathbf{k}\cdot\mathbf{r}''}$, gives the result $f = -\frac{2m}{\hbar^2}\frac{1}{4\pi}U_0$. This is seen in a frame where the target particle is in $\mathbf{r} = 0$, and stays there after the collision. But due to momentum conservation this can not be the case for identical particles. In that case we need to look in the center-of-mass frame where the mass appearing in the formula above is the reduced mass $m_r = m_1m_2/(m_1 + m_2)$, which reduces to $m_r = m/2$ if the two masses are equal, as they are in our case. This gives us the final relation between U_0 and the scattering length:

$$U_0 = \frac{4\pi\hbar^2 a}{m} \tag{4.12}$$

Reincluding the trap potential, the Hamiltonian for the total system becomes

$$\mathcal{H} = \sum_{i=1}^{N}\left(-\frac{\hbar^2}{2m}\nabla_i^2 + \frac{1}{2}m\omega^2 r_i^2 + U_0\sum_{j>i}\delta(\mathbf{r}_i - \mathbf{r}_j)\right) \tag{4.13}$$

and by taking the expectation value of (4.13), we can find[9] the average energy of the system to be

$$E = N\int \mathrm{d}\mathbf{r}\left(\frac{1}{2}|\nabla\varphi(\mathbf{r})|^2 + \frac{1}{2}\mathbf{r}^2|\varphi(\mathbf{r})|^2 + \frac{N-1}{2}U_0|\varphi(\mathbf{r})|^4\right) \tag{4.14}$$

where we have introduced the natural oscillator units which we will keep for the rest of the thesis. We wish to find the $\varphi(\mathbf{r})$ minimizing the energy, under the condition that the particle number N is kept constant. This can be done by minimizing the quantity $E - \mu N$ instead of E. This additional term can be introduced in (4.14) by including the term $-\mu|\varphi(\mathbf{r})|^2$ as part of the integrand in 4.14. In order to do the minimization, variational calculus is used. The 'central theorem' of variational calculus is

$$\delta\int f\big(x(t), \dot{x}(t)\big)\mathrm{d}t = 0 \Leftrightarrow \frac{\partial f}{\partial x} = \frac{d}{dt}\frac{\partial f}{\partial \dot{x}} \tag{4.15}$$

[8]This is the first order Born approximation. One can make a second order Born approximation by replacing ζ inside the integral with the result of the first order approximation, etc. See [b].

[9]Here, partial integration on the ∇^2-term is used, along with the assumption that $r \to \infty \Rightarrow \varphi(\mathbf{r}) \to 0$, a reasonable assumption given the shape of the potential. That is $\int_{-\infty}^{\infty}\varphi^*\nabla^2\varphi = -\int_{-\infty}^{\infty}|\nabla\varphi|^2$.

where $\dot{x} \equiv dx/dt$, and δ denotes a small variation. If we let $\mathbf{r}$ play the role as t, and $\varphi^*(\mathbf{r})$ play the role as $x(t)$, (4.15) and the modified (4.14) will give the Gross-Pitaevskii equation (in the following known as the GPE)

$$-\frac{1}{2}\nabla^2\psi(\mathbf{r}) + \frac{1}{2}\mathbf{r}^2\psi(\mathbf{r}) + U_0|\psi(\mathbf{r})|^2\psi(\mathbf{r}) = \mu\psi(\mathbf{r}) \tag{4.16}$$

where $N \gg 1$ is assumed and $\psi(\mathbf{r}) \equiv \sqrt{N}\varphi(\mathbf{r})$, indicating that ψ is a many-body wave function since it normalizes to N instead of to 1. With this latest definition $|\psi(\mathbf{r})|^2$ is the particle density of the condensate.

Going from (4.14) to second quantization[10], the Hamiltonian becomes

$$\hat{\mathcal{H}} = \int \mathrm{d}\mathbf{r}\left(-\hat{\Psi}^\dagger(\mathbf{r})\frac{1}{2}\nabla^2\hat{\Psi}(\mathbf{r}) + \frac{1}{2}r^2\hat{\Psi}^\dagger(\mathbf{r})\hat{\Psi}(\mathbf{r}) + \frac{U_0}{2}\hat{\Psi}^\dagger(\mathbf{r})\hat{\Psi}^\dagger(\mathbf{r})\hat{\Psi}(\mathbf{r})\hat{\Psi}(\mathbf{r})\right) \tag{4.17}$$

where the ∇^2-term has been reinserted. This Hamiltonian is known as the Gross-Pitaevskii (or GP) Hamiltonian, and it is essential to the following calculations. In order to find a time-dependent version of the GPE, we calculate the quantity $i\frac{\partial\hat{\Psi}}{\partial t}$ using the Heisenberg equation, with the result

$$i\frac{\partial\hat{\Psi}(\mathbf{r}')}{\partial t} = -\frac{1}{2}\nabla^2\hat{\Psi}(\mathbf{r}') + \frac{1}{2}r^2\hat{\Psi}(\mathbf{r}') + U_0\hat{\Psi}^\dagger(\mathbf{r}')\hat{\Psi}(\mathbf{r}')\hat{\Psi}(\mathbf{r}') \tag{4.18}$$

Going back to first quantization gives

$$i\frac{\partial\psi(\mathbf{r})}{\partial t} = -\frac{1}{2}\nabla^2\psi(\mathbf{r}) + \frac{1}{2}r^2\psi(\mathbf{r}) + U_0|\psi(\mathbf{r})|^2\psi(\mathbf{r}) \tag{4.19}$$

which is known as the time-dependent Gross-Pitaevskii equation.

4.3 Solutions to the Gross-Pitaevskii equation

The GPE (4.16) is a nonlinear differential equation and it has no general analytical solution. There are, however, ways to find approximate analytical solutions. In the absence of any interaction, ψ is given by (4.7)

$$\psi(\mathbf{r}) = \frac{\sqrt{N}}{\pi^{3/4}a^{3/2}}e^{-r^2/2a^2} \tag{4.20}$$

where $a = 1$ in NOU. An ansatz to finding our analytical solution could be to assume a solution of the same Gaussian form, but now with the width a replaced by another width a' minimizing the energy (4.14). This approach is denoted the Gaussian approximation[11]. The energy can be calculated to

$$E = \frac{3}{2}N\left(\frac{1}{a'^2} + a'^2\right) + \frac{N^2U_0}{2(2\pi)^{3/2}a'^3} \tag{4.21}$$

[10] See appendix A.
[11] See [a] p. 165 ff.

which is minimized by an a' that is a solution to

$$a'^5 - a' - \frac{NU_0}{(2\pi)^{\frac{3}{2}}} = 0 \tag{4.22}$$

When NU_0 is small compared to one, an approximate solution is

$$a' = 1 + \frac{NU_0}{4(2\pi)^{\frac{3}{2}}} \tag{4.23}$$

and when NU_0 is large compared to one, an approximate solution is

$$a' = \sqrt[5]{\frac{NU_0}{(2\pi)^{\frac{3}{2}}}} \tag{4.24}$$

Plots of these results can be seen in fig. 4.1.

We see from (4.21) that if U_0 is negative, corresponding to a negative scattering length, the energy will have a negative singularity in $a' = 0$. This means that the condensate eventually will collapse into a point[12]. Therefore we will only regard positive values of U_0 in this thesis.

Another convenient approximation known as the Thomas-Fermi approximation consists of neglecting the kinetic term in (4.16) giving

$$|\psi(\mathbf{r})|^2 = \frac{\mu - \frac{1}{2}r^2}{U_0} \tag{4.25}$$

from $r = 0$ to $r = \sqrt{2\mu}$ and $\psi = 0$ elsewhere. From the normalization μ can be found to be

$$\mu = \left(\frac{15NU_0}{16\sqrt{2}\pi}\right)^{2/5} \tag{4.26}$$

If we want to find a more precise result, it must be done numerically. Imagine that we want to find the lowest energy state for an equation similar to the time dependent Schrödinger equation

$$i\frac{\partial\psi(\mathbf{r},t)}{\partial t} = \hat{O}(\mathbf{r})\psi(\mathbf{r},t) \tag{4.27}$$

where $\hat{O}(\mathbf{r})$ is some linear operator. This can be done by making the variable shift $\tau \equiv it$ so the equation becomes[13]

$$\frac{\partial\psi(\mathbf{r},\tau)}{\partial\tau} = -\hat{O}(\mathbf{r})\psi(\mathbf{r},\tau) \tag{4.28}$$

[12]For some slightly negative values of U_0, we can calculate from (4.21) that $E(a')$ has a local minimum different from $a' = 0$ where a metastable condensate can exist. This point has $a' \approx -0.079 \cdot NU_0$ and it will only exist for $NU_0 \gtrsim -8.426$.

[13]If $\hat{O} = -\nabla^2$ as it is for the Schrödinger equation for a free particle, the equation becomes equivalent to Fick's second law, the diffusion equation.

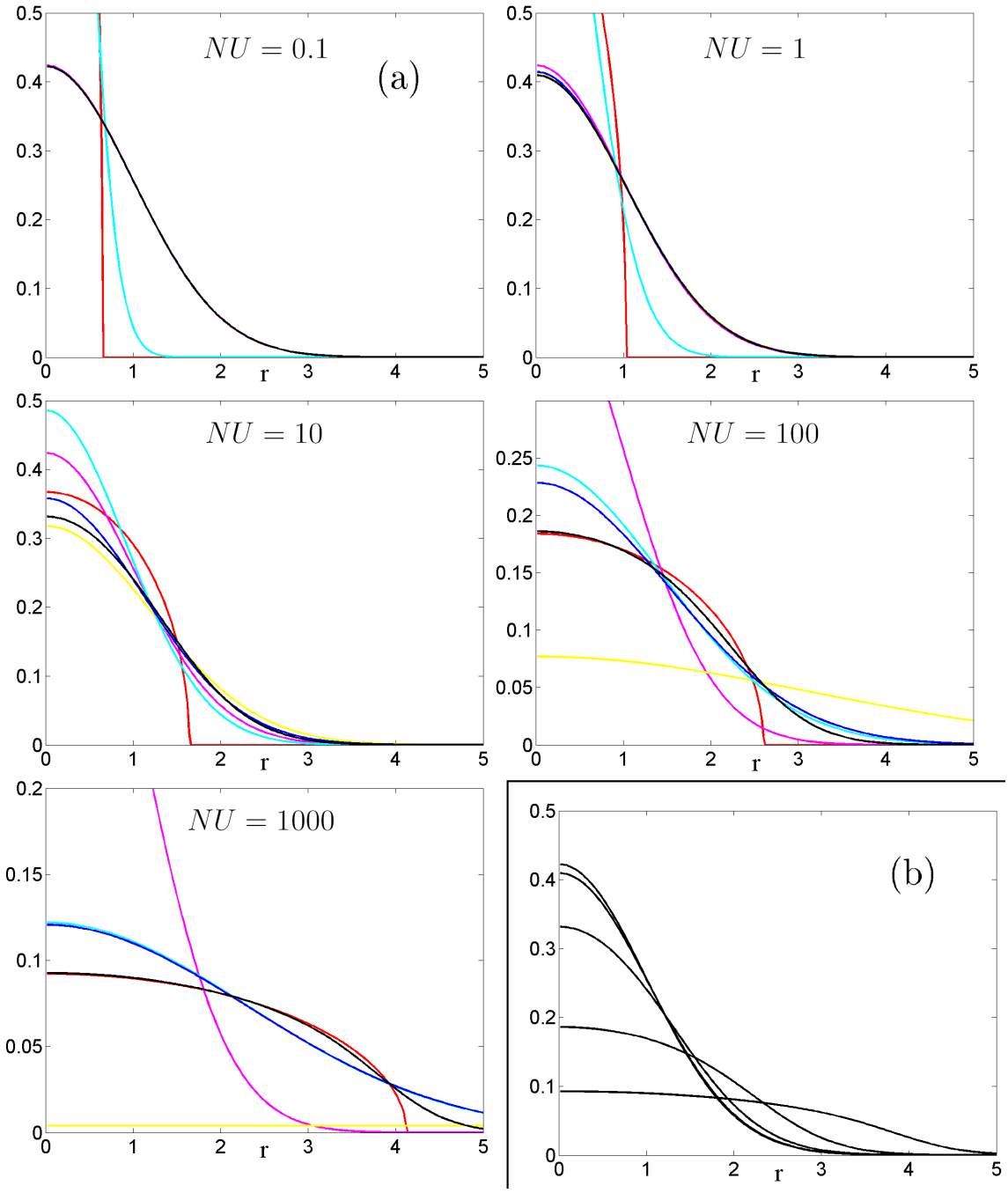

Figure 4.1: The five graphs in (a) show the exact and the approximated solutions to the GPE for various values of NU_0. The black curve is the exact result found using the imaginary time algorithm. The Blue curve is the result of the Gaussian approximation (4.20), and the yellow and cyan curves are the Gaussian approximation in the limits of small and large NU_0 respectively. The red curve is the result of the Thomas-Fermi approximation (4.25), and the pink curve is the result in absence of interaction given by (4.7). (b) shows the exact result for the five values of NU_0, the curves correspond to $NU_0 = 0.1$, 1, 10, 100, and 1000 from above near $r = 0$.

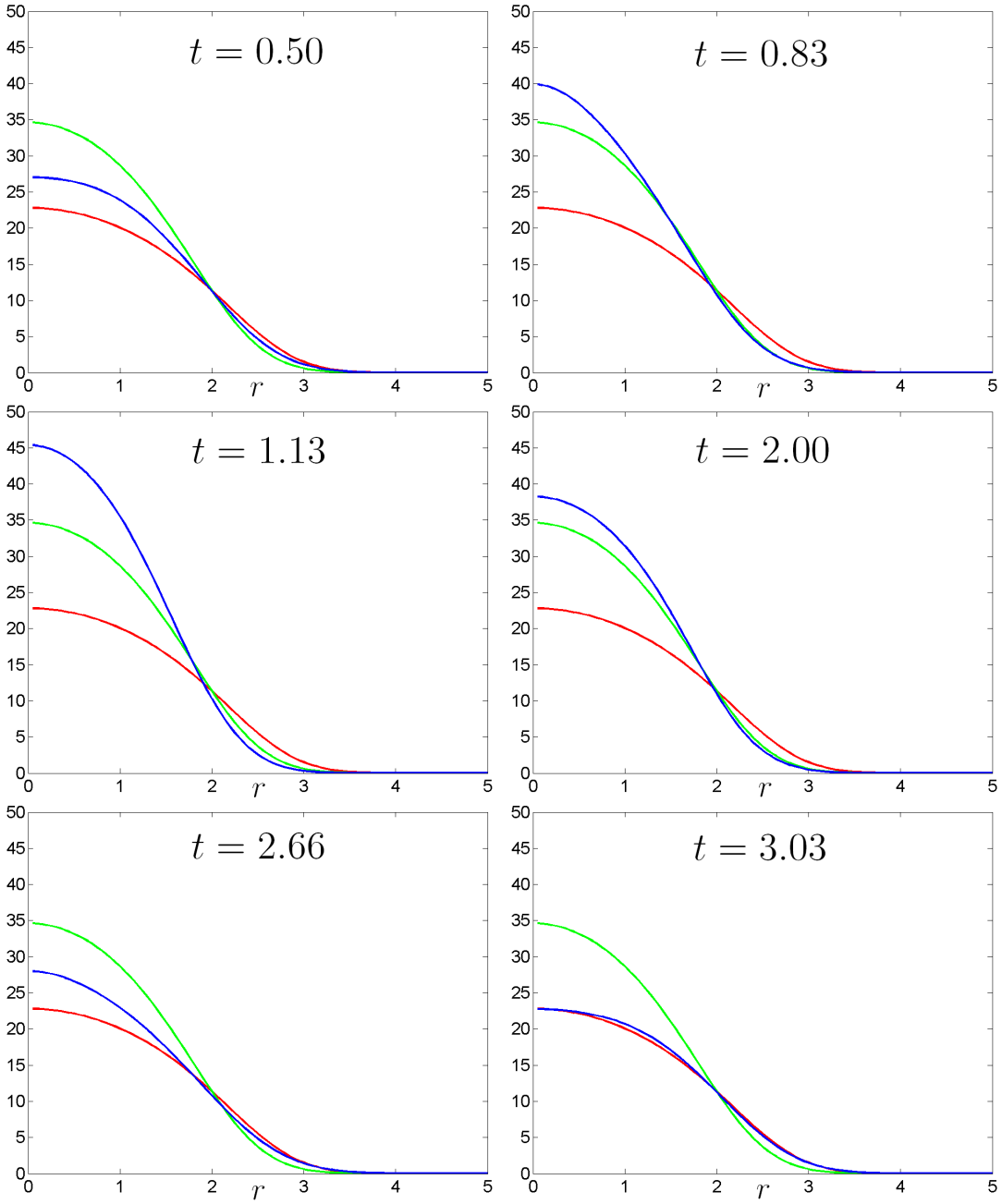

Figure 4.2: This plot shows the time evolution of the particle density for $N = 1000$ atoms and an interaction $U_0 = 0.1$, when the initial state is not an eigenstate to the GPE. In this case the initial state is the steady state wave function for $U_0 = 0.2$ found using the imaginary time-formalism, and plotted as the red curves. The blue curves show the result at different times, found by solving the time-dependent GPE. The steady-state result for $U_0 = 0.1$ is plotted as the green curves, and we see that the temporal behaviour of ψ is oscillations around that state. $t = 1.13$ is the point of maximal compression, and at $t = 3.03$ the oscillation has returned to its initial value, that of minimal compression.

ψ can be expanded into Fourier-components as $\psi(\mathbf{r}) = \sum_j k_j \psi_j(\mathbf{r})$ where the k_js are some constants, and the ψ_j-functions are a complete set of eigenfunctions to the operator $\hat{O}(\mathbf{r})$. From this we get the time evolution of ψ to be

$$\begin{aligned} \psi(\mathbf{r},t) &= e^{-i\hat{O}} \sum_j k_j \psi_j(\mathbf{r}) = \sum_j k_j e^{-i\omega_j t} \psi_j(\mathbf{r}) \;\rightarrow \\ \psi(\mathbf{r},\tau) &= \sum_j k_j e^{-\omega_j \tau} \psi_j(\mathbf{r}) \end{aligned} \tag{4.29}$$

where the ω_js are the eigenvalues corresponding to the ψ_j eigenfunctions. We see that in the limit $\tau \rightarrow \infty$ we get $\psi(\mathbf{r}) \propto \psi_0(\mathbf{r})$ since the term $e^{-\omega_0 \tau}$ decreases the slowest with τ. The limit can be taken by solving (4.28) numerically for an imaginary time long enough so that $e^{-(\omega_0 - \omega_1)\tau} \gg 1$.

The time dependent GPE is, however, not on the form (4.28), because of the cubic term $U_0|\psi(\mathbf{r})|^2\psi(\mathbf{r})$. But fortunately it turns out that the described method still works with a nonlinear term included, so this is the method that is used throughout this thesis for numerical determination of $\psi(\mathbf{r})$.

Finally, let us have a look at the behaviour of μ. Given an expression for ψ, μ can be found using the GPE (4.16), by multiplying both sides with ψ^* and integrating over $\mathbf{r}$. In the Gaussian approximation we find μ to be

$$\mu = \frac{3}{2a'^2} + \frac{3}{4}\left(a'^2 - \frac{1}{a'^2}\right) + \frac{NU_0}{(2\pi)^{\frac{2}{3}} a'^3} \tag{4.30}$$

where a' is given by the solution to (4.22), but simpler results can be obtained by using the approximations (4.23)[14] or (4.24). For the Thomas Fermi approximation the result is given by (4.26).

4.4 The two-species case

The atoms forming the clockwork of the atomic clock mentioned in chapter 2, need two internal states in order for the proposed clock-scheme to function. While these states in the experimental setting are two weakly exited states of the outermost electron of the atoms, the theory describes them as the spin-up and spin-down states of a spin-half particle[15]. The spin-squeezing in the headline of the thesis refers to this abstract spin. The second quantization Hamiltonian for a condensate

[14] In this limit the result turns out to be the same as we would get using the 'zeroth order' approximation $a' = 1$ namely $\mu = \frac{3}{2} + \frac{NU_0}{(2\pi)^{\frac{2}{3}}}$.

[15] This makes the theory in this thesis a theory about spin-$\frac{1}{2}$ bosons. This would of course have been impossible if the spin in question was a physical spin, and not this abstract spin.

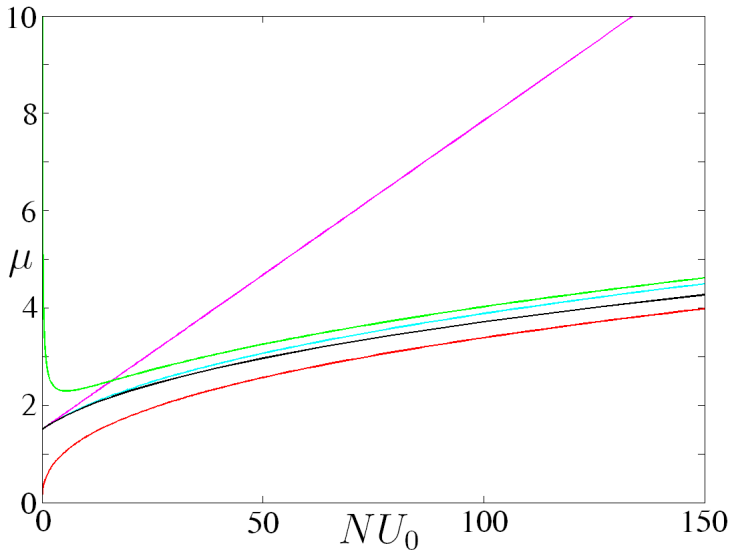

Figure 4.3: These graphs show μ as a function of NU_0. Black is the exact result, blue is the Gaussian approximation, magenta and green are the Gaussian approximation in the limits of small and large NU_0, and red is the result of the Thomas-Fermi approximation.

composed of particles of these two species, denoted a and b will be[16]

$$\begin{aligned}\hat{\mathcal{H}} &= \int \mathrm{d}\mathbf{r}\Big(\hat{\Psi}_a^\dagger(\mathbf{r})H_{0,a}\hat{\Psi}_a(\mathbf{r}) + \hat{\Psi}_b^\dagger(\mathbf{r})H_{0,b}\hat{\Psi}_b(\mathbf{r}) \\ &\quad + \frac{U_{aa}}{2}\hat{\Psi}_a^\dagger(\mathbf{r})\hat{\Psi}_a^\dagger(\mathbf{r})\hat{\Psi}_a(\mathbf{r})\hat{\Psi}_a(\mathbf{r}) + \frac{U_{bb}}{2}\hat{\Psi}_b^\dagger(\mathbf{r})\hat{\Psi}_b^\dagger(\mathbf{r})\hat{\Psi}_b(\mathbf{r})\hat{\Psi}_b(\mathbf{r}) \\ &\quad + U_{ab}\hat{\Psi}_a^\dagger(\mathbf{r})\hat{\Psi}_b^\dagger(\mathbf{r})\hat{\Psi}_a(\mathbf{r})\hat{\Psi}_b(\mathbf{r}) + \frac{\Omega}{2}\left(\hat{\Psi}_a^\dagger(\mathbf{r})\hat{\Psi}_b(\mathbf{r}) + \hat{\Psi}_b^\dagger(\mathbf{r})\hat{\Psi}_a(\mathbf{r})\right)\Big) \end{aligned} \quad (4.31)$$

where

$$H_0 \equiv -\frac{1}{2}\nabla^2 + \frac{1}{2}r^2 \quad (4.32)$$

$\hat{\Psi}_a(\mathbf{r})$ and $\hat{\Psi}_b(\mathbf{r})$ are the quantum field operators for the a and b-particles respectively, while U_{ij} is the U_0-constant for interactions between particles of type i and j. The major difference between (4.31) and the corresponding one-species Hamiltonian (4.17) is the Ω-term caused by interactions with an external field, which requires some extra explanation. The interaction Hamiltonian for an atom in a (classical) electrical field is $H_{int} = -\hat{\boldsymbol{d}} \cdot \boldsymbol{E}$, where $\hat{\boldsymbol{d}}$ is the dipole moment operator. Since $\langle a|\hat{\boldsymbol{d}}|a\rangle = \langle b|\hat{\boldsymbol{d}}|b\rangle = 0$, the dipole moment operator can be written $\hat{\boldsymbol{d}} = \boldsymbol{d}|a\rangle\langle b| + \boldsymbol{d}|b\rangle\langle a|$, where $\boldsymbol{d}$ is real. This means that H_{int} can be written

[16]This assumes that the two particle types do not differ with respect to the constants m or ω, since otherwise the rescaling (see (1.5)) cannot be done consistently, and (4.31) can not be written as it is. Later we will assume that $H_{0,a} = H_{0,b}$ which will solve this problem.

$H_{int} = (\Omega/2)(|a\rangle\langle b| + |b\rangle\langle a|) = (\Omega/2)\sigma_x = \Omega\hat{j}_x$ where $\Omega \equiv -2\boldsymbol{d}\cdot\boldsymbol{E}$ is denoted the Rabi frequency. When many atoms are present, we sum over them, giving $H_{int} = \Omega\hat{J}_x$. In second quantization this becomes

$$H_{int} = \frac{\Omega}{2}\left(\hat{\Psi}_a^\dagger(\mathbf{r})\hat{\Psi}_b(\mathbf{r}) + \hat{\Psi}_b^\dagger(\mathbf{r})\hat{\Psi}_a(\mathbf{r})\right) \tag{4.33}$$

which is the term in question in (4.31).

In the following we will assume that $H_{0,a} = H_{0,b} \equiv H_0$ and $U_{aa} = U_{bb} \equiv U$, that is, the two types of particles act identically[17]. If we insert this, (4.31) becomes

$$\begin{aligned}\hat{\mathcal{H}} &= \int \mathrm{d}\mathbf{r}\Bigg(\hat{\Psi}_a^\dagger(\mathbf{r})H_0\hat{\Psi}_a(\mathbf{r}) + \hat{\Psi}_b^\dagger(\mathbf{r})H_0\hat{\Psi}_b(\mathbf{r}) \\ &\quad + \frac{U}{2}\left(\hat{\Psi}_a^\dagger(\mathbf{r})\hat{\Psi}_a^\dagger(\mathbf{r})\hat{\Psi}_a(\mathbf{r})\hat{\Psi}_a(\mathbf{r}) + \hat{\Psi}_b^\dagger(\mathbf{r})\hat{\Psi}_b^\dagger(\mathbf{r})\hat{\Psi}_b(\mathbf{r})\hat{\Psi}_b(\mathbf{r})\right) \\ &\quad + U_{ab}\hat{\Psi}_a^\dagger(\mathbf{r})\hat{\Psi}_b^\dagger(\mathbf{r})\hat{\Psi}_a(\mathbf{r})\hat{\Psi}_b(\mathbf{r}) + \frac{\Omega}{2}\left(\hat{\Psi}_a^\dagger(\mathbf{r})\hat{\Psi}_b(\mathbf{r}) + \hat{\Psi}_b^\dagger(\mathbf{r})\hat{\Psi}_a(\mathbf{r})\right)\Bigg)\end{aligned} \tag{4.34}$$

which is the form of the GP-Hamiltonian we will use the most in the following calculations.

It is possible to calculate a Gross-Pitaevskii-like equation for the two species case as well. This can be done by converting (4.34) back to a first quantization energy expression, by replacing $\hat{\Psi}_a(\mathbf{r}) \to \psi_a(\mathbf{r})$ and $\hat{\Psi}_b(\mathbf{r}) \to \psi_b(\mathbf{r})$. Like we did when deriving the GPE, we use variational calculus to minimize[18] $E - \mu N$, with respect to the variables ψ_a^* and ψ_b^*. This results in the two-species GPE

$$H_0\psi_a(\mathbf{r}) + U|\psi_a(\mathbf{r})|^2\psi_a(\mathbf{r}) + U_{ab}|\psi_b(\mathbf{r})|^2\psi_a(\mathbf{r}) + \frac{\Omega}{2}\psi_b(\mathbf{r}) = \mu\psi_a(\mathbf{r}) \tag{4.35}$$

and a similar one with ψ_a and ψ_b interchanged.

[17] As we will see from (5.6), this ensures an absence of a $\hat{J}_z$-term in the expression for H, which keeps the Bloch-sphere from rotating.

[18] If no Ω-term had been present, N_a and N_b would be conserved individually, making two chemical potentials necessary.

Chapter 5

Spin-squeezing in Bose-Einstein condensates

In this chapter we are going to relate the theory on BEC to our efforts on minimizing the spin-squeezing, by showing how the former can be used as a tool for the latter. Even though other methods to produce spin-squeezing are available, like the quantum non-demolition measurement method described in [16], this thesis will only consider spin-squeezing using BEC. In the end we are going to calculate the spin-squeezing using a Bogoliubov method, but let us first show how spin-squeezing and BEC are related by doing the more simple two-mode approximation.

5.1 The two-mode approximation

In general a second quantization operator $\hat{\Psi}(\mathbf{r})$ can be written

$$\hat{\Psi}(\mathbf{r}) = \sum_i \hat{a}_i \varphi_i(\mathbf{r}) \tag{5.1}$$

If we assume that the vast majority of particles are placed in the lowest energy state as is the case for the BEC[1], we can do the single-mode approximation $\hat{\Psi}(\mathbf{r}) = \sum_i \hat{a}_i \varphi_i(\mathbf{r}) \approx \hat{a}_0 \varphi_0(\mathbf{r})$. When this is done for both $\hat{\Psi}_a(\mathbf{r})$ and $\hat{\Psi}_b(\mathbf{r})$ in (4.34) it is known as the two-mode approximation. If $U \geq U_{ab}$ the lowest energy state is one where the two species will mix, so in that case we see that if Ω is large and negative, the energy will be minimized if $\varphi_a \approx \varphi_b$. Inserting the two-mode approximation and $\varphi_a(\mathbf{r}) = \varphi_b(\mathbf{r}) \equiv \varphi(\mathbf{r})$ in (4.34) gives

$$\begin{aligned} \hat{\mathcal{H}} &= E\left(\hat{a}^\dagger \hat{a} + \hat{b}^\dagger \hat{b}\right) + \frac{U}{2}|\varphi|^4 \left(\hat{a}^\dagger \hat{a}^\dagger \hat{a}\hat{a} + \hat{b}^\dagger \hat{b}^\dagger \hat{b}\hat{b}\right) \\ &\quad + U_{ab}|\varphi|^4 \left(\hat{a}^\dagger \hat{b}^\dagger \hat{a}\hat{b}\right) + \frac{\Omega}{2}\left(\hat{a}^\dagger \hat{b} + \hat{b}^\dagger \hat{a}\right) \end{aligned} \tag{5.2}$$

[1] The discussion in connection with (4.4) indicates that all particles are in the lowest energy state at zero temperature. Later calculations show this to be not absolutely true due to the U and U_{ab}-terms.

where

$$E \equiv \int \mathrm{d}\mathbf{r}\varphi^*(\mathbf{r})H_0\varphi(\mathbf{r}) \quad \text{and} \quad |\varphi|^4 \equiv \int \mathrm{d}\mathbf{r}\varphi^*(\mathbf{r})\varphi^*(\mathbf{r})\varphi(\mathbf{r})\varphi(\mathbf{r}) \tag{5.3}$$

If on the other hand we had chosen the ferromagnetic regime $U < U_{ab}$, the lowest energy state will be one where the two atomic species are physically separate[2], so in that case this two-mode approximation will break down. This thesis will only consider the antiferromagnetic regime where $U \geq U_{ab}$.

In order to relate this to the discussion of squeezing, we must use the $\hat{J}$-operators expressed in second quantization, where they are given as[3]

$$\begin{aligned}
\hat{J}_x &= \frac{1}{2}\int \mathrm{d}\mathbf{r}\left(\hat{\Psi}_a^\dagger(\mathbf{r})\hat{\Psi}_b(\mathbf{r}) + \hat{\Psi}_b^\dagger(\mathbf{r})\hat{\Psi}_a(\mathbf{r})\right) \\
\hat{J}_y &= \frac{i}{2}\int \mathrm{d}\mathbf{r}\left(\hat{\Psi}_b^\dagger(\mathbf{r})\hat{\Psi}_a(\mathbf{r}) - \hat{\Psi}_a^\dagger(\mathbf{r})\hat{\Psi}_b(\mathbf{r})\right) \\
\hat{J}_z &= \frac{1}{2}\int \mathrm{d}\mathbf{r}\left(\hat{\Psi}_a^\dagger(\mathbf{r})\hat{\Psi}_a(\mathbf{r}) - \hat{\Psi}_b^\dagger(\mathbf{r})\hat{\Psi}_b(\mathbf{r})\right) \\
\hat{N} &= \int \mathrm{d}\mathbf{r}\left(\hat{\Psi}_a^\dagger(\mathbf{r})\hat{\Psi}_a(\mathbf{r}) + \hat{\Psi}_b^\dagger(\mathbf{r})\hat{\Psi}_b(\mathbf{r})\right)
\end{aligned} \tag{5.4}$$

which after applying the same two-mode approximation becomes

$$\begin{aligned}
\hat{N} = \left(\hat{a}^\dagger\hat{a} + \hat{b}^\dagger\hat{b}\right) \ , \quad \hat{J}_z = \tfrac{1}{2}\left(\hat{a}^\dagger\hat{a} - \hat{b}^\dagger\hat{b}\right) \ , \quad \hat{J}_x = \tfrac{1}{2}\left(\hat{a}^\dagger\hat{b} + \hat{b}^\dagger\hat{a}\right) \ , \\
\hat{N}^2 = \left(\hat{a}^\dagger\hat{a}\hat{a}^\dagger\hat{a} + \hat{b}^\dagger\hat{b}\hat{b}^\dagger\hat{b} + 2\hat{a}^\dagger\hat{a}\hat{b}^\dagger\hat{b}\right) \ , \quad \hat{J}_z^2 = \tfrac{1}{4}\left(\hat{a}^\dagger\hat{a}\hat{a}^\dagger\hat{a} + \hat{b}^\dagger\hat{b}\hat{b}^\dagger\hat{b} - 2\hat{a}^\dagger\hat{a}\hat{b}^\dagger\hat{b}\right)
\end{aligned} \tag{5.5}$$

where only the combinations relevant for this discussion are listed.

Inserting this into (5.2) gives[4]

$$\hat{\mathcal{H}} = \alpha\hat{N} + \beta\hat{N}^2 + \chi\hat{J}_z^2 + \Omega\hat{J}_x \tag{5.6}$$

where

$$\alpha \equiv E - \frac{U}{2}|\varphi|^4 \ , \quad \beta \equiv \frac{U + U_{ab}}{4}|\varphi|^4 \ , \quad \chi \equiv (U - U_{ab})|\varphi|^4 \ , \quad \Omega \equiv \Omega \tag{5.7}$$

Since the particle number is conserved[5], the $\hat{N}$- and the $\hat{N}^2$-terms will always give the same contributions to the energy independent of the state. This means that the essential part of the Hamiltonian is

$$\hat{\mathcal{H}} = \chi\hat{J}_z^2 + \Omega\hat{J}_x \tag{5.8}$$

[2] At least in the absence of Ω.

[3] See appendix B.

[4] If we had kept $U_{aa} \neq U_{bb}$ and $H_{0a} \neq H_{0b}$ there would also have been a $\hat{J}_z$ and a $\hat{N}\hat{J}_z$-term with coefficients $E_a - E_b - \frac{1}{2}(U_{aa} - U_{ab})|\psi|^4$ and $\frac{1}{2}(U_{aa} - U_{bb})|\psi|^4$ respectively.

[5] We assume this to be true physically, but now we can see it mathematically as well from the fact that $\hat{N}$ commutes with $\hat{\mathcal{H}}$.

which is proportional to the operator $\hat{M}$ from given by (3.33) with $\lambda = -\Omega/\chi$. This means that the ground state of (5.8) will be the state minimizing the squeezing parameter ξ_{J_z} for a given value of $\langle \hat{J}_x \rangle$, which can be regulated by changing Ω.

As mentioned in the section on the F-functions, it is not surprising that the ground state of 5.6 is squeezed, when Ω is large and negative. The $\hat{J}_z^2$-term is minimized by states on the equator of the Bloch sphere, and the $\hat{J}_x$-term is minimized by states like the coherent spin-state (3.24) close to the x-pole of the Bloch sphere. A compromise is a state elongated in the y-direction but still localized around $\langle \hat{J}_x \rangle = j$, and that is exactly a state squeezed in the z-direction, see fig. 3.5.

At this point it should be clear why BEC is interesting in the context of spin-squeezing.

5.2 The plus-minus basis

We see from the previous section that if $-\Omega \gg |\chi|$, the state minimizing the energy approaches an eigenstate to $\hat{J}_x$, and therefore it has $\psi_a \approx \psi_b$. In the following we are going to do perturbations around this state, so that motivates us to do a change of basis, and express (4.34) in terms of the new field operators

$$\hat{\Psi}_+ \equiv \frac{\hat{\Psi}_a + \hat{\Psi}_b}{\sqrt{2}} \quad , \quad \hat{\Psi}_- \equiv \frac{\hat{\Psi}_a - \hat{\Psi}_b}{\sqrt{2}} \tag{5.9}$$

which can be inverted to

$$\hat{\Psi}_a = \frac{\hat{\Psi}_+ + \hat{\Psi}_-}{\sqrt{2}} \quad , \quad \hat{\Psi}_b = \frac{\hat{\Psi}_+ - \hat{\Psi}_-}{\sqrt{2}} \tag{5.10}$$

We see that the SCS in the x-direction will have all the particles in the plus-mode.

Substituting the $\hat{\Psi}_\pm$-operators into (4.34) gives

$$\begin{aligned}
\hat{\mathcal{H}} \;=\; & \int \mathrm{d}\mathbf{r} \Big(\hat{\Psi}_+^\dagger(\mathbf{r}) H_0 \hat{\Psi}_+(\mathbf{r}) + \hat{\Psi}_-^\dagger(\mathbf{r}) H_0 \hat{\Psi}_-(\mathbf{r}) + U \left(\hat{\Psi}_+^\dagger(\mathbf{r}) \hat{\Psi}_-^\dagger(\mathbf{r}) \hat{\Psi}_+(\mathbf{r}) \hat{\Psi}_-(\mathbf{r}) \right) \\
& + \frac{U + U_{ab}}{4} \left(\hat{\Psi}_+^\dagger(\mathbf{r}) \hat{\Psi}_+^\dagger(\mathbf{r}) \hat{\Psi}_+(\mathbf{r}) \hat{\Psi}_+(\mathbf{r}) + \hat{\Psi}_-^\dagger(\mathbf{r}) \hat{\Psi}_-^\dagger(\mathbf{r}) \hat{\Psi}_-(\mathbf{r}) \hat{\Psi}_-(\mathbf{r}) \right) \\
& + \frac{U - U_{ab}}{4} \left(\hat{\Psi}_+^\dagger(\mathbf{r}) \hat{\Psi}_+^\dagger(\mathbf{r}) \hat{\Psi}_-(\mathbf{r}) \hat{\Psi}_-(\mathbf{r}) + \hat{\Psi}_-^\dagger(\mathbf{r}) \hat{\Psi}_-^\dagger(\mathbf{r}) \hat{\Psi}_+(\mathbf{r}) \hat{\Psi}_+(\mathbf{r}) \right) \\
& + \frac{\Omega}{2} \left(\hat{\Psi}_+^\dagger(\mathbf{r}) \hat{\Psi}_+(\mathbf{r}) - \hat{\Psi}_-^\dagger(\mathbf{r}) \hat{\Psi}_-(\mathbf{r}) \right) \Big)
\end{aligned} \tag{5.11}$$

which is the form of the GP-Hamiltonian we will use most often in the following calculations.

Let us try to calculate a GPE in the plus-minus basis. We saw that $\psi_a \approx \psi_b$ in the mentioned limit, which corresponds to $\psi_+ \approx \psi$ and $\psi_- \approx 0$ in the new basis.

ψ is normalized to N, the total particle number. So when rewriting (5.11) back to first quantization, we should use $\hat{\Psi}_+ \to \psi$ and $\hat{\Psi}_- \to 0$, and then use variational calculus to minimize with respect to ψ^*. The result is

$$H_0\psi(\mathbf{r}) + \frac{U+U_{ab}}{2}|\psi(\mathbf{r})|^2\psi(\mathbf{r}) + \frac{\Omega}{2}\psi(\mathbf{r}) \;=\; \mu\psi(\mathbf{r}) \tag{5.12}$$

and we see that we could have had the same result by inserting $\psi_a = \psi_b = \frac{1}{\sqrt{2}}\psi$ into (4.35). This form of the two-species GPE is similar to the one-species case given by (4.16) with the substitutions $\frac{U+U_{ab}}{2} \to U_0$ and $\mu - \frac{\Omega}{2} \to \mu$, meaning that the results found in section 4.3 are valid for the two-species case as well after the above substitutions.

The angular momentum operators and the number operator can be expressed in the plus-minus basis as well, with the results

$$\begin{aligned}
\hat{J}_x &= \frac{1}{2}\int \mathrm{d}\mathbf{r}\left(\hat{\Psi}_+^\dagger(\mathbf{r})\hat{\Psi}_+(\mathbf{r}) - \hat{\Psi}_-^\dagger(\mathbf{r})\hat{\Psi}_-(\mathbf{r})\right)\\
\hat{J}_y &= \frac{i}{2}\int \mathrm{d}\mathbf{r}\left(\hat{\Psi}_+^\dagger(\mathbf{r})\hat{\Psi}_-(\mathbf{r}) - \hat{\Psi}_-^\dagger(\mathbf{r})\hat{\Psi}_+(\mathbf{r})\right)\\
\hat{J}_z &= \frac{1}{2}\int \mathrm{d}\mathbf{r}\left(\hat{\Psi}_+^\dagger(\mathbf{r})\hat{\Psi}_-(\mathbf{r}) + \hat{\Psi}_-^\dagger(\mathbf{r})\hat{\Psi}_+(\mathbf{r})\right)\\
\hat{N} &= \int \mathrm{d}\mathbf{r}\left(\hat{\Psi}_+^\dagger(\mathbf{r})\hat{\Psi}_+(\mathbf{r}) + \hat{\Psi}_-^\dagger(\mathbf{r})\hat{\Psi}_-(\mathbf{r})\right)
\end{aligned} \tag{5.13}$$

We see that the form of the $\hat{N}$-operator is unchanged by the basis shift, while the form of $\hat{J}_x$ and the $\hat{J}_z$-operators are interchanged. The $\hat{J}_y$-operator changes sign compared to the ab-basis.

5.3 Previous theoretical results

Let me at this point introduce some of the previous results on spin-squeezing and BEC. This section is by no means a full introduction to everything that has been done in the field, it will only touch the surface. All the articles described in this section uses Hamiltonians including a $\hat{J}_z^2$-term, but with no $\Omega\hat{J}_x$-term unlike the one used in the theory developed in this thesis.

A pioneering article in the field of spin-squeezing was [7] "Squeezed spin states" by Kitagawa and Ueda. The article discusses the effects of applying the Hamiltonian

$$\hat{H}_s \;\equiv\; \chi\hat{J}_z^2 \tag{5.14}$$

to the SCS to the $\hat{J}_x$-operator given by (3.24), followed by a rotation around the x-axis with an angle ν. Kitagawa and Ueda name this scheme "One-axis twisting" and the effect of $\hat{H}_s$ is plotted in fig. 5.2.

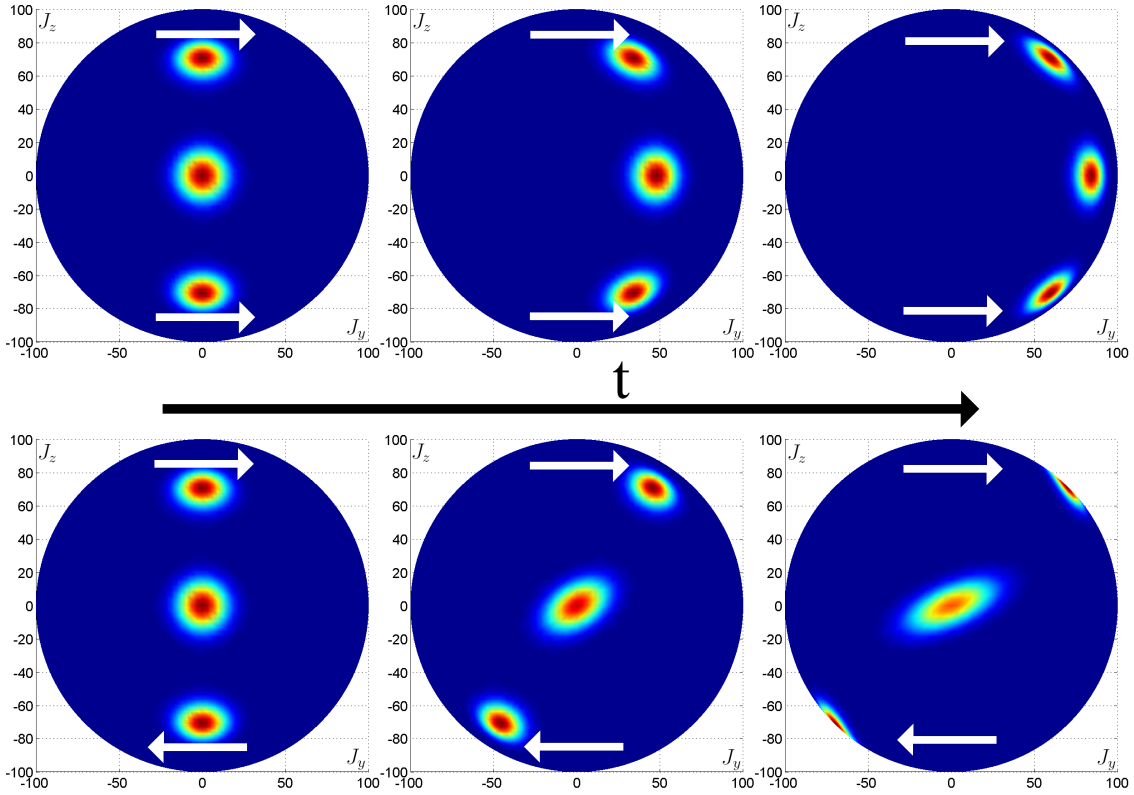

Figure 5.1: This figure explains the white arrows on the Bloch spheres in this chapter. The time evolution of the three angular momentum operators when applying the Hamiltonian $\mathcal{H}_\zeta \equiv \zeta \hat{J}_z$ is $\frac{d\hat{J}_x}{dt} = -\zeta \hat{J}_y$, $\frac{d\hat{J}_y}{dt} = \zeta \hat{J}_x$, and $\frac{d\hat{J}_z}{dt} = 0$. This corresponds to a rotation around the J_z-axis with angular frequency ζ as illustrated on the upper row of Bloch spheres where the Q-functions for the results of applying $\mathcal{H}_\zeta$ on some initial state for for $\zeta t = 0$, 0.5, and 1 are plotted. The white arrows indicate the direction of the rotation. In the lower row of Bloch spheres the Hamiltonian $\mathcal{H}_s \equiv \chi \hat{J}_z^2$ is applied instead. No movement in the J_z-direction can result from applying $\mathcal{H}_s$, so the effect must be some sort of rotation as well. On the 'northern hemisphere' of the Bloch sphere the sign of J_z^2 is the same as that of J_z, while they are opposite on the 'southern hemisphere' which means that the movement on the 'northern hemisphere' is expected to go in the same direction as when applying $\mathcal{H}_\zeta$, while the direction on the 'southern hemisphere' must be the opposite. This is shown by the white arrows and it is indeed what is seen on the movement of our initial state, where the Q-functions for the results for $j\chi t = 0$, 0.5 and 1 are plotted.

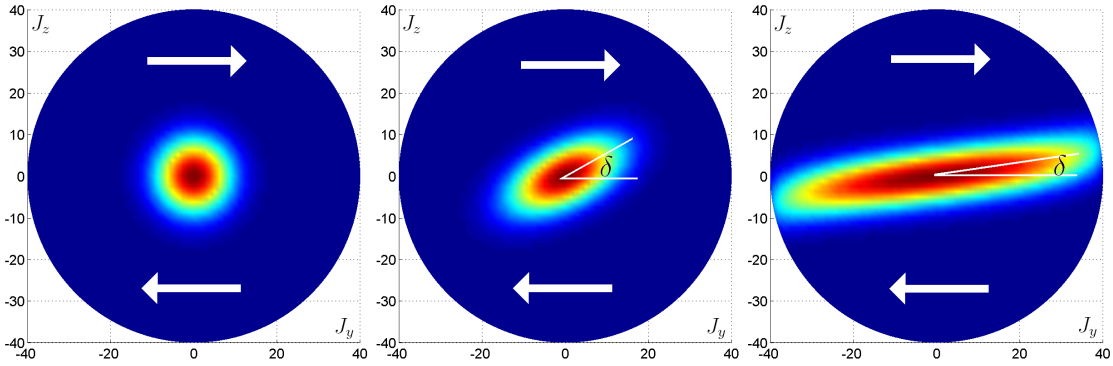

Figure 5.2: Illustration of the scheme of one-axis twisting, showing the results of applying $H_s \equiv \chi \hat{J}_z^2$ on the SCS (3.24) for a system with $j = 40$. The three subplots are for $\chi t = 0$, 0.05 and 0.1 respectively. The white arrows show qualitatively the effect of the Hamiltonian, see fig. 5.1. Indicated in the figure is the angle δ, an expression for which is given in the main text, and we see that $\nu = -\delta$ will produce the maximal squeezing in the J_z-direction. This figure is similar to FIG. 2. in [7].

After applying $\hat{H}_s$ and rotating, the expectation value of an operator $\hat{O}$ is

$$\langle \hat{O} \rangle = \langle x | \exp\left(i\chi t \hat{J}_z^2\right) \exp\left(i\nu \hat{J}_x\right) \hat{O} \exp\left(-i\nu \hat{J}_x\right) \exp\left(-i\chi t \hat{J}_z^2\right) | x \rangle \tag{5.15}$$

which can be calculated exactly[6] for the relevant operators with the results

$$\begin{aligned} \langle \hat{J}_z \rangle &= 0 \\ \langle \hat{J}_x \rangle &= j \cos^{2j-1}(\chi t) \\ \langle \hat{J}_z^2 \rangle &= \frac{j}{2}\left(1 + \tfrac{1}{2}(j - \tfrac{1}{2})\left(A - \sqrt{A^2 + B^2}\cos(2\nu + 2\delta)\right)\right) \end{aligned} \tag{5.16}$$

where $A \equiv 1 - \cos^{N-2}(2\chi t)$, $B \equiv 4\sin(\chi t)\cos^{N-2}(\chi t)$, and $\delta \equiv \frac{1}{2}\tan^{-1}\left(\frac{B}{A}\right)$. We see that $\nu = -\delta$ will minimize the squeezing, as indicated by fig. (5.2). The squeezing parameter as a function of time is

$$\xi^2(\nu, t) = \frac{1 + \frac{1}{4}(N-1)\left(A - \sqrt{A^2 + B^2}\cos(2\nu + 2\delta)\right)}{\cos^{2N-2}(\chi t)} \tag{5.17}$$

and for large N, the minimal squeezing is given as[7]

$$\xi^2 = \tfrac{1}{2}\left(\tfrac{3}{N}\right)^{2/3} \tag{5.18}$$

which should be compared to the ideal case of the F-functions (3.39) and to the Schwinger model (5.50) considered later in section 5.7.

[6] The calculations are sketched in [7], and the results are given. Doing it requires patience, and the relations $\sum_k \binom{n}{k} x^n = (1+x)^n$, $\sum_k k\binom{n}{k} x^n = \frac{nx}{1+x}(1+x)^n$, and $\sum_k k^2 \binom{n}{k} x^n = \left(\frac{nx}{1+x} + \frac{n(n-1)}{(1+x)^2}\right)(1+x)^n$.

[7] See [1]. Something similar to this result is stated wrong in [7].

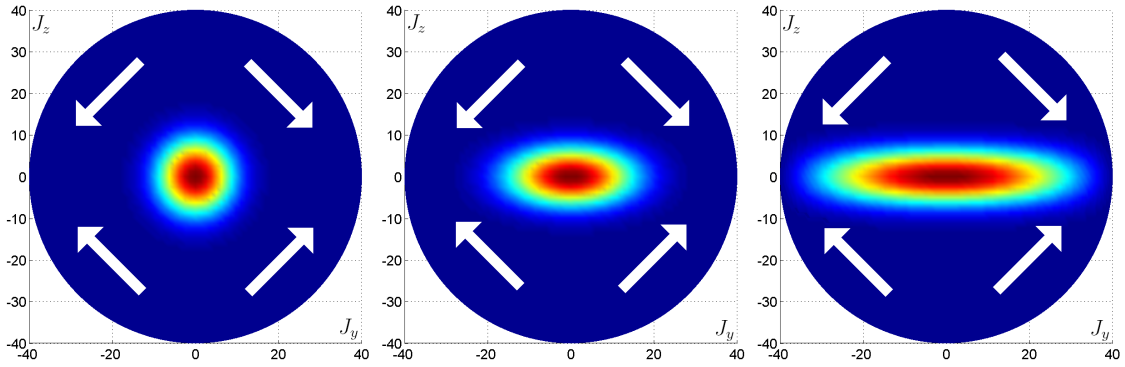

Figure 5.3: Illustration of the scheme of two-axis countertwisting showing the results of applying the Hamiltonian $\hat{H}_{2ac}$ given by (5.19) on the SCS in the J_x-direction (3.24). The plot is made for for a system with $j = 40$. The three subplots are for $\chi t = 0$, 0.01 and 0.02 respectively. The white arrows shows qualitatively the effect of the Hamiltonian, see fig. 5.1. This plot is similar to FIG. 3. in [7].

Kitagawa and Ueda discuss another scheme as well, by which one can obtain spin-squeezing. That scheme is denoted "Two-axis countertwisting" and works by applying the Hamiltonian

$$\hat{H}_{2ac} = \chi \left(\left(\frac{\hat{J}_y + \hat{J}_z}{\sqrt{2}} \right)^2 - \left(\frac{\hat{J}_y - \hat{J}_z}{\sqrt{2}} \right)^2 \right) \tag{5.19}$$

the effect of which can be seen in fig. 5.3 which explains the name, since we see that the twisting produced by each of the two components of (5.19) cancels each other out, thus requiring no ν-rotation at the end of the procedure. The amount of squeezing that can be obtained by two-axis countertwisting goes as[8] $\xi \propto N^{-1}$ for large N, which is better than the one-axis case.

Further theoretical results were found by Anders Sørensen, L.-M. Duan, J.I.Cirac, and P. Zoller in the Nature article [1] named "Many-particle entanglement with Bose-Einstein condensates". Instead of the toy model $\hat{H}_s$ they consider the full GP-Hamiltonian given by (4.34) without the Ω-term:

$$\begin{aligned} \hat{\mathcal{H}} \;=\; & \int \mathrm{d}\mathbf{r} \Big(\hat{\Psi}_a^\dagger(\mathbf{r}) H_0 \hat{\Psi}_a(\mathbf{r}) + \hat{\Psi}_b^\dagger(\mathbf{r}) H_0 \hat{\Psi}_b(\mathbf{r}) \\ & + \frac{U}{2} \left(\hat{\Psi}_a^\dagger(\mathbf{r}) \hat{\Psi}_a^\dagger(\mathbf{r}) \hat{\Psi}_a(\mathbf{r}) \hat{\Psi}_a(\mathbf{r}) + \hat{\Psi}_b^\dagger(\mathbf{r}) \hat{\Psi}_b^\dagger(\mathbf{r}) \hat{\Psi}_b(\mathbf{r}) \hat{\Psi}_b(\mathbf{r}) \right) \\ & + U_{ab} \hat{\Psi}_a^\dagger(\mathbf{r}) \hat{\Psi}_b^\dagger(\mathbf{r}) \hat{\Psi}_a(\mathbf{r}) \hat{\Psi}_b(\mathbf{r}) \Big) \end{aligned} \tag{5.20}$$

[8] See [7].

In the two-mode approximation, this Hamiltonian will reduce to

$$\hat{\mathcal{H}} = \alpha\hat{N} + \beta\hat{N}^2 + \chi\hat{J}_z^2 \tag{5.21}$$

where α, β and χ are given by (5.7), a result identical to $\hat{H}_s$ except for terms proportional to the particle number, which makes a comparison between the two models reasonable. The method[9] used by Sørensen, starts with a state with all the particles in the a-mode, which we can write $|N_a, N_b\rangle = |N, 0\rangle$ corresponding to a the SCS in the $-J_z$-direction. This state is rotated by $\pi/2$ around the y-axis so it becomes

$$|\psi\rangle = 2^{-N/2} \sum_{N_a} \sqrt{\frac{N!}{N_a!N_b!}} |N_a\phi(0), N_b\phi(0)\rangle \tag{5.22}$$

which is identical to the SCS in the J_x-direction given by (3.24) since $|j, m\rangle = |N_a, N_b\rangle$ with $j = N/2$ and $m = N_a/2$. This approach differs from the two-mode approximation considered previously in that it takes differences in the occupation number of the two modes into account. It has been shown that this is equivalent to the Bogoliubov calculations described in later sections. The procedure is to let the state evolve according to (5.20), and the time evolution can be written

$$|N_a\phi_0, N_b\phi_0\rangle \rightarrow C_{N_aN_b}(t)|N_a\phi_{a,N_a,N_b}(t), N_b\phi_{b,N_a,N_b}(t)\rangle \tag{5.23}$$

where $C_{N_aN_b}(t)$ is a complex phase factor $|C|^2 = 1$, and where all the parameters $C_{N_aN_b}(t)$, $\phi_{a,N_aN_b}(t)$, and $\phi_{b,N_aN_b}(t)$ can be calculated. Using (5.4), this result can be used to derive the expectation values $\langle\hat{J}_x\rangle$ and $\langle\hat{J}_z^2\rangle$ and thereby the squeezing parameter. The result of such a calculation is plotted in fig. 5.4 which is taken directly from [1]. We see that oscillations occur in the $\langle\hat{J}_x\rangle$ vs. $(\Delta J_z)^2$-function. This is due to oscillations in $\phi_a(t)$ and $\phi_b(t)$ similar to those plotted in fig. 4.2. If $U > U_{ab}$, most of the states in the sum in (5.22) will have less energy than the initial state $|N, 0\rangle$, and therefore the oscillations start at minimal compression like the situation plotted in fig. 4.2. We see that the 'dips' in the result in fig. 5.4 shifts between small and large ones, and the small ones correspond to the points of maximal compression, while the big ones correspond to minimal, or initial compression[10].

In another article named "Bogoliubov theory of entanglement in a Bose-Einstein condensate" [4], Anders Sørensen treats the same problem using a time-dependent version of the Bogoliubov method described in this thesis, and gets a similar result.

In [4] a plot is shown of the fraction of the physical value of χ to the value calculated for the two-mode approximation in (5.7), as function of the chemical potential. In general this fraction is different from one, and in the limit of large μ which corresponds to a large value of $N(U + U_{ab})$, the fraction approaches $\frac{7}{10}$. A derivation of this value can be found in [11], but the fact that it is different from one is due to perturbations in the condensate similar to the Bogoliubov-modes found in a later section, which makes the GPE less valid in this limit.

[9] The method is described in further detail in [11].

[10] See [1].

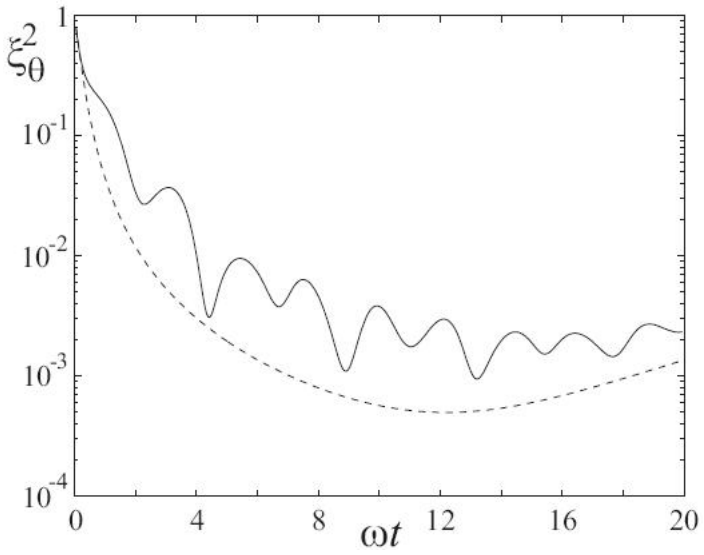

Figure 5.4: This figure is taken from [1], where it is denoted FIG. 1. The dotted line shows the result for one-axis twisting given by (5.17), and the solid line shows the result of the more realistic numerical calculation made in [1]. We see that the squeezing in some points approaches, but never reaches the one-axis twisting result. The value of χ used to draw the dotted line is corrected with the value of $\frac{7}{10}$ mentioned in the main text.

5.4 Previous experimental results

In this section some of the previous experimental results on spin-squeezing and BEC will be presented. Like the previous section, this section is not at all a full introduction to all experiments that have been done in the field, only a few selected experiments will be mentioned.

The first experiment that will be mentioned, is a recent one made by a group in Heidelberg led by Marcus Oberthaler. The experiment is described in the article [13] named "Nonlinear atom interferometer surpasses classical precision limit". The experiment had a trapped BEC going through the procedure of Ramsey spectroscopy described in section 2.1, and the reason for the word "interferometry" in the title is the parallel between Ramsey spectroscopy and Mach-Zehnder interferometry described in that section. It is however the initial step in which the experiment squeezes the state of the atoms that will concern us here, since that step essentially amounts to a realization of one-axis twisting.

The experiment used 2300 atoms of ^{87}Rb trapped in an (almost) isotropic harmonic oscillator potential with $\omega = 2\pi \times 425$ Hz. The $|a\rangle$ and $|b\rangle$-states were chosen as the hyperfine states $|F = 1, m_F = 1\rangle$ and $|F = 2, m_F = -1\rangle$. These states

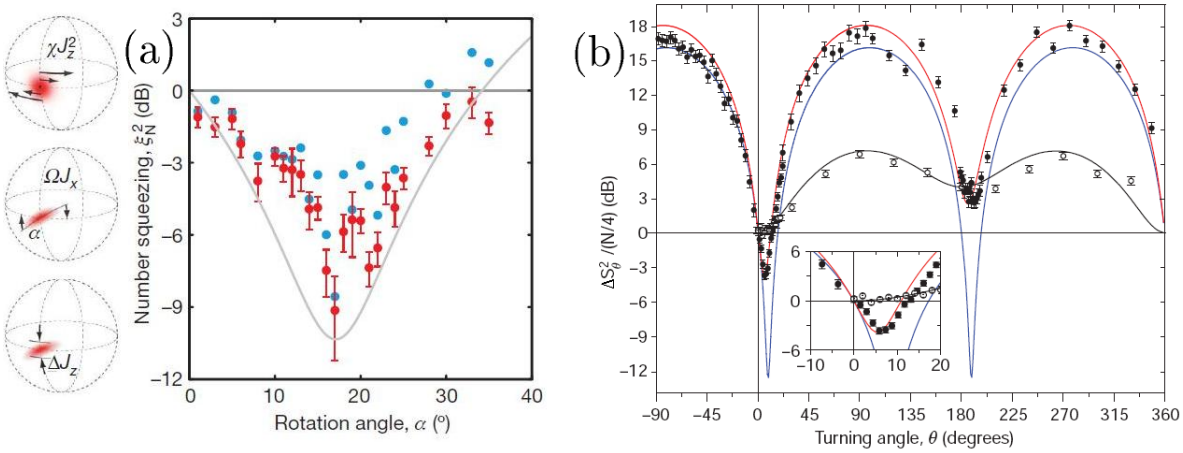

Figure 5.5: The experimental results by Oberthaler and Treutlein respectively. The figures are taken directly from the corresponding articles where they are denoted FIG. 3a and FIG. 2a. (a) is the result by Oberthaler from [13]. The blue data are the measurements corrected for shot noise, and the red data with the error bars is further corrected for technical noise. The gray line is a fit to (5.17) with $\alpha \equiv -\nu$, fitted after the parameter χ giving the result mentioned in the main text. The Bloch spheres to the left of the figure shows the one-axis twisting procedure, indicating the angle α. (b) is the result by Treutlein from [14], showing (what corresponds to) $4(\Delta J_z)^2/N$ as functions of an angle θ similar to α in the Oberthaler experiment. The closed circles show the measured data while the open circles are reference data for a coherent spin state. The solid blue line is a fit to an expression similar to (5.17), which takes losses into account, see [19]. The fit plotted as the red line takes technical noise into account as well. The black line is a similar fit to the reference data, and we see unsurprisingly that the SCS has $\xi > 1$ for all values of θ.

have the scattering lengths[11] $a_{aa} = 100a_0$, $a_{ab} = 97.7a_0$ and $a_{bb} = 95a_0$ where a_0 is the Bohr radius. We see that $a_{aa} + a_{bb} \approx 2a_{ab}$ making $\chi \approx 0$ and thereby making squeezing harder to obtain, but Oberthaler circumvented this by using a Feshbach resonance[12] induced by an external magnetic field to adjust the value of a_{ab} so he ended up with $\chi = 2\pi \times 0.063$ Hz. A side effect of the Feshbach resonance is that it increases the particle loss, 15% of the atoms were lost during the experiment.

In fig. 5.5a we see the amount of squeezing produced by the experiment, as function of an angle corresponding to the angle ν in (5.17). The optimal angle gives a squeezing of -8.2 dB corresponding to $\xi^2 \approx 0.15$.

The second experiment I am going to mention was carried out by a group led by Philipp Treutlein. The experiment is described in the article [14] named "Atom-chip-

[11] Oberthaler does strictly speaking not quote these values, he only writes that the fraction is 100 : 97.7 : 95. But I am comparing to Treutlein in [14] who uses the same atoms and almost the same states, and he uses the same fractional notation, but writes that the unit of the numbers is a_0.

[12] See [13] and [a] p. 143 ff.

based generation of entanglement for quantum metrology". Like Oberthaler, Treutlein's group used ^{87}Rb-atoms, of which they had 1250 trapped in an anisotropic trap with frequencies from $\omega_{\text{long}} = 2\pi \times 109Hz$ to $\omega_{\text{ax}} = 2\pi \times 500Hz$. As the $|a\rangle$ and $|b\rangle$ states they used the hyperfine states $|F = 1, m_F = -1\rangle$ and $|F = 2, m_F = 1\rangle$ with scattering lengths $a_{aa} = 100.4a_0$, $a_{ab} = 97.7a_0$ and $a_{bb} = 95.0a_0$ also giving $\chi \approx 0$. Treutlein solved this problem another way, namely by separating the a and the b-mode physically so the overlap between ψ_a and ψ_b diminishes, giving a $\chi = 0.49\text{s}^{-1}$. The squeezing procedure is one-axis twisting, and the squeezing as a function of an angle θ corresponding to the angle ν present in (5.17) is plotted in fig. 5.5 (b). The minimal measured value of $4(\Delta J_z)^2/N$ is -3.7 dB and the value of $\langle \hat{J}_x \rangle / N$ is 0.88 giving a squeezing of -2.5 dB corresponding to $\xi^2 = 0.56$. The experiment took place on a so-called atom-chip making the setup more portable than the one used by Oberthaler[13], but the drawback is the increased technical noise which is the reason why the amount of squeezing obtained by this experiment is not as large as the amount produced in the experiment by Oberthaler described in [13].

None of the experiments described above looked at a static situation which is what my theory is going to describe. This is, however, done in a previous experiment by Oberthaler described in [15]. In this experiment he used a one-dimensional lattice potential similar to the one used in [13], made up of a series of potential wells, which can be approximated with a harmonic oscillator potential near the bottom of each well. In this case the potential barrier is adjusted so there is some interaction between particles in different sites on the lattice. The particles do, however, not have any internal degrees of freedom, so it is the position of the particle that plays the role of spin. The maximal squeezing obtained in this experiment is $\xi^{(N)^2} = -7.2$ dB.

It should be noted that the theory that will be derived in this thesis describes a situation that is a combination of the two experiments by Oberthaler. It describes internal states like the experiment in [13], but it looks at a steady-state situation like the experiment in [15].

5.5 Parallel to xp-squeezing: a proposal

Let us return to the two-mode approximation for a moment. As we saw in section 5.1, the lowest energy eigenstate of the Hamiltonian (5.8) will be a squeezed state, indicating that the system will approach this state if it is left in peace. But in the dynamic case (5.8) will result in squeezing as well. In the limit $\langle \hat{J}_x \rangle \approx j$ we can use

$$\hat{J}_x \approx \sqrt{j(j+1) - (\hat{J}_z^2 + \hat{J}_y^2)} \approx j - \tfrac{1}{2j}\hat{J}_z^2 - \tfrac{1}{2j}\hat{J}_y^2 \tag{5.24}$$

to rewrite (5.8) to

$$\hat{\mathcal{H}} \approx \Omega j + \left(\chi - \tfrac{\Omega}{2j}\right)\hat{J}_z^2 + \tfrac{-\Omega}{2j}\hat{J}_y^2 \tag{5.25}$$

[13] See [12] and [14].

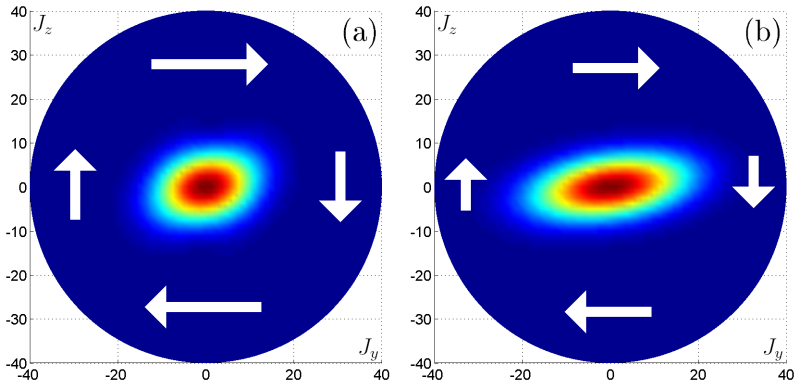

Figure 5.6: Q-functions for the states created by applying the Hamiltonian (5.25) for a time $\chi t = 1$ to the SCS in the J_x-direction. (a) and (b) differs by the value of $\lambda \equiv -\Omega/\chi$. (a) has $\lambda = 1$ and (b) has $\lambda = 0.1$. The resulting values of $\xi^2_{J_z}$ are 0.6606 and 0.2997 respectively. The white arrows show (qualitatively) the effect of the $\hat{J}_z^2$ and the $\hat{J}_y^2$ parts of the Hamiltonian, see fig. (5.1).

and the application of this Hamiltonian results in squeezing as can be seen from fig. 5.6 and the associated text.

We can, however, get even further results out of (5.25) in the dynamical case. In the $\pm$-basis we can make an interesting parallel to the squeezing operator as described in the section on xp-squeezing. If we assume that the vast majority of the particles are in the plus-mode, the $\hat{J}_y$ and $\hat{J}_z$ operators become

$$\begin{aligned} \hat{J}_y &\approx \frac{i\sqrt{N}}{2}\left(\hat{c}_- - \hat{c}_-^\dagger\right) \\ \hat{J}_z &\approx \frac{\sqrt{N}}{2}\left(\hat{c}_- + \hat{c}_-^\dagger\right) \end{aligned} \tag{5.26}$$

which we can compare to the results for $\hat{x}$ and $\hat{p}$ in (3.9). In addition the uncertainty relation for the spin operators becomes $\Delta J_y \Delta J_z \geq \frac{1}{4}N$, which we can compare to the Heisenberg relation $\Delta x \Delta p \geq \frac{1}{2}$. From these relations we may get the idea that we can make an analogy to xp-squeezing in this limit.

The most obvious identifications $\hat{J}_y \leftrightarrow \sqrt{\frac{N}{2}}\hat{p}$, $\hat{J}_z \leftrightarrow \sqrt{\frac{N}{2}}\hat{x}$, $\hat{c}_- \leftrightarrow \hat{a}$, and $\hat{c}_-^\dagger \leftrightarrow \hat{a}^\dagger$ create an inconsistency in the commutators. Instead the identifications $\hat{J}_y \leftrightarrow \sqrt{\frac{N}{2}}\hat{x}$ and $\hat{J}_z \leftrightarrow \sqrt{\frac{N}{2}}\hat{p}$ with $\hat{c}_- \leftrightarrow -i\hat{a}$ and $\hat{c}_-^\dagger \leftrightarrow i\hat{a}^\dagger$ will allow us to complete the analogy.

Writing (5.25) in the plus-minus basis gives

$$\hat{\mathcal{H}} = \Omega j + \frac{N\chi}{4}\left(\hat{c}_-\hat{c}_- + \hat{c}_-^\dagger\hat{c}_-^\dagger\right) + \frac{N}{4}\left(\chi - \Omega/j\right)\left(\hat{c}_-\hat{c}_-^\dagger + \hat{c}_-^\dagger\hat{c}_-\right) \tag{5.27}$$

using the approximations for $\hat{J}_y$ and $\hat{J}_z$ found in (5.26). If we choose Ω so $\chi = \Omega/j$,

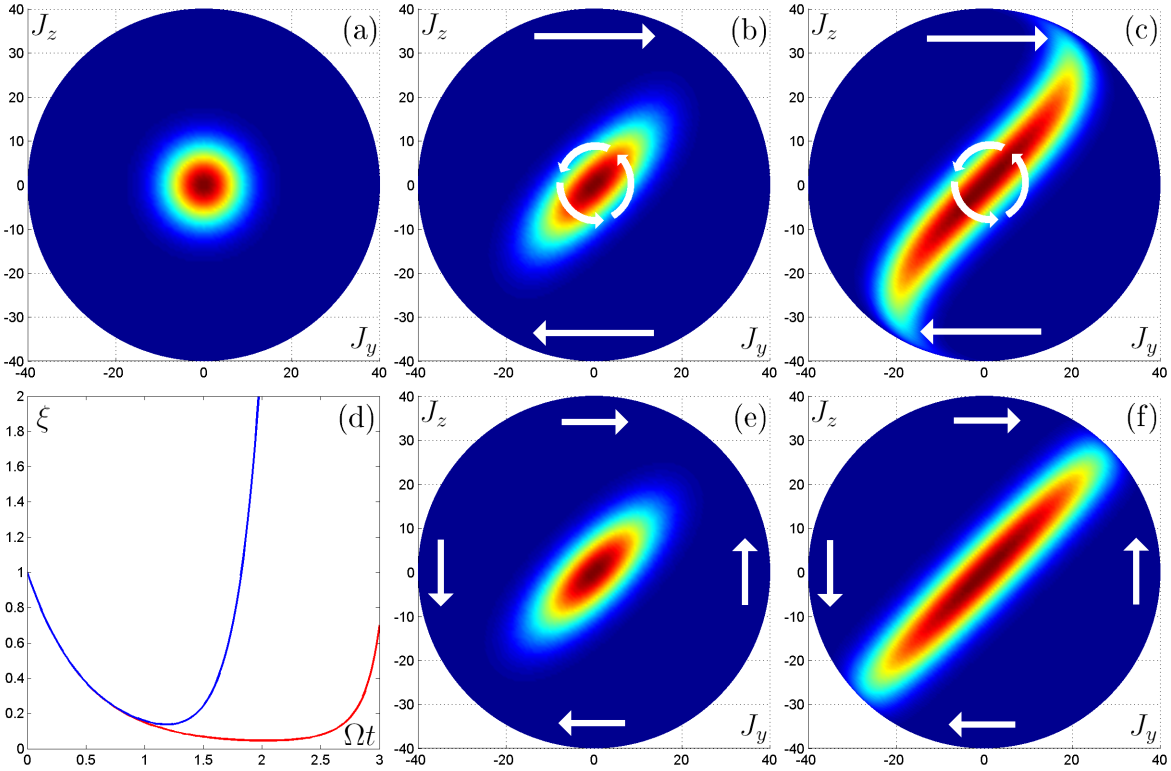

Figure 5.7: A way to create spin-squeezing dynamically that, to the best of my knowledge, have not been tried before experimentally. It consists of applying the Hamiltonian (5.8) with $\Omega = \chi j$ to the SCS in the J_x-direction. As shown in the main text (5.8) reduces to (5.25) in the limit of $\langle \hat{J}_x \rangle \approx j$, and if $\Omega = \chi j$ it is identical to $\mathcal{H}_{2ac}$ given by (5.19) in a rotated coordinate system. (a) shows the initial state, and (b) and (c) show the result of applying (5.8) for $\chi j t = 0.5$ and 1 respectively. (e) and (f) show the result of applying (5.25) with the chosen Ω for the same times. The graphs on (d) show the amount of squeezing produced by the two methods. The red curve is the result for two-axis countertwisting (5.25), and the blue curve shows the result of applying (5.8), both with the chosen value of Ω. We see that the amount of squeezing produced by (5.8) approaches, but never reaches the result for two-axis countertwisting. Still it seems like an approach worth trying experimentally.

and insert the identification $\hat{c}_- = -i\hat{a}$, the time evolution of some state $|\psi\rangle$ will be

$$|\psi(t)\rangle = \exp\left(\frac{-i\chi Nt}{4}\left(\hat{a}^\dagger\hat{a}^\dagger + \hat{a}\hat{a}\right)\right)|\psi(0)\rangle \tag{5.28}$$

if we ignore the phase coming from the constant Ωj-term. This can be rewritten as

$$|\psi(t)\rangle = \exp\left(\frac{r}{2}\left(\exp\left(i\tfrac{\pi}{2}\right)\hat{a}\hat{a} - \exp\left(-i\tfrac{\pi}{2}\right)\hat{a}^\dagger\hat{a}^\dagger\right)\right)|\psi(0)\rangle \tag{5.29}$$

where we have made the additional identification $r \equiv \frac{\chi Nt}{2}$. We see that this is identical to the effect of applying the squeeze operator $\hat{S}(r,\phi)$ as defined in (3.11) with $\phi = \pi/2$.

If we reinsert our relation $\Omega = \chi j$ directly into (5.25), we see that it becomes

$$\hat{\mathcal{H}} \;=\; \frac{\Omega}{2j}\hat{J}_z^2 - \frac{\Omega}{2j}\hat{J}_y^2 \tag{5.30}$$

which is identical to the Hamiltonian for two-axis countertwisting given by (5.19) in a rotated coordinate system rotated with the angle $\pi/4$, similar to what we found in the parallel to xp-squeezing (5.29). The results of applying (5.30) and (5.8) with $\Omega = \chi j$ are plotted in fig. 5.7. Even though we see that the squeezing produced by (5.8) does not match the amount produced by (5.30), I still assume that this approach to dynamical spin-squeezing production is worth trying experimentally, since the amount of squeezing obtainable by two-axis countertwisting exceeds what can be produced by one-axis twisting[14].

5.6 Bogoliubov transformations

The Bogoliubov method is a way by which one can diagonalize a second quantization Hamiltonian. In our case, the Bogoliubov transformation consists of two steps. The first step is a rewriting of the second quantization operators $\hat{\Psi}_\pm(\mathbf{r})$ as a sum of a mean-field term and a perturbation term denoted $\delta\hat{\psi}_\pm(\mathbf{r})$ which is considered small so one can discard higher order[15] terms. The second step, which strictly speaking is THE Bogoliubov transformation, consists of expressing[16] $\delta\hat{\psi}_\pm$ which in the original representation is a sum of terms $\delta\hat{\psi}_\pm(\mathbf{r}) = \sum_{i>0}\hat{c}_{i\pm}\varphi_{i\pm}(\mathbf{r})$, as another sum of some new operators $\delta\hat{\psi}_\pm(\mathbf{r}) = \sum_i\left(u_{i\pm}(\mathbf{r})\hat{\alpha}_{i\pm} + v_{i\pm}(\mathbf{r})\hat{\alpha}_{i\pm}^\dagger\right)$ having the property of diagonalizing the Hamiltonian so that it can be written as a constant term plus $\sum_i \varepsilon_i\alpha_i^\dagger\alpha_i$, indicating that the energy eigenstates are the eigenstates for the these new number operators. The complication arises when one tries to find the functions $u_i(\mathbf{r})$ and $v_i(\mathbf{r})$ making this diagonalization possible.

[14] See [7] and section 5.3.

[15] In the calculations in chapter 6, we discard terms of more than second order in $\delta\hat{\psi}$.

[16] In the calculations in chapter 6, this is not done to the $\delta\hat{\psi}$-operator but to a related operator denoted $\hat{\Lambda}$.

The details of the calculations may differ from case to case. In the case where the Hamiltonian in question is a one-species Gross-Pitaevskii Hamiltonian, differing from (4.17) by having the harmonic trap potential replaced with a box-shaped potential, the Bogoliubov calculations can be solved exactly[17]. But whenever a more complicated trap is present, even one as simple as the spherical symmetric one used in this thesis, this can not be done and numeric calculations are necessary.

It seems like a time-dependent approach to Bogoliubov transformations has been the most popular in the literature[18]. In this thesis however, the calculation is going to be done time independently which will give us the steady-state result. This explains the large focus in previous sections on time independent GPEs over the time dependent ones, which for a two-species case can be constructed exactly like (4.19) were for the one-species case. The advantage of a steady-state approach is that the conditions are more easily met experimentally since the experiment does not need to be timed precisely, in theory it can be done any time after the system has reached equilibrium. For some examples of time-dependent calculations, see appendix E.

Another choice that must be made is if we will do the calculations as though there is a condensate in both the plus- and the minus-mode, or in the plus-mode only. If we choose the plus-mode only, the rewriting for the minus-mode will be $\hat{\Psi}_- = \delta\hat{\psi}_-$ which means that we view the φ_{0-} mode as a part of the perturbation. One might imagine that a calculation with a condensate in both modes is more precise since we will do a smaller part of the calculation approximatively in that case. This is, however, not the case, since such a rewriting is unable to take the differences between the φ_{0+} and the φ_{0-}-mode into account as we would need to use $\varphi_{0+} = \varphi_{0-} = \varphi$ where φ is the condensate mode found by the GPE. Therefore the calculation in chapter 6 will be done with φ_{0+} as the only condensate mode. With this choice our interactions are as depicted in fig. 5.8.

The final choice we are faced with, is whether or not to make a symmetry-break in the approximation. This choice is between the symmetry-breaking rewriting $\hat{\Psi}_+(\mathbf{r}) = \psi(\mathbf{r}) + \delta\hat{\psi}_+(\mathbf{r})$ where ψ is the many-body wave function, and the more correct rewriting $\hat{\Psi}_+(\mathbf{r}) = \varphi(\mathbf{r})\hat{c} + \delta\hat{\psi}_+(\mathbf{r})$ where φ and $\hat{c}$ are short for the wave function and the annihilation operator for the condensate mode. The symmetry in question is the $U(1)$-symmetry imposed by the fact that the Hamiltonian (5.11) is invariant under the transformation $\hat{\Psi} \to \hat{\Psi}e^{i\theta}$. If we do the transformation and calculate $\langle\hat{\Psi}_+\rangle$ in the two approaches with a state $\bigotimes_i |n_i\rangle_i$, the result is $\psi e^{i\theta}$ for the symmetry-breaking rewriting, and 0 for the more correct non-symmetry-breaking one. We see that the phase is present in the result under the symmetry-breaking approach, thereby explaining the name. This gives a degree of freedom to the system that would not otherwise have been there, and the mode formed by this symmetry break is known as a Goldstone mode named after Goldstone's theorem predicting that 'a spontaneous breaking of a continuous symmetry generates a massless bosonic

[17] See [a] page 229ff.

[18] Examples are [4] and [6].

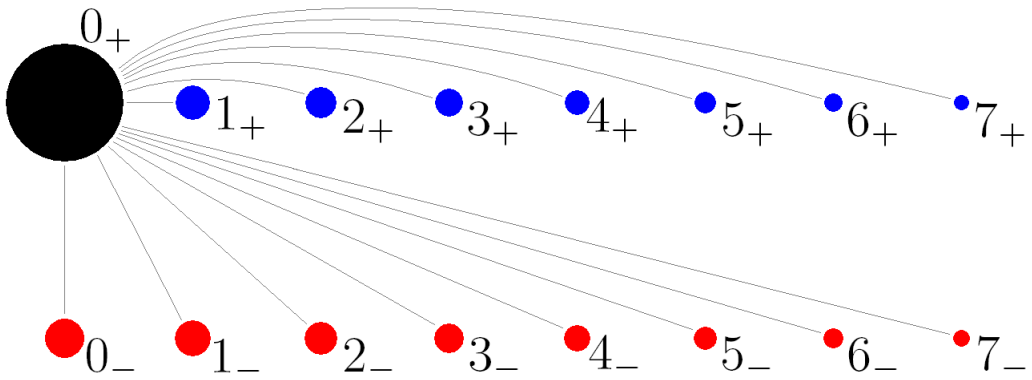

Figure 5.8: The various dots in this picture illustrate the individual Bogoliubov modes of our system. The interaction is modeled so that the condensate-mode 0_+ is interacting perturbatively with the other modes as illustrated by the gray lines. If we had chosen to treat the 0_--mode as a condensate-mode as well, the 0_+-0_--interaction would be done non-perturbatively, but not necessarily yielding a more precise result.

particle'. The Goldstone mode would, since it has zero energy, be occupied by an infinite amount of quasi-particles that would need to be artificially excluded from sums over all modes[19]. Other problems would arise as well, see section 6.4 which explains the problems caused by the symmetry-breaking approach in further detail.

The choice of the non-symmetry-breaking approach does bring a few complications as well. In this approach expressing $\delta\hat{\psi}(\mathbf{r})$ in terms of $\hat{\alpha}$-operators is not helpful, we have to relate $\delta\hat{\psi}$ to another operator $\hat{\Lambda}$ before changing to the $\hat{\alpha}$-operators using $\hat{\Lambda}(\mathbf{r}) = \sum_i \left(u_i(\mathbf{r})\hat{\alpha}_i + v_i(\mathbf{r})\hat{\alpha}_i^\dagger \right)$ instead. I addition we need to introduce a projection operator $\mathcal{Q}\circ$ that projects away from the 0_+-state. But these are complications that can be overcome, which is why we choose the non-symmetry-breaking approach for the main calculation in chapter 6.

5.7 The Schwinger model

Before doing the calculations for the full Hamiltonian (5.11), let us illustrate the use of Bogoliubov transformations on the simpler Hamiltonian (5.8)

$$\hat{\mathcal{H}} = \chi \hat{J}_z^2 + \Omega \hat{J}_x \tag{5.31}$$

and let us further make the two-mode approximation saying that we only regard the smallest energy state in each of the plus and minus-modes. This model is known as the Schwinger[20] model[21].

[19] Like those that would turn up in equations similar to those from (6.42) to (6.45), which would be expressed without excluding the sum over the 0_+-mode, corresponding to the Goldstone mode.

[20] The Schwinger in question is Julian Schwinger, one of the fathers of Quantum Electro-Dynamics.

[21] For more on the Schwinger model, see [b], page 217ff.

The relevant $\hat{J}$-operators can be written

$$\begin{aligned} \hat{J}_x &= \frac{1}{2}\left(\hat{c}_+^\dagger \hat{c}_+ - \hat{c}_-^\dagger \hat{c}_-\right) \\ \hat{J}_z &= \frac{1}{2}\left(\hat{c}_+^\dagger \hat{c}_- + \hat{c}_-^\dagger \hat{c}_+\right) \end{aligned} \tag{5.32}$$

since any spatial dependence will integrate out. Let us express these operators using the new operators[22]

$$\begin{aligned} \hat{\Lambda} &\equiv \frac{\hat{c}_+^\dagger \hat{c}_-}{\sqrt{N_0}} \\ \hat{N} &= \hat{c}_+^\dagger \hat{c}_+ + \hat{c}_-^\dagger \hat{c}_- \end{aligned} \tag{5.33}$$

where N_0 is the number of particles in the plus-mode. Assuming that $N_0 \gg 1$ allows us to calculate

$$\begin{aligned} \hat{J}_x &= \frac{1}{2}\hat{N} - \frac{1}{2}\left(\hat{\Lambda}^\dagger\hat{\Lambda} + \hat{\Lambda}\hat{\Lambda}^\dagger\right) \\ \hat{J}_z &= \frac{\sqrt{N_0}}{2}\left(\hat{\Lambda} + \hat{\Lambda}^\dagger\right) \\ \hat{J}_z^2 &= \frac{N_0}{4}\left(\hat{\Lambda}\hat{\Lambda} + \hat{\Lambda}\hat{\Lambda}^\dagger + \hat{\Lambda}^\dagger\hat{\Lambda} + \hat{\Lambda}^\dagger\hat{\Lambda}^\dagger\right) \end{aligned} \tag{5.34}$$

so now we can write the Hamiltonian (5.31) as[23]

$$\hat{\mathcal{H}} = \hat{\mathcal{H}}_0 + \frac{1}{2}\left(A\left(\hat{\Lambda}^\dagger\hat{\Lambda} + \hat{\Lambda}\hat{\Lambda}^\dagger\right) + B\left(\hat{\Lambda}\hat{\Lambda} + \hat{\Lambda}^\dagger\hat{\Lambda}^\dagger\right)\right) \tag{5.35}$$

where

$$\begin{aligned} \hat{\mathcal{H}}_0 &\equiv \frac{\Omega}{2}\hat{N} \\ A &\equiv \frac{\chi N_0}{2} - \Omega \\ B &\equiv \frac{\chi N_0}{2} \end{aligned} \tag{5.36}$$

[22] In the Schwinger model only one mode exists in each of the plus- and minus-states, and therefore the rewriting $\hat{\Psi}_+ = \hat{c}_+\varphi + \delta\hat{\psi}_+$ makes no sense. Only in the minus-mode where the full model uses $\hat{\Psi}_- = \delta\hat{\psi}_-$ the Schwinger model has a corresponding operator, and that is the $\hat{\Lambda}$-operator mentioned here.

[23] In the full calculation it makes sense to write this equation as a matrix equation, $\hat{\mathcal{H}} = \hat{\mathcal{H}}_0 + \bar{\Lambda}^\dagger\mathcal{M}\bar{\Lambda}$, where $\bar{\Lambda}$ is a vector with the elements $\hat{\Lambda}$ and $\hat{\Lambda}^\dagger$, and $\mathcal{M}$ is a matrix with A and B as elements arranged in a way similar to the matrix $\mathcal{L}$ which we will encounter later, except for the minuses. For this Schwinger calculation such a rewriting does not simplify anything, so it is avoided.

We want to diagonalize this Hamiltonian, but in order to do this we need to have a look at the commutator for the $\hat{\Lambda}$-operators.

$$\left[\hat{\Lambda}, \hat{\Lambda}^\dagger\right] = \frac{\hat{c}_+^\dagger \hat{c}_- \hat{c}_+ \hat{c}_-^\dagger - \hat{c}_+ \hat{c}_-^\dagger \hat{c}_+^\dagger \hat{c}_-}{N_0} = \frac{\hat{c}_+^\dagger \hat{c}_+ - \hat{c}_-^\dagger \hat{c}_-}{N_0} \approx 1 \tag{5.37}$$

where the approximation is known as the Holstein-Primakoff approximation, and consists of assuming that the vast majority of the particles are in the plus-mode, just like we are going to do in the full calculation in chapter 6.

Now we are ready to do the diagonalization. The first step consists of expressing $\hat{\Lambda}$ as a sum of some new operators

$$\hat{\Lambda} = u\hat{\alpha} + v\hat{\alpha}^\dagger \tag{5.38}$$

as described in the general section on Bogoliubov transforms. We want to find values for u and v so that the Hamiltonian is diagonal in the $\hat{\alpha}$-basis, meaning that it can be written

$$\hat{\mathcal{H}} = \hat{\mathcal{H}}_0 + \varepsilon\left(\hat{\alpha}^\dagger\hat{\alpha} + \hat{\alpha}\hat{\alpha}^\dagger\right) \tag{5.39}$$

Inserting the $\hat{\alpha}$-operators in the expression for the commutator gives

$$\begin{aligned}\left[\hat{\Lambda}, \hat{\Lambda}^\dagger\right] &= \left(u\hat{\alpha} + v\hat{\alpha}^\dagger\right)\left(u^*\hat{\alpha}^\dagger + v^*\hat{\alpha}\right) - \left(u^*\hat{\alpha}^\dagger + v^*\hat{\alpha}\right)\left(u\hat{\alpha} + v\hat{\alpha}^\dagger\right) \\ &= \left(uu^* - v^*v\right)\hat{\alpha}\hat{\alpha}^\dagger + \left(v^*v - uu^*\right)\hat{\alpha}^\dagger\hat{\alpha}\end{aligned} \tag{5.40}$$

where we see that if the commutator equals one as it should as a result of the Holstein-Primakoff approximation, we must require that

$$u^*u - vv^* = 1 \tag{5.41}$$

since we require the $\hat{\alpha}$-operators to obey $\left[\hat{\alpha}, \hat{\alpha}^\dagger\right] = 1$. Inserting the expression for $\hat{\Lambda}$ (5.38) into (5.35) gives

$$\begin{aligned}\hat{\mathcal{H}} &= \hat{\mathcal{H}}_0 + \frac{\chi N_0}{4}\Big(\left(uu + v^*v^* + v^*u + uv^*\right)\hat{\alpha}\hat{\alpha} + \left(vv + u^*u^* + u^*v + vu^*\right)\hat{\alpha}^\dagger\hat{\alpha}^\dagger \\ &\quad + \left(uv + v^*u^* + v^*v + uu^*\right)\hat{\alpha}\hat{\alpha}^\dagger + \left(vu + u^*v^* + u^*u + vv^*\right)\hat{\alpha}^\dagger\hat{\alpha}\Big) \\ &\quad - \frac{\Omega}{2}\Big(\left(uv^* + v^*u\right)\hat{\alpha}\hat{\alpha} + \left(vu^* + u^*v\right)\hat{\alpha}^\dagger\hat{\alpha}^\dagger + \left(uu^* + v^*v\right)\hat{\alpha}\hat{\alpha}^\dagger + \left(vv^* + u^*u\right)\hat{\alpha}^\dagger\hat{\alpha}\Big) \\ &= \hat{\mathcal{H}}_0 + \frac{1}{2}\Bigg(\left(\left(v^*,\ -u\right)\mathcal{L}\begin{pmatrix} u \\ v^* \end{pmatrix}\right)\hat{\alpha}\hat{\alpha} + \left(\left(v^*,\ -u\right)\mathcal{L}\begin{pmatrix} u \\ v^* \end{pmatrix}\right)^*\hat{\alpha}^\dagger\hat{\alpha}^\dagger \\ &\quad + \left(\left(u^*,\ -v\right)\mathcal{L}\begin{pmatrix} u \\ v^* \end{pmatrix}\right)\hat{\alpha}^\dagger\hat{\alpha} + \left(\left(u^*,\ -v\right)\mathcal{L}\begin{pmatrix} u \\ v^* \end{pmatrix}\right)\hat{\alpha}\hat{\alpha}^\dagger\Bigg)\end{aligned} \tag{5.42}$$

where

$$\mathcal{L} \equiv \begin{bmatrix} A & B \\ -B & -A \end{bmatrix} \tag{5.43}$$

Using (5.41), we see that if

$$\bar{w} \equiv \begin{pmatrix} u \\ v^* \end{pmatrix} \tag{5.44}$$

is an eigenvector to $\mathcal{L}$ with eigenvalue ε, (5.42) turns into (5.39) as desired, meaning that u and v can be found by diagonalizing $\mathcal{L}$.

The diagonalization can be done analytically, and the result is that one of the sets of eigenvalues and eigenstates is

$$\begin{aligned} \varepsilon &= \sqrt{A^2 - B^2} \\ u &= \frac{1}{\sqrt{1 - \left(\frac{\varepsilon - A}{B}\right)^2}} \\ v^* &= \frac{-1}{\sqrt{\left(\frac{B}{\varepsilon - A}\right)^2 - 1}} \end{aligned} \tag{5.45}$$

We see that since B is positive[24] and A and B are real, we can ensure the ε-eigenvalue to be real if $A > B$ which means that $\Omega < 0$. This just means that the energy of the $+$-mode is smaller than for the $-$-mode, and if that was not the case the approximation $n_+ \ll n_-$ would not make sense. The other eigenvalue is $\varepsilon' = -\varepsilon$ with $u' = iv^*$ and $v^{*\prime} = iu$, where the i is necessary if we still want the state to obey (5.41). We see that only one of the eigenvalues are positive and therefore physical. It turns out that a positive real eigenvalue corresponds to real u and v-functions. This can be seen from the fact that a real u corresponds to $B^2 > (\varepsilon - A)^2$ which can be rewritten to $\varepsilon > (A^2 - B^2)/A$, and since the right hand side is positive, so is the left hand side. If we insist on having real u and v, this result can be restated as a claim that only states with a positive eigenvalue can solve (5.41).

When we have found u and v we can use them to calculate the expectation values of our operators, under the assumption that no particles are in the $\hat{\alpha}$-mode, which is similar to the Holstein-Primakoff approximation made above. The results are

$$\begin{aligned} \langle \hat{J}_x \rangle &= \frac{N_0}{2} - \frac{1}{2} v^* v \\ \langle \hat{N} \rangle &= N_0 + v^* v \\ \langle \hat{J}_z^2 \rangle &= \frac{N_0}{4}\left(1 + 2v^* v + uv + u^* v^*\right) \\ \langle \hat{J}_z \rangle &= 0 \end{aligned} \tag{5.46}$$

[24] Which it is since we assume that $U > U_{ab}$.

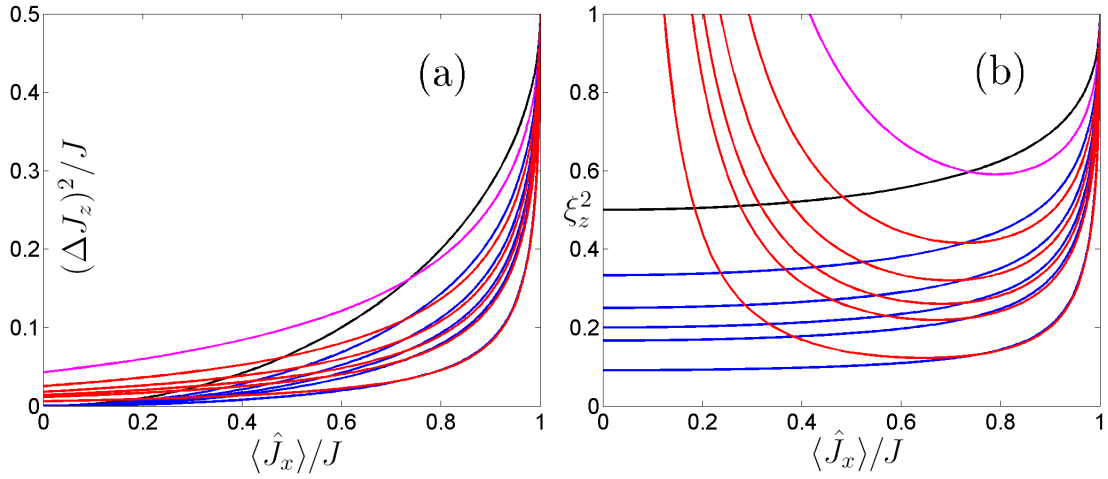

Figure 5.9: (a) shows $(\Delta J_z)^2$ as functions of $\langle \hat{J}_x \rangle$ for various values of N, while (b) shows the squeezing. The black and blue curves corresponds to the F-function case, and are similar to what is shown in fig. 3.6, while the pink and red curves shows the results of the Schwinger model. The black and the pink curves corresponds to $N = 2$, and the remaining curves corresponds to $N = 4$, 6, 8, 10, and 20 just like in fig. 3.6.

since among the terms in the expressions for these operators involving the $\hat{\alpha}$-operator, only those involving the combination $\hat{\alpha}\hat{\alpha}^\dagger$ will contribute. These results can be compared to the results for the full calculation obtained in the next chapter, given by (6.52).

From (5.46) we can calculate

$$N_0 = \frac{N}{2} + \langle \hat{J}_x \rangle \tag{5.47}$$

and

$$(\Delta J_z)^2 = \frac{\frac{N}{2} + \langle \hat{J}_x \rangle}{4} \left(1 + 2 \left(\frac{N}{2} - \langle \hat{J}_x \rangle \right) - 2\sqrt{\frac{N}{2} - \langle \hat{J}_x \rangle} \sqrt{1 + \frac{N}{2} - \langle \hat{J}_x \rangle} \right) \tag{5.48}$$

where $N \equiv \langle \hat{N} \rangle$ is the total particle number.

A plot of $(\Delta J_z)^2$ vs. $\langle \hat{J}_x \rangle$ similar to the F-function defined by (3.31) can be seen in fig. 5.9a. We see that as N increases, the result of the Schwinger model approaches the F-function, and for $N \gtrsim 1000$ the two functions are almost indistinguishable. This is a surprise, since we can calculate from (5.47) that the Holstein-Primakoff approximation becomes linearly worse the further we are from the point $\langle \hat{J}_x \rangle = J$ around which the perturbation is done. But regardless of the value of N, the value of $(\Delta J_z)^2$ in $\langle \hat{J}_x \rangle = 0$ will never become zero[25] entirely, indicating that the squeezing parameter will be infinite in that point. This was the point where the F-functions

[25] As $N \to \infty$, $(\Delta J_z)^2 \to 1/16$.

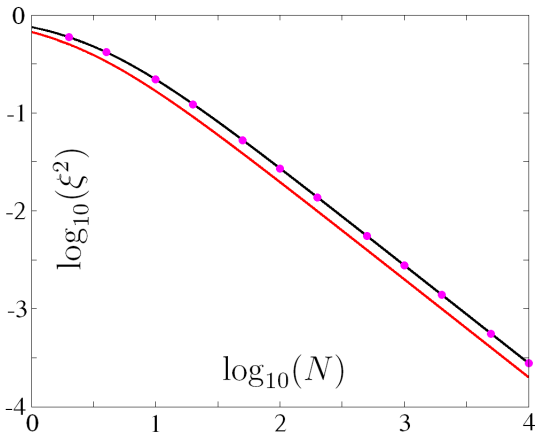

Figure 5.10: The black curve is the result given by (5.50), and the pink points are a few of the points to which (5.50) is fitted. The red curve shows the result for the F-functions given by (3.39).

had their maximal squeezing, but for the Schwinger model that point lies elsewhere. The squeezing parameter can be found to be

$$\xi^2 = N\frac{\frac{N}{2}+\langle\hat{J}_x\rangle}{4\langle\hat{J}_x\rangle^2}\left(1+2\left(\frac{N}{2}-\langle\hat{J}_x\rangle\right)-2\sqrt{\frac{N}{2}-\langle\hat{J}_x\rangle}\sqrt{1+\frac{N}{2}-\langle\hat{J}_x\rangle}\right) \tag{5.49}$$

and a plot of ξ^2 as a function of $\langle\hat{J}_x\rangle$ can be seen in fig. 5.9b.

We want to find the minimal squeezing for each value of N. This can be done numerically, and inspired by (3.39) we fit a function $\xi^2 = a/(N+b)$ to the results. This gives us an expression for the minimal squeezing parameter[26]

$$\xi^2 = \frac{2.784}{N+2.709} \tag{5.50}$$

which is plotted in fig. 5.10. A comparison with (3.39) shows that $\xi^2_{Sch} = 1.392\cdot\xi^2_F$ for large N, showing that less squeezing is produced by the Schwinger model than by the two-mode approximation, even though the scaling with the particle number is the same.

[26] The fit to $\xi^2 = a/(N+b)$ gives the values $a = 2.7839\pm0.0009$ and $b = 2.7086\pm0.0022$. Initially I fitted $a/(N+b)^c$ which gave a $c = 1.0044\pm0.0003$ almost but not entirely consistent with $c = 1$. On the other hand the other parameters gave $a = 2.8297\pm0.0029$ and $b = 2.7565\pm0.0031$ where we see that the uncertainties are greater than they are in the $c = 1$ case. Another option is to fit $a/(N+a)$ which gives $a = 2.8167\pm0.0034$, which also has a higher uncertainty than the ab case.

Chapter 6

The full Bogoliubov calculation

At last we are ready to do the full Bogoliubov calculation central to this thesis. The calculation will be split into a first and second part as described in section 5.6.

6.1 The full calculation: first part

We want to diagonalize the two-species Hamiltonian (5.11)

$$\begin{aligned}\hat{\mathcal{H}} &= \int \mathrm{d}\mathbf{r}\Big(\hat{\Psi}_+^\dagger(\mathbf{r})H_0\hat{\Psi}_+(\mathbf{r}) + \hat{\Psi}_-^\dagger(\mathbf{r})H_0\hat{\Psi}_-(\mathbf{r}) + U\left(\hat{\Psi}_+^\dagger(\mathbf{r})\hat{\Psi}_-^\dagger(\mathbf{r})\hat{\Psi}_+(\mathbf{r})\hat{\Psi}_-(\mathbf{r})\right) \\ &\quad + \frac{U+U_{ab}}{4}\left(\hat{\Psi}_+^\dagger(\mathbf{r})\hat{\Psi}_+^\dagger(\mathbf{r})\hat{\Psi}_+(\mathbf{r})\hat{\Psi}_+(\mathbf{r}) + \hat{\Psi}_-^\dagger(\mathbf{r})\hat{\Psi}_-^\dagger(\mathbf{r})\hat{\Psi}_-(\mathbf{r})\hat{\Psi}_-(\mathbf{r})\right) \\ &\quad + \frac{U-U_{ab}}{4}\left(\hat{\Psi}_+^\dagger(\mathbf{r})\hat{\Psi}_+^\dagger(\mathbf{r})\hat{\Psi}_-(\mathbf{r})\hat{\Psi}_-(\mathbf{r}) + \hat{\Psi}_-^\dagger(\mathbf{r})\hat{\Psi}_-^\dagger(\mathbf{r})\hat{\Psi}_+(\mathbf{r})\hat{\Psi}_+(\mathbf{r})\right) \\ &\quad + \frac{\Omega}{2}\left(\hat{\Psi}_+^\dagger(\mathbf{r})\hat{\Psi}_+(\mathbf{r}) - \hat{\Psi}_-^\dagger(\mathbf{r})\hat{\Psi}_-(\mathbf{r})\right)\Big) \end{aligned} \tag{6.1}$$

A large value of $-\Omega$ will cause the Ω-term in (6.1) to be dominant, so in that case the lowest energy state will be one where all the particles are in the $\hat{\Psi}_+$-state, which means that this is where the condensate will be. The following calculations will be perturbations around this state, which justifies the approximation of small $\delta\hat{\psi}$, where the $\delta\hat{\psi}$s are defined by the rewritings

$$\begin{aligned}\hat{\Psi}_+(\mathbf{r}) &= \sum_i \hat{c}_{i+}\varphi_{i+}(\mathbf{r}) = \hat{c}_{0+}\varphi_{0+}(\mathbf{r}) + \sum_{i>0}\hat{c}_{i+}\varphi_{i+}(\mathbf{r}) \equiv \hat{c}\varphi(\mathbf{r}) + \delta\hat{\psi}_+(\mathbf{r}) \\ \hat{\Psi}_-(\mathbf{r}) &= \sum_i \hat{c}_{i-}\varphi_{i-}(\mathbf{r}) \equiv \delta\hat{\psi}_-(\mathbf{r}) \end{aligned} \tag{6.2}$$

Assuming $\delta\hat{\psi}(\mathbf{r})$ to be small enables us to ignore terms of more than second order in $\delta\hat{\psi}$, which allow us to write $\hat{\mathcal{H}}$ as

$$\hat{\mathcal{H}} \equiv \hat{\mathcal{H}}_0 + \hat{\mathcal{H}}_1 + \hat{\mathcal{H}}_2 + \mathcal{O}(\delta\hat{\psi}^3) \tag{6.3}$$

where

$$\hat{\mathcal{H}}_0 \equiv \int \mathrm{d}\mathbf{r}\left(\varphi^* H_0 \varphi \hat{c}^\dagger \hat{c} + \frac{U+U_{ab}}{4}|\varphi|^4 \hat{c}^\dagger \hat{c}^\dagger \hat{c}\hat{c} + \frac{\Omega}{2}|\varphi|^2 \hat{c}^\dagger \hat{c}\right) \tag{6.4}$$

$$\begin{aligned}\hat{\mathcal{H}}_1 \equiv \int \mathrm{d}\mathbf{r}\Big(&\delta\hat{\psi}_+^\dagger H_0 \varphi \hat{c} + \varphi^* \hat{c}^\dagger H_0 \delta\hat{\psi}_+ + \frac{\Omega}{2}\left(\delta\hat{\psi}_+^\dagger \varphi \hat{c} + \varphi^* \hat{c}^\dagger \delta\hat{\psi}_+\right) \\ &+ \frac{U+U_{ab}}{4}\left(2\delta\hat{\psi}_+^\dagger |\varphi|^2 \varphi \hat{c}^\dagger \hat{c}\hat{c} + 2\varphi^* |\varphi|^2 \hat{c}^\dagger \hat{c}^\dagger \hat{c}\delta\hat{\psi}_+\right)\Big)\end{aligned} \tag{6.5}$$

$$\begin{aligned}\hat{\mathcal{H}}_2 = \int \mathrm{d}\mathbf{r}\Big(&\delta\hat{\psi}_+^\dagger H_0 \delta\hat{\psi}_+ + \delta\hat{\psi}_-^\dagger H_0 \delta\hat{\psi}_- + \frac{\Omega}{2}\left(\delta\hat{\psi}_+^\dagger \delta\hat{\psi}_+ - \delta\hat{\psi}_-^\dagger \delta\hat{\psi}_-\right) \\ &+ \frac{U+U_{ab}}{4}\left(\delta\hat{\psi}_+^\dagger \delta\hat{\psi}_+^\dagger \hat{c}\hat{c}(\varphi)^2 + \hat{c}^\dagger \hat{c}^\dagger (\varphi^*)^2 \delta\hat{\psi}_+ \delta\hat{\psi}_+ + 4\hat{c}^\dagger \hat{c}|\varphi|^2 \delta\hat{\psi}_+^\dagger \delta\hat{\psi}_+\right) \\ &+ \frac{U-U_{ab}}{4}\left(\hat{c}^\dagger \hat{c}^\dagger (\varphi^*)^2 \delta\hat{\psi}_- \delta\hat{\psi}_- + \delta\hat{\psi}_-^\dagger \delta\hat{\psi}_-^\dagger \hat{c}\hat{c}(\varphi)^2\right) + U\left(\hat{c}^\dagger \hat{c}|\varphi|^2 \delta\hat{\psi}_-^\dagger \delta\hat{\psi}_-\right)\Big)\end{aligned} \tag{6.6}$$

We see that $\hat{\mathcal{H}}_0$, $\hat{\mathcal{H}}_1$, and $\hat{\mathcal{H}}_2$ are terms of zeroth, first, and second order in $\delta\hat{\psi}$ respectively. For clarity, the $\mathbf{r}$-dependence is no longer written explicitly from (6.4) and onward. We see that the expression for $\hat{\mathcal{H}}_0$ (6.4) is equivalent to (5.2), the expression for $\hat{\mathcal{H}}$ derived using the two-mode approximation. This means that to zeroth order we expect the behaviour of $\Delta J_z(\langle \hat{J}_x \rangle)$ to be similar to the F-functions derived in section 3.4. But since the F-functions describes the absolute maximal squeezing, we expect the corrections coming from the higher order terms to be in the direction of decreased squeezing.

We want to rewrite $\hat{\mathcal{H}}_0$ to to be a function of a new operator $\hat{\mathfrak{c}}$ for which $\hat{N} = \hat{\mathfrak{c}}^\dagger \hat{\mathfrak{c}}$, is the total particle number operator. This should be compared to the usual $\hat{c}$-operators for which $\langle \hat{c}^\dagger \hat{c} \rangle = N_0$, the number of particles in the condensate. The reason for introducing the $\hat{\mathfrak{c}}$-operators is that while the number of particles in the condensate mode can fluctuate, the total number of particles is a constant, making terms in $\hat{\mathcal{H}}$ proportional only to this operator constant as well.

We can rewrite the $\hat{N}$-operator as

$$\begin{aligned}\hat{N} &= \int \mathrm{d}\mathbf{r}\left(\hat{\Psi}_+^\dagger \hat{\Psi}_+ + \hat{\Psi}_-^\dagger \hat{\Psi}_-\right) = \hat{c}^\dagger \hat{c} + \int \mathrm{d}\mathbf{r}\left(\delta\hat{\psi}_+^\dagger \delta\hat{\psi}_+ + \delta\hat{\psi}_-^\dagger \delta\hat{\psi}_-\right) \Leftrightarrow \\ \hat{c}^\dagger \hat{c} &= \hat{\mathfrak{c}}^\dagger \hat{\mathfrak{c}} - \delta\hat{n}\end{aligned} \tag{6.7}$$

where $\delta\hat{n} \equiv \int \mathrm{d}\mathbf{r}\left(\delta\hat{\psi}_+^\dagger \delta\hat{\psi}_+ + \delta\hat{\psi}_-^\dagger \delta\hat{\psi}_-\right)$. Since $\delta\hat{n}$ is of order $(\delta\hat{\psi})^2$, we can ignore terms of more than first order in $\delta\hat{n}$ when we insert the above in the expression for $\hat{\mathcal{H}}_0$.

$$\begin{aligned}
\hat{\mathcal{H}}_0 &= \int \mathrm{d}\mathbf{r}\Big(\varphi^* H_0 \varphi \left(\hat{\mathfrak{c}}^\dagger\hat{\mathfrak{c}} - \delta\hat{n}\right) + \frac{\Omega}{2}|\varphi|^2\left(\hat{\mathfrak{c}}^\dagger\hat{\mathfrak{c}} - \delta\hat{n}\right) \\
&\quad + \frac{U+U_{ab}}{4}|\varphi|^4\left(\left(\hat{\mathfrak{c}}^\dagger\hat{\mathfrak{c}} - \delta\hat{n}\right)^2 - \left(\hat{\mathfrak{c}}^\dagger\hat{\mathfrak{c}} - \delta\hat{n}\right)\right)\Big) \\
&\approx \int \mathrm{d}\mathbf{r}\Big(\varphi^* H_0\varphi\hat{\mathfrak{c}}^\dagger\hat{\mathfrak{c}} + \frac{U+U_{ab}}{4}|\varphi|^4\hat{\mathfrak{c}}^\dagger\hat{\mathfrak{c}}^\dagger\hat{\mathfrak{c}}\hat{\mathfrak{c}} + \frac{\Omega}{2}|\varphi|^2\hat{\mathfrak{c}}^\dagger\hat{\mathfrak{c}}\Big) \\
&\quad - \int \mathrm{d}\mathbf{r}\Big(\varphi^* H_0\varphi\delta\hat{n} + \frac{U+U_{ab}}{2}|\varphi|^4\delta\hat{n} + \frac{\Omega}{2}|\varphi|^2\delta\hat{n}\Big) \\
&= \hat{\mathfrak{H}}_0 - \int \mathrm{d}\mathbf{r}\varphi^*\mu\varphi\delta\hat{n} \;=\; \mathfrak{H}_0 - \mu\delta\hat{n} \\
&= \hat{\mathfrak{H}}_0 - \mu\int \mathrm{d}\mathbf{r}\left(\delta\hat{\psi}_+^\dagger\delta\hat{\psi}_+ + \delta\hat{\psi}_-^\dagger\delta\hat{\psi}_-\right) \qquad (6.8)
\end{aligned}$$

where

$$\hat{\mathfrak{H}}_0 \;\equiv\; \int \mathrm{d}\mathbf{r}\Big(\varphi^* H_0\varphi\hat{\mathfrak{c}}^\dagger\hat{\mathfrak{c}} + \frac{U+U_{ab}}{4}|\varphi|^4\hat{\mathfrak{c}}^\dagger\hat{\mathfrak{c}}^\dagger\hat{\mathfrak{c}}\hat{\mathfrak{c}} + \frac{\Omega}{2}|\varphi|^2\hat{\mathfrak{c}}^\dagger\hat{\mathfrak{c}}\Big) \qquad (6.9)$$

The approximation in (6.8) consists of assuming that $N \gg 1$ and of skipping terms of second order in $\delta\hat{n}$. As part of the calculation we used the GPE (5.12), where we identified the first quantization many-body wave functions ψ with the term $\varphi\hat{\mathfrak{c}}$.

When handling the $\hat{\mathcal{H}}_1$-term (6.5) we observe that by using[1] the GPE (5.12), it can be rewritten to

$$\hat{\mathcal{H}}_1 \;=\; \mu\int \mathrm{d}\mathbf{r}\Big(\delta\hat{\psi}_+^\dagger\varphi\hat{c} + \hat{c}^\dagger\varphi^*\delta\hat{\psi}_+\Big) = 0 \qquad (6.10)$$

where the last equality is true due to the orthonormality of the φ_i-functions in the expression $\hat{\Psi}(\mathbf{r}) = \sum_i \varphi_i(\mathbf{r})\hat{c}_i$. This means that $\mathcal{H}$ has no contributions to first order in $\delta\hat{\psi}$.

Let us now define an operator $\hat{\Lambda}$ as

$$\hat{\Lambda}_\pm(\mathbf{r}) \;\equiv\; \frac{\hat{c}^\dagger\delta\hat{\psi}_\pm(\mathbf{r})}{\sqrt{N}} \qquad (6.11)$$

and insert it in the results for $\hat{\mathcal{H}}_0$, $\hat{\mathcal{H}}_1$, and $\hat{\mathcal{H}}_2$. This gives us an expression for the total $\hat{\mathcal{H}}$

$$\begin{aligned}
\hat{\mathcal{H}} &= \hat{\mathfrak{H}}_0 + \int \mathrm{d}\mathbf{r}\Big(\hat{\Lambda}_+^\dagger(H_0-\mu)\hat{\Lambda}_+ + \hat{\Lambda}_-^\dagger(H_0-\mu)\hat{\Lambda}_- + \frac{\Omega}{2}\Big(\hat{\Lambda}_+^\dagger\hat{\Lambda}_+ - \hat{\Lambda}_-^\dagger\hat{\Lambda}_-\Big) \\
&\quad + \frac{U+U_{ab}}{4}\Big(\hat{\Lambda}_+^\dagger\hat{\Lambda}_+^\dagger(\psi)^2 + (\psi^*)^2\hat{\Lambda}_+\hat{\Lambda}_+ + 4|\psi|^2\hat{\Lambda}_+^\dagger\hat{\Lambda}_+\Big) \qquad (6.12) \\
&\quad + \frac{U-U_{ab}}{4}\Big((\psi^*)^2\hat{\Lambda}_-\hat{\Lambda}_- + \hat{\Lambda}_-^\dagger\hat{\Lambda}_-^\dagger(\psi)^2\Big) + U\Big(|\psi|^2\hat{\Lambda}_-^\dagger\hat{\Lambda}_-\Big)\Big)
\end{aligned}$$

[1] Here we identify the first quantization wave function ψ with the term $\varphi\hat{c}$.

which can be rewritten to[2]

$$\hat{\mathcal{H}} = \hat{\mathfrak{H}}_0 + \frac{1}{2}\int \mathrm{d}\mathbf{r}\bar{\Lambda}_+^\dagger \mathcal{M}_+ \bar{\Lambda}_+ + \frac{1}{2}\int \mathrm{d}\mathbf{r}\bar{\Lambda}_-^\dagger \mathcal{M}_- \bar{\Lambda}_- \tag{6.13}$$

where

$$\bar{\Lambda}_\pm \equiv \begin{pmatrix} \hat{\Lambda}_\pm(\mathbf{r}) \\ \hat{\Lambda}_\pm^\dagger(\mathbf{r}) \end{pmatrix} \tag{6.14}$$

and

$$\mathcal{M}_\pm \equiv \begin{bmatrix} A_\pm & B_\pm \\ B_\pm^* & A_\pm \end{bmatrix} \tag{6.15}$$

where

$$\begin{aligned} A_+ &\equiv H_0 - \mu + (U + U_{ab})|\psi|^2 + \frac{\Omega}{2} \\ B_+ &\equiv \frac{(U + U_{ab})}{2}(\psi)^2 \\ A_- &\equiv H_0 - \mu + U|\psi|^2 - \frac{\Omega}{2} \\ B_- &\equiv \frac{(U - U_{ab})}{2}(\psi)^2 \end{aligned} \tag{6.16}$$

With (6.13) we have written the Hamiltonian on a form that enables us to do the Bogoliubov transform, which is the subject of the next section.

6.2 The full calculation: second part

Let us define a function $\mathcal{Q}(\mathbf{r}, \mathbf{r}')$ as

$$\mathcal{Q}(\mathbf{r}, \mathbf{r}') \equiv \delta(\mathbf{r} - \mathbf{r}') - \varphi(\mathbf{r})\varphi^*(\mathbf{r}') \tag{6.17}$$

and a corresponding operator $\mathcal{Q}\circ$ as

$$\mathcal{Q}\circ f(\mathbf{r}) \equiv \int \mathrm{d}\mathbf{r}'\Big(\delta(\mathbf{r} - \mathbf{r}') - \varphi(\mathbf{r})\varphi^*(\mathbf{r}')\Big) f(\mathbf{r}') \tag{6.18}$$

This operator functions as a projection operator into the hyperplane perpendicular to $\varphi(\mathbf{r})$. This can be seen by considering a function $g(\mathbf{r}) = \kappa\xi(\mathbf{r}) + k\varphi(\mathbf{r})$ where $\xi(\mathbf{r})$

[2]This step may appear like cheating, since we disregard the commutator $\left[\delta\hat{\psi}^\dagger(\mathbf{r}), \delta\hat{\psi}(\mathbf{r})\right] = \varphi^*(\mathbf{r})\varphi(\mathbf{r}) - \delta(0)$, which is actually infinite. One can always disregard a constant term in a Hamiltonian, but when that term is infinite it seems questionable. Is is, however, all right, and this issue is a part of a larger discussion about renormalization which will not be discussed further here.

is perpendicular[3] to $\varphi(\mathbf{r})$ and k and κ are some constants. The result is $\mathcal{Q}\circ g(\mathbf{r}) = \kappa\xi(\mathbf{r})$, which is what defines a projection operator. We notice that the function $\mathcal{Q}(\mathbf{r},\mathbf{r}')$ obeys $\mathcal{Q}(\mathbf{r},\mathbf{r}') = \mathcal{Q}^*(\mathbf{r}',\mathbf{r})$ and $\int \mathrm{d}\mathbf{r}''\mathcal{Q}(\mathbf{r},\mathbf{r}'')\mathcal{Q}(\mathbf{r}'',\mathbf{r}') = \mathcal{Q}(\mathbf{r},\mathbf{r}')$, which are results we will use later.

Let us do the Bogoliubov transform by writing the functions $\hat{\Lambda}_+(\mathbf{r})$ and $\hat{\Lambda}_-(\mathbf{r})$ as

$$\begin{aligned}\hat{\Lambda}_+(\mathbf{r}) &= \sum_{i>0}\mathcal{Q}\circ\left(u_{i+}(\mathbf{r})\hat{\alpha}_{i+} + v_{i+}(\mathbf{r})\hat{\alpha}^\dagger_{i+}\right)\\ \hat{\Lambda}_-(\mathbf{r}) &= \sum_{i}\left(u_{i-}(\mathbf{r})\hat{\alpha}_{i-} + v_{i-}(\mathbf{r})\hat{\alpha}^\dagger_{i-}\right)\end{aligned} \tag{6.19}$$

The reason for the $\mathcal{Q}\circ$-operator and the counting from one in the expression for the $\hat{\Lambda}_+$-operator, is that the $\delta\hat{\psi}_+$-operator and therefore also the $\hat{\Lambda}_+$-operator has to be perpendicular to φ. When we have this extra requirement, we know that the terms on the right hand side of (6.19) must span a function space one dimension smaller than that of the φ_{i+}-functions, and this is ensured by skipping the 0+-mode. The requirement that the skipped function is φ_{0+} and not something arbitrary, is ensured by the $\mathcal{Q}$-operator.

The $u(\mathbf{r})$ and $v(\mathbf{r})$-functions should be found so that insertion of (6.19) results in

$$\begin{aligned}\int \mathrm{d}\mathbf{r}\bar{\Lambda}^\dagger_+\mathcal{M}_+\bar{\Lambda}_+ &= \sum_{i>0}\varepsilon_{i+}\left(\hat{\alpha}^\dagger_{i+}\hat{\alpha}_{i+} + \hat{\alpha}_{i+}\hat{\alpha}^\dagger_{i+}\right)\\ \int \mathrm{d}\mathbf{r}\bar{\Lambda}^\dagger_-\mathcal{M}_-\bar{\Lambda}_- &= \sum_{i}\varepsilon_{i-}\left(\hat{\alpha}^\dagger_{i-}\hat{\alpha}_{i-} + \hat{\alpha}_{i-}\hat{\alpha}^\dagger_{i-}\right)\end{aligned} \tag{6.20}$$

which will diagonalize the Hamiltonian (6.13) giving it the form[4]

$$\hat{\mathcal{H}} = \hat{\mathfrak{H}}_0 + \sum_{i>0}\left(\varepsilon_{i+}\hat{\alpha}^\dagger_{i+}\hat{\alpha}_{i+}\right) + \sum_{i}\left(\varepsilon_{i-}\hat{\alpha}^\dagger_{i-}\hat{\alpha}_{i-}\right) \tag{6.21}$$

The reason for this rewriting of the Hamiltonian is that it insures that the energy eigenstates are the same as the number states in the $\hat{\alpha}$-basis, which makes them much easier to calculate as long as the states are expressed in this basis.

The goal of this section is to find a way to calculate a set of $u(\mathbf{r})$ and $v(\mathbf{r})$-functions making this diagonalization possible, and in order to achieve this goal we will take a look at the commutators. The derivation will be made for the plus-operators since the calculation for the minus-operators is similar but simpler, so for the rest of this section $\hat{\alpha}_i$, u_i and v_i will refer to $\hat{\alpha}_{i+}$, u_{i+}, and v_{i+}.

[3] Perpendicular means that $\int \mathrm{d}\mathbf{r}\varphi^*(\mathbf{r})\xi(\mathbf{r}) = 0$.

[4] Yet again we skip an infinite but constant term in the Hamiltonian! This is the term $\sum_i(\varepsilon_i^+ + \varepsilon_i^-)$. Like in the previous case this is allowed for reasons related to renormalization.

We want all the involved operators to obey the canonical commutation relations. That is

$$\left[\hat{\alpha}_i, \hat{\alpha}_j^\dagger\right] = \delta_{ij} \ , \quad [\hat{\alpha}_i, \hat{\alpha}_j] = \left[\hat{\alpha}_i^\dagger, \hat{\alpha}_j^\dagger\right] = 0 \tag{6.22}$$

and

$$\left[\hat{\Psi}(\mathbf{r}), \hat{\Psi}^\dagger(\mathbf{r}')\right] = \delta(\mathbf{r}-\mathbf{r}') \ , \quad \left[\hat{\Psi}^\dagger(\mathbf{r}), \hat{\Psi}^\dagger(\mathbf{r}')\right] = \left[\hat{\Psi}(\mathbf{r}), \hat{\Psi}(\mathbf{r}')\right] = 0 \tag{6.23}$$

From the final set of these, we can derive

$$\left[\delta\hat{\psi}(\mathbf{r}), \delta\hat{\psi}^\dagger(\mathbf{r}')\right] = \mathcal{Q}(\mathbf{r},\mathbf{r}') \ , \quad \left[\delta\hat{\psi}^\dagger(\mathbf{r}), \delta\hat{\psi}^\dagger(\mathbf{r}')\right] = \left[\delta\hat{\psi}(\mathbf{r}), \delta\hat{\psi}(\mathbf{r}')\right] = 0 \tag{6.24}$$

and[5]

$$\left[\hat{\Lambda}(\mathbf{r}), \hat{\Lambda}^\dagger(\mathbf{r}')\right] = \mathcal{Q}(\mathbf{r},\mathbf{r}') \ , \quad \left[\hat{\Lambda}^\dagger(\mathbf{r}), \hat{\Lambda}^\dagger(\mathbf{r}')\right] = \left[\hat{\Lambda}(\mathbf{r}), \hat{\Lambda}(\mathbf{r}')\right] = 0 \tag{6.25}$$

Let us insert (6.19) in (6.25). Insertion in the $\left[\hat{\Lambda}, \hat{\Lambda}^\dagger\right]$-term gives

$$\begin{aligned}
\left[\hat{\Lambda}(\mathbf{r}), \hat{\Lambda}^\dagger(\mathbf{r}')\right] &= \sum_{ij>0} \Big(\mathcal{Q}\circ\Big(u_i(\mathbf{r})\hat{\alpha}_i + v_i(\mathbf{r})\hat{\alpha}_i^\dagger\Big)\ \mathcal{Q}^*\circ\Big(u_j^*(\mathbf{r}')\hat{\alpha}_j^\dagger + v_j^*(\mathbf{r}')\hat{\alpha}_j\Big) \\
&\qquad -\mathcal{Q}^*\circ\Big(u_j^*(\mathbf{r}')\hat{\alpha}_j^\dagger + v_j^*(\mathbf{r}')\hat{\alpha}_j\Big)\ \mathcal{Q}\circ\Big(u_i(\mathbf{r})\hat{\alpha}_i + v_i(\mathbf{r})\hat{\alpha}_i^\dagger\Big)\Big) \Leftrightarrow \\
\mathcal{Q}(\mathbf{r},\mathbf{r}') &= \sum_{i>0}\big(\mathcal{Q}\circ u_i(\mathbf{r})\ \mathcal{Q}^*\circ u_i^*(\mathbf{r}') - \mathcal{Q}\circ v_i(\mathbf{r})\ \mathcal{Q}^*\circ v_i^*(\mathbf{r}')\big)
\end{aligned} \tag{6.26}$$

and insertion in the $\left[\hat{\Lambda}, \hat{\Lambda}\right]$-term gives similarly

$$\begin{aligned}
\left[\hat{\Lambda}(\mathbf{r}), \hat{\Lambda}(\mathbf{r}')\right] &= \sum_{ij>0} \Big(\mathcal{Q}\circ\Big(u_i(\mathbf{r})\hat{\alpha}_i + v_i(\mathbf{r})\hat{\alpha}_i^\dagger\Big)\ \mathcal{Q}\circ\Big(u_j(\mathbf{r}')\hat{\alpha}_j + v_j(\mathbf{r}')\hat{\alpha}_j^\dagger\Big) \\
&\qquad -\mathcal{Q}\circ\Big(u_j(\mathbf{r}')\hat{\alpha}_j + v_j(\mathbf{r}')\hat{\alpha}_j^\dagger\Big)\ \mathcal{Q}\circ\Big(u_i(\mathbf{r})\hat{\alpha}_i + v_i(\mathbf{r})\hat{\alpha}_i^\dagger\Big)\Big) \Leftrightarrow \\
0 &= \sum_{i>0}\big(\mathcal{Q}\circ u_i(\mathbf{r})\ \mathcal{Q}\circ v_i(\mathbf{r}') - \mathcal{Q}\circ v_i(\mathbf{r})\ \mathcal{Q}\circ u_i(\mathbf{r}')\big)
\end{aligned} \tag{6.27}$$

(6.26) plays a role as a completeness relation for the u and v-functions.

We want to invert (6.19) in order to express the $\hat{\alpha}$-operators as functions of the $\hat{\Lambda}$-operators. We assume that (6.19) can be inverted to

$$\hat{\alpha}_i = \int \mathrm{d}\mathbf{r}\,\Big(h_i(\mathbf{r})\hat{\Lambda}(\mathbf{r}) + k_i(\mathbf{r})\hat{\Lambda}^\dagger(\mathbf{r})\Big) \tag{6.28}$$

[5] In all the $\left[\hat{\Lambda}, \hat{\Lambda}\right]$-terms we disregard a term of order N^{-1}.

where $h_i(\mathbf{r})$ and $k_i(\mathbf{r})$ are some functions, which we are going to derive. Inserting in (6.19) gives

$$\begin{aligned}\hat{\Lambda}(\mathbf{r}) &= \sum_{i>0}\mathcal{Q}\circ\Big(u_i(\mathbf{r})\int \mathrm{d}\mathbf{r}'\left(h_i(\mathbf{r}')\hat{\Lambda}(\mathbf{r}')+k_i(\mathbf{r}')\hat{\Lambda}^\dagger(\mathbf{r}')\right)\\ &\quad +v_i(\mathbf{r})\int \mathrm{d}\mathbf{r}''\left(h_i^*(\mathbf{r}'')\hat{\Lambda}^\dagger(\mathbf{r}'')+k_i^*(\mathbf{r}'')\hat{\Lambda}(\mathbf{r}'')\right)\Big)\\ &= \int \mathrm{d}\mathbf{r}'\sum_{i>0}\Big(\Big(\mathcal{Q}\circ u_i(\mathbf{r})h_i(\mathbf{r}')+\mathcal{Q}\circ v_i(\mathbf{r})k_i^*(\mathbf{r}')\Big)\hat{\Lambda}(\mathbf{r}')\\ &\quad +\Big(\mathcal{Q}\circ u_i(\mathbf{r})k_i(\mathbf{r}')+\mathcal{Q}\circ v_i(\mathbf{r})h_i^*(\mathbf{r}')\Big)\hat{\Lambda}^\dagger(\mathbf{r}')\Big) \qquad (6.29)\end{aligned}$$

which is consistent only if the functions $h_i(\mathbf{r})$ and $k_i(\mathbf{r})$ makes the right hand side equal to $\hat{\Lambda}(\mathbf{r})$ as it should be. If $h_i(\mathbf{r})=\mathcal{Q}^*\circ u_i^*(\mathbf{r})$ and $k_i(\mathbf{r})=-\mathcal{Q}\circ v_i(\mathbf{r})$ the $\hat{\Lambda}^\dagger$-term is seen from (6.27) to be zero as required, and the coefficient to the $\hat{\Lambda}$-term will become $\mathcal{Q}(\mathbf{r},\mathbf{r}')$ which can be seen to give one after the $\mathbf{r}'$-integration since $\hat{\Lambda}(\mathbf{r})$ is perpendicular to $\varphi(\mathbf{r})$. Therefore do this choice of h_i and k_i fulfil our requirement. This means that (6.28) should be written

$$\hat{\alpha}_i=\int \mathrm{d}\mathbf{r}\left(\mathcal{Q}^*\circ u_i^*(\mathbf{r})\hat{\Lambda}(\mathbf{r})-\mathcal{Q}\circ v_i(\mathbf{r})\hat{\Lambda}^\dagger(\mathbf{r})\right) \qquad (6.30)$$

which is consistent with (6.19).

Let us compare the commutators once again, this time the other way around, using the above relation:

$$\begin{aligned}\left[\hat{\alpha}_i,\hat{\alpha}_j^\dagger\right] &= \iint \mathrm{d}\mathbf{r}\mathrm{d}\mathbf{r}'\left(\mathcal{Q}^*\circ u_i^*(\mathbf{r})\hat{\Lambda}(\mathbf{r})-\mathcal{Q}\circ v_i(\mathbf{r})\hat{\Lambda}^\dagger(\mathbf{r})\right)\left(\mathcal{Q}\circ u_j(\mathbf{r}')\hat{\Lambda}^\dagger(\mathbf{r}')-\mathcal{Q}^*\circ v_j^*(\mathbf{r}')\hat{\Lambda}(\mathbf{r}')\right)\\ &\quad -\iint \mathrm{d}\mathbf{r}\mathrm{d}\mathbf{r}'\left(\mathcal{Q}\circ u_j(\mathbf{r})\hat{\Lambda}^\dagger(\mathbf{r})-\mathcal{Q}^*\circ v_j^*(\mathbf{r})\hat{\Lambda}(\mathbf{r})\right)\left(\mathcal{Q}^*\circ u_i^*(\mathbf{r}')\hat{\Lambda}(\mathbf{r}')-\mathcal{Q}\circ v_i(\mathbf{r}')\hat{\Lambda}^\dagger(\mathbf{r}')\right)\\ &= \iint \mathrm{d}\mathbf{r}\mathrm{d}\mathbf{r}'\Big(\mathcal{Q}^*\circ u_i^*(\mathbf{r})\;\mathcal{Q}\circ u_j(\mathbf{r}')\left[\hat{\Lambda}(\mathbf{r}),\hat{\Lambda}^\dagger(\mathbf{r}')\right]-\mathcal{Q}^*\circ u_i^*(\mathbf{r})\;\mathcal{Q}^*\circ v_j^*(\mathbf{r}')\left[\hat{\Lambda}(\mathbf{r}),\hat{\Lambda}(\mathbf{r}')\right]\\ &\quad -\mathcal{Q}\circ v_i(\mathbf{r})\;\mathcal{Q}\circ u_j(\mathbf{r}')\left[\hat{\Lambda}^\dagger(\mathbf{r}),\hat{\Lambda}^\dagger(\mathbf{r}')\right]+\mathcal{Q}\circ v_i(\mathbf{r})\;\mathcal{Q}^*\circ v_j^*(\mathbf{r}')\left[\hat{\Lambda}^\dagger(\mathbf{r}),\hat{\Lambda}(\mathbf{r}')\right]\Big)\Leftrightarrow\\ \delta_{ij} &= \iint \mathrm{d}\mathbf{r}\mathrm{d}\mathbf{r}'\Big(u_i^*(\mathbf{r})\mathcal{Q}(\mathbf{r},\mathbf{r}')u_j(\mathbf{r}')-v_i(\mathbf{r})\mathcal{Q}^*(\mathbf{r},\mathbf{r}')v_j^*(\mathbf{r}')\Big) \qquad (6.31)\end{aligned}$$

and

$$\begin{aligned}
[\hat{\alpha}_i, \hat{\alpha}_j] &= \iint \mathrm{d}\mathbf{r}\mathrm{d}\mathbf{r}' \left(\mathcal{Q}^*\circ u_i^*(\mathbf{r})\hat{\Lambda}(\mathbf{r}) - \mathcal{Q}\circ v_i(\mathbf{r})\hat{\Lambda}^\dagger(\mathbf{r})\right)\left(\mathcal{Q}^*\circ u_j^*(\mathbf{r}')\hat{\Lambda}(\mathbf{r}') - \mathcal{Q}\circ v_j(\mathbf{r}')\hat{\Lambda}^\dagger(\mathbf{r}')\right) \\
&\quad - \iint \mathrm{d}\mathbf{r}\mathrm{d}\mathbf{r}' \left(\mathcal{Q}^*\circ u_j^*(\mathbf{r})\hat{\Lambda}(\mathbf{r}) - \mathcal{Q}\circ v_j(\mathbf{r})\hat{\Lambda}^\dagger(\mathbf{r})\right)\left(\mathcal{Q}^*\circ u_i^*(\mathbf{r}')\hat{\Lambda}(\mathbf{r}') - \mathcal{Q}\circ v_i(\mathbf{r}')\hat{\Lambda}^\dagger(\mathbf{r}')\right) \\
&= \iint \mathrm{d}\mathbf{r}\mathrm{d}\mathbf{r}' \Big(\mathcal{Q}^*\circ u_i^*(\mathbf{r})\ \mathcal{Q}^*\circ u_j^*(\mathbf{r}')\left[\hat{\Lambda}(\mathbf{r}), \hat{\Lambda}(\mathbf{r}')\right] - \mathcal{Q}^*\circ u_i^*(\mathbf{r})\ \mathcal{Q}\circ v_j(\mathbf{r}')\left[\hat{\Lambda}(\mathbf{r}), \hat{\Lambda}^\dagger(\mathbf{r}')\right] \\
&\quad - \mathcal{Q}\circ v_i(\mathbf{r})\ \mathcal{Q}^*\circ u_j^*(\mathbf{r}')\left[\hat{\Lambda}^\dagger(\mathbf{r}), \hat{\Lambda}(\mathbf{r}')\right] + \mathcal{Q}\circ v_i(\mathbf{r})\ \mathcal{Q}\circ v_j(\mathbf{r}')\left[\hat{\Lambda}^\dagger(\mathbf{r}), \hat{\Lambda}^\dagger(\mathbf{r}')\right] \Big) \Leftrightarrow \\
0 &= \iint \mathrm{d}\mathbf{r}\mathrm{d}\mathbf{r}' \Big(v_i(\mathbf{r})\mathcal{Q}^*(\mathbf{r},\mathbf{r}')u_j^*(\mathbf{r}') - u_i^*(\mathbf{r})\mathcal{Q}(\mathbf{r},\mathbf{r}')v_j(\mathbf{r}') \Big) \qquad (6.32)
\end{aligned}$$

where (6.31) plays a role as an orthonormality criterion for the u and v-functions.

This can help us on in our search for expressions for $u_i(\mathbf{r})$ and $v_i(\mathbf{r})$. Let us insert the expressions for $\mathcal{M}$ and $\bar{\Lambda}$ into (6.20)

$$\begin{aligned}
&\int \mathrm{d}\mathbf{r}\bar{\Lambda}^\dagger\mathcal{M}\bar{\Lambda} \\
&= \int \mathrm{d}\mathbf{r} \sum_{ij>0} \Big(\mathcal{Q}^*\circ\Big(u_i^*\hat{\alpha}_i^\dagger + v_i^*\hat{\alpha}_i\Big)\ A\ \mathcal{Q}\circ\Big(u_j\hat{\alpha}_j + v_j\hat{\alpha}_j^\dagger\Big) \\
&\quad + \mathcal{Q}^*\circ\Big(u_i^*\hat{\alpha}_i^\dagger + v_i^*\hat{\alpha}_i\Big)\ B\ \mathcal{Q}^*\circ\Big(u_j^*\hat{\alpha}_j^\dagger + v_j^*\hat{\alpha}_j\Big) \\
&\quad + \mathcal{Q}\circ\Big(u_i\hat{\alpha}_i + v_i\hat{\alpha}_i^\dagger\Big)\ B^*\ \mathcal{Q}\circ\Big(u_j\hat{\alpha}_j + v_j\hat{\alpha}_j^\dagger\Big) \qquad (6.33) \\
&\quad + \mathcal{Q}\circ\Big(u_i\hat{\alpha}_i + v_i\hat{\alpha}_i^\dagger\Big)\ A\ \mathcal{Q}^*\circ\Big(u_j^*\hat{\alpha}_j^\dagger + v_j^*\hat{\alpha}_j\Big) \Big) \\
&= \int \mathrm{d}\mathbf{r} \sum_{ij>0} \Big(\left(\mathcal{Q}^*\circ v_i^* A\mathcal{Q}\circ u_j + B\mathcal{Q}^*\circ v_i^*\mathcal{Q}^*\circ v_j^* + B^*\mathcal{Q}\circ u_i\mathcal{Q}\circ u_j + \mathcal{Q}\circ u_i A\mathcal{Q}^*\circ v_j^*\right)\hat{\alpha}_i\hat{\alpha}_j \\
&\quad + \left(\mathcal{Q}^*\circ v_i^* A\mathcal{Q}\circ v_j + B\mathcal{Q}^*\circ v_i^*\mathcal{Q}^*\circ u_j^* + B^*\mathcal{Q}\circ u_i\mathcal{Q}\circ v_j + \mathcal{Q}\circ u_i A\mathcal{Q}^*\circ u_j^*\right)\hat{\alpha}_i\hat{\alpha}_j^\dagger \\
&\quad + \left(\mathcal{Q}^*\circ u_i^* A\mathcal{Q}\circ u_j + B\mathcal{Q}^*\circ u_i^*\mathcal{Q}^*\circ v_j^* + B^*\mathcal{Q}\circ v_i\mathcal{Q}\circ u_j + \mathcal{Q}\circ v_i A\mathcal{Q}^*\circ v_j^*\right)\hat{\alpha}_i^\dagger\hat{\alpha}_j \\
&\quad + \left(\mathcal{Q}^*\circ u_i^* A\mathcal{Q}\circ v_j + B\mathcal{Q}^*\circ u_i^*\mathcal{Q}^*\circ u_j^* + B^*\mathcal{Q}\circ v_i\mathcal{Q}\circ v_j + \mathcal{Q}\circ v_i A\mathcal{Q}^*\circ u_j^*\right)\hat{\alpha}_i^\dagger\hat{\alpha}_j^\dagger \Big)
\end{aligned}$$

We can see that a solution to (6.20) are the relations

$$\begin{aligned}
\varepsilon_i\delta_{ij} &= \int \mathrm{d}\mathbf{r}\Big(\mathcal{Q}^*\circ u_i^* A\mathcal{Q}\circ u_j + B\mathcal{Q}^*\circ u_i^*\mathcal{Q}^*\circ v_j^* + B^*\mathcal{Q}\circ v_i\mathcal{Q}\circ u_j + \mathcal{Q}\circ v_i A\mathcal{Q}^*\circ v_j^*\Big) \\
0 &= \int \mathrm{d}\mathbf{r}\Big(\mathcal{Q}^*\circ v_i^* A\mathcal{Q}\circ u_j + B\mathcal{Q}^*\circ v_i^*\mathcal{Q}^*\circ v_j^* + B^*\mathcal{Q}\circ u_i\mathcal{Q}\circ u_j + \mathcal{Q}\circ u_i A\mathcal{Q}^*\circ v_j^*\Big)
\end{aligned}$$

which can be rewritten to

$$\begin{aligned}\varepsilon_i\delta_{ij} &= \int \mathrm{d}\mathbf{r}\Big(\mathcal{Q}^*\circ u_i^* A\mathcal{Q}\circ u_j + B\mathcal{Q}^*\circ u_i^*\mathcal{Q}^*\circ v_j^* + B^*\mathcal{Q}\circ v_i\mathcal{Q}\circ u_j + \mathcal{Q}\circ v_i A\mathcal{Q}^*\circ v_j^*\Big)\\ &= \int \mathrm{d}\mathbf{r}\mathrm{d}\mathbf{s}\mathrm{d}\mathbf{t}\Big(u_i^*(\mathbf{s})\mathcal{Q}^*(\mathbf{r},\mathbf{s})A(\mathbf{r})\mathcal{Q}(\mathbf{r},\mathbf{t})u_j(\mathbf{t}) + u_i^*(\mathbf{s})\mathcal{Q}^*(\mathbf{r},\mathbf{s})B(\mathbf{r})\mathcal{Q}^*(\mathbf{r},\mathbf{t})v_j^*(\mathbf{t})\\ &\qquad v_i(\mathbf{s})\mathcal{Q}(\mathbf{r},\mathbf{s})B^*(\mathbf{r})\mathcal{Q}(\mathbf{r},\mathbf{t})u_j(\mathbf{t}) + v_i(\mathbf{s})\mathcal{Q}(\mathbf{r},\mathbf{s})A(\mathbf{r})\mathcal{Q}^*(\mathbf{r},\mathbf{t})v_j^*(\mathbf{t})\Big)\\ &= \int \mathrm{d}\mathbf{p}\mathrm{d}\mathbf{r}\mathrm{d}\mathbf{t}\Big(\mathcal{Q}^*\circ u_i^*(\mathbf{p})\ ,\ -\mathcal{Q}\circ v_i(\mathbf{p})\Big)\mathcal{L}(\mathbf{p},\mathbf{r},\mathbf{t})\begin{pmatrix} u_j(\mathbf{t})\\ v_j^*(\mathbf{t})\end{pmatrix} \qquad (6.34)\end{aligned}$$

and

$$\begin{aligned}0 &= \int \mathrm{d}\mathbf{r}\Big(\mathcal{Q}^*\circ v_i^* A\mathcal{Q}\circ u_j + B\mathcal{Q}^*\circ v_i^*\mathcal{Q}^*\circ v_j^* + B^*\mathcal{Q}\circ u_i\mathcal{Q}\circ u_j + \mathcal{Q}\circ u_i A\mathcal{Q}^*\circ v_j^*\Big)\\ &= \int \mathrm{d}\mathbf{r}\mathrm{d}\mathbf{s}\mathrm{d}\mathbf{t}\Big(v_i^*(\mathbf{s})\mathcal{Q}^*(\mathbf{r},\mathbf{s})A(\mathbf{r})\mathcal{Q}(\mathbf{r},\mathbf{t})u_j(\mathbf{t}) + v_i^*(\mathbf{s})\mathcal{Q}^*(\mathbf{r},\mathbf{s})B(\mathbf{r})\mathcal{Q}^*(\mathbf{r},\mathbf{t})v_j^*(\mathbf{t})\\ &\qquad u_i(\mathbf{s})\mathcal{Q}(\mathbf{r},\mathbf{s})B^*(\mathbf{r})\mathcal{Q}(\mathbf{r},\mathbf{t})u_j(\mathbf{t}) + u_i(\mathbf{s})\mathcal{Q}(\mathbf{r},\mathbf{s})A(\mathbf{r})\mathcal{Q}^*(\mathbf{r},\mathbf{t})v_j^*(\mathbf{t})\Big)\\ &= \int \mathrm{d}\mathbf{p}\mathrm{d}\mathbf{r}\mathrm{d}\mathbf{t}\Big(\mathcal{Q}^*\circ v_i^*(\mathbf{p})\ ,\ -\mathcal{Q}\circ u_i(\mathbf{p})\Big)\mathcal{L}(\mathbf{p},\mathbf{r},\mathbf{t})\begin{pmatrix} u_j(\mathbf{t})\\ v_j^*(\mathbf{t})\end{pmatrix} \qquad (6.35)\end{aligned}$$

where $\mathbf{p}$, $\mathbf{r}$, $\mathbf{s}$, and $\mathbf{t}$ are different positional variables, and $\mathcal{L}$ is a matrix defined as

$$\mathcal{L}(\mathbf{p},\mathbf{r},\mathbf{t}) \equiv \begin{bmatrix} \mathcal{Q}(\mathbf{p},\mathbf{r})A(\mathbf{r})\mathcal{Q}(\mathbf{r},\mathbf{t}) & \mathcal{Q}(\mathbf{p},\mathbf{r})B(\mathbf{r})\mathcal{Q}^*(\mathbf{r},\mathbf{t})\\ -\mathcal{Q}^*(\mathbf{p},\mathbf{r})B^*(\mathbf{r})\mathcal{Q}(\mathbf{r},\mathbf{t}) & -\mathcal{Q}^*(\mathbf{p},\mathbf{r})A(\mathbf{r})\mathcal{Q}^*(\mathbf{r},\mathbf{t})\end{bmatrix} \qquad (6.36)$$

A set of $u_i(\mathbf{r})$ and $v_i(\mathbf{r})$-functions making (6.34) and (6.35) true, is obtained if

$$\bar{w}_i(\mathbf{t}) \equiv \begin{pmatrix} u_i(\mathbf{t})\\ v_i^*(\mathbf{t})\end{pmatrix} \qquad (6.37)$$

is a solution to the eigenvalue equation

$$\int \mathrm{d}\mathbf{r}\mathrm{d}\mathbf{t}\mathcal{L}(\mathbf{p},\mathbf{r},\mathbf{t})\bar{w}_i(\mathbf{t}) = \varepsilon_i\bar{w}_i(\mathbf{p}) \qquad (6.38)$$

since this will allow us to rewrite (6.34) and (6.35) to

$$\begin{aligned}\varepsilon_j\delta_{ij} &= \varepsilon_j\int \mathrm{d}\mathbf{r}\mathrm{d}\mathbf{r}'\Big(u_i^*(\mathbf{r})\mathcal{Q}(\mathbf{r},\mathbf{r}')u_j(\mathbf{r}') - v_i(\mathbf{r})\mathcal{Q}^*(\mathbf{r},\mathbf{r}')v_j^*(\mathbf{r}')\Big)\\ 0 &= \varepsilon_j\int \mathrm{d}\mathbf{r}\mathrm{d}\mathbf{r}'\Big(v_i^*(\mathbf{r})\mathcal{Q}(\mathbf{r},\mathbf{r}')u_j(\mathbf{r}') - u_i(\mathbf{r})\mathcal{Q}^*(\mathbf{r},\mathbf{r}')v_j^*(\mathbf{r}')\Big) \qquad (6.39)\end{aligned}$$

which are both true, according to (6.31) and (6.32).

The corresponding calculation for the $u_{i-}(\mathbf{r})$ and $v_{i-}(\mathbf{r})$-terms is similar, just with the replacements $\mathcal{Q}(\mathbf{r},\mathbf{r}') \to \delta(\mathbf{r},\mathbf{r}')$, $\mathcal{Q}\circ \to 1$, and $\sum_{i>0} \to \sum_i$

So to summarize this long calculation: The Hamiltonian (6.1) can be expressed as a function of the set of operators $\hat{\Lambda}_\pm(\mathbf{r})$, which is done in (6.13). The sets of functions $u_{i\pm}(\mathbf{r})$ and $v_{i\pm}(\mathbf{r})$, which can be found by solving (6.38), enable us to express the operators $\hat{\Lambda}_\pm(\mathbf{r})$ as functions of another set of operators $\alpha_{i\pm}$ through the relations (6.19) and (6.30). The reason for doing this is that the $\hat{\alpha}_{i\pm}$-operators diagonalize the Hamiltonian giving it the form (6.21). This diagonalization procedure is known as a Bogoliubov transformation.

It turns out that some of the previous results can be simplified by introducing σ_z as the metric for the space in which the $\bar{w}_i$-vectors live, such that $\bar{w}_i \cdot \bar{w}_j = u_i^* u_j - v_i v_j^*$. If we in addition introduce the alternate $\bar{w}_i$-vectors

$$\bar{\mathfrak{w}}_{i+}(\mathbf{r}) \equiv \begin{pmatrix} \mathcal{Q}\circ u_{i+}(\mathbf{r}) \\ \mathcal{Q}^*\circ v_{i+}^*(\mathbf{r}) \end{pmatrix} \tag{6.40}$$

we see that (6.31) and (6.26) can be written

$$\begin{aligned} \delta_{ij} &= \int \mathrm{d}\mathbf{r}\ (\bar{\mathfrak{w}}_{i+}(\mathbf{r}) \cdot \bar{\mathfrak{w}}_{j+}(\mathbf{r})) \\ \delta(\mathbf{r},\mathbf{r}') &= \varphi^*(\mathbf{r})\varphi(\mathbf{r}') + \sum_{i>0} (\bar{\mathfrak{w}}_{i+}(\mathbf{r}) \cdot \bar{\mathfrak{w}}_{i+}(\mathbf{r}')) \end{aligned} \tag{6.41}$$

for the case of real u_i and v_i-functions. From (6.41) we clearly see how (6.31) and (6.26) correspond to orthonormality and completeness, something which was stated at the original expressions.

6.3 Rewriting the operators

In order to be able to use the results of the the calculation in previous sections to help us calculate the spin-squeezing, we need to express the various operators[6] involved in the calculation of the squeezing parameter in the new $\hat{\alpha}$-basis. This is done by first expressing the $\hat{\Psi}$ operators in terms of the $\delta\hat{\psi}$ operators, then expressing those in terms of the $\hat{\Lambda}$-operators, and finally expressing the $\hat{\Lambda}$-operators in terms of u, v and $\hat{\alpha}$-operators. This section will introduce some new notation. The summation $\sum_{ij*}$ indicates that the sum should go over all modes if it is a sum over minus-modes, but exclude the 0-mode if it is a sum over plus-modes, and the operator $\circ$ is defined as[7] $f \circ g \equiv \int \mathrm{d}\mathbf{r} f(\mathbf{r}) g(\mathbf{r})$.

[6] This refers to the operators $\hat{N}$, $\hat{J}_x$, $\hat{J}_z$, and $\hat{J}_z^2$.

[7] This definition is different from, but consistent with the $\circ$ in the $\mathcal{Q}\circ$-operator.

Let us start by calculating the $\hat{J}_x$-operator.

$$\begin{aligned}
\hat{J}_x &= \frac{1}{2}\int \mathrm{d}\mathbf{r}\left(\hat{\Psi}_+^\dagger\hat{\Psi}_+ - \hat{\Psi}_-^\dagger\hat{\Psi}_-\right)\\
&= \frac{1}{2}\int \mathrm{d}\mathbf{r}\Big(\left(\hat{c}_+^\dagger\varphi^* + \delta\hat{\psi}_+^\dagger\right)\left(\hat{c}_+\varphi + \delta\hat{\psi}_+\right) - \left(\delta\hat{\psi}_-^\dagger\right)\left(\delta\hat{\psi}_-\right)\Big)\\
&= \frac{\hat{c}_+^\dagger\hat{c}_+}{2} + \frac{1}{2}\int \mathrm{d}\mathbf{r}\left(\delta\hat{\psi}_+^\dagger\delta\hat{\psi}_+ - \delta\hat{\psi}_-^\dagger\delta\hat{\psi}_-\right)\\
&\approx \frac{\hat{c}_+^\dagger\hat{c}_+}{2} + \frac{1}{2}\int \mathrm{d}\mathbf{r}\left(\hat{\Lambda}_+^\dagger\hat{\Lambda}_+ - \hat{\Lambda}_-^\dagger\hat{\Lambda}_-\right)\\
&= \frac{1}{2}\int \mathrm{d}\mathbf{r}\sum_{i,j*}\Big(\mathcal{Q}^*\circ\left(u_{i+}^*\hat{\alpha}_{i+}^\dagger + v_{i+}^*\hat{\alpha}_{i+}\right)\ \mathcal{Q}\circ\left(u_{j+}\hat{\alpha}_{j+} + v_{j+}\hat{\alpha}_{j+}^\dagger\right)\\
&\quad - \left(u_{i-}\hat{\alpha}_{i-} + v_{i-}\hat{\alpha}_{i-}^\dagger\right)\left(u_{j-}^*\hat{\alpha}_{j-}^\dagger + v_{j-}^*\hat{\alpha}_{j-}\right)\Big) + \frac{\hat{c}_+^\dagger\hat{c}_+}{2}\\
&= \frac{1}{2}\sum_{i,j*}\Big(v_{i+}^*\circ\mathcal{Q}\circ u_{j+}\hat{\alpha}_{i+}\hat{\alpha}_{j+} + v_{i+}^*\circ\mathcal{Q}\circ v_{j+}\hat{\alpha}_{i+}\hat{\alpha}_{j+}^\dagger + u_{i+}^*\circ\mathcal{Q}\circ u_{j+}\hat{\alpha}_{i+}^\dagger\hat{\alpha}_{j+}\\
&\quad + u_{i+}^*\circ\mathcal{Q}\circ v_{j+}\hat{\alpha}_{i+}^\dagger\hat{\alpha}_{j+}^\dagger - v_{i-}^*\circ u_{j-}\hat{\alpha}_{i-}\hat{\alpha}_{j-} - v_{i-}^*\circ v_{j-}\hat{\alpha}_{i-}\hat{\alpha}_{j-}^\dagger\\
&\quad - u_{i-}^*\circ u_{j-}\hat{\alpha}_{i-}^\dagger\hat{\alpha}_{j-} - u_{i-}^*\circ v_{j-}\hat{\alpha}_{i-}^\dagger\hat{\alpha}_{j-}^\dagger\Big) + \frac{\hat{c}_+^\dagger\hat{c}_+}{2}
\end{aligned} \tag{6.42}$$

Similar calculations can be done[8] for the other operators, with the results

$$\begin{aligned}
\hat{N} &= \sum_{ij*}\Big(v_{i+}^*\circ\mathcal{Q}\circ u_{j+}\hat{\alpha}_{i+}\hat{\alpha}_{j+} + v_{i+}^*\circ\mathcal{Q}\circ v_{j+}\hat{\alpha}_{i+}\hat{\alpha}_{j+}^\dagger + u_{i+}^*\circ\mathcal{Q}\circ u_{j+}\hat{\alpha}_{i+}^\dagger\hat{\alpha}_{j+}\\
&\quad + u_{i+}^*\circ\mathcal{Q}\circ v_{j+}\hat{\alpha}_{i+}^\dagger\hat{\alpha}_{j+}^\dagger + v_{i-}^*\circ u_{j-}\hat{\alpha}_{i-}\hat{\alpha}_{j-} + v_{i-}^*\circ v_{j-}\hat{\alpha}_{i-}\hat{\alpha}_{j-}^\dagger\\
&\quad + u_{i-}^*\circ u_{j-}\hat{\alpha}_{i-}^\dagger\hat{\alpha}_{j-} + u_{i-}^*\circ v_{j-}\hat{\alpha}_{i-}^\dagger\hat{\alpha}_{j-}^\dagger\Big) + \hat{c}^\dagger\hat{c}
\end{aligned} \tag{6.43}$$

$$\begin{aligned}
\hat{J}_z &= \frac{1}{2}\sum_{ij*}\Big(\left(v_{i+}^*\circ\mathcal{Q}\circ u_{j-} + u_{i+}\circ\mathcal{Q}^*\circ v_{j-}^*\right)\hat{\alpha}_{i+}\hat{\alpha}_{j-} + \left(v_{i+}^*\circ\mathcal{Q}\circ v_{j-} + u_{i+}\circ\mathcal{Q}^*\circ u_{j-}^*\right)\hat{\alpha}_{i+}\hat{\alpha}_{j-}^\dagger\\
&\quad + \left(u_{i+}^*\circ\mathcal{Q}\circ u_{j-} + v_{i+}\circ\mathcal{Q}^*\circ v_{j-}^*\right)\hat{\alpha}_{i+}^\dagger\hat{\alpha}_{j-} + \left(u_{i+}^*\circ\mathcal{Q}\circ v_{j-} + v_{i+}\circ\mathcal{Q}^*\circ u_{j-}^*\right)\hat{\alpha}_{i+}^\dagger\hat{\alpha}_{j-}^\dagger\Big)\\
&\quad + \int \mathrm{d}\mathbf{r}\sum_i\Big(\left(\varphi^* u_{i-} + v_{i-}^*\varphi\right)\hat{\alpha}_{i-} + \left(\varphi^* v_{i-} + u_{i-}^*\varphi\right)\hat{\alpha}_{i-}^\dagger\Big)
\end{aligned} \tag{6.44}$$

[8]The full calculations for all $\hat{J}$-operators and combinations thereof, can be found in appendix D.

$$\begin{aligned}
\hat{J}_z^2 &= \frac{N_0}{4}\sum_{i,j}\Big(\Big(\varphi^*\circ u_{i-}\varphi^*\circ u_{j-} + 2v^*_{i-}\circ\varphi\varphi^*\circ u_{j-} + v^*_{i-}\circ\varphi v^*_{j-}\circ\varphi\Big)\hat{\alpha}_{i-}\hat{\alpha}_{j-} \\
&\quad + \Big(\varphi^*\circ u_{i-}\varphi^*\circ v_{j-} + 2v^*_{i-}\circ\varphi\varphi^*\circ v_{j-} + v^*_{i-}\circ\varphi u^*_{j-}\circ\varphi\Big)\hat{\alpha}_{i-}\hat{\alpha}^\dagger_{j-} \\
&\quad + \Big(\varphi^*\circ v_{i-}\varphi^*\circ u_{j-} + 2u^*_{i-}\circ\varphi\varphi^*\circ u_{j-} + u^*_{i-}\circ\varphi v^*_{j-}\circ\varphi\Big)\hat{\alpha}^\dagger_{i-}\hat{\alpha}_{j-} \\
&\quad + \Big(\varphi^*\circ v_{i-}\varphi^*\circ v_{j-} + 2u^*_{i-}\circ\varphi\varphi^*\circ v_{j-} + u^*_{i-}\circ\varphi u^*_{j-}\circ\varphi\Big)\hat{\alpha}^\dagger_{i-}\hat{\alpha}^\dagger_{j-}\Big) + \frac{\hat{c}^\dagger\hat{c}}{4} \\
&\quad + \frac{1}{4}\sum_{i,j}\Big(v^*_{i-}\circ u_{j-}\hat{\alpha}_{i-}\hat{\alpha}_{j-} + v^*_{i-}\circ v_{j-}\hat{\alpha}_{i-}\hat{\alpha}^\dagger_{j-} + u^*_{i-}\circ u_{j-}\hat{\alpha}^\dagger_{i-}\hat{\alpha}_{j-} + u^*_{i-}\circ v_{j-}\hat{\alpha}^\dagger_{i-}\hat{\alpha}^\dagger_{j-}\Big) \\
&\quad + \frac{1}{4}\sum_{i,j>0}\Big(v^*_{i+}\circ\mathcal{Q}\circ u_{j+}\hat{\alpha}_{i+}\hat{\alpha}_{j+} + v^*_{i+}\circ\mathcal{Q}\circ v_{j+}\hat{\alpha}_{i+}\hat{\alpha}^\dagger_{j+} \\
&\quad + u^*_{i+}\circ\mathcal{Q}\circ u_{j+}\hat{\alpha}^\dagger_{i+}\hat{\alpha}_{j+} + u^*_{i+}\circ\mathcal{Q}\circ v_{j+}\hat{\alpha}^\dagger_{i+}\hat{\alpha}^\dagger_{j+}\Big) \qquad (6.45)
\end{aligned}$$

Let us in the following assume that the occupation of the Bogoliubov modes is caused by thermal excitations alone. In order to investigate such thermal excitations, let us calculate the probability of having the system in the state x, which has n_{ix} excitations in the ith Bogoliubov state.

$$\begin{aligned}
p_x &= \frac{\exp\left(-\beta E_x\right)}{\sum_{x'}\exp\left(-\beta E_{x'}\right)} = \frac{\exp\left(-\beta\left(E_0+\sum_i\varepsilon_i n_{ix}\right)\right)}{\sum_{x'}\exp\left(-\beta\left(E_0+\sum_i\varepsilon_i n_{ix'}\right)\right)} = \frac{\prod_i\exp\left(-\beta\varepsilon_i n_{ix}\right)}{\sum_{x'}\prod_i\exp\left(-\beta\varepsilon_i n_{ix'}\right)} \\
&\approx \prod_i\frac{\exp\left(-\beta\varepsilon_i n_{ix}\right)}{\sum_{n_i}\exp\left(-\beta\varepsilon_i n_i\right)} \qquad (6.46)
\end{aligned}$$

where β is defined as $\beta\equiv\frac{1}{\mathcal{T}}$ where $\mathcal{T}$ is an unitless temperature defined as $\mathcal{T}\equiv\frac{k_BT}{\hbar\omega}$ where T is the temperature. The terms in the product on the final line of (6.46) are the probabilities of having n_{ix} excitations in the ith state, so if we want to calculate the average number of excitations in the ith state we can use these probabilities and get

$$\begin{aligned}
\langle n\rangle_i &= \sum_{n_i} n_i p_{i,n} = \sum_{n_i} n_i\frac{\exp\left(-\beta\varepsilon_i n_i\right)}{\sum_{n_i}\exp\left(-\beta\varepsilon_i n_i\right)} \equiv \frac{\sum_n na^n}{\sum_{n'}a^{n'}} = \frac{\frac{a}{(1-a)^2}}{\frac{1}{1-a}} = \frac{1}{a^{-1}-1} \\
&= \frac{1}{\exp\left(\beta\varepsilon_i\right)-1} \qquad (6.47)
\end{aligned}$$

where we have defined $a\equiv\exp\left(-\beta\varepsilon_i\right)$ along the way. This result is similar to the Bose-Einstein distribution, but differs by an absence of a chemical potential, which is caused by the number of excitations in the Bogoliubov modes not being fixed.

We can use this result to calculate the expectation value of the combinations of $\hat{\alpha}_i$-operators appearing in (6.42) to (6.45). $\langle\hat{\alpha}^\dagger_i\hat{\alpha}_i\rangle = \langle\hat{n}_i\rangle = \langle n\rangle_i$, and inserting this

in (6.42) to (6.45) gives

$$\begin{aligned}\langle\hat{N}\rangle &= N_0+\sum_{i*}\Big(v_{i+}^*\circ\mathcal{Q}\circ v_{i+}\Big(\langle n\rangle_{i+}+1\Big)+u_{i+}^*\circ\mathcal{Q}\circ u_{i+}\langle n\rangle_{i+}\\ &\quad +v_{i-}^*\circ v_{i-}\Big(\langle n\rangle_{i-}+1\Big)+u_{i-}^*\circ u_{i-}\langle n\rangle_{i-}\Big)\end{aligned}\tag{6.48}$$

$$\begin{aligned}\langle\hat{J}_x\rangle &= \frac{N_0}{2}+\frac{1}{2}\sum_{i*}\Big(v_{i+}^*\circ\mathcal{Q}\circ v_{i+}\Big(\langle n\rangle_{i+}+1\Big)+u_{i+}^*\circ\mathcal{Q}\circ u_{i+}\langle n\rangle_{i+}\\ &\quad -v_{i-}^*\circ v_{i-}\Big(\langle n\rangle_{i-}+1\Big)-u_{i-}^*\circ u_{i-}\langle n\rangle_{i-}\Big)\end{aligned}\tag{6.49}$$

$$\langle\hat{J}_z\rangle = 0\tag{6.50}$$

$$\begin{aligned}\langle\hat{J}_z^2\rangle &= \frac{N_0}{4}+\frac{N_0}{4}\sum_i\Big(\Big(\varphi^*\circ u_{i-}\varphi^*\circ v_{i-}+2v_{i-}^*\circ\varphi\varphi^*\circ v_{i-}+v_{i-}^*\circ\varphi u_{i-}^*\circ\varphi\Big)\Big(\langle n\rangle_{i-}+1\Big)\\ &\quad +\Big(\varphi^*\circ v_{i-}\varphi^*\circ u_{i-}+2u_{i-}^*\circ\varphi\varphi^*\circ u_{i-}+u_{i-}^*\circ\varphi v_{i-}^*\circ\varphi\Big)\langle n\rangle_{i-}\Big)\\ &\quad +\frac{1}{4}\sum_i\Big(v_{i-}^*\circ v_{i-}\Big(\langle n\rangle_{i-}+1\Big)+u_{i-}^*\circ u_{i-}\langle n\rangle_{i-}\Big)\\ &\quad +\frac{1}{4}\sum_{i>0}\Big(v_{i+}^*\circ\mathcal{Q}\circ v_{i+}\Big(\langle n\rangle_{i+}+1\Big)+u_{i+}^*\circ\mathcal{Q}\circ u_{i+}\langle n\rangle_{i+}\Big)\end{aligned}\tag{6.51}$$

which are the results we will use when doing calculations for non-zero temperatures.

For $\mathcal{T}=0$ the occupation number of all the Bogoliubov states goes to zero, and the result for the expectation values of our operators reduces further to

$$\begin{aligned}\langle\hat{J}_z\rangle &= 0\\ \langle\hat{J}_x\rangle &= \frac{N_0}{2}+\frac{1}{2}\sum_{i*}\big(v_{i+}^*\circ\mathcal{Q}\circ v_{i+}-v_{i-}^*\circ v_{i-}\big)\\ \langle\hat{N}\rangle &= N_0+\sum_{i*}\big(v_{i+}^*\circ\mathcal{Q}\circ v_{i+}+v_{i-}^*\circ v_{i-}\big)\\ \langle\hat{J}_z^2\rangle &= \frac{N_0}{4}+\frac{1}{4}\sum_{i*}\big(v_{i+}^*\circ\mathcal{Q}\circ v_{i+}+v_{i-}^*\circ v_{i-}\big)\\ &\quad +\frac{N_0}{4}\sum_i\big(\varphi^*\circ u_{i-}\varphi^*\circ v_{i-}+2v_{i-}^*\circ\varphi\varphi^*\circ v_{i-}+v_{i-}^*\circ\varphi u_{i-}^*\circ\varphi\big)\end{aligned}\tag{6.52}$$

which we will use when doing calculations for zero temperature.

When we know these expectation values, calculating the spin-squeezing using (3.30) is no problem.

6.4 The symmetry-breaking approach

In this section the consequences of trying to do the symmetry-breaking calculation will be described in more detail[9]. Some reasons to why the full calculation was done using the (in some aspects) more complicated non-symmetry-breaking approach are given, since we will show some of the problems arising from the symmetry-breaking approach.

As mentioned in section 5.6 the symmetry break arises if the rewritings in (6.2) are replaced with

$$\begin{aligned}\hat{\Psi}_+(\mathbf{r}) &\approx \psi(\mathbf{r}) + \delta\hat{\psi}_+(\mathbf{r}) \\ \hat{\Psi}_-(\mathbf{r}) &\approx \delta\hat{\psi}_-(\mathbf{r})\end{aligned} \tag{6.53}$$

which is an approximation, since it substitutes the operator $\hat{c}\varphi$ with the c-number ψ. The symmetry in question is the U(1)-symmetry induced by the fact that the Hamiltonian is invariant under the transformation $\hat{\Psi} \to \hat{\Psi}e^{i\theta}$, and the symmetry break can be seen from the fact that $\langle\hat{\Psi}_+\rangle = \psi e^{i\theta}$ after the transformation (6.53), where we would have had $\langle\hat{\Psi}_+\rangle = 0$ from the non-symmetry-breaking rewriting (6.2).

In the symmetry-breaking approach we do neither need to introduce the $\hat{\Lambda}$-operator, since the definition would become $\hat{\Lambda} \equiv \delta\hat{\psi}$, nor to introduce the $\mathcal{Q}\circ$-operators since there no longer is a demand for the φ_{i+}-functions to be orthogonal to ψ. When calculating the various operators, we can follow the same method as for the non-symmetry breaking approach used in section 6.3, and we get for most of the operators the same result as previously, except for the lack of $\mathcal{Q}\circ$-operators and the fact that all sums start from zero. But in the calculation of[10] $\hat{J}_z^2$ a problem arises. We can of course follow the same path as previously:

$$\begin{aligned}\hat{J}_z^2 &= \left(\frac{1}{2}\int \mathrm{d}\mathbf{r}\left(\hat{\Psi}_+^\dagger(\mathbf{r})\hat{\Psi}_-(\mathbf{r}) + \hat{\Psi}_-^\dagger(\mathbf{r})\hat{\Psi}_+(\mathbf{r})\right)\right)^2 \\ &= \frac{1}{4}\int \mathrm{d}\mathbf{r}\mathrm{d}\mathbf{r}'\Big(\hat{\Psi}_+^\dagger(\mathbf{r})\hat{\Psi}_-(\mathbf{r})\hat{\Psi}_+^\dagger(\mathbf{r}')\hat{\Psi}_-(\mathbf{r}') + \hat{\Psi}_-^\dagger(\mathbf{r})\hat{\Psi}_+(\mathbf{r})\hat{\Psi}_+^\dagger(\mathbf{r}')\hat{\Psi}_-(\mathbf{r}') \\ &\quad + \hat{\Psi}_-^\dagger(\mathbf{r})\hat{\Psi}_-^\dagger(\mathbf{r}')\hat{\Psi}_+(\mathbf{r})\hat{\Psi}_+(\mathbf{r}')\Big) + \frac{1}{4}\int \mathrm{d}\mathbf{r}\Big(\hat{\Psi}_+^\dagger(\mathbf{r})\hat{\Psi}_+(\mathbf{r}) + \hat{\Psi}_-^\dagger(\mathbf{r})\hat{\Psi}_-(\mathbf{r})\Big) \\ &\approx \frac{N}{4} + \frac{1}{4}\int \mathrm{d}\mathbf{r}\mathrm{d}\mathbf{r}'\Big(\psi^*(\mathbf{r})\psi^*(\mathbf{r}')\delta\hat{\psi}_-(\mathbf{r})\delta\hat{\psi}_-(\mathbf{r}') + 2\psi^*(\mathbf{r})\psi(\mathbf{r}')\delta\hat{\psi}_-^\dagger(\mathbf{r}')\delta\hat{\psi}_-(\mathbf{r}) \\ &\quad + \psi(\mathbf{r})\psi(\mathbf{r}')\delta\hat{\psi}_-^\dagger(\mathbf{r})\delta\hat{\psi}_-^\dagger(\mathbf{r}')\Big) + \frac{1}{4}\int \mathrm{d}\mathbf{r}\Big(\delta\hat{\psi}_+^\dagger(\mathbf{r})\delta\hat{\psi}_+(\mathbf{r}) + \delta\hat{\psi}_-^\dagger(\mathbf{r})\delta\hat{\psi}_-(\mathbf{r})\Big) \\ &= \ldots\end{aligned} \tag{6.54}$$

[9] For the full calculation of the main result (6.60) of this section, see appendix F.

[10] In section 6.3 the result of the calculation of $\hat{J}_z^2$ was just stated. For the full derivation of this result see appendix D.

which would give the same result as we got for the non-symmetry-breaking approach. But another option is to insert (6.53) before doing the normal ordering

$$\begin{aligned}
\hat{J}_z^2 &= \left(\frac{1}{2}\int \mathrm{d}\mathbf{r}\left(\hat{\Psi}_+^\dagger(\mathbf{r})\hat{\Psi}_-(\mathbf{r}) + \hat{\Psi}_-^\dagger(\mathbf{r})\hat{\Psi}_+(\mathbf{r})\right)\right)^2 \\
&= \left(\frac{1}{2}\int \mathrm{d}\mathbf{r}\left(\big(\psi^*(\mathbf{r}) + \delta\hat{\psi}_+(\mathbf{r})\big)\big(\delta\hat{\psi}_-(\mathbf{r})\big) + \big(\delta\hat{\psi}_-^\dagger(\mathbf{r})\big)\big(\psi(\mathbf{r}) + \delta\hat{\psi}_+(\mathbf{r})\big)\right)\right)^2 \\
&\approx \frac{1}{4}\int \mathrm{d}\mathbf{r}\mathrm{d}\mathbf{r}'\Big(\psi^*(\mathbf{r})\psi^*(\mathbf{r}')\delta\hat{\psi}_-(\mathbf{r})\delta\hat{\psi}_-(\mathbf{r}') + 2\psi^*(\mathbf{r})\psi(\mathbf{r}')\delta\hat{\psi}_-^\dagger(\mathbf{r}')\delta\hat{\psi}_-(\mathbf{r}) \\
&\quad + \psi(\mathbf{r})\psi(\mathbf{r}')\delta\hat{\psi}_-^\dagger(\mathbf{r})\delta\hat{\psi}_-^\dagger(\mathbf{r}')\Big) \\
&= \ldots
\end{aligned} \tag{6.55}$$

where we see that we get a different result. The difference arises from the fact that $\psi(\mathbf{r})$ and $\psi^*(\mathbf{r}')$ commute where $\hat{c}\varphi(\mathbf{r})$ and $\hat{c}^\dagger\varphi^*(\mathbf{r}')$ do not. Of course it should not be possible to get different results by calculating the same thing in two different ways, so this is an indication that the symmetry-breaking method is inadequate, and if we try the same for the non-symmetry-breaking approach this problem will not arise. But even if we by chance had the right result here and carried on the calculation, other problems would arise.

The u and v functions will be found to be those that solve the simpler version of (6.38)

$$\mathcal{L}(\mathbf{r})\bar{w}_i(\mathbf{r}) = \varepsilon_i\bar{w}_i(\mathbf{r}) \tag{6.56}$$

where

$$\mathcal{L}(\mathbf{r}) \equiv \begin{bmatrix} A(\mathbf{r}) & B(\mathbf{r}) \\ -B^*(\mathbf{r}) & -A(\mathbf{r}) \end{bmatrix} \tag{6.57}$$

and $\bar{w}_i(\mathbf{r}) \equiv (u_i(\mathbf{r}), v_i^*(\mathbf{r}))$ as in the main calculation. Insertion gives

$$\begin{aligned}
A(\mathbf{r})u_i(\mathbf{r}) + B(\mathbf{r})v_i^*(\mathbf{r}) &= \epsilon_i u_i(\mathbf{r}) \\
B(\mathbf{r})u_i(\mathbf{r}) + A(\mathbf{r})v_i^*(\mathbf{r}) &= -\epsilon_i v_i^*(\mathbf{r})
\end{aligned} \tag{6.58}$$

from which we see that if we interchange u and $-v$ we would have another eigenvector[11] with eigenvalue $-\varepsilon$. This means that if $\varepsilon = 0$, a possible solution is $u = -v$. For the plus-mode such a solution actually exists and by inserting the values of A_+ and B_+, we get

$$\left(H_0 - \mu + (U + U_{ab})|\psi|^2 + \frac{\Omega}{2}\right)u_{0+}(\mathbf{r}) - \frac{(U + U_{ab})}{2}(\psi)^2 u_{0+}^*(\mathbf{r}) = 0 \tag{6.59}$$

[11] One could argue that such an eigenvector can not fulfil (6.31) $u'^*\circ u' - v'\circ v'^* = 1$ which we require, but it could if one allows for complex eigenvectors and instead defines $u' = iv$ and $v' = iu$, where such a phase shift always is allowed in an eigenvalue equation. This is related to the discussion of positive and negative eigenvalues in the section on the Schwinger model.

and from the GPE (5.12) we see that a solution to this is $u_{0+}(\mathbf{r}) = -v_{0+}(\mathbf{r}) = \psi(\mathbf{r})$. Something is, however, wrong with this result, since we see that it never will fulfil (6.31) because $u^*_{0+} \circ u_{0+} - v_{0+} \circ v^*_{0+} = u_{0+} \circ u_{0+} - u_{0+} \circ u_{0+} = 0$. Fortunately it turns out[12] that we can find a possible other eigenvector with the same eigenvalue, and a superposition of the two turns out to be in accordance with (6.31). This new state is, however, not an eigenstate to the matrix $\mathcal{L}$, and therefore we can not diagonalize $\hat{\mathcal{H}}$ to the form given by (6.20). Instead we can write it as

$$\hat{\mathcal{H}} = \hat{\mathcal{H}}_0 + \frac{1}{2}\frac{d\mu}{dN}\hat{Q}^2 + 0\hat{P}^2 + \sum_{i>0}\varepsilon_{i+}\left(\hat{\alpha}^\dagger_{i+}\hat{\alpha}_{i+}\right) + \sum_i \varepsilon_{i-}\left(\hat{\alpha}^\dagger_{i-}\hat{\alpha}_{i-}\right) \quad (6.60)$$

where

$$\begin{aligned} \hat{Q} &\equiv \frac{1}{\sqrt{2}}(\hat{\alpha}_{0+} + \hat{\alpha}^\dagger_{0+}) \\ \hat{P} &\equiv \frac{1}{i\sqrt{2}}(\hat{\alpha}_{0+} - \hat{\alpha}^\dagger_{0+}) \end{aligned} \quad (6.61)$$

has been defined. We see from the expression (6.60), that the coefficient on the $\hat{P}^2$-term is zero, and the particles created by excitations in this P-mode are the massless Goldstone bosons mentioned in section 5.6. An illustration of the P and Q-modes[13] can be seen in fig. 6.1.

An infinite amount of particles could be created in this Goldstone-mode and we would need to exclude them artificially from sums over all modes, like those appearing in (6.42) to (6.45). It is in order to avoid this that the main calculation in this thesis uses the non-symmetry-breaking approach.

6.5 Numerical calculations

Unlike the case of the simpler Schwinger model, the u and v-functions can not be found analytically for our main calculation. So therefore we need to find a way to implement the calculation numerically[14]. In order to be able to do any of the calculations we must find the value of μ. This can be done by isolating it in the GPE (5.12), where the value of φ is found using the imaginary time formalism

[12] See appendix F.

[13] Excitations in the Q-mode play a role analogous to that of Higgs bosons in the standard model, with the coefficient $\frac{d\mu}{dN}$ playing the role of the Higgs mass. Using the Thomas-Fermi approximation (4.26), that value can be found to $\frac{d\mu}{dN} \approx 0.163 \cdot (U + U_{ab})^{2/5} N^{-3/5}$.

[14] In principle this sentence could have ended "which we have done.", and then we could have went on to the next chapter presenting the results. But in the introduction I wrote that the thesis is aimed at people at the same academical level as my own, and I am far from sure that everyone would find numerical solutions of differential matrix-equations a trivial task. This is the reason for the inclusion of this section in the main text, and not just as an appendix.

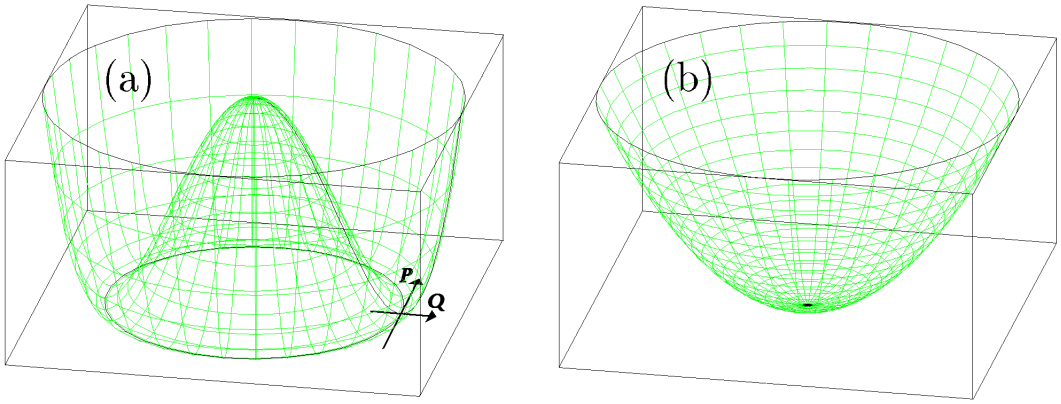

Figure 6.1: An illustration of the Goldstone mode, which is a consequence of the symmetry breaking approach. (a) represents the condensate-mode, while (b) represents the other modes. The vertical axis shows the energy, and the horizontal axis shows the real and the imaginary part of the wave-function for the mode in question. For modes different from the condensate-mode, we see that any excitation in the mode increases the energy, but for the condensate-mode the situation is different. The condensate contains per default N_0 particles, and any deviation from that number increases the energy, as shown by the Q-mode. However, the phase is not fixed due to the symmetry break ($\langle\hat{\Psi}_+\rangle = \psi e^{i\theta}$) and changing the phase changes none of the physics, which is shown by the fact that excitations in the Goldstone-mode P do not change the energy.

described in connection with (4.29), which can be solved using a fourth order Runge-Kutta algorithm[15]. How to implement the ∇^2-part of the H_0-operator in the time-dependent GPE is described below.

The u and v functions are the solutions to the equations[16] (6.38)

$$\int d\mathbf{r}' \mathcal{L}_\pm(\mathbf{r},\mathbf{r}')\bar{w}_{i\pm}(\mathbf{r}') = \varepsilon_{i\pm}\bar{w}_{i\pm}(\mathbf{r}) \tag{6.62}$$

where

$$\bar{w}_{i\pm}(\mathbf{r}) \equiv \begin{pmatrix} u_{i\pm}(\mathbf{r}) \\ v^*_{i\pm}(\mathbf{r}) \end{pmatrix} \tag{6.63}$$

$$\mathcal{L}_+(\mathbf{r},\mathbf{r}') \equiv \begin{bmatrix} \int d\mathbf{r}''\big(\mathcal{Q}(\mathbf{r},\mathbf{r}'')A_+(\mathbf{r}'')\mathcal{Q}(\mathbf{r}'',\mathbf{r}')\big) & \int d\mathbf{r}''\big(\mathcal{Q}(\mathbf{r},\mathbf{r}'')B_+(\mathbf{r}'')\mathcal{Q}^*(\mathbf{r}'',\mathbf{r}') \\ -\int d\mathbf{r}''\big(\mathcal{Q}^*(\mathbf{r},\mathbf{r}'')B^*_+(\mathbf{r}'')\mathcal{Q}(\mathbf{r}'',\mathbf{r}')\big) & -\int d\mathbf{r}''\big(\mathcal{Q}^*(\mathbf{r},\mathbf{r}'')A_+(\mathbf{r}'')\mathcal{Q}^*(\mathbf{r}'',\mathbf{r}')\big) \end{bmatrix} \tag{6.64}$$

and

$$\mathcal{L}_-(\mathbf{r},\mathbf{r}') \equiv \begin{bmatrix} \delta(\mathbf{r}-\mathbf{r}')A_-(\mathbf{r}') & \delta(\mathbf{r}-\mathbf{r}')B_-(\mathbf{r}') \\ -\delta(\mathbf{r}-\mathbf{r}')B^*_-(\mathbf{r}') & -\delta(\mathbf{r}-\mathbf{r}')A_-(\mathbf{r}') \end{bmatrix} \tag{6.65}$$

[15] See [f].

[16] Here we have redefined $\mathcal{L}$ so that the integration over the third variable which were called $\mathbf{r}$ in (6.38), is moved into the definition.

All of the variables $\mathbf{r}$, $\mathbf{r}'$ and $\mathbf{r}''$ are position variables, and when integrated they are integrated over all of three dimensional space. The functions $\mathcal{Q}$, $A_\pm$ and $B_\pm$ are functions of $\mathbf{r}$ through the function $\varphi(\mathbf{r})$, which is radially symmetric, and therefore a function of $r = |\mathbf{r}|$ only. In addition $A_\pm$ depends on H_0 which is a function of the differential operator ∇^2 which can be written

$$\nabla^2 f = \frac{1}{r}\frac{\partial^2}{\partial r^2}(rf) - \frac{1}{r^2}L^2 f \tag{6.66}$$

in spherical coordinates, where the differential operator L^2 is defined as

$$L^2 \equiv \frac{1}{\sin(\theta)}\frac{\partial}{\partial\theta}\left(\sin(\theta)\frac{\partial}{\partial\theta}\right) + \frac{1}{\sin^2(\theta)}\frac{\partial^2}{\partial\phi^2} \tag{6.67}$$

This means that the only part of the $\mathcal{L}$-matrix that depends on θ and ϕ is the operator L^2, and it turns out[17] that the spherical harmonics $Y_l^m(\theta,\phi)$ are eigenfunctions to L^2 with eigenvalue $l(l+1)$. This means that if our functions $\bar{w}$ can be separated[18] as $f(\mathbf{r}) = f(r)\cdot Y_l^m(\theta,\phi)$ the ∇^2-operator can be written $\nabla^2 f = \frac{1}{r}\frac{\partial^2}{\partial r^2}(rf) - \frac{l(l+1)}{r^2}f$, and thus $\mathcal{L}$ becomes a function of r only. For functions of a radial variable only, an integration over three dimensional space can be written

$$\int \mathrm{d}\mathbf{r} f(r) \;\; = \;\; 4\pi\int_0^\infty \mathrm{d}r\; r^2 f(r) \tag{6.68}$$

which is the result we will use for the integrations in (6.62) and (6.64).

We are now left with a one dimensional eigenvalue equation involving the variable r, which we (in principle) need to solve for each value of l. In order to solve this numerically we need to turn r into a discrete variable, with step-size dr, and write the four components of $\mathcal{L}$ as huge matrices. The local parts of A and B are easy to discritize, since they can be written as diagonal matrices, and the only nonlocal part of these operators is the $\frac{\partial^2}{\partial r^2}(rf)$-operator[19] in A, which can be discretized as

$$\frac{\partial^2}{\partial r^2}(rf) \to \frac{1}{\mathrm{dr}^2}\begin{bmatrix} -2 & 1 & 0 & 0 \\ 1 & \ddots & \ddots & 0 \\ 0 & \ddots & \ddots & 1 \\ 0 & 0 & 1 & -2 \end{bmatrix}\begin{pmatrix} \mathrm{dr}\cdot f(\mathrm{dr}) \\ 2\mathrm{dr}\cdot f(2\mathrm{dr}) \\ \vdots \\ r_{max}\cdot f(r_{max}) \end{pmatrix} \tag{6.69}$$

[17] See [f].

[18] This separation requires a little more explanation. A more general separation would be $f(\mathbf{r}) = f(r)\Theta(\theta,\phi)$, where Θ is some function. But any angular function can be written as a superposition of spherical harmonics and if some of the spherical harmonics in the expansion of Θ have different values of l, that function can no longer be an eigenfunction of anything for which the L^2-operator is the only angular dependent part. If all of the spherical harmonics in Θ have the same value of l they could be eigenfunctions, but so could other superpositions of the same harmonics perpendicular to the first one, and all these functions would have the same eigenvalue. In general if two functions solve the same eigenvalue-equation with the same eigenvalue, then so does some superposition of these two functions, implying that we can always pick Θ as being one single spherical harmonic.

[19] The operator is local in the limit $\mathrm{dr} \to 0$, but since we are doing a discretization this limit is not taken.

There are no errors at the endpoints since the function rf is 0 in $r = 0$, and also in $r \to \infty$ since the trap-part in H_0 would give an infinite contribution for $r \to \infty$ if the function had any other value than 0. If we choose $r_{\max}$ sufficiently large, correct behaviour is guaranteed for the functions with smallest eigenvalues[20]. The projection operator $\mathcal{Q}\circ f(\mathbf{r}) = \int \mathrm{d}\mathbf{r}'\mathcal{Q}(\mathbf{r},\mathbf{r}')f(\mathbf{r}')$ can be discretized as

$$\mathcal{Q}\circ \to \left(I - 4\pi \mathrm{dr} \begin{bmatrix} \varphi(\mathrm{dr})\varphi^*(\mathrm{dr})\mathrm{dr}^2 & \varphi(\mathrm{dr})\varphi^*(2\mathrm{dr})(2\mathrm{dr})^2 & \dots \\ \varphi(2\mathrm{dr})\varphi^*(\mathrm{dr})\mathrm{dr}^2 & \varphi(2\mathrm{dr})\varphi^*(2\mathrm{dr})(2\mathrm{dr})^2 & \dots \\ \vdots & \vdots & \ddots \end{bmatrix} \right) \tag{6.70}$$

for the spherical symmetric parts of $f(\mathbf{r})$, and as $\mathcal{Q}\circ \to I$ otherwise. This means that if f is proportional to a spherical harmonic $Y_l^m(\theta,\phi)$, we only should use the expression (6.70) if that spherical harmonic is Y_0^0, or rather when f has $l = 0$.

Using this we can write the left hand side of (6.62) as a compound matrix

$$\int \mathrm{d}r'\mathcal{L}_+(r,r')w_+(r') \;\to\; \begin{bmatrix} \left[\mathcal{Q}\circ A_+\mathcal{Q}\circ\right] & \left[\mathcal{Q}\circ B_+\mathcal{Q}^*\circ\right] \\ \left[-\mathcal{Q}^*\circ B_+^*\mathcal{Q}\circ\right] & \left[-\mathcal{Q}^*\circ A_+\mathcal{Q}^*\circ\right] \end{bmatrix} \begin{pmatrix} u_+(\mathrm{dr}) \\ \vdots \\ u_+(r_{\max}) \\ v_+^*(\mathrm{dr}) \\ \vdots \\ v_+^*(r_{\max}) \end{pmatrix}$$

$$\int \mathrm{d}r'\mathcal{L}_-(r,r')w(r') \;\to\; \begin{bmatrix} A_- & B_- \\ -B_-^* & -A_- \end{bmatrix} \begin{pmatrix} u_-(\mathrm{dr}) \\ \vdots \\ u_-(r_{\max}) \\ v_-^*(\mathrm{dr}) \\ \vdots \\ v_-^*(r_{\max}) \end{pmatrix} \tag{6.71}$$

and then we can find the w-functions as the eigenvectors to these matrices.

Since $\varphi(\mathbf{r})$ is a real function, $\mathcal{Q} = \mathcal{Q}^*$ and $B = B^*$, which means that both $\mathcal{L}_+$ and $\mathcal{L}_-$ are on the form $\begin{bmatrix} C & D \\ -D & -C \end{bmatrix}$. From this we see that if some $\bar{w}_i$ with $u_i(r) = x(r)$ and $v_i^*(r) = y(r)$ is a solution to (6.62) with eigenvalue ε, then so is another $\bar{w}_j$ with $u_j(r) = y(r)$ and $v_j^*(r) = x(r)$ with eigenvalue $-\varepsilon$. But we see from (6.31) that all solutions should fulfil

$$u_+^*\circ\mathcal{Q}\circ u_+ - v_+\circ\mathcal{Q}^*\circ v_+^* = 1 \quad \text{or} \quad u_-^*\circ u_- - v_-\circ v_-^* \tag{6.72}$$

and these equations cannot be solved by both of the two functions $\bar{w}_i$ and $\bar{w}_j$ simultaneously. It turns out[21] that the $\bar{w}$-functions solving (6.72) are those with a

[20] See appendix H.

[21] In the Schwinger model we proved this to be the case, and for the the full model the result is the same.

positive energy eigenvalue, i.e. the physical ones, so after discarding the negative eigenvalue eigenstates we are left with a number of k-states equal to the number of steps in the discretization, as would be expected. When we have found the correct set of $\bar{w}$s, we can use them to find the expectation values of the $\hat{J}$-operators using the results (6.52) from the previous section.

After the numerical solution procedure, we get each $\bar{w}$ labeled with three quantum numbers k, l and m. But in (6.52) the states are labeled using only one number i, so each i must correspond to a unique combination[22] of k, l and m. This means that whenever a sum over all states occurs, we should do the replacement

$$\sum_{i=0}^{\infty} f_i \to \sum_{k=0}^{k_{\max}} \sum_{l=0}^{l_{\max}} \sum_{m=-l}^{l} f_{klm} = \sum_{k=0}^{k_{\max}} \sum_{l=0}^{l_{\max}} (2l+1) f_{kl} \tag{6.73}$$

where the equality is true because there are $(2l+1)$ m-states for each l-state, and the results of the above calculations are independent of the m quantum number.

The source code to a program doing the calculations described in this section can be found in appendix G. The code is commented so it should be understandable using the results from this section. For a discussion of the precision of the numerical calculations, see appendix H.

[22] What exact relation we use does not matter as long as $i = 0$ corresponds to $k = l = m = 0$. If we use a maximum l-number $l_{\max}$ a possible indexing is $i = \big((l_{\max}+1)^2 \cdot k + l(l+1) + m\big)$. If we use an infinite number of l-states a possible indexing is $i = \big(\,(l(l+1)+m)\cdot(k_{\max}+1)+k\big)$ where $k_{\max}$ is the number of the final step in the discretization of the r-axis. Even if both $k_{\max}$ and $l_{\max}$ are infinite an indexing is possible. Inspired by the proof of the fact that the cardinality of $\mathbb{Q}$ is the same as for $\mathbb{N}$, we find a possible indexing to be $i = \Big(\frac{(k+l)(k+l+1)(k+l+2)}{3} - \frac{(k+l)(k+l+1)}{2} + l(l+1) + m\Big)$.

Chapter 7

Results

In this chapter the results produced by an implementation of the theory derived in the previous chapter, will be presented. The source code to the program producing these results can be found in appendix G. A discussion of the numerical input parameters (like the resolution and the length of the r-axis) is presented in appendix H, which concludes that the values of $\langle \hat{J}_x \rangle$ and $(\Delta J_z)^2$ found in this section are correct within a margin of error of 0.5%, while the calculated values of ξ^2 are correct within a margin of error of 1%. Not all results will be presented in this chapter, for further results without the thorough discussion found here see appendix I. Some of the figures in this chapter are shown in higher resolution in appendix J.

7.1 Structure of the equations: preliminary results

In this section we will discuss the structure of the equations and present some preliminary results, before discussing the main results about spin-squeezing in the next sections.

As we now know, the equation (6.38) can not be solved analytically, and it will therefore be solved numerically using the results from section 6.5. We can, however, look at the equation in various limits, and thereby try to get some ideas about how we expect the solutions to behave. As mentioned in section 6.4, the solutions will come in pairs[1], such that if $\bar{w}$ is a solution with eigenvalue ε, then so is $\bar{w}'$ with $u' = v$, $v' = u$ and $\varepsilon' = -\varepsilon$. All the negative eigenvalues can be discarded as unphysical, which leaves us with eigenvalues that we know to be ≥ 0. Let us write out the equation for the plus-states.

$$\begin{aligned} \mathcal{Q}\circ A_+ \mathcal{Q}\circ u_+(\mathbf{r}) + \mathcal{Q}\circ B_+ \mathcal{Q}^*\circ v_+^*(\mathbf{r}) &= \varepsilon u_+(\mathbf{r}) \\ \mathcal{Q}^*\circ B_+^* \mathcal{Q}\circ u_+(\mathbf{r}) + \mathcal{Q}^*\circ A_+ \mathcal{Q}^*\circ v_+^*(\mathbf{r}) &= -\varepsilon v_+^*(\mathbf{r}) \end{aligned} \tag{7.1}$$

[1] In the mentioned section this was calculated using the symmetry breaking approach where the $\mathcal{Q}$-functions were absent. But the same calculation can be done with $\mathcal{L}$ as given by (6.36).

where A and B are given by (6.16)

$$\begin{aligned} A_+ &\equiv H_0 - \mu + (U + U_{ab})|\psi|^2 + \frac{\Omega}{2} \\ B_+ &\equiv \frac{(U + U_{ab})}{2}(\psi)^2 \\ A_- &\equiv H_0 - \mu + U|\psi|^2 - \frac{\Omega}{2} \\ B_- &\equiv \frac{(U - U_{ab})}{2}(\psi)^2 \end{aligned} \tag{7.2}$$

We see that a solution to (7.1) is $u(\mathbf{r}) = \psi(r)$ and $v(\mathbf{r}) = -\psi(r)$ with eigenvalue $\varepsilon = 0$ because $\mathcal{Q}\circ\psi(r) = \mathcal{Q}^*\circ\psi^*(r) = 0$. A problem could arise from this solution, namely that it can not be properly normalized since (6.31) would always give zero and not one as required, as we saw in section 6.4. But luckily this problem does not concern us: We know that this ψ-eigenstate must have $l = 0$ because ψ is spherically symmetric. And because none of the eigenvalues are negative, we know that this is the lowest one, which assigns it $k = 0$ as well. This means that this ψ-eigenstate can be identified as the $\bar{w}_{0+}$-eigenstate which was excluded from all the sums from (6.42) to (6.45), and therefore it will never influence our physical results. The physical $\bar{w}_{0+}$-mode is of course the condensate-mode described by the $\hat{c}$-operator, but is is not a part of the perturbation and it is not treated as such. With the exception of the $\bar{w}_{0+}$-mode all the rest of the plus-modes will be orthogonal to ψ thanks to the $\mathcal{Q}$-operators, and ensuring this is the only function of these operators. In the following we will disregard the $\mathcal{Q}$-operators in order to simplify the equations.

Let us first have a look at the limit $U = U_{ab} = 0$. In this case $B_+ = 0$, so our equation for the radial part of the plus-states will become

$$\begin{aligned} (\check{\mu} + \varepsilon_{i+})\, u_{i+}(r) &= \frac{1}{2}\left(-\frac{1}{r}\frac{\partial^2}{\partial r^2}(r u_{i+}(r)) + \frac{l(l+1)}{r^2}u_{i+}(r) + r^2 u_{i+}(r)\right) \\ (\check{\mu} - \varepsilon_{i+})\, v^*_{i+}(r) &= \frac{1}{2}\left(-\frac{1}{r}\frac{\partial^2}{\partial r^2}(r v^*_{i+}(r)) + \frac{l(l+1)}{r^2}v^*_{i+}(r) + r^2 v^*_{i+}(r)\right) \end{aligned} \tag{7.3}$$

where

$$\check{\mu} \equiv \mu - \frac{\Omega}{2} \tag{7.4}$$

We see that the equations for u and v^* are uncoupled in this limit, and that both equations are identical to the Schrödinger equation for the three dimensional harmonic oscillator[2], with $E_u = \check{\mu} + \varepsilon$ and $E_{v^*} = \check{\mu} - \varepsilon$. From (4.6) and (5.12) we know that $\check{\mu} = \frac{3}{2}$ (in this limit), so this means that E_u always will be positive, while E_v will

[2]This is not surprising since our GP-Hamiltonian (4.17) was constructed by adding an interaction term to the 3D harmonic oscillator Hamiltonian, and the limit regarded here consists of setting that interaction to zero.

be negative if $\varepsilon > \frac{3}{2}$. The Schrödinger equation has no negative energy solutions, so the only way a contradiction can be avoided is if $v_+ = 0$ in all cases. This means that

$$\bar{w}_{klm+}(\mathbf{r}) = \begin{pmatrix} \phi_{kl}(r) \cdot Y_{lm}(\theta, \phi) \\ 0 \end{pmatrix} \tag{7.5}$$

is the correct solution to (7.3), where $\phi_{kl}(r)$ is the radial part of the wave function for the three dimensional harmonic oscillator with quantum numbers k, l, and m. The Schrödinger equation can be solved analytically in this case, and the solution (in NOU) is

$$\phi_{kl}(r) = N_{kl} r^l e^{-\frac{1}{2}r^2} L_k^{(l+\frac{1}{2})}(r^2) \tag{7.6}$$

where N_{kl} is a normalization constant and where the $L_n^{(\alpha)}(x)$-functions are known as the generalized[3] Laguerre polynomials defined by

$$L_n^{(\alpha)}(x) \equiv \frac{x^{-\alpha}e^x}{n!} \frac{\partial^n}{\partial x^n} \left(e^{-x} x^{n+\alpha}\right) \tag{7.7}$$

The associated energies are $E_{klm} = 2k + l + \frac{3}{2}$ which translate to

$$\varepsilon_{kl+} = 2k + l \tag{7.8}$$

The equation for the minus-modes is identical to (7.3) with the exception that $\Omega \to -\Omega$ or $\check{\mu} \to \check{\mu} + \Omega$. This transformation leaves the eigenfunctions the same $\bar{w}_{kl-} = \bar{w}_{kl+}$, and the energies are $\varepsilon_{kl-} = 2k + l - \Omega$. This means that the energy difference between a plus- and a minus-mode with the same quantum numbers is $E_{i-} - E_{i+} = \varepsilon_{i-} - \varepsilon_{i+} = -\Omega$.

The calculated energies and ϕ-functions are plotted in fig. 7.1. We see from fig. 7.1 and from (7.6) that the u-functions go as r^l close to $r = 0$ and that the functions have value zero at k different points[4]. So even though reincluding the interaction terms will change the form of the u-functions, these features are essential enough to remain after including the U-terms. Another effect of reincluding the U-terms is that the Bs in (7.2) become non-zero, which makes the vs different from zero, as we see in fig. 7.2 where the u and v-functions are plotted for non-zero values of U and U_{ab}.

Also the energies will change when the non-linear terms are included. Let us calculate the expectation values of $\hat{\mathcal{H}}$ in the states $|N\rangle_{0+}$, $|N-1\rangle_{0+} \otimes |1\rangle_{i+}$, and

[3] These differ from the ordinary Laguerre polynomials by the constant α. If we set $\alpha = 0$ we get the ordinary Laguerre polynomials.

[4] Excluding the zero at the limit $r \to \infty$ and for $l \neq 0$ the zero at $r = 0$.

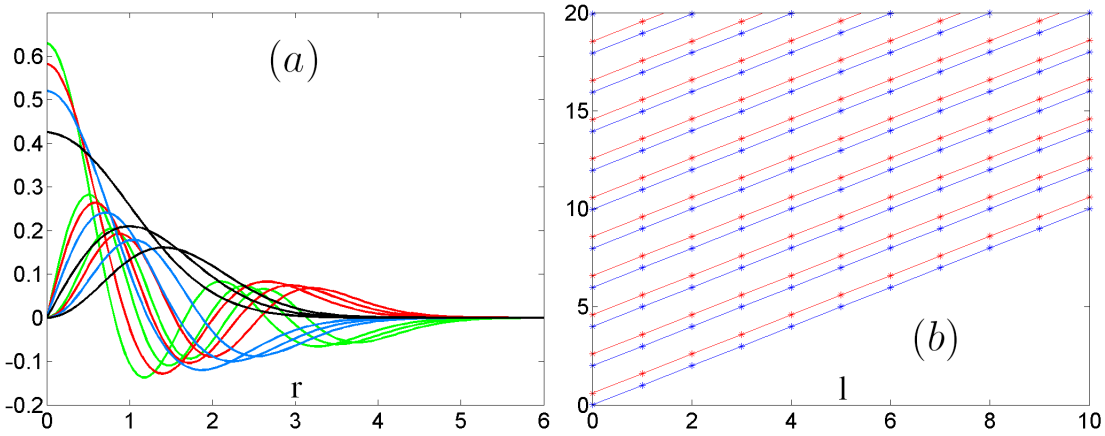

Figure 7.1: The solution to the three dimensional harmonic oscillator, corresponding to $U = U_{ab} = 0$. (a) shows the $\phi_{kl}(r)$-functions (or $u_{kl}(r)$-function) for various values of k and l. Black curves correspond to $k = 0$, blue correspond to $k = 1$, red to $k = 2$ and green to $k = 3$. For each k value a curve is plotted for $l = 0$, 1, and 2. (b) shows the values of ε_{kl}. Blue points are the results for the plus-modes and red points are the minus-modes. The l quantum number is on the horizontal axis and each curve corresponds to a fixed value of the k quantum number starting from zero from below. The plus- and minus-states are split by $-\Omega = 0.6$.

$|N-1\rangle_{0+} \otimes |1\rangle_{i-}$ using (5.11). The results are

$$\begin{aligned}
E_{0+} &= \int \mathrm{d}\mathbf{r} \left(N\varphi_{0+}^* H_0 \varphi_{0+} + N(N-1)\frac{U+U_{ab}}{4}|\varphi_{0+}|^4 \right) + N\frac{\Omega}{2} \\
E_{i+} &= \int \mathrm{d}\mathbf{r} \Big((N-1)\varphi_{0+}^* H_0 \varphi_{0+} + \varphi_{i+}^* H_0 \varphi_{i+} + (N-1)(N-2)\frac{U+U_{ab}}{4}|\varphi_{0+}|^4 \\
&\quad + (N-1)(U+U_{ab})|\varphi_{0+}|^2|\varphi_{i+}|^2 \Big) + N\frac{\Omega}{2} \\
E_{i-} &= \int \mathrm{d}\mathbf{r} \Big((N-1)\varphi_{0+}^* H_0 \varphi_{0+} + \varphi_{i-}^* H_0 \varphi_{i-} + (N-1)(N-2)\frac{U+U_{ab}}{4}|\varphi_{0+}|^4 \\
&\quad + (N-1)U|\varphi_{0+}|^2|\varphi_{i-}|^2 \Big) + (N-2)\frac{\Omega}{2} \qquad (7.9)
\end{aligned}$$

where as usual E_{i-} includes $i = 0$ while E_{i+} does not. In order to get a quantity similar to the ε_is, we can calculate the energy relative to the ground state

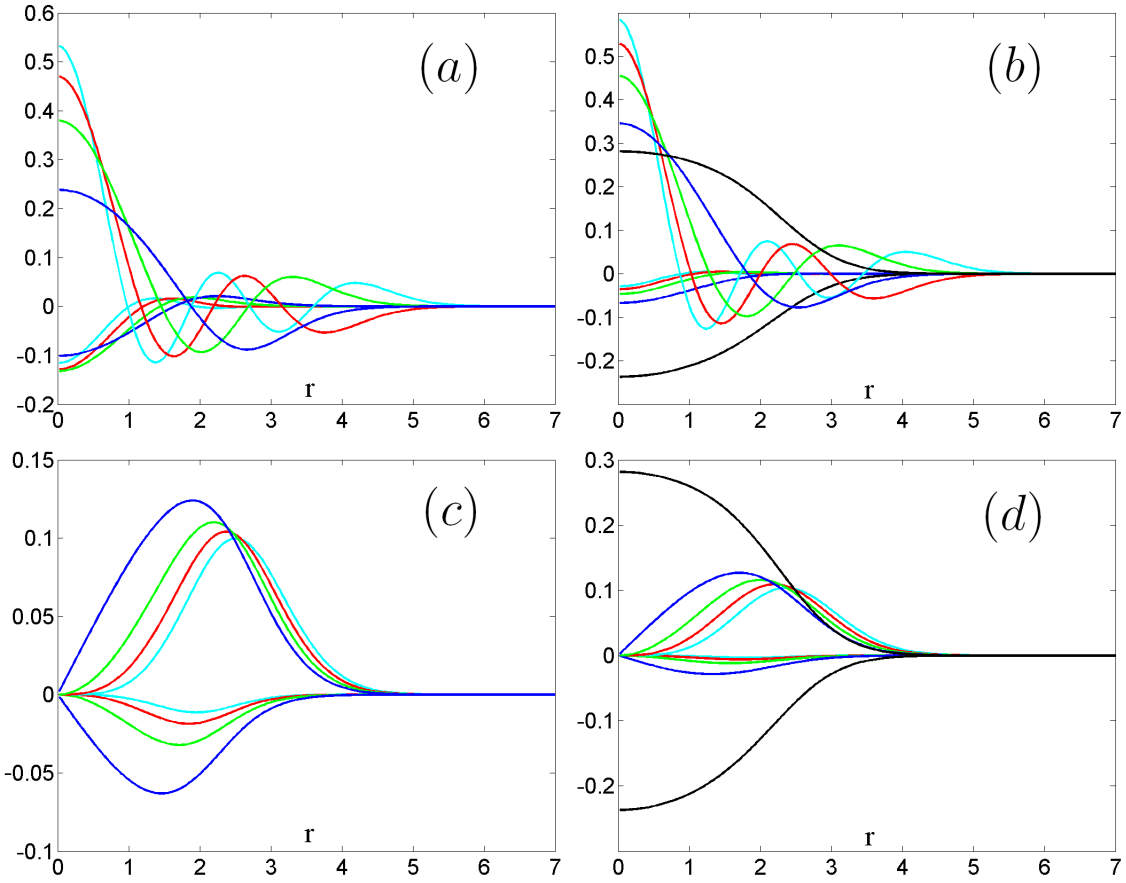

Figure 7.2: Some of the u and v functions as functions of r, for the parameters $N = 1000$, $U = 0.06$, $U_{ab} = 0.04$, and $\Omega = -0.01$. u and v have been normalized so the u function always starts out as positive, and all the plots show both of the functions. (a) and (b) show the functions for various values of the k-quantum number, while $l = 0$. (a) shows the plus-states while (b) shows the minus states. Black, blue, green, red, and azure correspond to $k = 0$, 1, 2, 3, and 4 respectively. (c) and (d) show the function for varying l while k is fixed at 0. (c) shows the plus-states and (d) shows the minus-states, while black, blue, green, red, and azure correspond to $l = 0$, 1, 2, 3, and 4 respectively. We notice on (a) and (c) that the u_{0+}-mode is absent. This is due to the mode being a numerical artifact as discussed in the main text.

$\mathcal{E}_{i\pm} \equiv E_{i\pm} - E_{0+}$, with the results

$$\begin{aligned}
\mathcal{E}_{i+} &= \int \mathrm{d}\mathbf{r}\Big(\varphi_{i+}^* H_0 \varphi_{i+} - \varphi_{0+}^* H_0 \varphi_{0+} - (N-1)\frac{U+U_{ab}}{2}|\psi_{0+}|^4 \\
&\quad + (N-1)(U+U_{ab})|\psi_{0+}|^2|\psi_{i+}|^2\Big) \\
\mathcal{E}_{i-} &= \int \mathrm{d}\mathbf{r}\Big(\varphi_{i-}^* H_0 \varphi_{i-} - \varphi_{0+}^* H_0 \varphi_{0+} - (N-1)\frac{U+U_{ab}}{2}|\psi_{0+}|^4 \\
&\quad + (N-1)U|\psi_{0-}|^2|\psi_{i+}|^2\Big) - \Omega
\end{aligned} \tag{7.10}$$

The i-numbering of the states in (7.10) refers to the index of the φ_i-functions. This is contrary to the use in the greater part of this thesis, where the i-numbering refers to the index of the u_i- and v_i-functions[5]. We have seen that in the case of $U = U_{ab} = 0$ there is a one to one correspondence between the two indices, so this means that $\mathcal{E}_i \approx \varepsilon_i$ can be regarded as true in the limit of small U and U_{ab}.

From (7.10) we can calculate the energy difference between a plus-state and a minus-state with the same value of i. Under the approximation $\varphi_{i+} = \varphi_{i-}$, we obtain the results

$$\begin{aligned}
\Delta\mathcal{E}_0 &\equiv \mathcal{E}_{0-} - \mathcal{E}_{0+} = -\Omega + (N-1)\frac{U-U_{ab}}{2}\int \mathrm{d}\mathbf{r}|\varphi_0|^4 \\
\Delta\mathcal{E}_i &\equiv \mathcal{E}_{i-} - \mathcal{E}_{i+} = -\Omega - (N-1)U_{ab}\int \mathrm{d}\mathbf{r}|\varphi_0|^2|\varphi_i|^2
\end{aligned} \tag{7.11}$$

where $i \neq 0$.

We see that in the limit $U = U_{ab} = 0$, both of these reduce to $\Delta\mathcal{E} = \Omega$ like we found previously. When this limit is not taken we get that $\Delta\mathcal{E}_0$ increases with the interaction, as long as $U > U_{ab}$. $\Delta\mathcal{E}_{\neq 0}$ on the other hand decreases with U, showing that given a large enough U, the sign of $\Delta\mathcal{E}_{\neq 0}$ can change so that $\mathcal{E}_{i+} > \mathcal{E}_{i-}$. In fig. 7.3 the simulated values of ε_i are plotted for a non-zero value of the U-terms. We see that the values behave in accordance with what is expected from (7.11).

As we saw in section 5.1 the two-mode approximation predicts that $\Omega = 0$ corresponds to $\langle \hat{J}_x \rangle = 0$. But as we will see later, that is not the case for the full Bogoliubov calculation, where a slightly positive Ω is needed in order to get $\langle \hat{J}_x \rangle = 0$. This can be explained by the positive extra term in the expression for $\Delta\mathcal{E}_0$ in (7.11). The expressions (7.10) and their similarity to the ε_is will be of further use in the coming sections where they are used to explain other details of our results.

[5]If we split the two different i-indices in k, l and m quantum numbers, we get that the l and m quantum numbers has a one to one correspondence between the two different numberings, while the k has not, except in the limit of $U = U_{ab} = 0$ as we have seen.

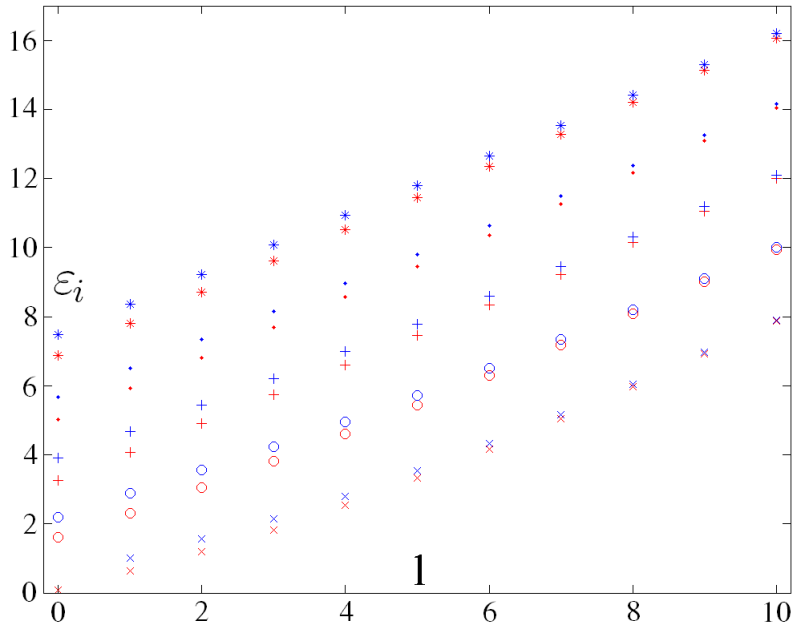

Figure 7.3: Some of the energy eigenvalues for the parameters $N = 1000$, $U = 0.06$, $U_{ab} = 0.04$, and $\Omega = -0.01$. Blue points correspond to plus-modes and red to minus-modes, and $\times$, $\circ$, $+$, $\bullet$, and $*$ correspond to $k = 0$, 1, 2, 3, and 4 respectively. The l quantum number is on the horizontal axis.

Let us have a look at the expectation values of the $\hat{J}$- operators. For the case of zero temperature they are given by (6.52), which can be written

$$\begin{aligned} \langle \hat{J}_x \rangle &= \frac{N}{2} - V_- \\ (\Delta J_z)^2 &= \frac{N}{4} + \frac{N - V_- - V_+}{4} W_- \end{aligned} \tag{7.12}$$

where

$$\begin{aligned} V_- &\equiv \sum_i \left(v_{i-}^* \circ v_{i-} \right) \\ V_+ &= \sum_{i \neq 0} \left(v_{i+}^* \circ \mathcal{Q} \circ v_{i+} \right) \\ W_- &= \sum_i \left(\varphi^* \circ u_{i-} \varphi^* \circ v_{i-} + 2 v_{i-}^* \circ \varphi \varphi^* \circ v_{i-} + v_{i-}^* \circ \varphi u_{i-}^* \circ \varphi \right) \end{aligned} \tag{7.13}$$

We see that if $v_i = 0$ for all i, we get $V_- = V_+ = W_- = 0$ corresponding to $\langle \hat{J}_x \rangle = \frac{N}{2}$ and $(\Delta J_z)^2 = \frac{N}{4}$, which are the values we get for the SCS in the J_x-direction. This indicates that at the point of perturbation, we expect $v_i = 0$ for all i. In order to explain this and predict the behaviour away from that point, we will make a model where we ignore the r-dependence of the u and v-functions. In that

case we can find a crude expression for v like we did in the case of the Schwinger model, by diagonalizing $\mathcal{L}$ analytically. The result is similar to (5.45), and is given by

$$v_i = \frac{-1}{\sqrt{C_i^2 - 1}} \tag{7.14}$$

where

$$C_i \equiv \frac{B_i}{\sqrt{A_i^2 - B_i^2} - A_i} \tag{7.15}$$

A similar expression for u can be found using $u_i \circ u_i - v_i \circ v_i = 1$. If we define $\Phi_i \equiv B_i/A_i$, we can rewrite the expression for C_i to

$$C_i = \frac{\Phi_i}{\sqrt{1 - \Phi_i^2} - 1} \tag{7.16}$$

from which we see that only the proportion between A_i and B_i matters, and not their absolute values. We see that C_i^2 is a decreasing function of $|\Phi_i|$, and that $-v_i$ is a decreasing function of C_i^2, showing that $-v_i$ is an increasing function of $|\Phi_i|$. The function is plotted in fig. 7.7a in the next section, and we can calculate that near $|\Phi_i| = 0$ it goes as $v_i = -\frac{1}{2}|\Phi_i|$.

As $\Omega \to -\infty$ we see from (7.2) that $A_{i-} \to \infty$ while B_{i-} stays unchanged, making $\Phi_{i-} \to 0$ and thereby $v_{i-} \to 0$. This explains why $v_{i-} = 0$ corresponds to the point of perturbation, since the perturbation is made around the point where $-\Omega \gg 1$.

7.2 Results for zero temperature

In this section the results for the spin-squeezing at zero temperature will be presented. In figs. (7.4) and (7.5) we show $(\Delta J_z)^2$ vs $\langle \hat{J}_x \rangle$ for different values of $s \equiv U + U_{ab}$ and $f \equiv U_{ab}/U$, and using (3.30) we can easily calculate that all the included values of s and f produce some amount of spin-squeezing[6]. The curves have been made by doing the calculation for different values of Ω, and each value of Ω corresponds to a point on the curve in question. We see that some values of s and f bring the curve closer to the F-function which is plotted in red as comparison, and since the curves do not cross each other, we know that the curve closest to the F-function gives the most spin-squeezing. We see that the point of maximal squeezing is relatively close to $\langle \hat{J}_x \rangle = N/2$ which is unlike the result for the two-mode function where the minimum was found to be at $\langle \hat{J}_x \rangle = 0$. $\mathfrak{Q}$-functions[7] for the produced states are shown in fig. 7.6, for one combination of parameters.

[6] As mentioned in sections 4.3 and 5.1 we limit the discussion to U and $U_{ab} \geq 0$, and $U \geq U_{ab}$. This corresponds to $s \geq 0$ and $0 \leq f \leq 1$.

[7] We have to use the $\mathfrak{Q}$-function defined by (3.29) instead of the more physical Q-function, since we do not have the Bogoliubov states expressed in the $|j, m\rangle$-basis. See sections 3.3 and 8.2.

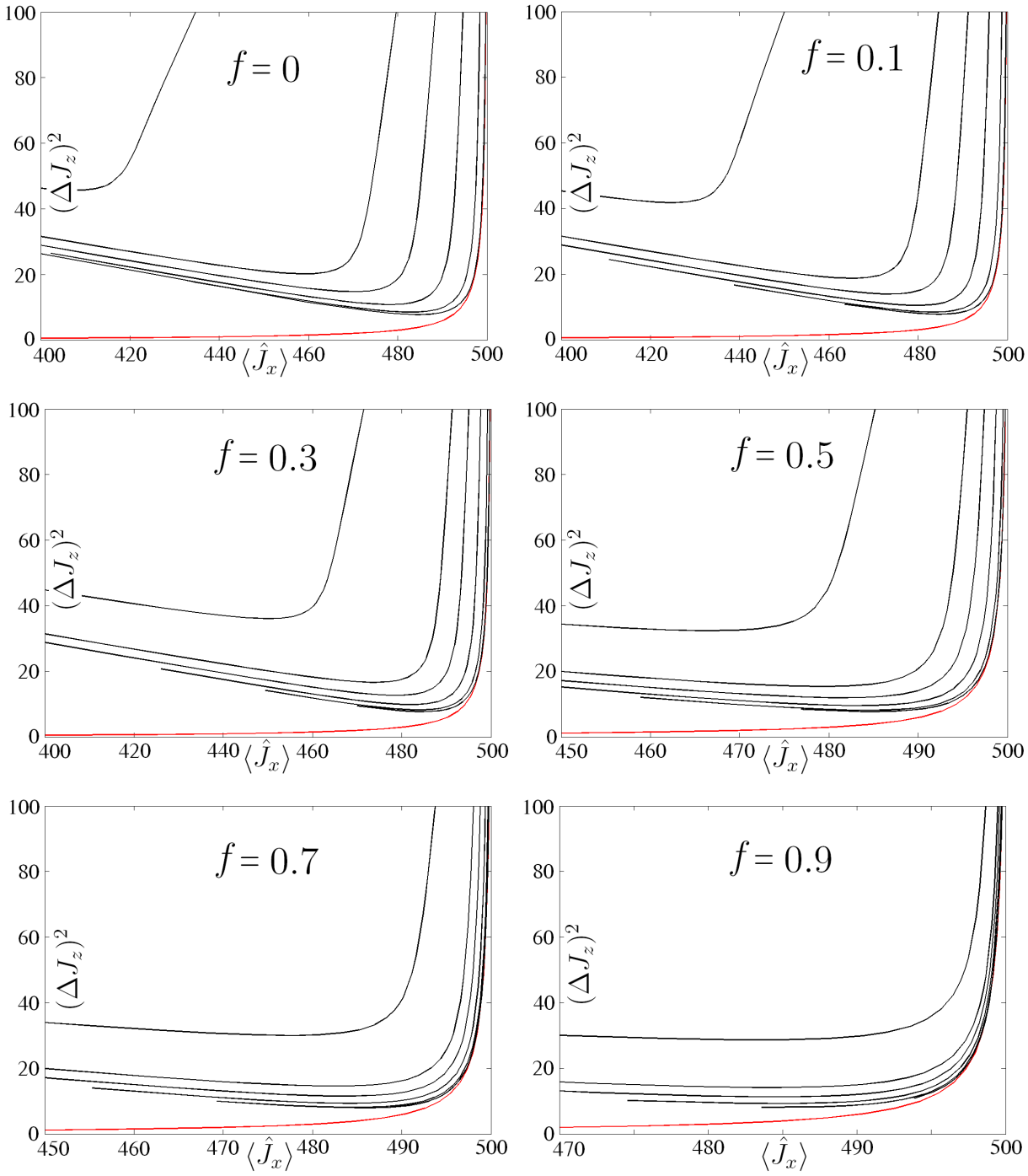

Figure 7.4: Graphs for $(\Delta J_z)^2$ vs $\langle \hat{J}_x \rangle$ for zero temperature and $N = 1000$. Each subplot corresponds to a fixed values of U_{ab}/U and each of the black curves to some value of $U + U_{ab}$. The values of $U + U_{ab}$ are 0.01, 0.1, 0.3, 0.6, 1, and 3 from below. The red curve is the ideal result given by the F-function. We see that as $U + U_{ab}$ approaches zero, the curves approach the ideal curve, indicating that for zero temperature, the parameters maximizing the squeezing are $U + U_{ab} \approx 0$. The data plotted here are the same as those plotted in fig. 7.5.

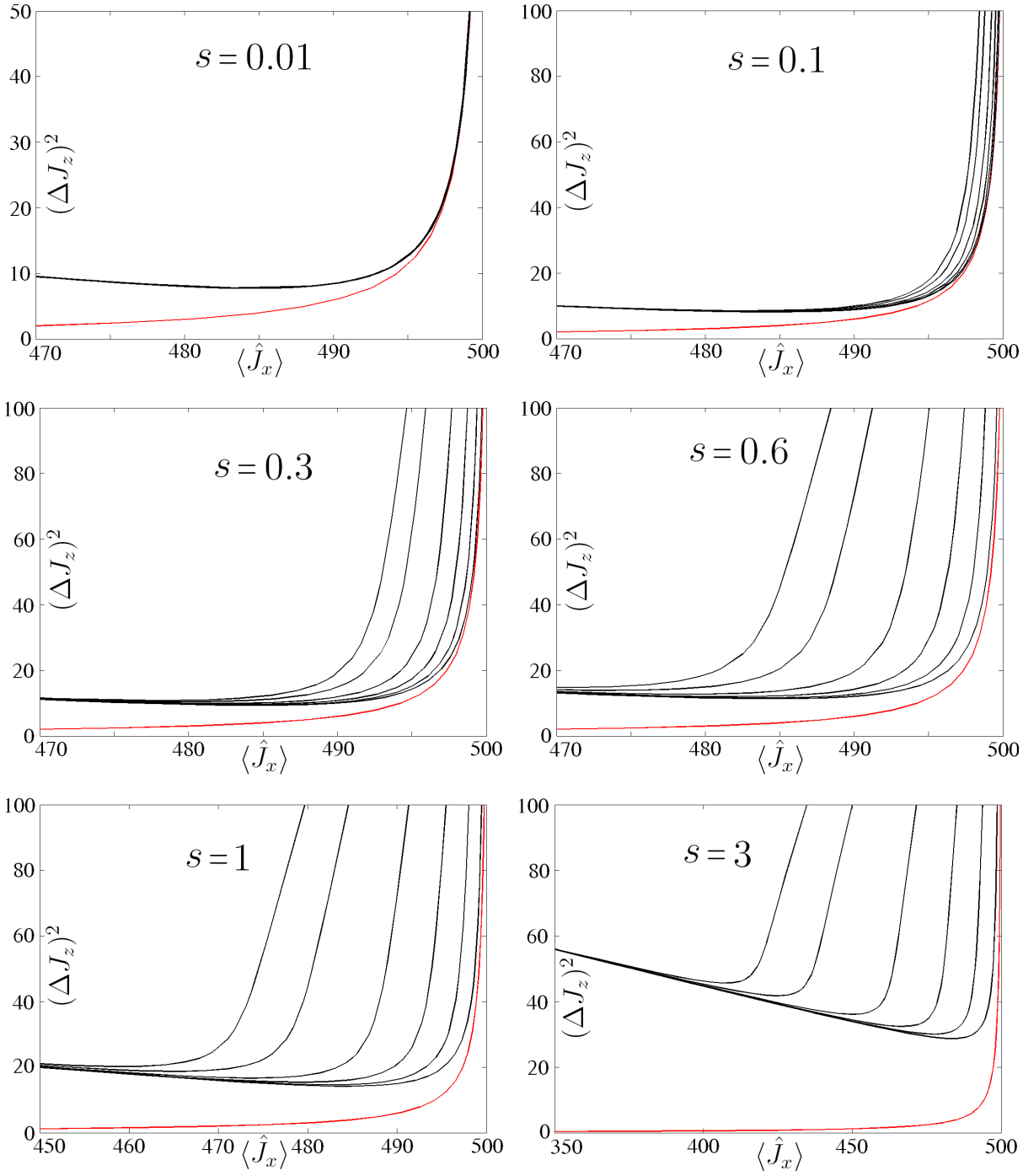

Figure 7.5: Graphs for $(\Delta J_z)^2$ vs $\langle \hat{J}_x \rangle$ for zero temperature and $N = 1000$. Each subplot corresponds to a fixed values of $U + U_{ab}$ and each of the black curves to some value of U_{ab}/U. The values of U_{ab}/U are 0, 0.1, 0.3, 0.5, 0.7, and 0.9 from above. The red curve is the ideal result given by the F-function. We see that as U_{ab}/U approaches one, the curves approach the ideal curve, indicating that for zero temperature, the parameters maximizing the squeezing have $U \approx U_{ab}$. The data plotted here are the same as those plotted in fig. 7.4.

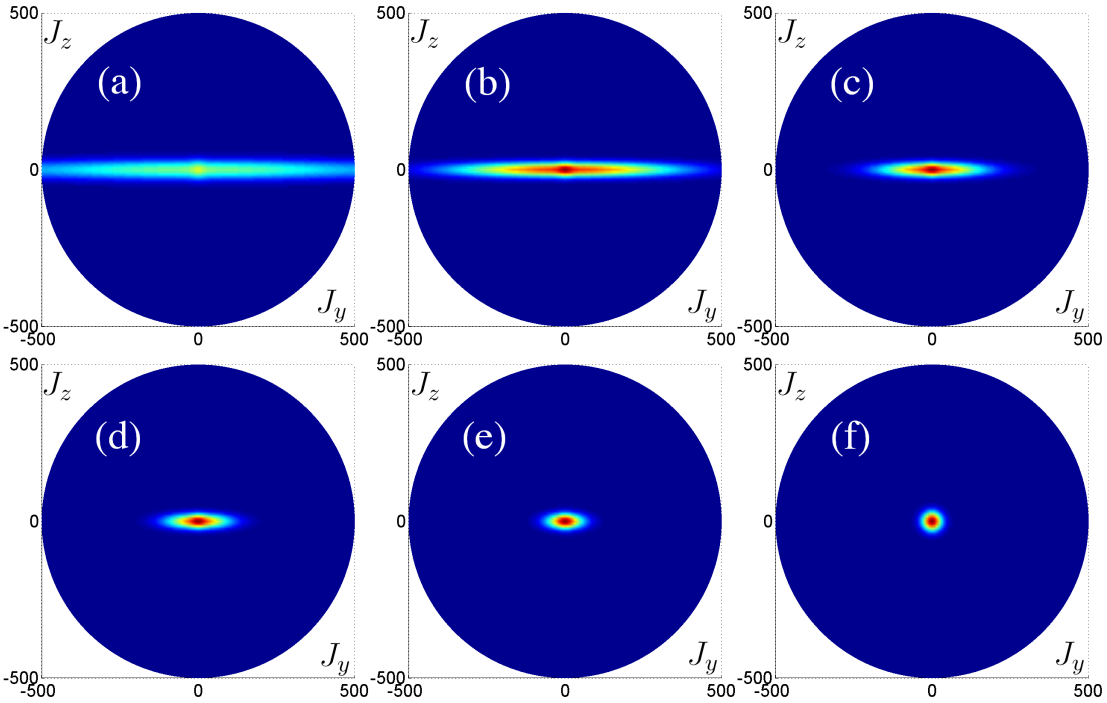

Figure 7.6: $\mathfrak{Q}$-functions for the states at different values of Ω, for $U = 0.06$, $U_{ab} = 0.04$, $N = 1000$ and $\mathcal{T} = 0$. The values of Ω from (a) to (f) are 0.00015, 0.00012, -0.000005, -0.001 -0.01, and -1 respectively. $\Omega = -0.000005$ gives a squeezing very close to the maximum for these parameters, the value is $\xi^2 = 0.0346$. The plot for $\Omega = 0.00015$ has $\langle \hat{J}_x \rangle = -365.30$, and at that point the approximation $N \approx N_0$ has broken down.

It turns out that small values of s and values of f close to one, bring the curves closest to the F-function. In section 4.3 we saw that a larger value of the constant U_0, which for the one-species case discussed there played the same role as $s/2$ does in two-species GPE (5.12), corresponds to a broader $\psi(\mathbf{r})$-function. From the classical expression for the angular momentum $L = \mathbf{r} \times \mathbf{p}$ we see that a broader ψ therefore makes the value of $\mathbf{p}$ needed to access a state with some angular momentum, smaller, which is equivalent to stating that less energy[8] is needed to access modes with $l \neq 0$. This will decrease the value of the $\sum_i (\varphi \circ \varphi_{i-})$-terms in the expression for $(\Delta J_z)^2$, since the terms in the sum with $l \neq 0$ give zero contribution. The consequence of this is that the curves will be moved in the direction of less squeezing, which explains why a small value of s gives the most squeezing.

The observed f-dependence can be explained from the time-energy uncertainty relation, from which we see that a smaller characteristic time of an excitation of the system corresponds to a greater uncertainty of the energy, meaning that the

[8]This can also be seen directly from the classical expression for energy in terms of angular momentum $E = \frac{L^2}{2I}$ where I is the moment of inertia which in general goes as r^2 and therefore increases when s does.

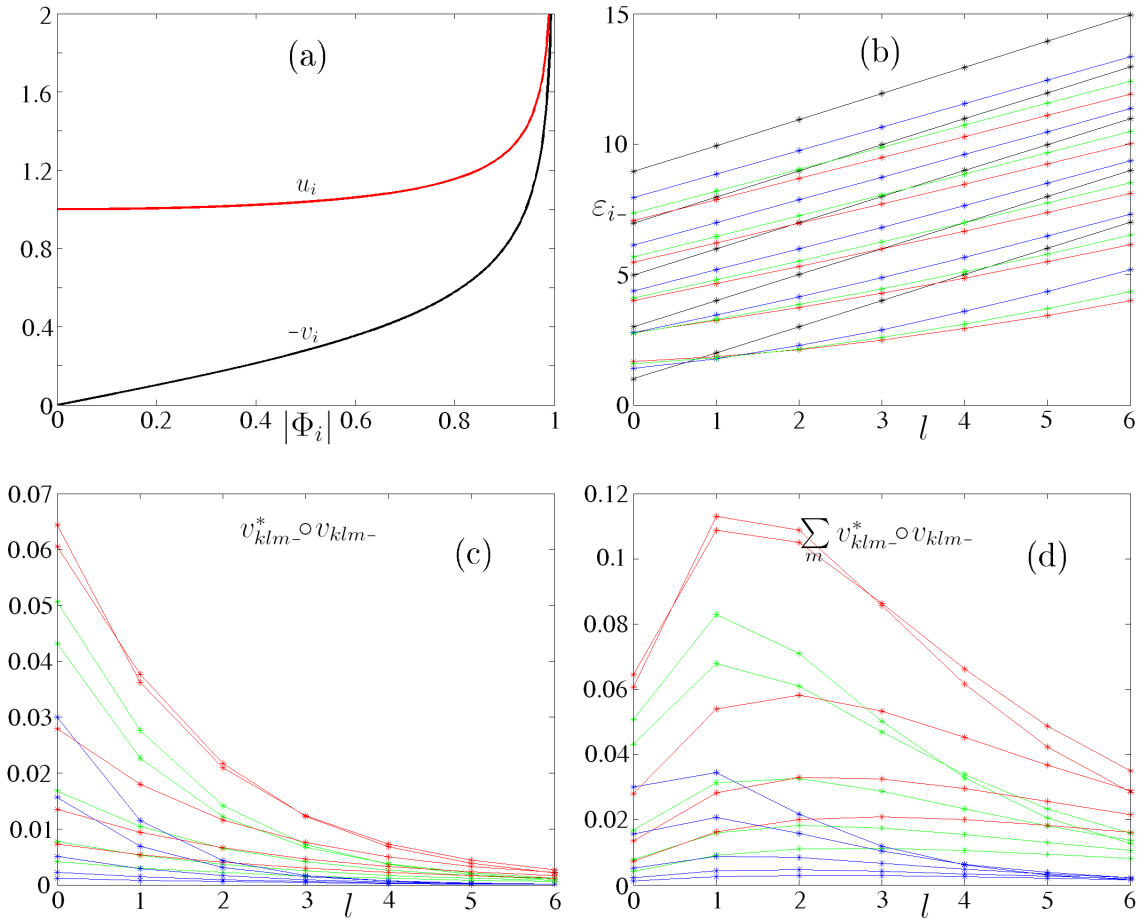

Figure 7.7: These graphs explain the behaviour of the subplots in figs. 7.4 and 7.5. (a) is a plot of the simplified functions u_i and $-v_i$ as functions of the fraction $\Phi_i \equiv B_i/A_i$, given by (7.14) and (7.16). (b) is similar to fig 7.3 and shows the values of ε_{kl-} for different values of $s \equiv U + U_{ab}$. Black points correspond to $s = 0$, blue to $s = 0.2$, green to $s = 0.6$ and red to $s = 1$. The l-quantum number is on the horizontal axis and each set of curves corresponds to values of $k = 0$, 1, 2, 3, and 4 from below. (c) shows values of $v^*_{kl-} \circ v_{kl-}$ with the same colour code as (b) excluding $s = 0$ which gives $v_{kl-} = 0$, and (d) shows the same values multiplied with $2l + 1$ showing how large s ensures that only a small part of W_- comes from the $l = 0$-states. On (c) and (d) each set of curves correspond to $k = 0$, 1, 2, 3, and 4 this time starting from above.

chance of the excitation being to a higher energy state is larger which decreases the squeezing. The characteristic time is inversely proportional to χ which goes as $\chi \propto s(1 - f)/(1 + f)$ from which we see that χ decreases when f increases. This explains why values of f close to one maximizes the squeezing.

A more mathematical explanation of these results can be seen from our position-independent model from the previous section. Around the point of perturbation, each Φ_i and consequently every v_i will be small, meaning that we can disregard the

v_i^2-terms and set $u = 1$, giving

$$(\Delta J_z)^2 = \frac{N}{4} + \frac{N}{4} W_- \quad , \quad W_- \propto \sum_i \varphi^* \circ v_{i-} \tag{7.17}$$

indicating that all the relevant contributions come from the minus-states. Keeping f fixed and increasing s will have the effect of increasing Φ_{i-}, $-v_{i-}$, and thereby V_- and $-W_-$. But we see that only terms with $l = 0$ give a contribution to W_- since the other terms have $\varphi^* \circ v_{i-} = 0$, so the value of W_- will be most sensitive to change, in configurations where a large part of the contribution to V_- comes from the $l = 0$-terms.

From (7.2) we see that a higher value of s corresponds to a higher value of Φ_{i-} for high values of $-\Omega$. A higher Φ_{i-} causes a higher v_{i-} for each value of i, which means that configurations with high s has more of the contribution to V_- coming from the $l \neq 0$-states which makes the response in W_- to changes in Ω relatively smaller, giving higher values of $(\Delta J_z)^2$ for a given value of $\langle \hat{J}_x \rangle$. Another way to formulate this is that higher s corresponds to lower values of $\frac{\mathrm{d}W_-}{\mathrm{d}V_-}$, thereby making the slope of the $(\Delta J_z)^2$ vs. $\langle \hat{J}_x \rangle$-curves smaller close to $\langle \hat{J}_x \rangle = N/2$ which takes it further away from the F-function in the direction of less squeezing, just as we see from fig 7.4. Likewise we see from (7.2) that higher values of f correspond to a higher value of Φ_{i-} which indicates that increasing f has the same effect as decreasing s, which is just what we see from fig. 7.5.

We notice that isolating N_0 in (7.12) gives $N_0 = \frac{1}{2}N - V_+ + \langle \hat{J}_x \rangle$. This means that if $V_+ \ll \langle \hat{J}_x \rangle$ as is the case close to the point of perturbation, we have that the "correctness-parameter" for the approximation of discarding higher order terms in $\delta\hat{\psi}$ is given as $\frac{N-N_0}{N} = \frac{1}{2} - \frac{\langle \hat{J}_x \rangle}{N}$ showing that for the values plotted in figs. 7.4 and 7.5 the approximation is still valid.

For the ideal case of the F-functions (3.39), the Schwinger model (5.50), and for the time-dependent two-mode model described by (5.18) in the "Kitagawa and Ueda"-part of section 5.3, we were able to find an expression for the squeezing as function of the particle number. For the F-functions and for the Schwinger model we had $\xi^2 \propto N^{-1}$ for large N, while the time dependent case had $\xi^2 \propto N^{-\frac{2}{3}}$ as we saw in (5.18). For the Schwinger model the result was found by fitting a function to the numerical results, and the same technique will be used here. We keep the value of $N(U + U_{ab})$ in order to keep the value of[9] $\breve{\mu}$. In addition we have the free variables f, Ω, and the temperature $\mathcal{T}$, so we limit the discussion to some fixed values of these parameters: zero temperature, $N(U + U_{ab}) = 100$, and $f = \frac{2}{3}$. A plot of $(\Delta J_z)^2/J$ vs. $\langle \hat{J}_x \rangle / J$ is shown in fig. 7.8 for different values of N, and from these results we

[9] As we saw in section 4.3, μ is a function of N and U only through the product NU in both the Gaussian approximation and the Thomas-Fermi approximation. This result is also valid for the two-species model, with the replacements $\mu \to \breve{\mu}$ and $U_0 \to \frac{1}{2}(U + U_{ab})$

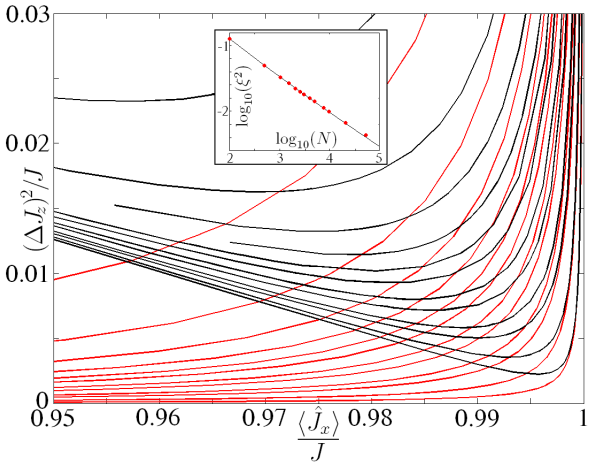

Figure 7.8: This plot shows $\langle \hat{J}_x \rangle / J$ vs. $(\Delta J_z)^2/J$ for different N, but constant $N(U + U_{ab}) = 100$ and $U_{ab}/U = \frac{2}{3}$. The black curves are the results, while the red curves are the F-functions as comparison. The values of N are 500, 1000, 1500, 2000, 2500, 3000, 4000, 5000, 7500, 10000, 20000, and 50000 from above. The insert shows the curve given by (7.18) and the points of data to which it is fitted.

get that the Ω minimizing ξ gives the squeezing parameter[10]

$$\xi^2 \approx \frac{1.31}{(N-17)^{0.527}} \tag{7.18}$$

where we see that the scaling with N is less advantageous than for all the previous models. (7.18) is plotted in the insert in fig. 7.8, along with the data points. The fact that the scaling with N is worse than for the squeezing produced by the F-functions is not surprising, since the existence of the Bogoliubov modes bring the system away from the two-mode approximation as argued above. The fact that the scaling with N is worse than what was calculated from the time-dependent approach, is, however, bad for the usefulness of the steady-state approach presented in this thesis.

7.3 Results for non-zero temperatures

The results of a simulation of how the squeezing depends on the temperature, can be seen in fig. 7.9. We see that the $(\Delta J_z)^2$ vs. $\langle \hat{J}_x \rangle$-curves for high temperatures lie above those for low temperatures, giving rise to less spin-squeezing. Fig. 7.9b shows a zoom on the rightmost part of these functions, and we see that independent of the temperature, some amount of squeezing is obtained very close to the point of perturbation. $\mathfrak{Q}$-functions for a non-zero temperature are plotted in fig. 7.10.

[10] The fitted function had the form $\frac{a}{(N+b)^c}$, and the fitting result was $a = 1.30648 \pm 0.02111$, $b = -17.792 \pm 1.067$, and $c = 0.526847 \pm 0.002174$. The fit was made to the 13 points seen in the insert in fig. 7.8.

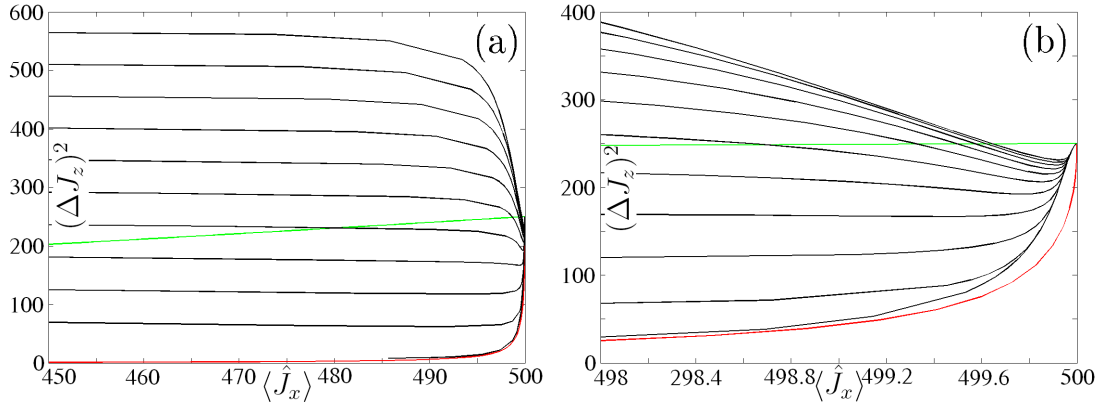

Figure 7.9: The black curves on these figures show $(\Delta J_z)^2$ vs. $\langle \hat{J}_x \rangle$ for different temperatures. The red curve shows the F-function describing the ideal case as comparison, while the green curve shows the function corresponding to $\xi = 1$. The temperatures go from 0 to 0.49 with an interval of 0.049 from below. For the trap-frequency mentioned in [13], $\mathcal{T} = 0.049$ corresponds to $T = 1$nK. The interaction constants are $U = 0.06$ and $U_{ab} = 0.04$, and $N = 1000$. The two subfigures differ by the zoom only.

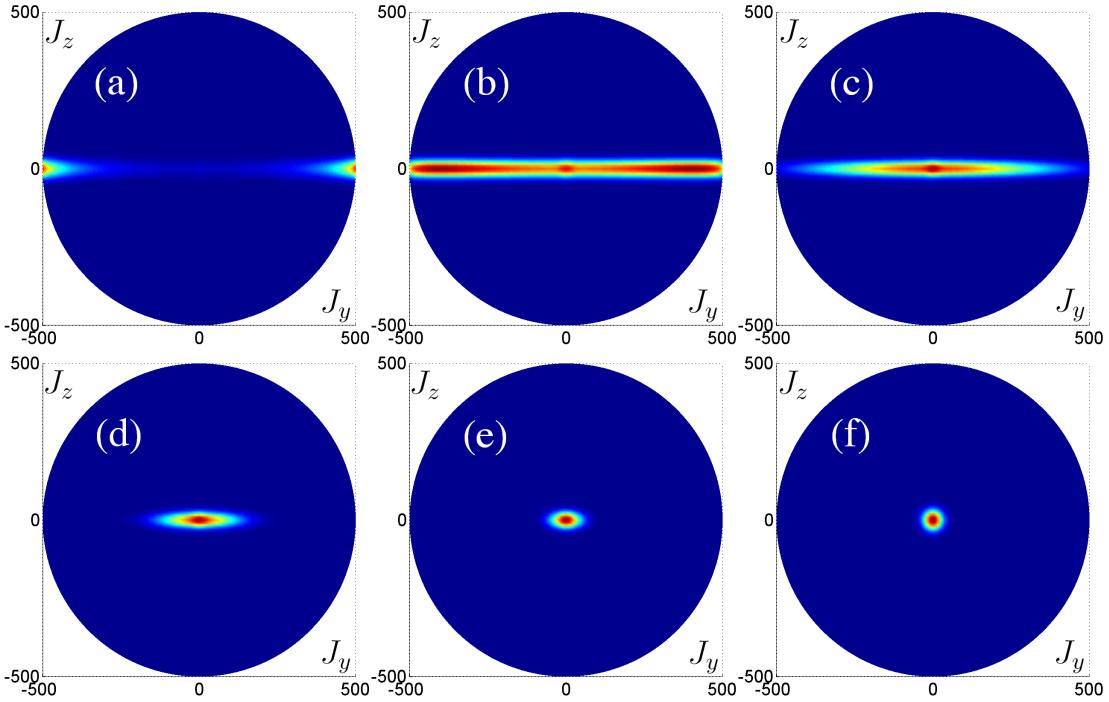

Figure 7.10: $\mathfrak{Q}$-functions for the states at different values of Ω for $\mathcal{T} = 0.049$. The shown states have $U = 0.4$, $U_{ab} = 0.2$, and $N = 1000$. The values of Ω from (a) to (f) are 0.00006, 0, -0.00025, -0.004 -0.1, and -10 respectively. $\Omega = -0.00025$ gives a squeezing very close to the maximum for these parameters, the value is $\xi^2 = 0.1039$. The plot for $\Omega = 0.00006$ has $\langle \hat{J}_x \rangle = -80.29$, and at that point the approximation $N \approx N_0$ has broken down.

It is not surprising that higher temperatures corresponds to lower squeezing, since higher temperatures will give rise to higher occupation levels of the Bogoliubov modes, as seen from (6.47). We see that further away from the point of perturbation where $-\Omega$ is small, $(\Delta J_z)^2$ takes an almost constant value proportional to the temperature. This can be explained by the parallel to the xp-case explained in section 5.5, where we see from (5.26) that $\hat{J}_z$ behaves as $\sqrt{N/2}\ \hat{x}$ near the point of perturbation. This means that the Hamiltonian can be written as $\mathcal{H} \propto \frac{\chi N}{2}\hat{x}^2$ ignoring the Ω-term. This is similar to the classical expression for the potential energy in a harmonic oscillator $E = \frac{1}{2}kx^2$ with $k = \chi N$. For a classical harmonic oscillator the thermal probability distribution is $p(x) = \sqrt{k/(2\pi\mathcal{T})}\exp\left(-kx^2/(2\mathcal{T})\right)$ from which we can calculate $\langle\hat{x}^2\rangle = \mathcal{T}/k$ which is proportional to $\mathcal{T}$, as we see for $(\Delta J_z)^2$ in fig. 7.9.

For a more detailed explanation of the behaviour shown in fig. 7.9, we use our position-independent model. As we can see from (6.48)-(6.51), we can let (7.12) maintain its form if (7.13) is redefined to

$$\begin{aligned}
V_- &= \sum_i \Big(v_{i-}^* \circ v_{i-} \big(\langle n \rangle_{i-} + 1 \big) + u_{i-}^* \circ u_{i-} \langle n \rangle_{i-} \Big) \\
V_+ &= \sum_{i>0} \Big(v_{i+}^* \circ \mathcal{Q} \circ v_{i+} \big(\langle n \rangle_{i+} + 1 \big) + u_{i+}^* \circ \mathcal{Q} \circ u_{i+} \langle n \rangle_{i+} \Big) \\
W_- &= \sum_i \Bigg(\Big(\varphi^* \circ u_{i-} \varphi^* \circ v_{i-} + 2 v_{i-}^* \circ \varphi \varphi^* \circ v_{i-} + v_{i-}^* \circ \varphi u_{i-}^* \circ \varphi \Big) \Big(\langle n \rangle_{i-} + 1 \Big) \\
&\qquad + \Big(\varphi^* \circ v_{i-} \varphi^* \circ u_{i-} + 2 u_{i-}^* \circ \varphi \varphi^* \circ u_{i-} + u_{i-}^* \circ \varphi v_{i-}^* \circ \varphi \Big) \langle n \rangle_{i-} \Big)
\end{aligned} \tag{7.19}$$

where the final result can be approximated as

$$W_- \propto \sum_i \Big(\varphi^* \circ v_{i-} + \varphi^* \circ u_{i-} \langle n \rangle_{i-} \Big) \tag{7.20}$$

near the point of perturbation.

$v_i = 0$ and $u_i = 1$ at the point of perturbation as we have seen, and from (7.10) we see that $\mathcal{E}_{i-}$, and therefore ε_{i-}, is infinite at that point, which makes $V_- = V_+ = W_i = 0$. This ensures that $(\Delta J_z)^2 = N/4$ and $\langle \hat{J}_x \rangle = N/2$ at the point of perturbation, as we saw in the temperature independent case.

We know that near the point of perturbation, the points of maximal squeezing will almost coincide with the minima of the $(\Delta J_z)^2$ vs. $\langle \hat{J}_x \rangle^2$-curves. These points can be found by finding the minimum of (7.20), which will be where the $\varphi \circ v_{i-}$-term dominates the most over the $\varphi^* \circ u_{i-}\langle n \rangle_{i-}$-term. A higher temperature will give more weight to the $\varphi^* \circ u_{i-}\langle n \rangle_{i-}$-term, which makes the values of $-\Omega$ required to make the energy high enough to make the $\varphi \circ v_{i-}$-term dominant even larger. This ensures that the curve will diverge from the zero-temperature case even

closer to the point of perturbation, thus giving less squeezing as we see from fig. 7.9.

A simulation with varying s and f, similar to the zero temperature case from the previous section, has been made for non-zero temperatures as well. In figs. 7.11 and 7.12 the results are plotted for one value of $\mathcal{T}$, and for other values of $\mathcal{T}$ the results can be found in appendix I. The same values of s and f have been used as in the previous section.

We see that it is no longer the case that a low s and a f close to one maximizes the squeezing, as we saw in the zero-temperature case. In fact the limit becomes the opposite for sufficiently high temperatures[11], and for the temperature used in figs. 7.11 and 7.12 we see that the optimal values are somewhere in between the two extrema. This can be understood from the fact that inclusion of a temperature introduces a new energy-scale, that of $\mathcal{T}$, in the system. The effects of the temperature will be smallest when $\mathcal{T} \ll \chi$, and χ is largest for large s and small f.

Our position-independent model can explain these results as well. We remember that the points of maximal squeezing are the points making the $\varphi \circ v_{i-}$-term in (7.20) dominant. For low temperatures, the $\varphi \circ v_{i-}$-term will always be dominant and the behaviour will be as described for the zero-temperature case. But for the high-temperature case we want some values of s and f that give as much weight to the $\varphi \circ v_{i-}$-term as possible for a given value of Ω, and we saw in the previous section that $-v_{i-}$ is maximized by high s and low f, indicating that for high temperatures the squeezing will be maximized in this opposite limit. For temperatures between the two limits, some set of s and f between the two extrema is expected to maximize the squeezing, just as we see in figs. 7.11 and 7.12.

I have tried to make a detailed calculation which imitates the values used in the experiment by Marcus Oberthaler described in [13] and in section 5.4. When calculating the value of U the average of a_{aa} and a_{bb} is used resulting in the scattering length $a = 97.5a_0$. From this we can calculate U using (4.12) with the result[12] $U = 4.99 \cdot 10^{-51}$ Jm^2 which corresponds to $U = 0.124$ in the natural oscillator units. As described in section 5.4, the experiment adjusts the value of a_{ab} using a Feshbach resonance, so that the measured value of χ becomes $\chi = 2\pi \times 0.063$Hz corresponding to $\chi = 148 \cdot 10^{-6}$ in NOU. We know, however, that in the limit of large interaction $Ns \gg 1$ the physical value of χ is[13] $\frac{7}{10}$ times the value $\chi = |\varphi|^4(U - U_{ab})$ given by (5.7). This means that the value of χ we should use when finding U_{ab} using (5.7) is $\chi = 212 \cdot 10^{-6}$. From this we can calculate[14] U_{ab} with the result[15] $U_{ab} = 0.103$. The

[11] We can not see this from figs. 7.11 and 7.12 alone. Similar plots for different temperatures are shown appendix I. See specifically fig. I.3 in that appendix.

[12] The values for ω and m used in these calculations are $\omega = 2\pi \times 425$Hz and $m = 87u$ where u is the atomic mass unit. Both values are listed in the relevant part of section 5.4.

[13] See section 5.3, and the papers [4] and [11]

[14] Since the value of U_{ab} affects the value of $\varphi(\mathbf{r})$, this must be done by numerical iteration.

[15] This result corresponds to $U_{ab} = 4.14 \cdot 10^{-51}$ Jm^2 and $a_{ab} = 81.0a_0$ corresponding to a decrease of 17% from the original value of a_{ab}.

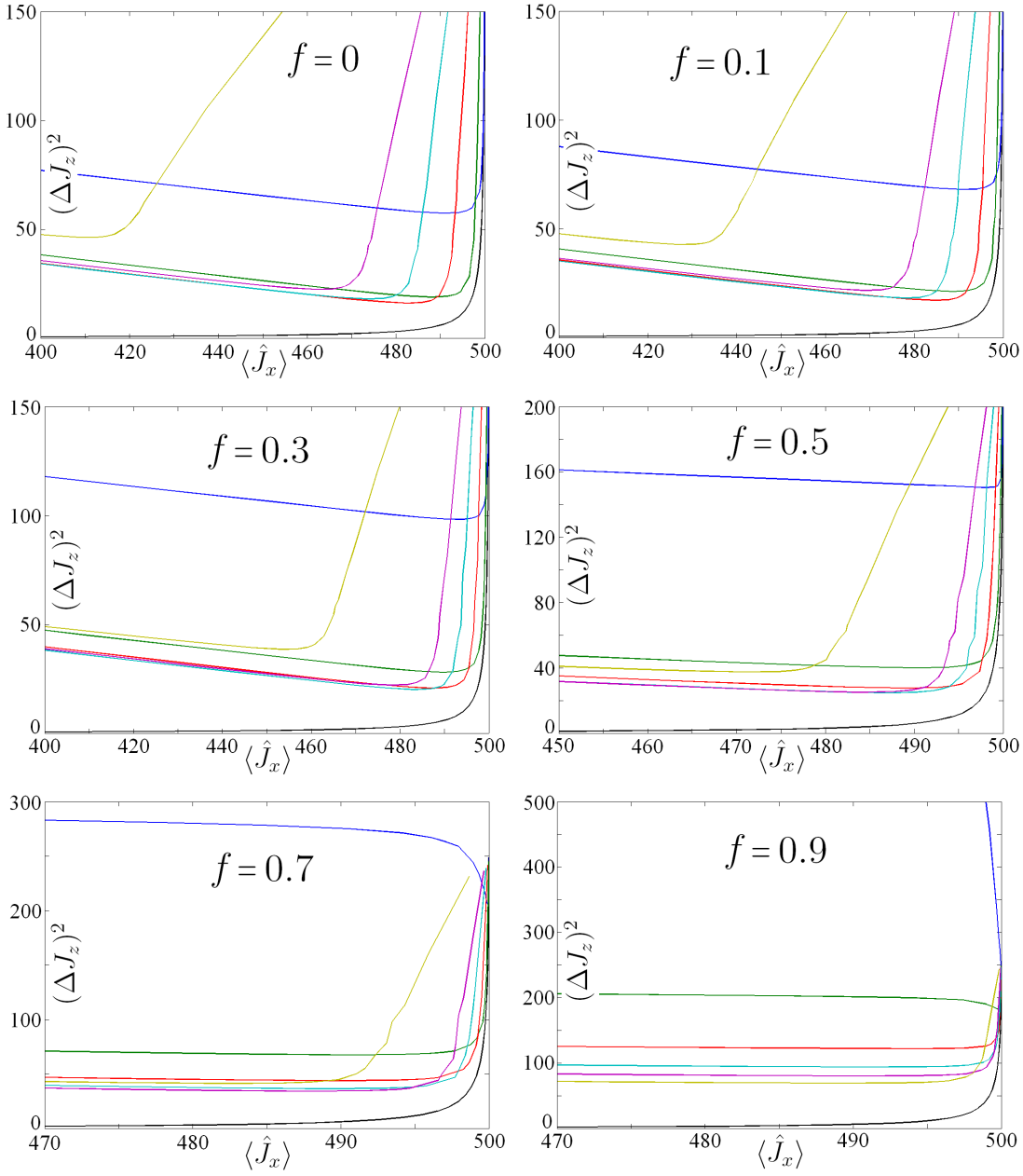

Figure 7.11: Graphs for $(\Delta J_z)^2$ vs $\langle \hat{J}_x \rangle$ for $N = 1000$ and a temperature of $\mathcal{T} = 0.049$. Each subplot corresponds to a fixed value of f while s is varied. The blue, dark green, red, cyan, violet, and brass curves correspond to $s = 0.01$, 0.1, 0.3, 0.6, 1, and 3 respectively, while the black curve is the ideal result given by the F-function. The data plotted here are the same as those plotted in fig 7.12, and the values of s and f are the same as those in fig. 7.4.

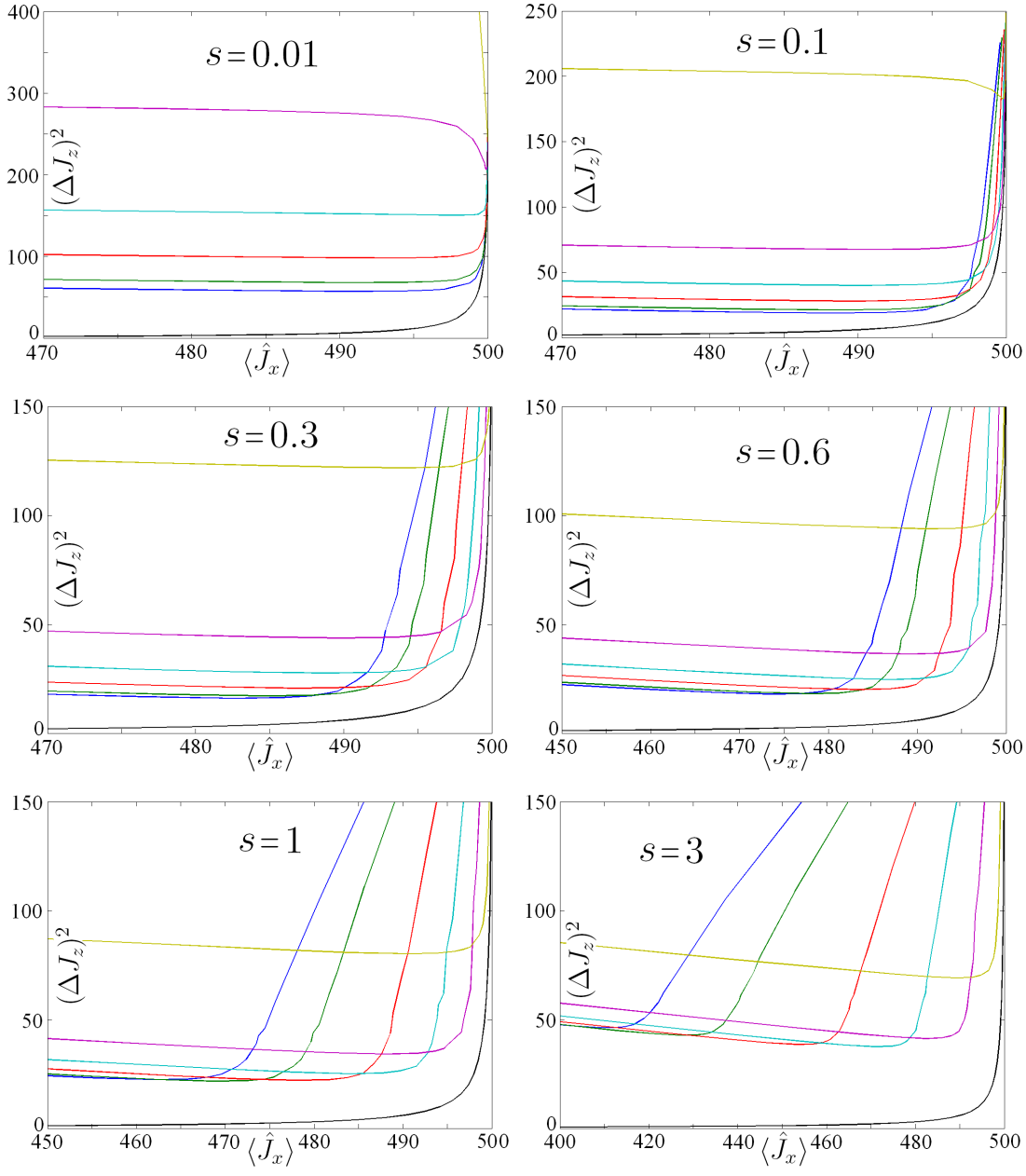

Figure 7.12: Graphs for $(\Delta J_z)^2$ vs $\langle \hat{J}_x \rangle$ for $N = 1000$ and a temperature of $\mathcal{T} = 0.049$. Each subplot corresponds to a fixed value of s while f is varied. The blue, dark green, red, cyan, violet, and brass curves correspond to $f = 0$, 0.1, 0.3, 0.5, 0.7, and 0.9 respectively, while the black curve is the ideal result given by the F-function. The data plotted here are the same as those plotted in fig 7.11, and the values of s and f are the same as those in fig. 7.5.

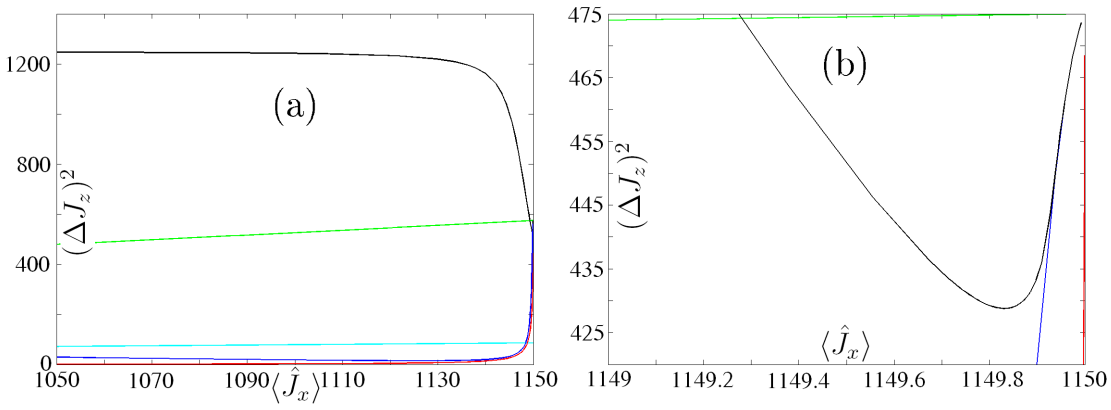

Figure 7.13: Graphs for $(\Delta J_z)^2$ vs $\langle \hat{J}_x \rangle$ for the values of U, U_{ab}, N and $\mathcal{T}$ used in the experiment described in [13]. The black curve is the result, and the dark blue curve shows the result for similar values at zero temperature. The red curve shows the F-function for comparison, and the green and cyan curves correspond to $\xi^2 = 1$ and $\xi^2 = 0.15$ respectively. The two subfigures differ by the zoom only.

temperature at which the experiment takes place is not reported in [13], but since the experimental setup is similar to the one described in [15], I will assume that the temperature is half of the smallest of those described in [15] namely $T = 10$nK corresponding to $\mathcal{T} = 0.49$. The particle number is $N = 2300$ which I will use ignoring the 15% particle loss reported in [13].

The result of a simulation using these parameters is plotted in fig. 7.13. The minimal value the squeezing parameter may assume is $\xi^2 = 0.9199$ which should be compared to the $\xi^2 = 0.15$ obtained in [13]. This does not contradict my theory since the experiment described in [13] uses a time-dependent approach to generation of spin-squeezing, as described in section 5.4, which is different from the steady-state approach described by my theory. The conclusion we can derive from this is that when the temperature is as high as 10nK a dynamical approach to production of squeezing is preferable. In fig 7.13 the steady-state result for zero temperature is plotted as well. We see that if zero temperature was to be obtained, it would be possible to obtain more squeezing than was done by Oberthaler. The point of maximal squeezing corresponds to $\xi^2 = 0.0271$ in this case.

Chapter 8

Conclusions and outlooks

8.1 Conclusions

As stated in the introduction, the purpose of this thesis is to derive a steady-state Bogoliubov model of a Bose-Einstein condensate, use the result to calculate the spin-squeezing, and investigate the results. This derivation was done in chapter 6, and the results are shown and analyzed in chapter 7.

The result of the derivation is that the two-species Gross-Pitaevskii Hamiltonian (5.11) can be diagonalized by expressing the quantum-field operator for the particles according to (6.2), (6.11), and (6.19), where the u_i and v_i-functions are eigenstates to the matrix $\mathcal{L}$ as given by (6.38). The expectation value of the angular momentum operators and thereby the squeezing, can be calculated from the u_i and v_i-functions using (3.30) and (6.48) to (6.51). How the calculations are implemented numerically is described in section 6.5.

Simpler models, like the Two-mode model and the Schwinger model, result in a squeezing scaling with the number of particles as $\xi^2 \propto N^{-1}$, showing that a large number of particles gives better squeezing. This is still true for the case described by my theory, even though the scaling is not as good as for the simpler models. For one set of parameters the relation was found to be $\xi^2 \propto N^{-0.527}$ for a fixed value of the chemical potential. The results for various particle numbers can be seen in fig. 7.8.

The best results for the spin-squeezing are obtained at low temperatures. This is not surprising since the system is closer to that described by the two-mode model in that limit. The results for various temperatures can be seen in fig. 7.9, and in appendix I.

For the case of zero temperature, the optimal squeezing is obtained for atoms with $U \approx U_{ab}$ and $U + U_{ab} \approx 0$, which can be seen in figs. 7.4 and 7.5. But for higher temperatures, like the 10 nK that were used in the discussion of the experiment by Oberthaler, the limit is the opposite, in this case atoms with $U \gg U_{ab}$ and $U + U_{ab} \gg 1$ optimizes the squeezing. The results for non-zero temperatures giving rise to this conclusion can be seen in figs. 7.11 and 7.12, and in appendix I.

A comparison with the experiment by Oberthaler described in [13] shows that for physical temperatures like 10nK, the dynamical approach used there results in an amount of squeezing surpassing the amount that can be obtained using the method developed in this thesis. Therefore I must conclude that a dynamical approach to creation of spin-squeezing is to be preferred, if the only concern is to squeeze as much as possible. The results of this comparison can be seen in fig. 7.13.

8.2 Outlooks

The ultimate result of this thesis would have been a formula for the squeezing parameter ξ_{J_z} as function of all the free parameters U, U_{ab}, N, Ω, and $\mathcal{T}$. Since ξ_{J_z} cannot be found analytically, such a formula could only have been made by fitting some function to the numerical results, like we did for the N-dependence alone in (7.18). The reason this has not been done is that the time needed to make the required number of simulations for all possible combinations of the free variables simply was not available.

If one was to realize the method described in this thesis experimentally, the primary limit on the amount of squeezing would be particle losses from the trap[1]. Such atomic losses are not part of the model in this thesis, since it is hard to assign reason to the notion of particle loss in a steady-state formulation requiring a system in equilibrium. If this thesis was to be improved, I would need to find a way to include such effects in the model anyway. In order to do this, one would presumably need to go into further detail on the experimental setup than what is done in this thesis, in order to find some optimal time being long enough to allow the system to obtain equilibrium, but short enough that only a few atoms will have escaped the trap. A similar calculation for the time-dependent approach can be found in [19].

Not the entire space of parameters was explored in this thesis. The discussion was limited to the cases of positive scattering lengths $U \geq 0$ and $U_{ab} \geq 0$, and to the antiferromagnetic regime $U \geq U_{ab}$. As we saw in section 4.3 the condensate collapses for large negative values of U and U_{ab}, and as mentioned in section 5.1 $U < U_{ab}$ results in a physical split of the a and b modes. Still it could have been interesting to investigate the behaviour a little into these 'forbidden' parts of parameter space, since we saw that for zero temperature, the squeezing is optimal for $U \approx U_{ab} \approx 0$, which is close to the forbidden area. Another possibility could have been not to make the assumption $U_{aa} = U_{bb}$. If the two constants were kept separate, the two-mode approximation would have included terms proportional to $\hat{J}_z$, which would imply that the maximally squeezed states would not be at the equator of the Bloch sphere. The full calculation could have been done without this assumption[2]. The result would have been that the plus- and minus-modes would not separate as they do in (6.13), which in this case could be written $\hat{\mathcal{H}} = \hat{\mathfrak{H}}_0 + \frac{1}{2}\bar{\Lambda}^\dagger \mathcal{M} \bar{\Lambda}$ where $\mathcal{M}$ would

[1] Marcus Oberthaler: Private correspondence.

[2] See [4].

be a 4×4-matrix.

In section 5.6 some choices that had to be made in order to do the full calculation were discussed. One of them was the choice of the non-symmetry-breaking approach, and the consequences of a different choice are discussed in detail in section 6.4. But another choice that was taken in section 5.6, was the choice of treating the φ_{0-}mode as part of the perturbation, and not as a condensate-mode. We see in fig. I.2 in appendix I, that the occupation number of that mode is much larger than of all the other modes[3], which makes the choice a little questionable. The reason for this treatment of the φ_{0-}mode is that otherwise we would have to choose $\varphi_{0-} \propto \varphi$ analogous to the case of φ_{0+} since it is not obvious how else we could find φ_{0-}. This choice would, however, be wrong, as the small differences in φ_a and φ_b would not be taken into account[4]. Finding a way to solve this problem would be another possible improvement of the thesis.

In order to plot the states resulting from an implementation of my theory, we used the $\mathfrak{Q}$-function instead of the more physical Q-functions. The reason for this is that we do not have an expression for the Bogoliubov-states in the $|j,m\rangle$-basis, and finding such an expression would be another possible improvement[5].

Finally I should mention the efficiency of my numerical simulations. I have chosen to do all my programming in the programming language 'Matlab', since that language is perfect for handling matrices, like those in (6.71) that have to be diagonalized in order to find the squeezing. 'Matlab' is however not that efficient in handling loops, of which my programs[6] contain plenty. It is very likely that implementing the code in a lower level language, like 'C', would be more efficient. For handling the matrices undoubtedly some C-algorithms exist, which I could have used for those parts of the calculations.

[3] At least for the value of Ω used to produce that plot. In fig. 7.7c the difference is not nearly as large.

[4] $\varphi_+ \propto \varphi_a + \varphi_b$, so in that case small differences in φ_a and φ_b does not matter. But $\varphi_- \propto \varphi_a - \varphi_b$, in which case any small differences would be blown up, and $\varphi_- \propto \varphi$ would accordingly be very wrong.

[5] A way to do this inspired by the Bogoliubov transform could be to express the $\hat{\alpha}$-operators using some new $\hat{\beta}$ operators $\hat{\alpha}_i \equiv \sum_j (\mu_{ij}\hat{\beta}_{ij} + \nu_{ij}\hat{\beta}^\dagger_{ij})$ where μ_{ij} and ν_{ij} are chosen so the operator $\hat{\mathbf{J}}^2 \equiv \hat{J}_x^2 + \hat{J}_y^2 + \hat{J}_z^2$ becomes diagonal. In that case the eigenstates to the $\hat{\beta}^\dagger\hat{\beta}$-operator will be eigenstates to $\hat{\mathbf{J}}^2$, and thus similar to the $|j,m\rangle$-states. This leaves the problem of how to find the m-quantum number. Whether this proposed method will work, is yet to be investigated.

[6] See appendix G.

Appendix A

Second quantization

The state vector for a pure state made up of N particles can be written as

$$|\psi\rangle = \sum_{\nu_1,\nu_2,\ldots} C_{\nu_1,\nu_2,\ldots} \cdot |\psi\rangle_{\nu_1}^{(1)} \otimes |\psi\rangle_{\nu_2}^{(2)} \otimes \ldots \otimes |\psi\rangle_{\nu_N}^{(N)} \tag{A.1}$$

where $|\psi\rangle_{\nu_i}^{(i)}$ is the ν_ith quantum state of the ith particle. We assume the set of $|\psi\rangle_{\nu_i}^{(i)}$ for a given i to be complete. In this thesis we will only consider bosons, and for bosons the many-particle wave function is (per definition) symmetric under exchange of two identical particles. So if our particles are indistinguishable, the $C_{\nu_1,\nu_2,\ldots}$-coefficients must be symmetric under exchange of ν_i and ν_j, for any i and j. When the particles are indistinguishable it makes no sense to enumerate them like we do in (A.1), and we can get rid of the enumeration by changing to the so called number basis. In this case we notice that all the ν_is can assume the same values, named $1, 2, 3, \ldots$, so in the number basis $|\psi\rangle$ is written[1] as

$$|\psi\rangle = \sum_{n_1,n_2,\ldots} K_{n_1,n_2,\ldots} \cdot |n_1\rangle_1 \otimes |n_2\rangle_2 \otimes \ldots \tag{A.2}$$

where $|n_i\rangle_i$ means n_i particles in the ν-state i.

Inspired by the quantum-harmonic oscillator we define a set of annihilation and creation operators $\hat{a}_i$ and $\hat{a}_i^\dagger$ which remove or add particles from the $\nu = i$ quantum state respectively. These operators are defined to have the commutation relations

$$\left[\hat{a}_i, \hat{a}_j^\dagger\right] = \delta_{ij} \quad , \quad \left[\hat{a}_i, \hat{a}_j\right] = \left[\hat{a}_i^\dagger, \hat{a}_j^\dagger\right] = 0 \tag{A.3}$$

which lead to the relations

$$\hat{a}_i|n\rangle_i = \sqrt{n}|n-1\rangle_i \quad , \quad \hat{a}_i^\dagger|n\rangle_i = \sqrt{n+1}|n+1\rangle_i \tag{A.4}$$

from which we see that the number operator $\hat{n}_i$ can be written as

$$\hat{a}_i^\dagger \hat{a}_i|n\rangle_i = n|n\rangle_i = \hat{n}_i|n\rangle_i \tag{A.5}$$

[1] The expression for the $K_{n_1,n_2,\ldots}$-coefficients must be $K_{n_1,n_2,\ldots} = \frac{N!}{n_1!n_2!\ldots} C_{1_1,\ldots,1_{n_1},2_1,\ldots,2_{n_2},\ldots}$, but this result is never used.

Let us have a look at a basis change from the complete basis enumerated by ν to another complete basis enumerated by μ

$$|\psi\rangle_\mu = \sum_\nu |\psi\rangle_\nu \langle\psi|_\nu |\psi\rangle_\mu = \sum_\nu \langle\psi_\mu|\psi_\nu\rangle^* |\psi\rangle_\nu \tag{A.6}$$

If we write $|\psi\rangle_\mu = \hat{a}_\mu^\dagger|0\rangle$ and $|\psi\rangle_\nu = \hat{a}_\nu^\dagger|0\rangle$, we can deduce the transformation relations for $\hat{a}$ to be

$$\hat{a}_\mu^\dagger = \sum_\nu \langle\psi_\mu|\psi_\nu\rangle^* \hat{a}_\nu^\dagger \quad , \quad \hat{a}_\mu = \sum_\nu \langle\psi_\mu|\psi_\nu\rangle \hat{a}_\nu \tag{A.7}$$

We see that the total particle number operator is given as

$$\begin{aligned} \hat{N} &= \sum_\mu \hat{a}_\mu^\dagger \hat{a}_\mu = \sum_\mu \sum_\nu \langle\psi_\nu|\psi_\mu\rangle \hat{a}_\nu^\dagger \sum_{\nu'} \langle\psi_\mu|\psi_{\nu'}\rangle \hat{a}_{\nu'} \\ &= \sum_{\nu\nu'} \langle\psi_\nu|\psi_{\nu'}\rangle \hat{a}_\nu^\dagger \hat{a}_{\nu'} = \sum_\nu \hat{a}_\nu^\dagger \hat{a}_\nu \end{aligned} \tag{A.8}$$

showing that the total particle number is unchanged by the transformation. If we let the μ-basis be the continuous $\mathbf{r}$-basis with $|\psi\rangle_\mu = |\mathbf{r}\rangle$, then the transformation becomes

$$\hat{\Psi}(\mathbf{r}) = \sum_\nu \langle\mathbf{r}|\psi_\nu\rangle \hat{a}_\nu = \sum_\nu \psi_\nu(\mathbf{r}) \hat{a}_\nu \tag{A.9}$$

where $\hat{a}_\mathbf{r}$ has been named $\hat{\Psi}(\mathbf{r})$ and is known as a quantum field operator. We see that the total particle number operator is given as

$$\hat{N} = \int \mathrm{d}\mathbf{r} \hat{\Psi}^\dagger(\mathbf{r}) \hat{\Psi}(\mathbf{r}) \tag{A.10}$$

Let us for a moment go back to first quantization and have a look at the local, one-particle operator $\hat{O}$. Inserting the completeness relations and transforming to the $\mathbf{r}$-basis, allows us to reexpress this operator as

$$\begin{aligned} \hat{O} &= \sum_{\nu'} |\psi\rangle_{\nu'} \langle\psi|_{\nu'} \int \mathrm{d}\mathbf{r} |\mathbf{r}\rangle\langle\mathbf{r}| \hat{O} \int \mathrm{d}\mathbf{r}' |\mathbf{r}'\rangle\langle\mathbf{r}'| \sum_{\nu''} |\psi\rangle_{\nu''} \langle\psi|_{\nu''} \\ &= \sum_{\nu'\nu''} \hat{O}_{\nu'\nu''} |\psi\rangle_{\nu'} \langle\psi|_{\nu''} \end{aligned} \tag{A.11}$$

where

$$\hat{O}_{\nu'\nu''} \equiv \int \mathrm{d}\mathbf{r} \psi_{\nu'}^*(\mathbf{r}) \hat{O} \psi_{\nu''}(\mathbf{r}) \tag{A.12}$$

The second integral has vanished due to the delta function coming from the locality of $\hat{O}$. The many-particle generalization of $\hat{O}$ is

$$\hat{\mathcal{O}} \equiv \hat{O}^{(1)} \otimes \hat{I}^{(2)} \otimes \ldots \otimes \hat{I}^{(N)} + \ldots + \hat{I}^{(1)} \otimes \ldots \otimes \hat{I}^{(N-1)} \otimes \hat{O}^{(N)} \tag{A.13}$$

and acting with that operator on the many-particle state

$$|\psi\rangle \;=\; |\psi\rangle^{(1)}_{\nu_1} \otimes |\psi\rangle^{(2)}_{\nu_2} \otimes \ldots \otimes |\psi\rangle^{(j)}_{\nu_j} \otimes \ldots \otimes |\psi\rangle^{(N)}_{\nu_N} \tag{A.14}$$

gives

$$\hat{\mathcal{O}}|\psi\rangle \;=\; \sum_j \sum_{\nu'} \hat{O}_{\nu'\nu_j} |\psi\rangle^{(1)}_{\nu_1} \otimes |\psi\rangle^{(2)}_{\nu_2} \otimes \ldots \otimes |\psi\rangle^{(j)}_{\nu'} \otimes \ldots \otimes |\psi\rangle^{(N)}_{\nu_N} \tag{A.15}$$

where we have used the fact that $\langle \psi_{\nu''} | \psi_{\nu_j} \rangle = \delta_{\nu''\nu_j}$. Rewriting the above using creation operators gives

$$|\psi\rangle \;=\; \hat{a}^\dagger_{\nu_1} \hat{a}^\dagger_{\nu_2} \ldots \hat{a}^\dagger_{\nu_j} \ldots \hat{a}^\dagger_{\nu_N} |0\rangle \tag{A.16}$$

and

$$\begin{aligned} \hat{\mathcal{O}}|\psi\rangle \;&=\; \sum_j \sum_{\nu'} \hat{O}_{\nu'\nu_j} \hat{a}^\dagger_{\nu_1} \hat{a}^\dagger_{\nu_2} \ldots \hat{a}^\dagger_{\nu'} \ldots \hat{a}^\dagger_{\nu_N} |0\rangle \\ &=\; \sum_{\nu'\nu''} \hat{O}_{\nu'\nu''} \hat{a}^\dagger_{\nu'} \hat{a}_{\nu''} |\psi\rangle \end{aligned} \tag{A.17}$$

where the final equation has renamed $\nu_j \;\nu''$. Reinserting the expression for $\hat{O}_{\nu'\nu''}$ gives us

$$\begin{aligned} \hat{\mathcal{O}}|\psi\rangle \;&=\; \sum_{\nu'\nu''} \int \mathrm{d}\mathbf{r} \psi^*_{\nu'}(\mathbf{r}) \hat{O} \psi_{\nu''}(\mathbf{r}) \hat{a}^\dagger_{\nu'} \hat{a}_{\nu''} |\psi\rangle \\ &=\; \int \mathrm{d}\mathbf{r} \hat{\Psi}^\dagger(\mathbf{r}) \hat{O} \hat{\Psi}(\mathbf{r}) \end{aligned} \tag{A.18}$$

with the definition of $\hat{\Psi}(\mathbf{r})$ inserted. By comparing this to the expression for the expectation value of $\hat{O}$

$$\langle \hat{O} \rangle \;=\; \int \mathrm{d}\mathbf{r} \psi^*(\mathbf{r}) \hat{O} \psi(\mathbf{r}) \tag{A.19}$$

we see that the form of these two expressions are the same. This is a general principle true not only for one-particle functions[2]. So if we have an expression for the expectation value of some operator, we can immediately generalize this to second quantization using[3]

$$\langle \hat{O} \rangle = \int \mathrm{d}\mathbf{r} f\big(\psi(\mathbf{r})\big) \rightarrow \hat{\mathcal{O}} = \int \mathrm{d}\mathbf{r} f\big(\hat{\Psi}(\mathbf{r})\big) \tag{A.20}$$

This principle will be used when going to second quantization throughout the thesis.

[2] In [e] the same calculation is done for two-particle operators, with the note that higher order operators will not be encountered. This is true for this thesis as well.

[3] This is not entirely well defined, since the ψs commute, while the $\hat{\Psi}$s do not. The rule of thumb is that the $\hat{\Psi}$-operators should appear in normal order. When the particle number is large we have that $\langle \hat{\Psi}^\dagger \hat{\Psi} \rangle \approx \langle \hat{\Psi} \hat{\Psi}^\dagger \rangle$ which makes the order of the $\hat{\Psi}$-operators less important in this limit.

Appendix B

Angular momentum in quantum mechanics

In classical mechanics angular momentum is defined as

$$\boldsymbol{L} = \boldsymbol{r} \times \boldsymbol{p} \tag{B.1}$$

This is generalized to first quantization by inserting the position operator $\hat{r}$ and the momentum operator $\hat{p} = -i\nabla$ giving

$$\hat{L}_l = -i\left(x_m \frac{\partial}{\partial x_n} - x_n \frac{\partial}{\partial x_m}\right)\epsilon_{lmn} \tag{B.2}$$

where the Einstein summation convention is used. From this we can derive that the commutation relation for angular momentum-like[1] operators should be

$$\left[\hat{J}_l, \hat{J}_m\right] = i\epsilon_{lmn}\hat{J}_n \tag{B.3}$$

We see that the operator $\hat{J}^2 \equiv \hat{J}_x^2 + \hat{J}_y^2 + \hat{J}_z^2$ commutes with $\hat{J}_z$ (or any of the other $\hat{J}_l$-operators), which means that we can find a common complete set of eigenstates to the two operators. Such states are denoted $|j, m\rangle$ and obey[2]

$$\begin{aligned} \hat{J}^2|j,m\rangle &= j(j+1)|j,m\rangle \\ \hat{J}_z|j,m\rangle &= m|j,m\rangle \end{aligned} \tag{B.4}$$

where j can take integer or half-integer values, and m can take values from $-j$ to j with integer steps. j can be thought of as the total angular momentum, while m

[1] By angular momentum-like operators is meant operators that obey these commutation relations. Examples are the orbital angular momentum $\hat{L}$, but also the spin $\hat{S}$ and the total angular momentum $\hat{J}$. $\hat{J}$ is the standard name for angular momentum-like operators, which is why it is used in this thesis even when there is no orbital component.

[2] See [b].

can be thought of as the component in the J_z-direction. When calculating J_x or J_y for states in the $|j,m\rangle$-basis it is useful to introduce the operators

$$\hat{J}_+ \equiv \hat{J}_x + i\hat{J}_y \quad , \quad \hat{J}_- \equiv \hat{J}_x - i\hat{J}_y \tag{B.5}$$

invertible to

$$\hat{J}_x = \frac{1}{2}\left(\hat{J}_- + \hat{J}_+\right) \quad , \quad \hat{J}_y = \frac{i}{2}\left(\hat{J}_- - \hat{J}_+\right) \tag{B.6}$$

since the $\hat{J}_\pm$-operators obey the relations

$$\begin{aligned} \hat{J}_+|j,m\rangle &= \sqrt{(j-m)(j+m+1)}|j,m+1\rangle \\ \hat{J}_-|j,m\rangle &= \sqrt{(j+m)(j-m+1)}|j,m-1\rangle \end{aligned} \tag{B.7}$$

in the $|j,m\rangle$-basis. The related commutation relations are

$$\begin{aligned} \left[\hat{J}_+, \hat{J}_-\right] &= 2\hat{J}_z \\ \left[\hat{J}_z, \hat{J}_\pm\right] &= \hat{J}_\pm \end{aligned} \tag{B.8}$$

The lowest dimensional representation of the algebra defined by (B.3) is $\hat{j}_m = \frac{1}{2}\sigma_m$ where

$$\sigma_x = \begin{bmatrix} 0 & 1 \\ 1 & 0 \end{bmatrix} \ , \ \sigma_y = \begin{bmatrix} 0 & -i \\ i & 0 \end{bmatrix} \ , \ \sigma_z = \begin{bmatrix} 1 & 0 \\ 0 & -1 \end{bmatrix} \tag{B.9}$$

are the Pauli spin-matrices. These $\hat{j}$-operators are angular momentum operators for particles with total angular momentum $\frac{1}{2}$, and for this specific representation of the $\hat{j}$-operators, the $(1,0)$ and $(0,1)$-states are eigenstates for the $\hat{j}_z$-operator. For particles with total angular momentum $> \frac{1}{2}$ a higher dimensional representation is needed. A representation for the $\hat{J}$-operators for particles with total angular momentum j is

$$\hat{J}_x = \begin{pmatrix} 0 & \sqrt{\frac{1}{2}\cdot j} & 0 & \cdots & 0 \\ \sqrt{\frac{1}{2}\cdot j} & 0 & \sqrt{1\cdot(j-\frac{1}{2})} & & 0 \\ 0 & \sqrt{1\cdot(j-\frac{1}{2})} & 0 & \ddots & \vdots \\ \vdots & & \ddots & \ddots & \sqrt{j\cdot\frac{1}{2}} \\ 0 & 0 & \cdots & \sqrt{j\cdot\frac{1}{2}} & 0 \end{pmatrix} \tag{B.10}$$

$$\hat{J}_y = i\begin{pmatrix} 0 & -\sqrt{\frac{1}{2}\cdot j} & 0 & \cdots & 0 \\ \sqrt{\frac{1}{2}\cdot j} & 0 & -\sqrt{1\cdot(j-\frac{1}{2})} & & 0 \\ 0 & \sqrt{1\cdot(j-\frac{1}{2})} & 0 & \ddots & \vdots \\ \vdots & & \ddots & \ddots & -\sqrt{j\cdot\frac{1}{2}} \\ 0 & 0 & \cdots & \sqrt{j\cdot\frac{1}{2}} & 0 \end{pmatrix} \tag{B.11}$$

$$\hat{J}_z = \begin{pmatrix} j & 0 & 0 & \cdots & 0 \\ 0 & j-1 & 0 & \cdots & 0 \\ 0 & 0 & j-2 & & 0 \\ \vdots & \vdots & & \ddots & \vdots \\ 0 & 0 & 0 & \cdots & -j \end{pmatrix} \tag{B.12}$$

where each matrix is square with dimension $2j+1$. The basis vectors in this representation are the states $|j,m\rangle$ mentioned previously, and the parts of the matrix representations of $\hat{J}_x$ and $\hat{J}_y$ above and below the diagonal may therefore be regarded as a matrix representation of the operators $\hat{J}_+$ and $\hat{J}_-$ respectively.

For a spin-$\frac{1}{2}$ particle in the state $|\varphi\rangle = \varphi_a(\mathbf{r})|a\rangle + \varphi_b(\mathbf{r})|b\rangle$ where a and b correspond to spin up and spin down[3] and where $\int \mathrm{d}\mathbf{r}\varphi_i^*(\mathbf{r})\varphi_i(\mathbf{r})$ is the probability of measuring the particle in the ith state, the expectation value of $\hat{j}_x$ will be

$$\langle\varphi|\hat{j}_x|\varphi\rangle = \frac{1}{2}\int \mathrm{d}\mathbf{r}\big(\varphi_a^*(\mathbf{r})\varphi_b(\mathbf{r}) + \varphi_b^*(\mathbf{r})\varphi_a(\mathbf{r})\big) \tag{B.13}$$

For an ensemble of N particles the total angular momentum operator is defined as

$$\hat{J}_k \equiv \hat{j}_k^{(1)}\otimes\hat{I}^{(2)}\otimes\cdots\otimes\hat{I}^{(N)} + \cdots + \hat{I}^{(1)}\otimes\cdots\otimes\hat{I}^{(N-1)}\otimes\hat{j}_k^{(N)} \tag{B.14}$$

and if the particles are identical[4] with spin $\frac{1}{2}$, the resulting expectation value is

$$\langle\psi|\hat{J}_x|\psi\rangle = \frac{1}{2}\int \mathrm{d}\mathbf{r}\big(\psi_a^*(\mathbf{r})\psi_b(\mathbf{r}) + \psi_b^*(\mathbf{r})\psi_a(\mathbf{r})\big) \tag{B.15}$$

where $\psi \equiv \sqrt{N}\phi$ fulfils

$$\int \mathrm{d}\mathbf{r}\big(\psi_a^*(\mathbf{r})\psi_a(\mathbf{r}) + \psi_b^*(\mathbf{r})\psi_b(\mathbf{r})\big) = N \tag{B.16}$$

Results similar to (B.15) can be obtained for the $\hat{J}_y$ and $\hat{J}_z$-operators. Going to second quantization[5] corresponds to doing the substitution $\psi(\mathbf{r}) \to \hat{\Psi}(\mathbf{r})$ with the

[3] In strict notation $|a\rangle = |\frac{1}{2},\frac{1}{2}\rangle$ and $|b\rangle = |\frac{1}{2},-\frac{1}{2}\rangle$.

[4] This does not require the particles to be strictly identical. The requirement is that $\varphi_{ai}(\mathbf{r}) = \varphi_{aj}(\mathbf{r})$ and similarly for b, for two particles numbered i and j.

[5] See appendix A.

results

$$\hat{\mathcal{J}}_x = \frac{1}{2}\int \mathrm{d}\mathbf{r}\big(\hat{\Psi}_a^\dagger(\mathbf{r})\hat{\Psi}_b(\mathbf{r}) + \hat{\Psi}_b^\dagger(\mathbf{r})\hat{\Psi}_a(\mathbf{r})\big) \tag{B.17}$$

$$\hat{\mathcal{J}}_y = \frac{1}{2i}\int \mathrm{d}\mathbf{r}\big(\hat{\Psi}_a^\dagger(\mathbf{r})\hat{\Psi}_b(\mathbf{r}) - \hat{\Psi}_b^\dagger(\mathbf{r})\hat{\Psi}_a(\mathbf{r})\big) \tag{B.18}$$

$$\hat{\mathcal{J}}_z = \frac{1}{2}\int \mathrm{d}\mathbf{r}\big(\hat{\Psi}_a^\dagger(\mathbf{r})\hat{\Psi}_a(\mathbf{r}) - \hat{\Psi}_b^\dagger(\mathbf{r})\hat{\Psi}_b(\mathbf{r})\big) \tag{B.19}$$

and likewise (B.16) in second quantization corresponds to the particle number operator

$$\hat{\mathcal{N}} = \int \mathrm{d}\mathbf{r}\big(\hat{\Psi}_a^\dagger(\mathbf{r})\hat{\Psi}_a(\mathbf{r}) + \hat{\Psi}_b^\dagger(\mathbf{r})\hat{\Psi}_b(\mathbf{r})\big) \tag{B.20}$$

In the main thesis we will denote these operators as $\hat{J}_i$ and $\hat{N}$ respectively.

Appendix C

Squeezing implies entanglement

In this section the "squeezing implies entanglement"-proof will be presented in full detail. For the same derivation with less equations but more discussion, see section 3.6.

$$(\Delta J_z)^2 \;=\; \langle \hat{J}_z^2 \rangle - \langle \hat{J}_z \rangle^2 \tag{C.1}$$

Let us calculate the two terms using the separability-criterion

$$\rho = \sum_i p_i \rho_i^{(1)} \otimes \rho_i^{(2)} \otimes \ldots \otimes \rho_i^{(n)} \tag{C.2}$$

$$\begin{aligned}
\langle J_z \rangle &= \mathrm{Tr}(\hat{J}_z \hat{\rho}) \\
&= \mathrm{Tr}\left(\sum_i p_i \left(\hat{j}_z^{(1)} \otimes 1 \otimes \ldots \otimes 1 + \ldots + 1 \otimes \ldots \otimes 1 \otimes \hat{j}_z^{(n)} \right) \hat{\rho}_i^{(1)} \otimes \ldots \otimes \hat{\rho}_i^{(n)} \right) \\
&= \sum_i p_i \left(\mathrm{Tr}(\hat{j}_z^{(1)} \hat{\rho}_i^{(1)}) + \ldots + \mathrm{Tr}(\hat{j}_z^{(n)} \hat{\rho}_i^{(n)}) \right) \\
&= \sum_i p_i \left(\langle \hat{j}_z^{(1)} \rangle_i + \ldots + \langle \hat{j}_z^{(n)} \rangle_i \right) = \sum_i p_i \langle \hat{J}_z \rangle_i
\end{aligned} \tag{C.3}$$

$$
\begin{aligned}
\langle J_z^2\rangle &= \mathrm{Tr}(\hat{J}_z^2\hat{\rho}) \\
&= \mathrm{Tr}\left(\sum_i p_i \left(\hat{j}_z^{(1)}\otimes 1\otimes\ldots\otimes 1+\ldots+1\otimes\ldots\otimes 1\otimes\hat{j}_z^{(n)}\right)^2 \hat{\rho}_i^{(1)}\otimes\ldots\otimes\hat{\rho}_i^{(n)}\right) \\
&= \sum_i p_i\left(\sum_k \mathrm{Tr}((\hat{j}_z^{(k)})^2\hat{\rho}_i^{(k)}) + \sum_{k\neq k'}\mathrm{Tr}\Big((\hat{j}_z^{(k)}\otimes\hat{j}_z^{(k')})(\hat{\rho}_i^{(k)}\otimes\hat{\rho}_i^{(k')})\Big)\right) \\
&= \sum_i p_i\left(\sum_k \langle(\hat{j}_z^{(k)})^2\rangle_i + \sum_{k\neq k'}\langle\hat{j}_z^{(k)}\rangle_i\langle\hat{j}_z^{(k')}\rangle_i\right) \\
&= \sum_i p_i\left(\sum_k \langle(\hat{j}_z^{(k)})^2\rangle_i - \sum_k\langle\hat{j}_z^{(k)}\rangle_i^2 + \sum_k\langle\hat{j}_z^{(k)}\rangle_i^2 + \sum_{k\neq k'}\langle\hat{j}_z^{(k)}\rangle_i\langle\hat{j}_z^{(k')}\rangle_i\right) \\
&= \sum_i p_i\left(\sum_k(\Delta j_z^{(k)})_i^2 + \left(\sum_k\langle\hat{j}_z^{(k)}\rangle_i\right)^2\right) \\
&= \sum_i p_i\left(\sum_k(\Delta j_z^{(k)})_i^2 + \langle\hat{J}_z\rangle_i^2\right) \qquad \text{(C.4)}
\end{aligned}
$$

giving

$$
\begin{aligned}
(\Delta J_z)^2 &= \langle\hat{J}_z^2\rangle - \langle\hat{J}_z\rangle^2 \\
&= \sum_i p_i\left(\sum_k(\Delta j_z^{(k)})_i^2 + \langle\hat{J}_z\rangle_i^2\right) - \left(\sum_i p_i\langle\hat{J}_z\rangle_i\right)\left(\sum_{i'} p_{i'}\langle\hat{J}_z\rangle_{i'}\right) \\
&= \sum_i p_i\left(\sum_k(\Delta j_z^{(k)})_i^2\right) + (\boldsymbol{A}\cdot\boldsymbol{A})(\boldsymbol{B}\cdot\boldsymbol{B}) - (\boldsymbol{A}\cdot\boldsymbol{B})^2 \qquad \text{(C.5)}
\end{aligned}
$$

where $A_i = \sqrt{p_i}$ and $B_i = \sqrt{p_i}\langle\hat{J}_z\rangle_i$. Now we can use the Cauchy-Schwartz inequality stating that $(\boldsymbol{A}\cdot\boldsymbol{A})(\boldsymbol{B}\cdot\boldsymbol{B}) \geq (\boldsymbol{A}\cdot\boldsymbol{B})^2$ for any set of vectors $\boldsymbol{A}$ and $\boldsymbol{B}$, to give us

$$
(\Delta J_z)^2 \geq \sum_i p_i \sum_k (\Delta j_z^{(k)})_i^2 \qquad \text{(C.6)}
$$

We know that $(\Delta j_z)^2 \geq jF_j(\langle\hat{j}_x\rangle/j)$, so therefore

$$
(\Delta J_z)^2 \geq \sum_i p_i \sum_k jF_j(\langle\hat{j}_x^{(k)}\rangle_i/j) \qquad \text{(C.7)}
$$

where we have used that all the subsystems have the same j. Since F is a convex function, we can use Jensen's inequality, stating that

$$
\sum_k^N a_k F(x_k) \geq \left(\sum_k^N a_k\right) F\left(\frac{\sum_k^N a_k x_k}{\sum_k^N a_k}\right) \qquad \text{(C.8)}
$$

if F is convex. If used twice, once on the k-sum where the as are 1, and once on the i-sum where the as are p_i, Jensen's inequality gives

$$\begin{aligned}
(\Delta J_z)^2 &\geq \sum_i p_i \sum_k jF_j\left(\frac{\langle\hat{j}_x^{(k)}\rangle_i}{j}\right) \Rightarrow \\
(\Delta J_z)^2 &\geq \sum_i p_i Njf_j\left(\frac{\sum_k\langle\hat{j}_x^{(k)}\rangle_i}{jN}\right) \Rightarrow \\
(\Delta J_z)^2 &\geq Njf_j\left(\frac{\sum_i p_i\sum_k\langle\hat{j}_x^{(k)}\rangle_i}{jN}\right) \Leftrightarrow \\
(\Delta J_z)^2 &\geq Njf_j\left(\frac{\langle\hat{J}_x\rangle}{jN}\right) \qquad \text{(C.9)}
\end{aligned}$$

where the final step uses a result similar to (C.3) for $\hat{J}_x$. Let us now use that $j=\frac{1}{2}$ and calculate the corresponding F-function. For a state $|\psi\rangle = c|\uparrow\rangle + s|\downarrow\rangle$ where c and s are short for cosine and sine to an angle, we get $\langle\hat{J}_z\rangle = 0.5C$, $\langle\hat{J}_x\rangle = 0.5S$ and $\langle\hat{J}_z^2\rangle = 0.25$, where C and S are short for cosine and sine to twice the angle. This gives $(\Delta J_z)^2 = \langle\hat{J}_x\rangle^2$ or

$$F_{\frac{1}{2}}(x) = \tfrac{1}{2}x^2 \qquad \text{(C.10)}$$

and insertion gives

$$\begin{aligned}
(\Delta J_z)^2 &\geq \frac{\langle\hat{J}_x\rangle^2}{N} \Leftrightarrow \\
\frac{\sqrt{N}(\Delta J_z)}{\langle\hat{J}_x\rangle} &\geq 1 \Leftrightarrow \\
\xi_{J_z} &\geq 1 \qquad \text{(C.11)}
\end{aligned}$$

showing that the state is not squeezed. So if the state is squeezed, we know that our initial assumption about separability was wrong, proving that if a state is squeezed, the state is entangled.

The discussions in the final part of section 3.6 showing a way to find a minimum for the amount of entangled particles giving rise to a state with certain values of $\langle\hat{J}_x\rangle$ and $(\Delta J_z)^2$, are based on the following calculation

$$
\begin{aligned}
(\Delta J_z)^2 &\geq \sum_i p_i \sum_k j_i^{(k)} F_{j_i^{(k)}} \left(\frac{\langle \hat{j}_x^{(k)} \rangle_i}{j_i^{(k)}} \right) \\
&\geq \sum_i p_i \sum_k j_i^{(k)} F_{j_{\max}} \left(\frac{\langle \hat{j}_x^{(k)} \rangle_i}{j_i^{(k)}} \right) \\
&\geq \sum_i p_i \left(\sum_k j_i^{(k)} \right) F_{j_{\max}} \left(\frac{\sum_k \langle \hat{j}_x^{(k)} \rangle_i}{\sum_k j_i^{(k)}} \right) \\
&\geq \tfrac{1}{2} N \sum_i p_i F_{j_{\max}} \left(\frac{\sum_k \langle \hat{j}_x^{(k)} \rangle_i}{\frac{1}{2}N} \right) \\
&\geq \tfrac{1}{2} N F_{j_{\max}} \left(\frac{\sum_i p_i \sum_k \langle \hat{j}_x^{(k)} \rangle_i}{\frac{1}{2}N} \right) \Leftrightarrow \\
(\Delta J_z)^2 &\geq \tfrac{1}{2} N F_{j_{\max}} \left(\frac{\langle \hat{J}_x \rangle}{\frac{1}{2}N} \right) \qquad \text{(C.12)}
\end{aligned}
$$

where we have used the fact that any convex, positive function with $f(0) = 0$ obeys $f(|x|) \geq a f(|x|/a)$ where $a \geq 1$. In this case $a = \frac{\frac{1}{2}N}{\sum_k j_i^{(k)}}$.

Appendix D

Calculation of combinations of J-operators

In this appendix we are going to express the $\hat{J}_i$-operators and combinations thereof using the results of the Bogoliubov approximation. Some of the results are stated in section 6.3, and the rest are used when drawing the $\mathfrak{Q}$-functions for the results of the main calculation in figs. 7.6 and 7.10.

$$
\begin{aligned}
\hat{N} &= \int \mathrm{d}\mathbf{r} \left(\hat{\Psi}_a^\dagger \hat{\Psi}_a + \hat{\Psi}_b^\dagger \hat{\Psi}_b \right) \\
&= \int \mathrm{d}\mathbf{r} \left(\frac{\hat{\Psi}_+^\dagger + \hat{\Psi}_-^\dagger}{\sqrt{2}} \cdot \frac{\hat{\Psi}_+ + \hat{\Psi}_-}{\sqrt{2}} + \frac{\hat{\Psi}_+^\dagger - \hat{\Psi}_-^\dagger}{\sqrt{2}} \cdot \frac{\hat{\Psi}_+ - \hat{\Psi}_-}{\sqrt{2}} \right) \\
&= \int \mathrm{d}\mathbf{r} \left(\hat{\Psi}_+^\dagger \hat{\Psi}_+ + \hat{\Psi}_-^\dagger \hat{\Psi}_- \right) \\
&= \int \mathrm{d}\mathbf{r} \Big(\left(\hat{c}_+^\dagger \varphi^* + \delta\hat{\psi}_+^\dagger \right) \left(\hat{c}_+ \varphi + \delta\hat{\psi}_+ \right) + \left(\delta\hat{\psi}_-^\dagger \right) \left(\delta\hat{\psi}_- \right) \Big) \\
&= \hat{c}_+^\dagger \hat{c}_+ + \int \mathrm{d}\mathbf{r} \left(\delta\hat{\psi}_+^\dagger \delta\hat{\psi}_+ + \delta\hat{\psi}_-^\dagger \delta\hat{\psi}_- \right) \\
&\approx \hat{c}_+^\dagger \hat{c}_+ + \int \mathrm{d}\mathbf{r} \left(\hat{\Lambda}_+^\dagger \hat{\Lambda}_+ + \hat{\Lambda}_-^\dagger \hat{\Lambda}_- \right) \\
&= \int \mathrm{d}\mathbf{r} \sum_{i,j*} \Big(\mathcal{Q}^* \circ \left(u_{i+}^* \hat{\alpha}_{i+}^\dagger + v_{i+}^* \hat{\alpha}_{i+} \right) \; \mathcal{Q} \circ \left(u_{j+} \hat{\alpha}_{j+} + v_{j+} \hat{\alpha}_{j+}^\dagger \right) \\
&\qquad + \left(u_{i-} \hat{\alpha}_{i-} + v_{i-} \hat{\alpha}_{i-}^\dagger \right) \left(u_{j-}^* \hat{\alpha}_{j-}^\dagger + v_{j-}^* \hat{\alpha}_{j-} \right) \Big) + \hat{c}_+^\dagger \hat{c}_+ \\
&= \sum_{i,j*} \Big(v_{i+}^* \circ \mathcal{Q} \circ u_{j+} \hat{\alpha}_{i+} \hat{\alpha}_{j+} + v_{i+}^* \circ \mathcal{Q} \circ v_{j+} \hat{\alpha}_{i+} \hat{\alpha}_{j+}^\dagger + u_{i+}^* \circ \mathcal{Q} \circ u_{j+} \hat{\alpha}_{i+}^\dagger \hat{\alpha}_{j+} \\
&\qquad + u_{i+}^* \circ \mathcal{Q} \circ v_{j+} \hat{\alpha}_{i+}^\dagger \hat{\alpha}_{j+}^\dagger + v_{i-}^* \circ u_{j-} \hat{\alpha}_{i-} \hat{\alpha}_{j-} + v_{i-}^* \circ v_{j-} \hat{\alpha}_{i-} \hat{\alpha}_{j-}^\dagger \\
&\qquad + u_{i-}^* \circ u_{j-} \hat{\alpha}_{i-}^\dagger \hat{\alpha}_{j-} + u_{i-}^* \circ v_{j-} \hat{\alpha}_{i-}^\dagger \hat{\alpha}_{j-}^\dagger \Big) + \hat{c}_+^\dagger \hat{c}_+
\end{aligned}
\tag{D.1}
$$

$$
\begin{aligned}
\hat{J}_x &= \frac{1}{2}\int \mathrm{d}\mathbf{r}\left(\hat{\Psi}_a^\dagger\hat{\Psi}_b + \hat{\Psi}_b^\dagger\hat{\Psi}_a\right) \\
&= \frac{1}{2}\int \mathrm{d}\mathbf{r}\left(\frac{\hat{\Psi}_+^\dagger + \hat{\Psi}_-^\dagger}{\sqrt{2}}\cdot\frac{\hat{\Psi}_+ - \hat{\Psi}_-}{\sqrt{2}} + \frac{\hat{\Psi}_+^\dagger - \hat{\Psi}_-^\dagger}{\sqrt{2}}\cdot\frac{\hat{\Psi}_+ + \hat{\Psi}_-}{\sqrt{2}}\right) \\
&= \frac{1}{2}\int \mathrm{d}\mathbf{r}\left(\hat{\Psi}_+^\dagger\hat{\Psi}_+ - \hat{\Psi}_-^\dagger\hat{\Psi}_-\right) \\
&= \frac{1}{2}\int \mathrm{d}\mathbf{r}\Big(\left(\hat{c}_+^\dagger\varphi^* + \delta\hat{\psi}_+^\dagger\right)\left(\hat{c}_+\varphi + \delta\hat{\psi}_+\right) - \left(\delta\hat{\psi}_-^\dagger\right)\left(\delta\hat{\psi}_-\right)\Big) \\
&= \frac{\hat{c}_+^\dagger\hat{c}_+}{2} + \frac{1}{2}\int \mathrm{d}\mathbf{r}\left(\delta\hat{\psi}_+^\dagger\delta\hat{\psi}_+ - \delta\hat{\psi}_-^\dagger\delta\hat{\psi}_-\right) \\
&\approx \frac{\hat{c}_+^\dagger\hat{c}_+}{2} + \frac{1}{2}\int \mathrm{d}\mathbf{r}\left(\hat{\Lambda}_+^\dagger\hat{\Lambda}_+ - \hat{\Lambda}_-^\dagger\hat{\Lambda}_-\right) \\
&= \frac{1}{2}\int \mathrm{d}\mathbf{r}\sum_{i,j*}\Big(\mathcal{Q}^*\circ\left(u_{i+}^*\hat{\alpha}_{i+}^\dagger + v_{i+}^*\hat{\alpha}_{i+}\right)\ \mathcal{Q}\circ\left(u_{j+}\hat{\alpha}_{j+} + v_{j+}\hat{\alpha}_{j+}^\dagger\right) \\
&\quad - \left(u_{i-}\hat{\alpha}_{i-} + v_{i-}\hat{\alpha}_{i-}^\dagger\right)\left(u_{j-}^*\hat{\alpha}_{j-}^\dagger + v_{j-}^*\hat{\alpha}_{j-}\right)\Big) + \frac{\hat{c}_+^\dagger\hat{c}_+}{2} \\
&= \frac{1}{2}\sum_{i,j*}\Big(v_{i+}^*\circ\mathcal{Q}\circ u_{j+}\hat{\alpha}_{i+}\hat{\alpha}_{j+} + v_{i+}^*\circ\mathcal{Q}\circ v_{j+}\hat{\alpha}_{i+}\hat{\alpha}_{j+}^\dagger + u_{i+}^*\circ\mathcal{Q}\circ u_{j+}\hat{\alpha}_{i+}^\dagger\hat{\alpha}_{j+} \\
&\quad + u_{i+}^*\circ\mathcal{Q}\circ v_{j+}\hat{\alpha}_{i+}^\dagger\hat{\alpha}_{j+}^\dagger - v_{i-}^*\circ u_{j-}\hat{\alpha}_{i-}\hat{\alpha}_{j-} - v_{i-}^*\circ v_{j-}\hat{\alpha}_{i-}\hat{\alpha}_{j-}^\dagger \\
&\quad - u_{i-}^*\circ u_{j-}\hat{\alpha}_{i-}^\dagger\hat{\alpha}_{j-} - u_{i-}^*\circ v_{j-}\hat{\alpha}_{i-}^\dagger\hat{\alpha}_{j-}^\dagger\Big) + \frac{\hat{c}_+^\dagger\hat{c}_+}{2}
\end{aligned}
\tag{D.2}
$$

$$
\begin{aligned}
\hat{J}_y &= \frac{i}{2}\int \mathrm{d}\mathbf{r}\left(\hat{\Psi}_b^\dagger\hat{\Psi}_a - \hat{\Psi}_a^\dagger\hat{\Psi}_b\right)\\
&= \frac{i}{2}\int \mathrm{d}\mathbf{r}\left(\frac{\hat{\Psi}_+^\dagger - \hat{\Psi}_-^\dagger}{\sqrt{2}}\cdot\frac{\hat{\Psi}_+ + \hat{\Psi}_-}{\sqrt{2}} + \frac{\hat{\Psi}_+^\dagger + \hat{\Psi}_-^\dagger}{\sqrt{2}}\cdot\frac{\hat{\Psi}_+ - \hat{\Psi}_-}{\sqrt{2}}\right)\\
&= \frac{i}{2}\int \mathrm{d}\mathbf{r}\left(\hat{\Psi}_+^\dagger\hat{\Psi}_- - \hat{\Psi}_-^\dagger\hat{\Psi}_+\right)\\
&= \frac{i}{2}\int \mathrm{d}\mathbf{r}\Big(\left(\hat{c}_+^\dagger\varphi^* + \delta\hat{\psi}_+^\dagger\right)\left(\delta\hat{\psi}_-^\dagger\right) - \left(\delta\hat{\psi}_-^\dagger\right)\left(\hat{c}_+\varphi + \delta\hat{\psi}_+\right)\Big)\\
&= \frac{i}{2}\int \mathrm{d}\mathbf{r}\Big(\left(\hat{c}_+^\dagger\varphi^*\delta\hat{\psi}_- - \hat{c}_+\delta\hat{\psi}_-^\dagger\varphi\right) + \left(\delta\hat{\psi}_{+-}^\dagger - {}_{-+}^\dagger\right)\Big)\\
&\approx \frac{i}{2}\int \mathrm{d}\mathbf{r}\left(\hat{\Lambda}_+^\dagger\hat{\Lambda}_- - \hat{\Lambda}_-^\dagger\hat{\Lambda}_+\right) + \frac{i\sqrt{N_0}}{2}\int \mathrm{d}\mathbf{r}\left(\varphi^*\hat{\Lambda}_- - \hat{\Lambda}_-^\dagger\varphi\right)\\
&= \frac{i}{2}\int \mathrm{d}\mathbf{r}\sum_{i>0}\sum_j\Big(\mathcal{Q}^*\circ\left(u_{i+}^*\hat{\alpha}_{i+}^\dagger + v_{i+}^*\hat{\alpha}_{i+}\right)\left(u_{j-}\hat{\alpha}_{j-} + v_{j-}\hat{\alpha}_{j-}^\dagger\right)\\
&\quad - \mathcal{Q}\circ\left(u_{i+}\hat{\alpha}_{i+} + v_{i+}\hat{\alpha}_{i+}^\dagger\right)\left(u_{j-}^*\hat{\alpha}_{j-}^\dagger + v_{j-}^*\hat{\alpha}_{j-}\right)\Big)\\
&\quad + \frac{i\sqrt{N_0}}{2}\sum_i\int \mathrm{d}\mathbf{r}\Big(\varphi^*\left(u_{i-}\hat{\alpha}_{i-} + v_{i-}\hat{\alpha}_{i-}^\dagger\right) - \left(u_{i-}^*\hat{\alpha}_{i-}^\dagger + v_{i-}^*\hat{\alpha}_{i-}\right)\varphi\Big)\\
&= \frac{i}{2}\sum_{i>0}\sum_j\Big(\left(v_{i+}^*\circ\mathcal{Q}\circ u_{j-} - u_{i+}\circ\mathcal{Q}^*\circ v_{j-}^*\right)\hat{\alpha}_{i+}\hat{\alpha}_{j-} + \left(v_{i+}^*\circ\mathcal{Q}\circ v_{j-} - u_{i+}\circ\mathcal{Q}^*\circ u_{j-}^*\right)\hat{\alpha}_{i+}\hat{\alpha}_{j-}^\dagger\\
&\quad + \left(u_{i+}^*\circ\mathcal{Q}\circ u_{j-} - v_{i+}\circ\mathcal{Q}^*\circ v_{j-}^*\right)\hat{\alpha}_{i+}^\dagger\hat{\alpha}_{j-} + \left(u_{i+}^*\circ\mathcal{Q}\circ v_{j-} - v_{i+}\circ\mathcal{Q}^*\circ u_{j-}^*\right)\hat{\alpha}_{i+}^\dagger\hat{\alpha}_{j-}^\dagger\Big)\\
&\quad + \frac{i\sqrt{N_0}}{2}\int \mathrm{d}\mathbf{r}\sum_i\Big(\left(\varphi^*u_{i-} - v_{i-}^*\varphi\right)\hat{\alpha}_{i-} + \left(\varphi^*v_{i-} - u_{i-}^*\varphi\right)\hat{\alpha}_{i-}^\dagger\Big) \qquad \text{(D.3)}
\end{aligned}
$$

$$
\begin{aligned}
\hat{J}_z &= \frac{1}{2}\int \mathrm{d}\mathbf{r}\left(\hat{\Psi}_a^\dagger\hat{\Psi}_a - \hat{\Psi}_b^\dagger\hat{\Psi}_b\right)\\
&= \frac{1}{2}\int \mathrm{d}\mathbf{r}\left(\frac{\hat{\Psi}_+^\dagger+\hat{\Psi}_-^\dagger}{\sqrt{2}}\cdot\frac{\hat{\Psi}_++\hat{\Psi}_-}{\sqrt{2}} - \frac{\hat{\Psi}_+^\dagger-\hat{\Psi}_-^\dagger}{\sqrt{2}}\cdot\frac{\hat{\Psi}_+-\hat{\Psi}_-}{\sqrt{2}}\right)\\
&= \frac{1}{2}\int \mathrm{d}\mathbf{r}\left(\hat{\Psi}_+^\dagger\hat{\Psi}_- + \hat{\Psi}_-^\dagger\hat{\Psi}_+\right)\\
&= \frac{1}{2}\int \mathrm{d}\mathbf{r}\Big(\left(\hat{c}_+^\dagger\varphi^* + \delta\hat{\psi}_+^\dagger\right)\left(\delta\hat{\psi}_-\right) + \left(\delta\hat{\psi}_-^\dagger\right)\left(\hat{c}_+\varphi+\delta\hat{\psi}_+\right)\Big)\\
&= \frac{1}{2}\int \mathrm{d}\mathbf{r}\left(\delta\hat{\psi}_+^\dagger\delta\hat{\psi}_- + \delta\hat{\psi}_-^\dagger\delta\hat{\psi}_+\right) + \frac{1}{2}\int \mathrm{d}\mathbf{r}\left(\varphi^*\hat{c}_+^\dagger\delta\hat{\psi}_- + \delta\hat{\psi}_-^\dagger\hat{c}_+\varphi\right)\\
&\approx \frac{1}{2}\int \mathrm{d}\mathbf{r}\left(\hat{\Lambda}_+^\dagger\hat{\Lambda}_- + \hat{\Lambda}_-^\dagger\hat{\Lambda}_+\right) + \frac{\sqrt{N_0}}{2}\int \mathrm{d}\mathbf{r}\left(\varphi^*\hat{\Lambda}_- + \hat{\Lambda}_-^\dagger\varphi\right)\\
&= \frac{1}{2}\int \mathrm{d}\mathbf{r}\sum_{i>0}\sum_j\Big(\mathcal{Q}^*\circ\left(u_{i+}^*\hat{\alpha}_{i+}^\dagger + v_{i+}^*\hat{\alpha}_{i+}\right)\left(u_{j-}\hat{\alpha}_{j-} + v_{j-}\hat{\alpha}_{j-}^\dagger\right)\\
&\quad + \mathcal{Q}\circ\left(u_{i+}\hat{\alpha}_{i+} + v_{i+}\hat{\alpha}_{i+}^\dagger\right)\left(u_{j-}^*\hat{\alpha}_{j-}^\dagger + v_{j-}^*\hat{\alpha}_{j-}\right)\Big)\\
&\quad + \frac{\sqrt{N_0}}{2}\sum_i\int \mathrm{d}\mathbf{r}\left(\varphi^*\left(u_{i-}\hat{\alpha}_{i-} + v_{i-}\hat{\alpha}_{i-}^\dagger\right) + \left(u_{i-}^*\hat{\alpha}_{i-}^\dagger + v_{i-}^*\hat{\alpha}_{i-}\right)\varphi\right)\\
&= \frac{1}{2}\sum_{i>0}\sum_j\Big(\left(v_{i+}^*\circ\mathcal{Q}\circ u_{j-} + u_{i+}\circ\mathcal{Q}^*\circ v_{j-}^*\right)\hat{\alpha}_{i+}\hat{\alpha}_{j-} + \left(v_{i+}^*\circ\mathcal{Q}\circ v_{j-} + u_{i+}\circ\mathcal{Q}^*\circ u_{j-}^*\right)\hat{\alpha}_{i+}\hat{\alpha}_{j-}^\dagger\\
&\quad + \left(u_{i+}^*\circ\mathcal{Q}\circ u_{j-} + v_{i+}\circ\mathcal{Q}^*\circ v_{j-}^*\right)\hat{\alpha}_{i+}^\dagger\hat{\alpha}_{j-} + \left(u_{i+}^*\circ\mathcal{Q}\circ v_{j-} + v_{i+}\circ\mathcal{Q}^*\circ u_{j-}^*\right)\hat{\alpha}_{i+}^\dagger\hat{\alpha}_{j-}^\dagger\Big)\\
&\quad + \frac{\sqrt{N_0}}{2}\int \mathrm{d}\mathbf{r}\sum_i\Big(\left(\varphi^*u_{i-} + v_{i-}^*\varphi\right)\hat{\alpha}_{i-} + \left(\varphi^*v_{i-} + u_{i-}^*\varphi\right)\hat{\alpha}_{i-}^\dagger\Big)
\end{aligned}
\tag{D.4}
$$

$$
\begin{aligned}
\hat{J}_x^2 &= \left(\frac{1}{2}\int \mathrm{d}\mathbf{r}\left(\hat{\Psi}_+^\dagger(\mathbf{r})\hat{\Psi}_+(\mathbf{r}) - \hat{\Psi}_-^\dagger(\mathbf{r})\hat{\Psi}_-(\mathbf{r})\right)\right)^2 \\
&= \frac{1}{4}\int \mathrm{d}\mathbf{r}\mathrm{d}\mathbf{r}'\Big(\hat{\Psi}_+^\dagger(\mathbf{r})\hat{\Psi}_+^\dagger(\mathbf{r}')\hat{\Psi}_+(\mathbf{r})\hat{\Psi}_+(\mathbf{r}') - 2\hat{\Psi}_+^\dagger(\mathbf{r})\hat{\Psi}_+(\mathbf{r})\hat{\Psi}_-^\dagger(\mathbf{r}')\hat{\Psi}_-(\mathbf{r}') \\
&\quad + \hat{\Psi}_-^\dagger(\mathbf{r})\hat{\Psi}_-^\dagger(\mathbf{r}')\hat{\Psi}_-(\mathbf{r})\hat{\Psi}_-(\mathbf{r}')\Big) + \frac{1}{4}\int \mathrm{d}\mathbf{r}\Big(\hat{\Psi}_+^\dagger(\mathbf{r})\hat{\Psi}_+(\mathbf{r}) + \hat{\Psi}_-^\dagger(\mathbf{r})\hat{\Psi}_-(\mathbf{r})\Big) \\
&\approx \frac{\hat{c}_+^\dagger\hat{c}_+\hat{c}_+^\dagger\hat{c}_+}{4} + \frac{1}{4}\int \mathrm{d}\mathbf{r}\Big(2\hat{c}_+^\dagger\hat{c}_+\delta\hat{\psi}_+^\dagger(\mathbf{r})\delta\hat{\psi}_+(\mathbf{r}) - 2\hat{c}_+^\dagger\hat{c}_+\delta\hat{\psi}_-^\dagger(\mathbf{r})\delta\hat{\psi}_-(\mathbf{r}) \\
&\quad + \delta\hat{\phi}_+^\dagger(\mathbf{r})\delta\hat{\phi}_+(\mathbf{r}) + \delta\hat{\phi}_-^\dagger(\mathbf{r})\delta\hat{\phi}_-(\mathbf{r})\Big) \\
&\approx \frac{\hat{c}_+^\dagger\hat{c}_+\hat{c}_+^\dagger\hat{c}_+}{4} + \frac{N_0}{2}\int \mathrm{d}\mathbf{r}\Big(\hat{\Lambda}_+^\dagger(\mathbf{r})\hat{\Lambda}_+(\mathbf{r}) - \hat{\Lambda}_-^\dagger(\mathbf{r})\hat{\Lambda}_-(\mathbf{r})\Big) \\
&\quad + \frac{1}{4}\int \mathrm{d}\mathbf{r}\Big(\hat{\Lambda}_+^\dagger(\mathbf{r})\hat{\Lambda}_+(\mathbf{r}) + \hat{\Lambda}_-^\dagger(\mathbf{r})\hat{\Lambda}_-(\mathbf{r})\Big) \\
&= \left(\frac{1}{4} + \frac{N_0}{2}\right)\int \mathrm{d}\mathbf{r}\sum_{i,j*}\left(\mathcal{Q}^*\circ\Big(u_{i+}^*\hat{\alpha}_{i+}^\dagger + v_{i+}^*\hat{\alpha}_{i+}\Big)\ \mathcal{Q}\circ\Big(u_{j+}\hat{\alpha}_{j+} + v_{j+}\hat{\alpha}_{j+}^\dagger\Big)\right) \\
&\quad + \left(\frac{1}{4} - \frac{N_0}{2}\right)\int \mathrm{d}\mathbf{r}\sum_{i,j}\left(\Big(u_{i-}\hat{\alpha}_{i-} + v_{i-}\hat{\alpha}_{i-}^\dagger\Big)\Big(u_{j-}^*\hat{\alpha}_{j-}^\dagger + v_{j-}^*\hat{\alpha}_{j-}\Big)\right) + \frac{\hat{c}_+^\dagger\hat{c}_+\hat{c}_+^\dagger\hat{c}_+}{4} \\
&= \left(\frac{1}{4} + \frac{N_0}{2}\right)\sum_{i,j*}\Big(v_{i+}^*\circ\mathcal{Q}\circ u_{j+}\hat{\alpha}_{i+}\hat{\alpha}_{j+} + v_{i+}^*\circ\mathcal{Q}\circ v_{j+}\hat{\alpha}_{i+}\hat{\alpha}_{j+}^\dagger + u_{i+}^*\circ\mathcal{Q}\circ u_{j+}\hat{\alpha}_{i+}^\dagger\hat{\alpha}_{j+} \\
&\quad + u_{i+}^*\circ\mathcal{Q}\circ v_{j+}\hat{\alpha}_{i+}^\dagger\hat{\alpha}_{j+}^\dagger\Big) + \left(\frac{1}{4} - \frac{N_0}{2}\right)\Big(v_{i-}^*\circ u_{j-}\hat{\alpha}_{i-}\hat{\alpha}_{j-} + v_{i-}^*\circ v_{j-}\hat{\alpha}_{i-}\hat{\alpha}_{j-}^\dagger \\
&\quad + u_{i-}^*\circ u_{j-}\hat{\alpha}_{i-}^\dagger\hat{\alpha}_{j-} + u_{i-}^*\circ v_{j-}\hat{\alpha}_{i-}^\dagger\hat{\alpha}_{j-}^\dagger\Big) + \frac{\hat{c}_+^\dagger\hat{c}_+\hat{c}_+^\dagger\hat{c}_+}{4} \qquad \text{(D.5)}
\end{aligned}
$$

$$
\begin{aligned}
\hat{J}_y^2 &= \left(\frac{i}{2}\int \mathrm{d}\mathbf{r}\left(\hat{\Psi}_+^\dagger(\mathbf{r})\hat{\Psi}_-(\mathbf{r}) - \hat{\Psi}_-^\dagger(\mathbf{r})\hat{\Psi}_+(\mathbf{r})\right)\right)^2 \\
&= \frac{1}{4}\int \mathrm{d}\mathbf{r}\mathrm{d}\mathbf{r}'\Big(2\hat{\Psi}_+^\dagger(\mathbf{r})\hat{\Psi}_-^\dagger(\mathbf{r}')\hat{\Psi}_+(\mathbf{r}')\hat{\Psi}_-(\mathbf{r}) - \hat{\Psi}_+^\dagger(\mathbf{r})\hat{\Psi}_+^\dagger(\mathbf{r}')\hat{\Psi}_-(\mathbf{r})\hat{\Psi}_-(\mathbf{r}') \\
&\quad - \hat{\Psi}_-^\dagger(\mathbf{r})\hat{\Psi}_-^\dagger(\mathbf{r}')\hat{\Psi}_+(\mathbf{r})\hat{\Psi}_+(\mathbf{r}')\Big) + \frac{1}{4}\int \mathrm{d}\mathbf{r}\Big(\hat{\Psi}_+^\dagger(\mathbf{r})\hat{\Psi}_+(\mathbf{r}) + \hat{\Psi}_-^\dagger(\mathbf{r})\hat{\Psi}_-(\mathbf{r})\Big) \\
&\approx \frac{\hat{c}_+^\dagger\hat{c}_+}{4} + \frac{1}{4}\int \mathrm{d}\mathbf{r}\mathrm{d}\mathbf{r}'\Big(2\hat{c}_+^\dagger\hat{c}_+\varphi^*(\mathbf{r})\varphi(\mathbf{r}')\delta\hat{\psi}_-^\dagger(\mathbf{r}')\delta\hat{\psi}_-(\mathbf{r}) - \hat{c}_+^\dagger\hat{c}_+^\dagger\varphi^*(\mathbf{r})\varphi^*(\mathbf{r}')\delta\hat{\psi}_-(\mathbf{r})\delta\hat{\psi}_-(\mathbf{r}') \\
&\quad - \hat{c}_+\hat{c}_+\varphi(\mathbf{r})\varphi(\mathbf{r}')\delta\hat{\psi}_-^\dagger(\mathbf{r})\delta\hat{\psi}_-^\dagger(\mathbf{r}')\Big) + \frac{1}{4}\int \mathrm{d}\mathbf{r}\Big(\delta\hat{\psi}_+^\dagger(\mathbf{r})\delta\hat{\psi}_+(\mathbf{r}) + \delta\hat{\psi}_-^\dagger(\mathbf{r})\delta\hat{\psi}_-(\mathbf{r})\Big) \\
&\approx \frac{\hat{c}_+^\dagger\hat{c}_+}{4} + \frac{N_0}{4}\int \mathrm{d}\mathbf{r}\mathrm{d}\mathbf{r}'\Big(2\varphi^*(\mathbf{r}')\varphi(\mathbf{r})\hat{\Lambda}_-^\dagger(\mathbf{r})\hat{\Lambda}_-(\mathbf{r}') - \varphi^*(\mathbf{r})\varphi^*(\mathbf{r}')\hat{\Lambda}_-(\mathbf{r})\hat{\Lambda}_-(\mathbf{r}') \\
&\quad - \varphi(\mathbf{r})\varphi(\mathbf{r}')\hat{\Lambda}_-^\dagger(\mathbf{r})\hat{\Lambda}_-^\dagger(\mathbf{r}')\Big) + \frac{1}{4}\int \mathrm{d}\mathbf{r}\Big(\hat{\Lambda}_+^\dagger(\mathbf{r})\hat{\Lambda}_+(\mathbf{r}) + \hat{\Lambda}_-^\dagger(\mathbf{r})\hat{\Lambda}_-(\mathbf{r})\Big) \\
&= \frac{N_0}{4}\sum_{i,j}\Bigg(\Big(2v_{i-}^*\circ\varphi\varphi^*\circ u_{j-} - \varphi^*\circ u_{i-}\varphi^*\circ u_{j-} - v_{i-}^*\circ\varphi v_{j-}^*\circ\varphi\Big)\hat{\alpha}_{i-}\hat{\alpha}_{j-} \\
&\quad + \Big(2v_{i-}^*\circ\varphi\varphi^*\circ v_{j-} - \varphi^*\circ u_{i-}\varphi^*\circ v_{j-} - v_{i-}^*\circ\varphi u_{j-}^*\circ\varphi\Big)\hat{\alpha}_{i-}\hat{\alpha}_{j-}^\dagger \\
&\quad + \Big(2u_{i-}^*\circ\varphi\varphi^*\circ u_{j-} - \varphi^*\circ v_{i-}\varphi^*\circ u_{j-} - u_{i-}^*\circ\varphi v_{j-}^*\circ\varphi\Big)\hat{\alpha}_{i-}^\dagger\hat{\alpha}_{j-} \\
&\quad + \Big(2u_{i-}^*\circ\varphi\varphi^*\circ v_{j-} - \varphi^*\circ v_{i-}\varphi^*\circ v_{j-} - u_{i-}^*\circ\varphi u_{j-}^*\circ\varphi\Big)\hat{\alpha}_{i-}^\dagger\hat{\alpha}_{j-}^\dagger\Bigg) + \frac{\hat{c}_+^\dagger\hat{c}_+}{4} \\
&\quad + \frac{1}{4}\sum_{i,j}\Big(v_{i-}^*\circ u_{j-}\hat{\alpha}_{i-}\hat{\alpha}_{j-} + v_{i-}^*\circ v_{j-}\hat{\alpha}_{i-}\hat{\alpha}_{j-}^\dagger + u_{i-}^*\circ u_{j-}\hat{\alpha}_{i-}^\dagger\hat{\alpha}_{j-} + u_{i-}^*\circ v_{j-}\hat{\alpha}_{i-}^\dagger\hat{\alpha}_{j-}^\dagger\Big) \\
&\quad + \frac{1}{4}\sum_{i,j>0}\Big(v_{i+}^*\circ\mathcal{Q}\circ u_{j+}\hat{\alpha}_{i+}\hat{\alpha}_{j+} + v_{i+}^*\circ\mathcal{Q}\circ v_{j+}\hat{\alpha}_{i+}\hat{\alpha}_{j+}^\dagger \\
&\quad + u_{i+}^*\circ\mathcal{Q}\circ u_{j+}\hat{\alpha}_{i+}^\dagger\hat{\alpha}_{j+} + u_{i+}^*\circ\mathcal{Q}\circ v_{j+}\hat{\alpha}_{i+}^\dagger\hat{\alpha}_{j+}^\dagger\Big) \qquad \text{(D.6)}
\end{aligned}
$$

$$
\begin{aligned}
\hat{J}_z^2 &= \left(\frac{1}{2}\int \mathrm{d}\mathbf{r}\left(\hat{\Psi}_a^\dagger(\mathbf{r})\hat{\Psi}_a(\mathbf{r}) - \hat{\Psi}_b^\dagger(\mathbf{r})\hat{\Psi}_b(\mathbf{r})\right)\right)^2 = \left(\frac{1}{2}\int \mathrm{d}\mathbf{r}\left(\hat{\Psi}_+^\dagger(\mathbf{r})\hat{\Psi}_-(\mathbf{r}) + \hat{\Psi}_-^\dagger(\mathbf{r})\hat{\Psi}_+(\mathbf{r})\right)\right)^2 \\
&= \frac{1}{4}\int \mathrm{d}\mathbf{r}\mathrm{d}\mathbf{r}'\Big(\hat{\Psi}_+^\dagger(\mathbf{r})\hat{\Psi}_-(\mathbf{r})\hat{\Psi}_+^\dagger(\mathbf{r}')\hat{\Psi}_-(\mathbf{r}') + \hat{\Psi}_-^\dagger(\mathbf{r})\hat{\Psi}_+(\mathbf{r})\hat{\Psi}_+^\dagger(\mathbf{r}')\hat{\Psi}_-(\mathbf{r}') \\
&\quad + \hat{\Psi}_+^\dagger(\mathbf{r})\hat{\Psi}_-(\mathbf{r})\hat{\Psi}_-^\dagger(\mathbf{r}')\hat{\Psi}_+(\mathbf{r}') + \hat{\Psi}_-^\dagger(\mathbf{r})\hat{\Psi}_+(\mathbf{r})\hat{\Psi}_-^\dagger(\mathbf{r}')\hat{\Psi}_+(\mathbf{r}')\Big) \\
&= \frac{1}{4}\int \mathrm{d}\mathbf{r}\mathrm{d}\mathbf{r}'\Big(\hat{\Psi}_+^\dagger(\mathbf{r})\hat{\Psi}_+^\dagger(\mathbf{r}')\hat{\Psi}_-(\mathbf{r})\hat{\Psi}_-(\mathbf{r}') + 2\hat{\Psi}_+^\dagger(\mathbf{r})\hat{\Psi}_-^\dagger(\mathbf{r}')\hat{\Psi}_+(\mathbf{r}')\hat{\Psi}_-(\mathbf{r}) \\
&\quad + \hat{\Psi}_-^\dagger(\mathbf{r})\hat{\Psi}_-^\dagger(\mathbf{r}')\hat{\Psi}_+(\mathbf{r})\hat{\Psi}_+(\mathbf{r}')\Big) + \frac{1}{4}\int \mathrm{d}\mathbf{r}\Big(\hat{\Psi}_+^\dagger(\mathbf{r})\hat{\Psi}_+(\mathbf{r}) + \hat{\Psi}_-^\dagger(\mathbf{r})\hat{\Psi}_-(\mathbf{r})\Big) \\
&\approx \frac{\hat{c}_+^\dagger\hat{c}_+}{4} + \frac{1}{4}\int \mathrm{d}\mathbf{r}\mathrm{d}\mathbf{r}'\Big(\hat{c}_+^\dagger\hat{c}_+^\dagger\varphi^*(\mathbf{r})\varphi^*(\mathbf{r}')\delta\hat{\psi}_-(\mathbf{r})\delta\hat{\psi}_-(\mathbf{r}') + 2\hat{c}_+^\dagger\hat{c}_+\varphi^*(\mathbf{r})\varphi(\mathbf{r}')\delta\hat{\psi}_-^\dagger(\mathbf{r}')\delta\hat{\psi}_-(\mathbf{r}) \\
&\quad + \hat{c}_+\hat{c}_+\varphi(\mathbf{r})\varphi(\mathbf{r}')\delta\hat{\psi}_-^\dagger(\mathbf{r})\delta\hat{\psi}_-^\dagger(\mathbf{r}')\Big) + \frac{1}{4}\int \mathrm{d}\mathbf{r}\Big(\delta\hat{\psi}_+^\dagger(\mathbf{r})\delta\hat{\psi}_+(\mathbf{r}) + \delta\hat{\psi}_-^\dagger(\mathbf{r})\delta\hat{\psi}_-(\mathbf{r})\Big) \\
&\approx \frac{\hat{c}_+^\dagger\hat{c}_+}{4} + \frac{N_0}{4}\int \mathrm{d}\mathbf{r}\mathrm{d}\mathbf{r}'\Big(\varphi^*(\mathbf{r})\varphi^*(\mathbf{r}')\hat{\Lambda}_-(\mathbf{r})\hat{\Lambda}_-(\mathbf{r}') + 2\varphi^*(\mathbf{r}')\varphi(\mathbf{r})\hat{\Lambda}_-^\dagger(\mathbf{r})\hat{\Lambda}_-(\mathbf{r}') \\
&\quad + \varphi(\mathbf{r})\varphi(\mathbf{r}')\hat{\Lambda}_-^\dagger(\mathbf{r})\hat{\Lambda}_-^\dagger(\mathbf{r}')\Big) + \frac{1}{4}\int \mathrm{d}\mathbf{r}\Big(\hat{\Lambda}_+^\dagger(\mathbf{r})\hat{\Lambda}_+(\mathbf{r}) + \hat{\Lambda}_-^\dagger(\mathbf{r})\hat{\Lambda}_-(\mathbf{r})\Big) \\
&= \frac{N_0}{4}\sum_{i,j}\Bigg(\Big(\varphi^*\circ u_{i-}\varphi^*\circ u_{j-} + 2v_{i-}^*\circ\varphi\varphi^*\circ u_{j-} + v_{i-}^*\circ\varphi v_{j-}^*\circ\varphi\Big)\hat{\alpha}_{i-}\hat{\alpha}_{j-} \\
&\quad + \Big(\varphi^*\circ u_{i-}\varphi^*\circ v_{j-} + 2v_{i-}^*\circ\varphi\varphi^*\circ v_{j-} + v_{i-}^*\circ\varphi u_{j-}^*\circ\varphi\Big)\hat{\alpha}_{i-}\hat{\alpha}_{j-}^\dagger \\
&\quad + \Big(\varphi^*\circ v_{i-}\varphi^*\circ u_{j-} + 2u_{i-}^*\circ\varphi\varphi^*\circ u_{j-} + u_{i-}^*\circ\varphi v_{j-}^*\circ\varphi\Big)\hat{\alpha}_{i-}^\dagger\hat{\alpha}_{j-} \\
&\quad + \Big(\varphi^*\circ v_{i-}\varphi^*\circ v_{j-} + 2u_{i-}^*\circ\varphi\varphi^*\circ v_{j-} + u_{i-}^*\circ\varphi u_{j-}^*\circ\varphi\Big)\hat{\alpha}_{i-}^\dagger\hat{\alpha}_{j-}^\dagger\Bigg) + \frac{\hat{c}_+^\dagger\hat{c}_+}{4} \\
&\quad + \frac{1}{4}\sum_{i,j}\Big(v_{i-}^*\circ u_{j-}\hat{\alpha}_{i-}\hat{\alpha}_{j-} + v_{i-}^*\circ v_{j-}\hat{\alpha}_{i-}\hat{\alpha}_{j-}^\dagger + u_{i-}^*\circ u_{j-}\hat{\alpha}_{i-}^\dagger\hat{\alpha}_{j-} + u_{i-}^*\circ v_{j-}\hat{\alpha}_{i-}^\dagger\hat{\alpha}_{j-}^\dagger\Big) \\
&\quad + \frac{1}{4}\sum_{i,j>0}\Big(v_{i+}^*\circ\mathcal{Q}\circ u_{j+}\hat{\alpha}_{i+}\hat{\alpha}_{j+} + v_{i+}^*\circ\mathcal{Q}\circ v_{j+}\hat{\alpha}_{i+}\hat{\alpha}_{j+}^\dagger \\
&\quad + u_{i+}^*\circ\mathcal{Q}\circ u_{j+}\hat{\alpha}_{i+}^\dagger\hat{\alpha}_{j+} + u_{i+}^*\circ\mathcal{Q}\circ v_{j+}\hat{\alpha}_{i+}^\dagger\hat{\alpha}_{j+}^\dagger\Big) \qquad \text{(D.7)}
\end{aligned}
$$

$$
\begin{aligned}
\hat{J}_x\hat{J}_y &= \frac{i}{4}\int \mathrm{d}\mathbf{r}\int \mathrm{d}\mathbf{r}'\left(\hat{\Psi}_+^\dagger(\mathbf{r})\hat{\Psi}_+(\mathbf{r})-\hat{\Psi}_-^\dagger(\mathbf{r})\hat{\Psi}_-(\mathbf{r})\right)\left(\hat{\Psi}_+^\dagger(\mathbf{r}')\hat{\Psi}_-(\mathbf{r}')-\hat{\Psi}_-^\dagger(\mathbf{r}')\hat{\Psi}_+(\mathbf{r}')\right)\\
&\approx \frac{i}{4}\hat{c}_+^\dagger\hat{c}_+\int \mathrm{d}\mathbf{r}\Bigg(\left(\hat{c}_+^\dagger\varphi^*\delta\hat{\psi}_- - \hat{c}_+\delta\hat{\psi}_-^\dagger\varphi\right)+\left(\delta\hat{\psi}_{+-}^\dagger - -_-^\dagger{}_+\right)\Bigg)\\
&\approx \frac{i}{4}\int \mathrm{d}\mathbf{r}\Bigg(N_0\left(\hat{\Lambda}_+^\dagger\hat{\Lambda}_- - \hat{\Lambda}_-^\dagger\hat{\Lambda}_+\right)+\sqrt{N_0}\hat{c}_+^\dagger\hat{c}_+\left(\varphi^*\hat{\Lambda}_- - \hat{\Lambda}_-^\dagger\varphi\right)\Bigg)\\
&= \frac{i}{4}N_0\int \mathrm{d}\mathbf{r}\sum_{i>0}\sum_j\Bigg(\mathcal{Q}^*\circ\left(u_{i+}^*\hat{\alpha}_{i+}^\dagger+v_{i+}^*\hat{\alpha}_{i+}\right)\left(u_{j-}\hat{\alpha}_{j-}+v_{j-}\hat{\alpha}_{j-}^\dagger\right)\\
&\quad -\mathcal{Q}\circ\left(u_{i+}\hat{\alpha}_{i+}+v_{i+}\hat{\alpha}_{i+}^\dagger\right)\left(u_{j-}^*\hat{\alpha}_{j-}^\dagger+v_{j-}^*\hat{\alpha}_{j-}\right)\Bigg)\\
&\quad +\frac{i\sqrt{N_0}}{4}\hat{c}_+^\dagger\hat{c}_+\sum_i\int \mathrm{d}\mathbf{r}\left(\varphi^*\left(u_{i-}\hat{\alpha}_{i-}+v_{i-}\hat{\alpha}_{i-}^\dagger\right)-\left(u_{i-}^*\hat{\alpha}_{i-}^\dagger+v_{i-}^*\hat{\alpha}_{i-}\right)\varphi\right)\\
&= \frac{i}{4}N_0\sum_{i>0}\sum_j\Bigg(\left(v_{i+}^*\circ\mathcal{Q}\circ u_{j-}-u_{i+}\circ\mathcal{Q}^*\circ v_{j-}^*\right)\hat{\alpha}_{i+}\hat{\alpha}_{j-}\\
&\quad +\left(v_{i+}^*\circ\mathcal{Q}\circ v_{j-}-u_{i+}\circ\mathcal{Q}^*\circ u_{j-}^*\right)\hat{\alpha}_{i+}\hat{\alpha}_{j-}^\dagger\\
&\quad +\left(u_{i+}^*\circ\mathcal{Q}\circ u_{j-}-v_{i+}\circ\mathcal{Q}^*\circ v_{j-}^*\right)\hat{\alpha}_{i+}^\dagger\hat{\alpha}_{j-}\\
&\quad +\left(u_{i+}^*\circ\mathcal{Q}\circ v_{j-}-v_{i+}\circ\mathcal{Q}^*\circ u_{j-}^*\right)\hat{\alpha}_{i+}^\dagger\hat{\alpha}_{j-}^\dagger\Bigg)\\
&\quad +\frac{i\sqrt{N_0}}{4}\hat{c}_+^\dagger\hat{c}_+\int \mathrm{d}\mathbf{r}\sum_i\Bigg(\left(\varphi^*u_{i-}-v_{i-}^*\varphi\right)\hat{\alpha}_{i-}+\left(\varphi^*v_{i-}-u_{i-}^*\varphi\right)\hat{\alpha}_{i-}^\dagger\Bigg)
\end{aligned}
\tag{D.8}
$$

$$
\begin{aligned}
\hat{J}_y\hat{J}_x &= \frac{i}{4}N_0\sum_{i>0}\sum_j\Bigg(\left(v_{i+}^*\circ\mathcal{Q}\circ u_{j-}-u_{i+}\circ\mathcal{Q}^*\circ v_{j-}^*\right)\hat{\alpha}_{i+}\hat{\alpha}_{j-}\\
&\quad +\left(v_{i+}^*\circ\mathcal{Q}\circ v_{j-}-u_{i+}\circ\mathcal{Q}^*\circ u_{j-}^*\right)\hat{\alpha}_{i+}\hat{\alpha}_{j-}^\dagger\\
&\quad +\left(u_{i+}^*\circ\mathcal{Q}\circ u_{j-}-v_{i+}\circ\mathcal{Q}^*\circ v_{j-}^*\right)\hat{\alpha}_{i+}^\dagger\hat{\alpha}_{j-}\\
&\quad +\left(u_{i+}^*\circ\mathcal{Q}\circ v_{j-}-v_{i+}\circ\mathcal{Q}^*\circ u_{j-}^*\right)\hat{\alpha}_{i+}^\dagger\hat{\alpha}_{j-}^\dagger\Bigg)\\
&\quad +\frac{i\sqrt{N_0}}{4}\int \mathrm{d}\mathbf{r}\sum_i\Bigg(\left(\varphi^*u_{i-}-v_{i-}^*\varphi\right)\hat{\alpha}_{i-}+\left(\varphi^*v_{i-}-u_{i-}^*\varphi\right)\hat{\alpha}_{i-}^\dagger\Bigg)\hat{c}_+^\dagger\hat{c}_+
\end{aligned}
\tag{D.9}
$$

$$
\begin{aligned}
\hat{J}_x\hat{J}_z &= \frac{1}{4}\int \mathrm{d}\mathbf{r}\int \mathrm{d}\mathbf{r}'\left(\hat{\Psi}_+^\dagger(\mathbf{r})\hat{\Psi}_+(\mathbf{r})+-\hat{\Psi}_-^\dagger(\mathbf{r})\hat{\Psi}_-(\mathbf{r})\right)\left(\hat{\Psi}_+^\dagger(\mathbf{r}')\hat{\Psi}_-(\mathbf{r}')+\hat{\Psi}_-^\dagger(\mathbf{r}')\hat{\Psi}_+(\mathbf{r})\right)\\
&= \frac{1}{4}\hat{c}_+^\dagger\hat{c}_+\int \mathrm{d}\mathbf{r}\Big(\left(\hat{c}_+^\dagger\varphi^*+\delta\hat{\psi}_+^\dagger\right)\left(\delta\hat{\psi}_-\right)+\left(\delta\hat{\psi}_-^\dagger\right)\left(\hat{c}_+\varphi+\delta\hat{\psi}_+\right)\Big)\\
&= \frac{1}{4}\hat{c}_+^\dagger\hat{c}_+\int \mathrm{d}\mathbf{r}\Big(\left(\delta\hat{\psi}_+^\dagger\delta\hat{\psi}_-+\delta\hat{\psi}_-^\dagger\delta\hat{\psi}_+\right)+\left(\varphi^*\hat{c}_+^\dagger\delta\hat{\psi}_-+\delta\hat{\psi}_-^\dagger\hat{c}_+\varphi\right)\Big)\\
&\approx \frac{N_0}{4}\int \mathrm{d}\mathbf{r}\left(\hat{\Lambda}_+^\dagger\hat{\Lambda}_-+\hat{\Lambda}_-^\dagger\hat{\Lambda}_+\right)+\frac{\sqrt{N_0}}{4}\hat{c}_+^\dagger\hat{c}_+\int \mathrm{d}\mathbf{r}\left(\varphi^*\hat{\Lambda}_-+\hat{\Lambda}_-^\dagger\varphi\right)\\
&= \frac{N_0}{4}\int \mathrm{d}\mathbf{r}\sum_{i>0}\sum_j\Big(\mathcal{Q}^*\circ\left(u_{i+}^*\hat{\alpha}_{i+}^\dagger+v_{i+}^*\hat{\alpha}_{i+}\right)\left(u_{j-}\hat{\alpha}_{j-}+v_{j-}\hat{\alpha}_{j-}^\dagger\right)\\
&\quad+\mathcal{Q}\circ\left(u_{i+}\hat{\alpha}_{i+}+v_{i+}\hat{\alpha}_{i+}^\dagger\right)\left(u_{j-}^*\hat{\alpha}_{j-}^\dagger+v_{j-}^*\hat{\alpha}_{j-}\right)\Big)\\
&\quad+\frac{\sqrt{N_0}}{4}\hat{c}_+^\dagger\hat{c}_+\sum_i\int \mathrm{d}\mathbf{r}\left(\varphi^*\left(u_{i-}\hat{\alpha}_{i-}+v_{i-}\hat{\alpha}_{i-}^\dagger\right)+\left(u_{i-}^*\hat{\alpha}_{i-}^\dagger+v_{i-}^*\hat{\alpha}_{i-}\right)\varphi\right)\\
&= \frac{N_0}{4}\sum_{i>0}\sum_j\Big(\left(v_{i+}^*\circ\mathcal{Q}\circ u_{j-}+u_{i+}\circ\mathcal{Q}^*\circ v_{j-}^*\right)\hat{\alpha}_{i+}\hat{\alpha}_{j-}\\
&\quad+\left(v_{i+}^*\circ\mathcal{Q}\circ v_{j-}+u_{i+}\circ\mathcal{Q}^*\circ u_{j-}^*\right)\hat{\alpha}_{i+}\hat{\alpha}_{j-}^\dagger\\
&\quad+\left(u_{i+}^*\circ\mathcal{Q}\circ u_{j-}+v_{i+}\circ\mathcal{Q}^*\circ v_{j-}^*\right)\hat{\alpha}_{i+}^\dagger\hat{\alpha}_{j-}\\
&\quad+\left(u_{i+}^*\circ\mathcal{Q}\circ v_{j-}+v_{i+}\circ\mathcal{Q}^*\circ u_{j-}^*\right)\hat{\alpha}_{i+}^\dagger\hat{\alpha}_{j-}^\dagger\Big)\\
&\quad+\frac{\sqrt{N_0}}{4}\hat{c}_+^\dagger\hat{c}_+\int \mathrm{d}\mathbf{r}\sum_i\Big(\left(\varphi^*u_{i-}+v_{i-}^*\varphi\right)\hat{\alpha}_{i-}+\left(\varphi^*v_{i-}+u_{i-}^*\varphi\right)\hat{\alpha}_{i-}^\dagger\Big)
\end{aligned}
\tag{D.10}
$$

$$
\begin{aligned}
\hat{J}_x\hat{J}_z &= \frac{N_0}{4}\sum_{i>0}\sum_j\Big(\left(v_{i+}^*\circ\mathcal{Q}\circ u_{j-}+u_{i+}\circ\mathcal{Q}^*\circ v_{j-}^*\right)\hat{\alpha}_{i+}\hat{\alpha}_{j-}\\
&\quad+\left(v_{i+}^*\circ\mathcal{Q}\circ v_{j-}+u_{i+}\circ\mathcal{Q}^*\circ u_{j-}^*\right)\hat{\alpha}_{i+}\hat{\alpha}_{j-}^\dagger\\
&\quad+\left(u_{i+}^*\circ\mathcal{Q}\circ u_{j-}+v_{i+}\circ\mathcal{Q}^*\circ v_{j-}^*\right)\hat{\alpha}_{i+}^\dagger\hat{\alpha}_{j-}\\
&\quad+\left(u_{i+}^*\circ\mathcal{Q}\circ v_{j-}+v_{i+}\circ\mathcal{Q}^*\circ u_{j-}^*\right)\hat{\alpha}_{i+}^\dagger\hat{\alpha}_{j-}^\dagger\Big)\\
&\quad+\frac{\sqrt{N_0}}{4}\int \mathrm{d}\mathbf{r}\sum_i\Big(\left(\varphi^*u_{i-}+v_{i-}^*\varphi\right)\hat{\alpha}_{i-}+\left(\varphi^*v_{i-}+u_{i-}^*\varphi\right)\hat{\alpha}_{i-}^\dagger\Big)\hat{c}_+^\dagger\hat{c}_+
\end{aligned}
\tag{D.11}
$$

$$
\begin{aligned}
\frac{1}{2}\left(\hat{J}_y\hat{J}_z+\hat{J}_z\hat{J}_y\right) &= \frac{i}{4}\int \mathrm{d}\mathbf{r}\int \mathrm{d}\mathbf{r}'\left(\hat{\Psi}_+^\dagger(\mathbf{r})\Psi_-(\mathbf{r})\hat{\Psi}_+^\dagger(\mathbf{r}')\hat{\Psi}_-(\mathbf{r}')-\hat{\Psi}_-^{\hat{\dagger}}(\mathbf{r})\hat{\Psi}_+(\mathbf{r})\hat{\Psi}_-^\dagger(\mathbf{r}')\hat{\Psi}_+(\mathbf{r}')\right)\\
&\approx \frac{i}{4}\left(\hat{c}_+^\dagger\hat{c}_+^\dagger\varphi^*\circ_-\varphi^*\circ_--\hat{c}_+\hat{c}_+{}^*_-\circ\varphi^*_-\circ\varphi\right)\\
&\approx \frac{iN}{4}\left(\varphi^*\circ\hat{\Lambda}_-\;\varphi^*\circ\hat{\Lambda}_--\hat{\Lambda}_-^\dagger!\circ\varphi\;\hat{\Lambda}_-^\dagger\circ\varphi\right)\\
&= \frac{iN}{4}\sum_{ij}\Bigg(\varphi^*\circ\left(u_{i-}\hat{\alpha}_{i-}+v_{i-}\hat{\alpha}_{i-}^\dagger\right)\;\varphi^*\circ\left(u_{j-}\hat{\alpha}_{j-}+v_{j-}\hat{\alpha}_{j-}^\dagger\right)\\
&\quad-\left(u_{i-}^*\hat{\alpha}_{i-}^\dagger+v_{i-}^*\hat{\alpha}_{i-}\right)\circ\varphi\;\left(u_{j-}^*\hat{\alpha}_{j-}^\dagger+v_{j-}^*\hat{\alpha}_{j-}\right)\circ\varphi\Bigg)\\
&= \frac{iN}{4}\sum_{ij}\Bigg(\left(\varphi^*\circ u_{i-}\;\varphi^*\circ u_{j-}-v_{i-}^*\circ\varphi\;v_{j-}^*\circ\varphi\right)\hat{\alpha}_{i-}\hat{\alpha}_{j-}\\
&\quad+\left(\varphi^*\circ v_{i-}\;\varphi^*\circ v_{j-}-u_{i-}^*\circ\varphi\;u_{j-}^*\circ\varphi\right)\hat{\alpha}_{i-}^\dagger\hat{\alpha}_{j-}^\dagger\\
&\quad+\left(\varphi^*\circ v_{i-}\;\varphi^*\circ u_{j-}-u_{i-}^*\circ\varphi\;v_{j-}^*\circ\varphi\right)\hat{\alpha}_{i-}^\dagger\hat{\alpha}_{j-}\\
&\quad+\left(\varphi^*\circ u_{i-}\;\varphi^*\circ v_{j-}-v_{i-}^*\circ\varphi\;u_{j-}^*\circ\varphi\right)\hat{\alpha}_{i-}\hat{\alpha}_{j-}^\dagger\Bigg)
\end{aligned}
\tag{D.12}
$$

In case of a product state $|\psi\rangle = |n_{0+}\rangle_{0+}\otimes|n_{0-}\rangle_{0-}\otimes|n_{1+}\rangle_{1+}\otimes\ldots$ the expectation values of our operators becomes

$$
\langle\hat{J}_z\rangle=\langle\hat{J}_y\rangle=\frac{\langle\hat{J}_x\hat{J}_y+\hat{J}_y\hat{J}_x\rangle}{2}=\frac{\langle\hat{J}_y\hat{J}_z+\hat{J}_z\hat{J}_y\rangle}{2}=\frac{\langle\hat{J}_z\hat{J}_x+\hat{J}_x\hat{J}_z\rangle}{2}=0 \tag{D.13}
$$

and

$$
\begin{aligned}
\langle\hat{N}\rangle &= N_0 + \sum_{i*}\Big(v^*_{i+}\circ\mathcal{Q}\circ v_{i+}\big(\langle n\rangle_{i+}+1\big) + u^*_{i+}\circ\mathcal{Q}\circ u_{i+}\langle n\rangle_{i+} \\
&\quad + v^*_{i-}\circ v_{i-}\big(\langle n\rangle_{i-}+1\big) + u^*_{i-}\circ u_{i-}\langle n\rangle_{i-}\Big) \\
\langle\hat{J}_x\rangle &= \frac{N_0}{2} + \frac{1}{2}\sum_{i*}\Big(v^*_{i+}\circ\mathcal{Q}\circ v_{i+}\big(\langle n\rangle_{i+}+1\big) + u^*_{i+}\circ\mathcal{Q}\circ u_{i+}\langle n\rangle_{i+} \\
&\quad - v^*_{i-}\circ v_{i-}\Big(\langle n\rangle_{i-}+1\Big) - u^*_{i-}\circ u_{i-}\langle n\rangle_{i-}\Big) \\
\langle\hat{J}_x^2\rangle &= \frac{N_0^2}{4} + \left(\frac{1}{4}+\frac{N_0}{2}\right)\sum_{i>i}\Big(v^*_{i+}\circ\mathcal{Q}\circ v_{i+}\Big(\langle n\rangle_{i+}+1\Big) + u^*_{i+}\circ\mathcal{Q}\circ u_{i+}\langle n\rangle_{i+}\Big) \\
&\quad + \left(\frac{1}{4}-\frac{N_0}{2}\right)\sum_{i}\Big(v^*_{i-}\circ v_{i-}\Big(\langle n\rangle_{i-}+1\Big) + u^*_{i-}\circ u_{i-}\langle n\rangle_{i-}\Big) \\
\langle\hat{J}_y^2\rangle &= \frac{N_0}{4} + \frac{N_0}{4}\sum_{i}\Big(\Big(2v^*_{i-}\circ\varphi\varphi^*\circ v_{i-} - \varphi^*\circ u_{i-}\varphi^*\circ v_{i-} - v^*_{i-}\circ\varphi u^*_{i-}\circ\varphi\Big)\big(\langle n\rangle_{i-}+1\big) \\
&\quad + \Big(2u^*_{i-}\circ\varphi\varphi^*\circ u_{i-} - \varphi^*\circ v_{i-}\varphi^*\circ u_{i-} - u^*_{i-}\circ\varphi v^*_{i-}\circ\varphi\Big)\langle n\rangle_{i-}\Big) \\
&\quad + \frac{1}{4}\sum_{i}\Big(v^*_{i-}\circ v_{i-}\Big(\langle n\rangle_{i-}+1\Big) + u^*_{i-}\circ u_{i-}\langle n\rangle_{i-}\Big) \\
&\quad + \frac{1}{4}\sum_{i>0}\Big(v^*_{i+}\circ\mathcal{Q}\circ v_{i+}\Big(\langle n\rangle_{i+}+1\Big) + u^*_{i+}\circ\mathcal{Q}\circ u_{i+}\langle n\rangle_{i+}\Big) \\
\langle\hat{J}_z^2\rangle &= \frac{N_0}{4} + \frac{N_0}{4}\sum_{i}\Big(\Big(\varphi^*\circ u_{i-}\varphi^*\circ v_{i-} + 2v^*_{i-}\circ\varphi\varphi^*\circ v_{i-} + v^*_{i-}\circ\varphi u^*_{i-}\circ\varphi\Big)\big(\langle n\rangle_{i-}+1\big) \\
&\quad + \Big(\varphi^*\circ v_{i-}\varphi^*\circ u_{i-} + 2u^*_{i-}\circ\varphi\varphi^*\circ u_{i-} + u^*_{i-}\circ\varphi v^*_{i-}\circ\varphi\Big)\langle n\rangle_{i-}\Big) \\
&\quad + \frac{1}{4}\sum_{i}\Big(v^*_{i-}\circ v_{i-}\Big(\langle n\rangle_{i-}+1\Big) + u^*_{i-}\circ u_{i-}\langle n\rangle_{i-}\Big) \\
&\quad + \frac{1}{4}\sum_{i>0}\Big(v^*_{i+}\circ\mathcal{Q}\circ v_{i+}\Big(\langle n\rangle_{i+}+1\Big) + u^*_{i+}\circ\mathcal{Q}\circ u_{i+}\langle n\rangle_{i+}\Big) \qquad \text{(D.14)}
\end{aligned}
$$

If we try to use the above results to calculate $(\Delta J_x)^2 = \langle\hat{J}_x^2\rangle - \langle\hat{J}_x\rangle^2$, the result becomes inconsistent, since the $\langle\hat{J}_x\rangle^2$-term would contain terms proportional to $(\delta\hat{\psi})^4$, while those terms were discarded in the calculation of $\langle\hat{J}_x^2\rangle$. Therefore we need to calculate a specific expression for $(\Delta J_x)^2$ containing all terms to all orders!

The calculations are tedious, but the result is

$$
\begin{aligned}
(\Delta J_x)^2 \;=\; & \frac{1}{4}\sum_{i*}\Bigg(v^*_{i+}\circ\mathcal{Q}\circ u_{i+}u^*_{i+}\circ\mathcal{Q}\circ v_{i+}\Big(\langle n_{i+}\rangle^2+3\langle n_{i+}\rangle+2\Big) \\
& + u^*_{i+}\circ\mathcal{Q}\circ v_{i+}v^*_{i+}\circ\mathcal{Q}\circ u_{i+}\Big(\langle n_{i+}\rangle-1\Big)\langle n_{i+}\rangle \\
& + v^*_{i-}\circ u_{i-}u^*_{i-}\circ v_{i-}\Big(\langle n_{i-}\rangle^2+3\langle n_{i-}\rangle+2\Big) \\
& + u^*_{i-}\circ v_{i-}v^*_{i-}\circ u_{i-}\Big(\langle n_{i-}\rangle-1\Big)\langle n_{i-}\rangle \\
& + \sum_{(j\neq i)*}\Bigg(v^*_{i+}\circ\mathcal{Q}\circ u_{j+}u^*_{i+}\circ\mathcal{Q}\circ v_{j+}\Big(\langle n_{i+}\rangle+1\Big)\Big(\langle n_{j+}\rangle+1\Big) \\
& + v^*_{i+}\circ\mathcal{Q}\circ u_{j+}u^*_{j+}\circ\mathcal{Q}\circ v_{i+}\Big(\langle n_{i+}\rangle+1\Big)\Big(\langle n_{j+}\rangle+1\Big) \\
& + v^*_{i+}\circ\mathcal{Q}\circ v_{j+}v^*_{j+}\circ\mathcal{Q}\circ v_{i+}\Big(\langle n_{i+}\rangle+1\Big)\langle n_{j+}\rangle \\
& + v^*_{i+}\circ\mathcal{Q}\circ v_{j+}u^*_{i+}\circ\mathcal{Q}\circ u_{j+}\Big(\langle n_{i+}\rangle+1\Big)\Big(\langle n_{j+}\rangle+1\Big) \\
& + u^*_{i+}\circ\mathcal{Q}\circ u_{j+}v^*_{i+}\circ\mathcal{Q}\circ u_{j+}\langle n_{i+}\rangle\Big(\langle n_{j+}\rangle+1\Big) \\
& + u^*_{i+}\circ\mathcal{Q}\circ u_{j+}u^*_{j+}\circ\mathcal{Q}\circ u_{i+}\langle n_{i+}\rangle\Big(\langle n_{j+}\rangle+1\Big) \\
& + u^*_{i+}\circ\mathcal{Q}\circ v_{j+}v^*_{i+}\circ\mathcal{Q}\circ u_{j+}\langle n_{i+}\rangle\langle n_{j+}\rangle \\
& + u^*_{i+}\circ\mathcal{Q}\circ v_{j+}v^*_{j+}\circ\mathcal{Q}\circ u_{i+}\langle n_{i+}\rangle\langle n_{j+}\rangle \\
& + v^*_{i-}\circ u_{j-}u^*_{i-}\circ v_{j-}\Big(\langle n_{i-}\rangle+1\Big)\Big(\langle n_{j-}\rangle+1\Big) \\
& + v^*_{i-}\circ u_{j-}u^*_{j-}\circ v_{i-}\Big(\langle n_{i-}\rangle+1\Big)\Big(\langle n_{j-}\rangle+1\Big) \\
& + v^*_{i-}\circ v_{j-}v^*_{j-}\circ v_{i-}\Big(\langle n_{i-}\rangle+1\Big)\langle n_{j-}\rangle \\
& + v^*_{i-}\circ v_{j-}u^*_{i-}\circ u_{j-}\Big(\langle n_{i-}\rangle+1\Big)\Big(\langle n_{j-}\rangle+1\Big) \\
& + u^*_{i-}\circ u_{j-}v^*_{i-}\circ u_{j-}\langle n_{i-}\rangle\Big(\langle n_{j-}\rangle+1\Big) \\
& + u^*_{i-}\circ u_{j-}u^*_{j-}\circ u_{i-}\langle n_{i-}\rangle\Big(\langle n_{j-}\rangle+1\Big) \\
& + u^*_{i-}\circ v_{j-}v^*_{i-}\circ u_{j-}\langle n_{i-}\rangle\langle n_{j-}\rangle \\
& + u^*_{i-}\circ v_{j-}v^*_{j-}\circ u_{i-}\langle n_{i-}\rangle\langle n_{j-}\rangle\Bigg)\Bigg)
\end{aligned}
\tag{D.15}
$$

If the state in question is $|\psi\rangle = |N\rangle_{0+}\otimes|0\rangle_{0-}\otimes|0\rangle_{1+}\otimes\ldots$ the results (D.14) and (D.15) reduces further to

$$
\begin{aligned}
\langle \hat{N} \rangle &= N_0 + \sum_{i*} \Big(v^*_{i+} \circ \mathcal{Q} \circ v_{i+} + v^*_{i-} \circ v_{i-} \Big) \\
\langle \hat{J}_x \rangle &= \frac{N_0}{2} + \frac{1}{2} \sum_{i*} \Big(v^*_{i+} \circ \mathcal{Q} \circ v_{i+} - v^*_{i-} \circ v_{i-} \Big) \\
\langle \hat{J}_x^2 \rangle &= \frac{N_0^2}{4} + \left(\frac{1}{4} + \frac{N_0}{2} \right) \sum_{i>0} v^*_{i+} \circ \mathcal{Q} \circ v_{i+} + \left(\frac{1}{4} - \frac{N_0}{2} \right) \sum_i v^*_{i-} \circ v_{i-} \\
\langle \hat{J}_y^2 \rangle &= \frac{N_0}{4} + \frac{N_0}{4} \sum_i \Big(2 v^*_{i-} \circ \varphi \varphi^* \circ v_{i-} - \varphi^* \circ u_{i-} \varphi^* \circ v_{i-} - v^*_{i-} \circ \varphi u^*_{i-} \circ \varphi \Big) \\
&\quad + \frac{1}{4} \sum_{i*} \Big(v^*_{i-} \circ v_{i-} + v^*_{i+} \circ \mathcal{Q} \circ v_{i+} \Big) \\
\langle \hat{J}_z^2 \rangle &= \frac{N_0}{4} + \frac{N_0}{4} \sum_i \Big(2 v^*_{i-} \circ \varphi \varphi^* \circ v_{i-} + \varphi^* \circ u_{i-} \varphi^* \circ v_{i-} + v^*_{i-} \circ \varphi u^*_{i-} \circ \varphi \Big) \\
&\quad + \frac{1}{4} \sum_{i*} \Big(v^*_{i-} \circ v_{i-} + v^*_{i+} \circ \mathcal{Q} \circ v_{i+} \Big) \\
(\Delta J_x)^2 &= \frac{1}{4} \sum_{i*} \Bigg(2 v^*_{i+} \circ \mathcal{Q} \circ u_{i+} u^*_{i+} \circ \mathcal{Q} \circ v_{i+} + 2 v^*_{i-} \circ u_{i-} u^*_{i-} \circ v_{i-} \\
&\quad + \sum_{(j \neq i)*} \Big(v^*_{i+} \circ \mathcal{Q} \circ u_{j+} u^*_{i+} \circ \mathcal{Q} \circ v_{j+} + v^*_{i+} \circ \mathcal{Q} \circ u_{j+} u^*_{j+} \circ \mathcal{Q} \circ v_{i+} \\
&\quad + v^*_{i+} \circ \mathcal{Q} \circ v_{j+} u^*_{i+} \circ \mathcal{Q} \circ u_{j+} + v^*_{i-} \circ u_{j-} u^*_{i-} \circ v_{j-} \\
&\quad + v^*_{i-} \circ u_{j-} u^*_{j-} \circ v_{i-} + v^*_{i-} \circ v_{j-} u^*_{i-} \circ \mathcal{Q} \circ u_{j-} \Big) \Bigg) \qquad \text{(D.16)}
\end{aligned}
$$

Appendix E

Time dependence

In this appendix we will calculate the equations of motion for the $\hat{\Lambda}$-operator and show that the time-dependent approach gives the same form of the matrix $\mathcal{L}$ as the time-independent steady-state calculations done in the main text. Before carrying out the calculation for the full theory, we will do it for a two-mode approximation and for the Schwinger approximation.

As these calculations are similar to the time-independent calculations in the main text, they will be done with a minimum of discussion.

A two-mode calculation

In this subsection we will use the two-mode approximation $\hat{\Psi}(\mathbf{r}) \to \hat{c}$ on the Hamiltonian

$$\begin{aligned}\hat{\mathcal{H}} &= \int \mathrm{d}\mathbf{r}\Big(\hat{\Psi}_+^\dagger(\mathbf{r})H_0\hat{\Psi}_+(\mathbf{r}) + \hat{\Psi}_-^\dagger(\mathbf{r})H_0\hat{\Psi}_-(\mathbf{r}) + U\left(\hat{\Psi}_+^\dagger(\mathbf{r})\hat{\Psi}_-^\dagger(\mathbf{r})\hat{\Psi}_+(\mathbf{r})\hat{\Psi}_-(\mathbf{r})\right) \\ &\quad + \frac{U+U_{ab}}{4}\left(\hat{\Psi}_+^\dagger(\mathbf{r})\hat{\Psi}_+^\dagger(\mathbf{r})\hat{\Psi}_+(\mathbf{r})\hat{\Psi}_+(\mathbf{r}) + \hat{\Psi}_-^\dagger(\mathbf{r})\hat{\Psi}_-^\dagger(\mathbf{r})\hat{\Psi}_-(\mathbf{r})\hat{\Psi}_-(\mathbf{r})\right) \\ &\quad + \frac{U-U_{ab}}{4}\left(\hat{\Psi}_+^\dagger(\mathbf{r})\hat{\Psi}_+^\dagger(\mathbf{r})\hat{\Psi}_-(\mathbf{r})\hat{\Psi}_-(\mathbf{r}) + \hat{\Psi}_-^\dagger(\mathbf{r})\hat{\Psi}_-^\dagger(\mathbf{r})\hat{\Psi}_+(\mathbf{r})\hat{\Psi}_+(\mathbf{r})\right) \\ &\quad + \frac{\Omega}{2}\left(\hat{\Psi}_+^\dagger(\mathbf{r})\hat{\Psi}_+(\mathbf{r}) - \hat{\Psi}_-^\dagger(\mathbf{r})\hat{\Psi}_-(\mathbf{r})\right)\Big) \end{aligned} \tag{E.1}$$

giving

$$\begin{aligned}\hat{\mathcal{H}} &= \hat{c}_+^\dagger E\hat{c}_+ + \hat{c}_-^\dagger E\hat{c}_- + \frac{\Omega}{2}\left(\hat{c}_+^\dagger\hat{c}_+ - \hat{c}_-^\dagger\hat{c}_-\right) + \frac{U+U_{ab}}{4}\left(\hat{c}_+^\dagger\hat{c}_+^\dagger\hat{c}_+\hat{c}_+ + \hat{c}_-^\dagger\hat{c}_-^\dagger\hat{c}_-\hat{c}_-\right) \\ &\quad + \frac{U-U_{ab}}{4}\left(\hat{c}_+^\dagger\hat{c}_+^\dagger\hat{c}_-\hat{c}_- + \hat{c}_-^\dagger\hat{c}_-^\dagger\hat{c}_+\hat{c}_+\right) + U\left(\hat{c}_+^\dagger\hat{c}_-^\dagger\hat{c}_+\hat{c}_-\right) \end{aligned} \tag{E.2}$$

We wish to find the time dependence of $\hat{\Lambda}$ as it was defined by (5.33) in the context of the Schwinger model. This is done using the Heisenberg equation with the result

$$-i\dot{\hat{\Lambda}} = \left[\hat{\mathcal{H}}, \frac{\hat{c}_+^\dagger \hat{c}_-}{\sqrt{N}}\right] = \left[\hat{\mathcal{H}}, \hat{c}_+^\dagger\right] \frac{\hat{c}_-}{\sqrt{N}} + \frac{\hat{c}_+^\dagger}{\sqrt{N}} \left[\hat{\mathcal{H}}, \hat{c}_-\right] \tag{E.3}$$

Let us find the various commutators

$$\begin{aligned} \left[\hat{c}_+^\dagger \hat{c}_+, \hat{c}_+^\dagger\right] &= \hat{c}_+^\dagger \\ \left[\hat{c}_+ \hat{c}_+, \hat{c}_+^\dagger\right] &= 2\hat{c}_+ \\ \left[\hat{c}_+^\dagger \hat{c}_+^\dagger \hat{c}_+ \hat{c}_+, \hat{c}_+^\dagger\right] &= 2\hat{c}_+^\dagger \hat{c}_+^\dagger \hat{c}_+ \end{aligned} \tag{E.4}$$

$$\begin{aligned} \left[\hat{c}_-^\dagger \hat{c}_-, \hat{c}_-\right] &= -\hat{c}_- \\ \left[\hat{c}_-^\dagger \hat{c}_-^\dagger, \hat{c}_-\right] &= -2\hat{c}_-^\dagger \\ \left[\hat{c}_-^\dagger \hat{c}_-^\dagger \hat{c}_- \hat{c}_-, \hat{c}_-\right] &= -2\hat{c}_-^\dagger \hat{c}_- \hat{c}_- \end{aligned} \tag{E.5}$$

This gives

$$\begin{aligned} \left[\hat{\mathcal{H}}, \hat{c}_+^\dagger\right] &= E\hat{c}_+^\dagger + \frac{\Omega}{2}\hat{c}_+^\dagger + \frac{U+U_{ab}}{2}\hat{c}_+^\dagger \hat{c}_+^\dagger \hat{c}_+ + \frac{U-U_{ab}}{2}\hat{c}_-^\dagger \hat{c}_-^\dagger \hat{c}_+ + U\hat{c}_-^\dagger \hat{c}_+^\dagger \hat{c}_- \\ \left[\hat{\mathcal{H}}, \hat{c}_-\right] &= -E\hat{c}_- + \frac{\Omega}{2}\hat{c}_- - \frac{U+U_{ab}}{2}\hat{c}_-^\dagger \hat{c}_- \hat{c}_- - \frac{U-U_{ab}}{2}\hat{c}_-^\dagger \hat{c}_+ \hat{c}_+ - U\hat{c}_+^\dagger \hat{c}_+ \hat{c}_- \end{aligned} \tag{E.6}$$

which gives

$$\begin{aligned} -i\sqrt{N}\dot{\hat{\Lambda}} &= E\hat{c}_+^\dagger \hat{c}_- + \frac{\Omega}{2}\hat{c}_+^\dagger \hat{c}_- + \frac{U+U_{ab}}{2}\hat{c}_+^\dagger \hat{c}_+^\dagger \hat{c}_+ \hat{c}_- + \frac{U-U_{ab}}{2}\hat{c}_-^\dagger \hat{c}_-^\dagger \hat{c}_+ \hat{c}_- \\ &\quad + U\hat{c}_-^\dagger \hat{c}_+^\dagger \hat{c}_- \hat{c}_- - E\hat{c}_+^\dagger \hat{c}_- + \frac{\Omega}{2}\hat{c}_+^\dagger \hat{c}_- - \frac{U+U_{ab}}{2}\hat{c}_+^\dagger \hat{c}_-^\dagger \hat{c}_- \hat{c}_- \\ &\quad - \frac{U-U_{ab}}{2}\hat{c}_+^\dagger \hat{c}_-^\dagger \hat{c}_+ \hat{c}_+ - U\hat{c}_+^\dagger \hat{c}_+^\dagger \hat{c}_+ \hat{c}_- \Leftrightarrow \\ -i\dot{\hat{\Lambda}} &= \Omega\hat{\Lambda} + \frac{U+U_{ab}}{2}\left(\hat{c}_+^\dagger \hat{c}_+ - \hat{c}_-^\dagger \hat{c}_- - 1\right)\hat{\Lambda} \\ &\quad + \frac{U-U_{ab}}{2}\left(\hat{c}_-^\dagger \hat{c}_- - \hat{c}_+^\dagger \hat{c}_+ - 1\right)\hat{\Lambda}^\dagger \\ &\quad + U\left(\hat{c}_-^\dagger \hat{c}_- - \hat{c}_+^\dagger \hat{c}_+ + 1\right)\hat{\Lambda} \end{aligned} \tag{E.7}$$

Let us do the same for $\hat{\Lambda}^\dagger$

$$-i\dot{\hat{\Lambda}}^\dagger = \left[\hat{\mathcal{H}}, \frac{\hat{c}_+ \hat{c}_-^\dagger}{\sqrt{N}}\right] = \left[\hat{\mathcal{H}}, \hat{c}_+\right] \frac{\hat{c}_-^\dagger}{\sqrt{N}} + \frac{\hat{c}_+}{\sqrt{N}} \left[\hat{\mathcal{H}}, \hat{c}_-^\dagger\right] \tag{E.8}$$

The commutators are

$$\begin{aligned}\left[\hat{c}_+^\dagger\hat{c}_+,\hat{c}_+\right] &= -\hat{c}_+\\ \left[\hat{c}_+^\dagger\hat{c}_+^\dagger,\hat{c}_+\right] &= -2\hat{c}_+^\dagger\\ \left[\hat{c}_+^\dagger\hat{c}_+^\dagger\hat{c}_+\hat{c}_+,\hat{c}_+\right] &= -2\hat{c}_+^\dagger\hat{c}_+\hat{c}_+\end{aligned} \tag{E.9}$$

$$\begin{aligned}\left[\hat{c}_-^\dagger\hat{c}_-,\hat{c}_-^\dagger\right] &= \hat{c}_-^\dagger\\ \left[\hat{c}_-\hat{c}_-,\hat{c}_-^\dagger\right] &= 2\hat{c}_-\\ \left[\hat{c}_-^\dagger\hat{c}_-^\dagger\hat{c}_-\hat{c}_-,\hat{c}_-^\dagger\right] &= 2\hat{c}_-^\dagger\hat{c}_-^\dagger\hat{c}_-\end{aligned} \tag{E.10}$$

which gives

$$\begin{aligned}[\mathcal{H},\hat{c}_+] &= -E\hat{c}_+ - \frac{\Omega}{2}\hat{c}_+ - \frac{U+U_{ab}}{2}\hat{c}_+^\dagger\hat{c}_+\hat{c}_+ - \frac{U-U_{ab}}{2}\hat{c}_+^\dagger\hat{c}_-\hat{c}_- - U\hat{c}_-^\dagger\hat{c}_-\hat{c}_+\\ \left[\mathcal{H},\hat{c}_-^\dagger\right] &= E\hat{c}_-^\dagger - \frac{\Omega}{2}\hat{c}_-^\dagger + \frac{U+U_{ab}}{2}\hat{c}_-^\dagger\hat{c}_-^\dagger\hat{c}_- + \frac{U-U_{ab}}{2}\hat{c}_+^\dagger\hat{c}_+^\dagger\hat{c}_- + U\hat{c}_+^\dagger\hat{c}_-^\dagger\hat{c}_+\end{aligned} \tag{E.11}$$

with the result

$$\begin{aligned}-i\sqrt{N}\dot{\Lambda}^\dagger &= -E\hat{c}_+\hat{c}_-^\dagger - \frac{\Omega}{2}\hat{c}_+\hat{c}_-^\dagger - \frac{U+U_{ab}}{2}\hat{c}_+^\dagger\hat{c}_+\hat{c}_+\hat{c}_-^\dagger - \frac{U-U_{ab}}{2}\hat{c}_+^\dagger\hat{c}_-\hat{c}_-\hat{c}_-^\dagger\\ &\quad -U\hat{c}_-^\dagger\hat{c}_-\hat{c}_+\hat{c}_-^\dagger + E\hat{c}_+\hat{c}_-^\dagger - \frac{\Omega}{2}\hat{c}_+\hat{c}_-^\dagger + \frac{U+U_{ab}}{2}\hat{c}_+\hat{c}_-^\dagger\hat{c}_-^\dagger\hat{c}_-\\ &\quad +\frac{U-U_{ab}}{2}\hat{c}_+\hat{c}_+^\dagger\hat{c}_+^\dagger\hat{c}_- + U\hat{c}_+\hat{c}_+^\dagger\hat{c}_-^\dagger\hat{c}_+ \Leftrightarrow\\ -i\dot{\Lambda}^\dagger &= -\Omega\hat{\Lambda}^\dagger + \frac{U+U_{ab}}{2}\left(\hat{c}_-^\dagger\hat{c}_- - \hat{c}_+^\dagger\hat{c}_+ - 1\right)\hat{\Lambda}^\dagger\\ &\quad + \frac{U-U_{ab}}{2}\left(\hat{c}_+^\dagger\hat{c}_+ - \hat{c}_-^\dagger\hat{c}_- - 1\right)\hat{\Lambda}\\ &\quad + U\left(\hat{c}_+^\dagger\hat{c}_+ - \hat{c}_-^\dagger\hat{c}_- + 1\right)\hat{\Lambda}^\dagger\end{aligned} \tag{E.12}$$

If we replace $\hat{c}_\pm^\dagger\hat{c}_\pm \to N_\pm$ and assume that $N_+ \gg N_-$, the above results (E.7) and (E.12) can be written on matrix form as

$$i\dot{\bar{\Lambda}} = \mathcal{L}\bar{\Lambda} \tag{E.13}$$

where

$$\bar{\Lambda} \equiv \begin{pmatrix}\hat{\Lambda}\\ \hat{\Lambda}^\dagger\end{pmatrix} \tag{E.14}$$

and

$$\mathcal{L} \equiv \begin{pmatrix} A & B \\ -B & -A \end{pmatrix} \tag{E.15}$$

where

$$\begin{aligned} A &\equiv -\Omega - \frac{U+U_{ab}}{2}N + UN \\ B &\equiv \frac{U-U_{ab}}{2}N \end{aligned} \tag{E.16}$$

If we use the GP-like equation

$$\mu = E + \frac{U+U_{ab}}{2}N + \frac{\Omega}{2} \tag{E.17}$$

we get

$$\begin{aligned} A &= (E-\mu) - \frac{\Omega}{2} + UN \\ B &= \frac{U-U_{ab}}{2}N \end{aligned} \tag{E.18}$$

which is just the result we want, since it is just as similar to A_- and B_- as given by (6.16) in the time independent calculation, as the two-mode approximation allows.

The Schwinger calculation

In this subsection we will do the time-dependent calculation for the Schwinger approximation, see section 5.7.

$$\begin{aligned} \hat{\mathcal{H}} &= \chi \hat{J}_z^2 + \Omega \hat{J}_x \\ &= \frac{\chi}{4}\left(\hat{c}_+^\dagger \hat{c}_+^\dagger \hat{c}_- \hat{c}_- + \hat{c}_-^\dagger \hat{c}_-^\dagger \hat{c}_+ \hat{c}_+ + 2\hat{c}_+^\dagger \hat{c}_+ \hat{c}_-^\dagger \hat{c}_- + \hat{c}_+^\dagger \hat{c}_+ + \hat{c}_-^\dagger \hat{c}_-\right) + \frac{\Omega}{2}\left(\hat{c}_+^\dagger \hat{c}_+ - \hat{c}_-^\dagger \hat{c}_-\right) \end{aligned} \tag{E.19}$$

The commutation relations for the $\hat{c}$-operators found in the previous subsection gives for the $\hat{\Lambda}$-operator

$$\begin{aligned} \sqrt{N} i\dot{\Lambda} &= \left[\hat{c}_+^\dagger \hat{c}_-, \hat{\mathcal{H}}\right] = \left[\hat{c}_+^\dagger, \hat{\mathcal{H}}\right]\hat{c}_- + \hat{c}_+^\dagger \left[\hat{c}_-, \hat{\mathcal{H}}\right] \\ &= \frac{\chi}{2}\left(\hat{c}_+^\dagger \hat{c}_-^\dagger \hat{c}_+ \hat{c}_+ + \hat{c}_+^\dagger \hat{c}_+^\dagger \hat{c}_+ \hat{c}_- - \hat{c}_-^\dagger \hat{c}_-^\dagger \hat{c}_+ \hat{c}_- - \hat{c}_-^\dagger \hat{c}_- \hat{c}_+^\dagger \hat{c}_-\right) - \Omega \hat{c}_+^\dagger \hat{c}_- \Leftrightarrow \\ i\dot{\Lambda} &= \left(\frac{\chi}{2}\left(\hat{c}_+^\dagger \hat{c}_+ - \hat{c}_-^\dagger \hat{c}_- - 1\right) - \Omega\right)\hat{\Lambda} + \frac{\chi}{2}\left(\hat{c}_+^\dagger \hat{c}_+ - \hat{c}_-^\dagger \hat{c}_- + 1\right)\hat{\Lambda}^\dagger \end{aligned} \tag{E.20}$$

and for the $\hat{\Lambda}^\dagger$-operator we get

$$\begin{aligned} \sqrt{N} i\dot{\Lambda}^\dagger &= \left[\hat{c}_+ \hat{c}_-^\dagger, \hat{\mathcal{H}}\right] = \left[\hat{c}_+, \hat{\mathcal{H}}\right]\hat{c}_-^\dagger + \hat{c}_+ \left[\hat{c}_-^\dagger, \hat{\mathcal{H}}\right] \\ &= \frac{\chi}{2}\left(\hat{c}_+^\dagger \hat{c}_- \hat{c}_- \hat{c}_-^\dagger + \hat{c}_+ \hat{c}_-^\dagger \hat{c}_- \hat{c}_-^\dagger - \hat{c}_+ \hat{c}_+^\dagger \hat{c}_+^\dagger \hat{c}_- - \hat{c}_+ \hat{c}_+^\dagger \hat{c}_+ \hat{c}_-^\dagger\right) + \Omega \hat{c}_+ \hat{c}_-^\dagger \Leftrightarrow \\ i\dot{\Lambda}^\dagger &= \frac{\chi}{2}\left(\hat{c}_-^\dagger \hat{c}_- - \hat{c}_+^\dagger \hat{c}_+ + 1\right)\hat{\Lambda} + \left(\frac{\chi}{2}\left(\hat{c}_-^\dagger \hat{c}_- - \hat{c}_+^\dagger \hat{c}_+ - 1\right) + \Omega\right)\hat{\Lambda}^\dagger \end{aligned} \tag{E.21}$$

If we, as in the previous subsection, replace $\hat{c}^\dagger\hat{c} \to N$ and assume that $N_+ \gg N_-$, the above results can be written on matrix form as

$$i\dot{\bar{\Lambda}} = \mathcal{L}\bar{\Lambda} \tag{E.22}$$

where

$$\mathcal{L} \equiv \begin{pmatrix} A & B \\ -B & -A \end{pmatrix} \tag{E.23}$$

and where

$$\begin{aligned} A &\equiv \frac{N_+\chi}{2} - \Omega \\ B &\equiv \frac{N_+\chi}{2} \end{aligned} \tag{E.24}$$

which is the same result as for the time independent Schwinger calculation in the main text.

The full calculation

Finally we will do a time-dependent version of the full calculation.

$$\begin{aligned} \hat{\mathcal{H}} &= \int \mathrm{d}\mathbf{r}\Big(\hat{\Psi}_+^\dagger(\mathbf{r}) H_0 \hat{\Psi}_+(\mathbf{r}) + \hat{\Psi}_-^\dagger(\mathbf{r}) H_0 \hat{\Psi}_-(\mathbf{r}) \\ &\quad + \frac{U+U_{ab}}{4}\left(\hat{\Psi}_+^\dagger(\mathbf{r})\hat{\Psi}_+^\dagger(\mathbf{r})\hat{\Psi}_+(\mathbf{r})\hat{\Psi}_+(\mathbf{r}) + \hat{\Psi}_-^\dagger(\mathbf{r})\hat{\Psi}_-^\dagger(\mathbf{r})\hat{\Psi}_-(\mathbf{r})\hat{\Psi}_-(\mathbf{r})\right) \\ &\quad + \frac{U-U_{ab}}{4}\left(\hat{\Psi}_+^\dagger(\mathbf{r})\hat{\Psi}_+^\dagger(\mathbf{r})\hat{\Psi}_-(\mathbf{r})\hat{\Psi}_-(\mathbf{r}) + \hat{\Psi}_-^\dagger(\mathbf{r})\hat{\Psi}_-^\dagger(\mathbf{r})\hat{\Psi}_+(\mathbf{r})\hat{\Psi}_+(\mathbf{r})\right) \\ &\quad + U\left(\hat{\Psi}_+^\dagger(\mathbf{r})\hat{\Psi}_-^\dagger(\mathbf{r})\hat{\Psi}_+(\mathbf{r})\hat{\Psi}_-(\mathbf{r})\right) + \frac{\Omega}{2}\left(\hat{\Psi}_+^\dagger(\mathbf{r})\hat{\Psi}_+(\mathbf{r}) - \hat{\Psi}_-^\dagger(\mathbf{r})\hat{\Psi}_-(\mathbf{r})\right)\Big) \end{aligned}$$

$$\begin{aligned} &= \int \mathrm{d}\mathbf{r}\Big(\varphi^* H_0 \varphi \hat{c}_+^\dagger\hat{c}_+ + \varphi^*\hat{c}_+^\dagger H_0 \delta\hat{\psi}_+ + \delta\hat{\psi}_+^\dagger H_0 \varphi\hat{c}_+ + \delta\hat{\psi}_+^\dagger(H_0)\delta\hat{\psi}_+ + \delta\hat{\psi}_-^\dagger(H_0)\delta\hat{\psi}_- \\ &\quad + \frac{U+U_{ab}}{4}\Big(|\varphi|^4\hat{c}_+^\dagger\hat{c}_+^\dagger\hat{c}_+\hat{c}_+ + 2\varphi^*\hat{c}_+^\dagger|\varphi|^2\hat{c}_+^\dagger\hat{c}_+\delta\hat{\psi}_+ + 2\delta\hat{\psi}_+^\dagger|\varphi|^2\hat{c}_+^\dagger\hat{c}_+\varphi\hat{c}_+ \\ &\quad + (\varphi^*)^2\hat{c}_+^\dagger\hat{c}_+^\dagger\delta\hat{\psi}_+\delta\hat{\psi}_+\delta\hat{\psi}_+^\dagger\delta\hat{\psi}_+^\dagger(\varphi)^2\hat{c}_+\hat{c}_+ + 4|\varphi|^2\hat{c}_+^\dagger\hat{c}_+\delta\hat{\psi}_+^\dagger\delta\hat{\psi}_+ \\ &\quad + 2\varphi^*\hat{c}_+^\dagger\delta\hat{\psi}_+^\dagger\delta\hat{\psi}_+\delta\hat{\psi}_+ + 2\delta\hat{\psi}_+^\dagger\delta\hat{\psi}_+^\dagger\delta\hat{\psi}_+\varphi\hat{c}_+\delta\hat{\psi}_+^\dagger\delta\hat{\psi}_+^\dagger\delta\hat{\psi}_+\delta\hat{\psi}_+ + \delta\hat{\psi}_-^\dagger\delta\hat{\psi}_-^\dagger\delta\hat{\psi}_-\delta\hat{\psi}_-\Big) \\ &\quad + \frac{U-U_{ab}}{4}\Big((\varphi^*)^2\hat{c}_+^\dagger\hat{c}_+^\dagger\delta\hat{\psi}_-\delta\hat{\psi}_- + 2\varphi^*\hat{c}_+^\dagger\delta\hat{\psi}_+^\dagger\delta\hat{\psi}_-\delta\hat{\psi}_- + \delta\hat{\psi}_+^\dagger\delta\hat{\psi}_+^\dagger\delta\hat{\psi}_-\delta\hat{\psi}_- \\ &\quad + \delta\hat{\psi}_-^\dagger\delta\hat{\psi}_-^\dagger(\varphi)^2\hat{c}_+\hat{c}_+ + 2\delta\hat{\psi}_-^\dagger\delta\hat{\psi}_-^\dagger\varphi\hat{c}_+\delta\hat{\psi}_+ + \delta\hat{\psi}_-^\dagger\delta\hat{\psi}_-^\dagger\delta\hat{\psi}_+\delta\hat{\psi}_+\Big) \\ &\quad + U\Big(|\varphi|^2\hat{c}_+^\dagger\hat{c}_+\delta\hat{\psi}_-^\dagger\delta\hat{\psi}_- + \varphi^*\hat{c}_+^\dagger\delta\hat{\psi}_+\delta\hat{\psi}_-^\dagger\delta\hat{\psi}_- + \delta\hat{\psi}_+^\dagger\varphi\hat{c}_+\delta\hat{\psi}_-^\dagger\delta\hat{\psi}_- + \delta\hat{\psi}_+^\dagger\delta\hat{\psi}_+\delta\hat{\psi}_-^\dagger\delta\hat{\psi}_-\Big) \\ &\quad + \frac{\Omega}{2}\Big(|\varphi|^2\hat{c}_+^\dagger\hat{c}_+ + \varphi^*\hat{c}_+^\dagger\delta\hat{\psi}_+ + \delta\hat{\psi}_+^\dagger\varphi\hat{c}_+ + \delta\hat{\psi}_+^\dagger\delta\hat{\psi}_+ - \delta\hat{\psi}_-^\dagger\delta\hat{\psi}_-\Big)\Big) \end{aligned} \tag{E.25}$$

Let us calculate the equation of motion for $\hat{\Lambda}$ and $\hat{\Lambda}^\dagger$ by calculating the commutators:

$$\begin{aligned}\left[\hat{c}_+^\dagger, \hat{\mathcal{H}}\right] &= \int \mathrm{d}\mathbf{r}\Big(- \varphi^* H_0 \varphi \hat{c}_+^\dagger - \delta\hat{\psi}_+^\dagger H_0 \varphi - \frac{\Omega}{2}\Big(|\varphi|^2 \hat{c}_+^\dagger + \delta\hat{\psi}_+^\dagger \varphi\Big) \\ &- \frac{U+U_{ab}}{2}\Big(|\varphi|^2|\varphi|^2 \hat{c}_+^\dagger \hat{c}_+^\dagger \hat{c}_+ + \varphi^*|\varphi|^2 \hat{c}_+^\dagger \hat{c}_+^\dagger \delta\hat{\psi}_+ + 2|\varphi|^2 \varphi \delta\hat{\psi}_+^\dagger \hat{c}_+^\dagger \hat{c}_+ \\ &+ \delta\hat{\psi}_+^\dagger \delta\hat{\psi}_+^\dagger (\varphi)^2 \hat{c}_+ + 2|\varphi|^2 \hat{c}_+^\dagger \delta\hat{\psi}_+^\dagger \delta\hat{\psi}_+ + \delta\hat{\psi}_+^\dagger \delta\hat{\psi}_+^\dagger \delta\hat{\psi}_+ \varphi\Big) \\ &- \frac{U-U_{ab}}{2}\Big(\delta\hat{\psi}_-^\dagger \delta\hat{\psi}_-^\dagger (\varphi)^2 \hat{c}_+ + \delta\hat{\psi}_-^\dagger \delta\hat{\psi}_-^\dagger \varphi \delta\hat{\psi}_+\Big) \\ &- U\Big(|\varphi|^2 \hat{c}_+^\dagger \delta\hat{\psi}_-^\dagger \delta\hat{\psi}_- + \delta\hat{\psi}_+^\dagger \varphi \delta\hat{\psi}_-^\dagger \delta\hat{\psi}_-\Big)\Big) \end{aligned} \tag{E.26}$$

$$\begin{aligned}\left[\delta\hat{\psi}_+, \hat{\mathcal{H}}\right] &= H_0 \varphi \hat{c}_+ + H_0 \delta\hat{\psi}_+ + \frac{U+U_{ab}}{2}\Big(|\varphi|^2 \hat{c}_+^\dagger \hat{c}_+ \varphi \hat{c}_+ + \delta\hat{\psi}(\varphi)^2 \hat{c}_+ \hat{c}_+ \\ &+ 2|\varphi|^2 \hat{c}_+^\dagger \hat{c}_+ \delta\hat{\psi}_+ + \varphi^* \hat{c}_+^\dagger \delta\hat{\psi}_+ \delta\hat{\psi}_+ + 2\delta\hat{\psi}_+^\dagger \delta\hat{\psi} \varphi \hat{c}_+ + \delta\hat{\psi}_+^\dagger \delta\hat{\psi}_+ \delta\hat{\psi}_+\Big) \\ &+ \frac{U-U_{ab}}{2}\Big(\varphi^* \hat{c}_+^\dagger \delta\hat{\psi}_- \delta\hat{\psi}_- + \delta\hat{\psi}_+^\dagger \delta\hat{\psi}_- \delta\hat{\psi}_-\Big) \\ &+ U\Big(\varphi \hat{c}_+ \delta\hat{\psi}_-^\dagger \delta\hat{\psi}_- + \delta\hat{\psi}_+ \delta\hat{\psi}_-^\dagger \delta\hat{\psi}_-\Big) + \frac{\Omega}{2}\Big(\varphi \hat{c}_+ + \delta\hat{\psi}_+\Big) \end{aligned} \tag{E.27}$$

$$\begin{aligned}\left[\delta\hat{\psi}_-, \hat{\mathcal{H}}\right] &= (H_0)\delta\hat{\psi}_- + \frac{U+U_{ab}}{2}\delta\hat{\psi}_-^\dagger \delta\hat{\psi}_- \delta\hat{\psi}_- - \frac{\Omega}{2}\delta\hat{\psi}_- \\ &+ \frac{U-U_{ab}}{2}\Big(\delta\hat{\psi}_-^\dagger (\varphi)^2 \hat{c}_+ \hat{c}_+ + 2\delta\hat{\psi}_-^\dagger \varphi \hat{c}_+ \delta\hat{\psi}_+ + \delta\hat{\psi}_-^\dagger \delta\hat{\psi}_+ \delta\hat{\psi}_+\Big) \\ &+ U\Big(|\varphi|^2 \hat{c}_+^\dagger \hat{c}_+ \delta\hat{\psi}_- + \varphi^* \hat{c}_+^\dagger \delta\hat{\psi}_+ \delta\hat{\psi}_- + \delta\hat{\psi}_+^\dagger \varphi \hat{c}_+ \delta\hat{\psi}_- + \delta\hat{\psi}_+^\dagger \delta\hat{\psi}_+ \delta\hat{\psi}_-\Big) \end{aligned} \tag{E.28}$$

which gives

$$\begin{aligned} i\sqrt{N}\dot{\Lambda}_+ &= \left[\hat{c}_+^\dagger, \hat{\mathcal{H}}\right]\delta\hat{\psi}_+ + \hat{c}_+^\dagger \left[\delta\hat{\psi}_+, \hat{\mathcal{H}}\right] \\ &= D_{0+} + D_{1+} + D_{2+} + \mathcal{O}(\delta\hat{\psi}^2) \end{aligned} \tag{E.29}$$

and

$$\begin{aligned} i\sqrt{N}\dot{\Lambda}_- &= \left[\hat{c}_+^\dagger, \hat{\mathcal{H}}\right]\delta\hat{\psi}_- + \hat{c}_+^\dagger \left[\delta\hat{\psi}_-, \hat{\mathcal{H}}\right] \\ &= D_{1-} + D_{2-} + \mathcal{O}(\delta\hat{\psi}^2) \end{aligned} \tag{E.30}$$

where

$$\begin{aligned}
D_{0+}(\mathbf{r}) &= \hat{c}_+^\dagger \left(H_0 + \frac{U+U_{ab}}{2}\left(|\varphi|^2 \hat{c}_+^\dagger \hat{c}_+\right) + \frac{\Omega}{2}\right) \varphi \hat{c}_+ \delta\hat{\psi}_+ \\
D_{1\pm}(\mathbf{r}) &= -\int \mathrm{d}\mathbf{r}' \left(\varphi^*(\mathbf{r}')\hat{c}_+^\dagger \left(H_0 + \frac{\Omega}{2} + \frac{U+U_{ab}}{2}|\varphi(\mathbf{r}')|^2 \hat{c}_+^\dagger \hat{c}_+ \right) \varphi(\mathbf{r}') \right) \delta\hat{\psi}_\pm(\mathbf{r}) \\
D_{2+}(\mathbf{r}) &= \left(H_0 + (U+U_{ab})|\varphi|^2 \left(\hat{c}_+^\dagger \hat{c}_+ - 1 \right) + \frac{\Omega}{2} \right) \hat{c}_+^\dagger \delta\hat{\psi}_+(\mathbf{r}) \\
&\quad + \left(\frac{U+U_{ab}}{2}(\varphi)^2 \hat{c}_+^\dagger \hat{c}_+ \right) \hat{c}_+ \delta\hat{\psi}_-^\dagger(\mathbf{r}) \\
D_{2-}(\mathbf{r}) &= \left(H_0 + U|\varphi|^2 \left(\hat{c}_+^\dagger \hat{c}_+ - 1 \right) - \frac{\Omega}{2} \right) \hat{c}_+^\dagger \delta\hat{\psi}_-(\mathbf{r}) \\
&\quad + \left(\frac{U-U_{ab}}{2}(\varphi)^2 \hat{c}_+^\dagger \hat{c}_+ \right) \hat{c}_+ \delta\hat{\psi}_-^\dagger(\mathbf{r})
\end{aligned} \tag{E.31}$$

If we make the identification $\psi = \varphi\hat{c}_+$, we can use the GPE to transform the the D_{0+}-term into $N\mu\varphi\delta\hat{\psi}_+(\mathbf{r})$ and the $D_{1\pm}$-term into $-\mu\hat{c}_+^\dagger\delta\hat{\psi}_\pm(\mathbf{r})$. The D_{0+}-term is just the $\mathfrak{H}_0$-term from the time independent theory, so ignoring that, and approximating $N \approx N-1$ we get the equation of motion

$$i\dot{\Lambda}_\pm = A_\pm\hat{\Lambda}_\pm + B_\pm\hat{\Lambda}_\pm \tag{E.32}$$

where

$$\begin{aligned}
A_+ &\equiv H_0 - \mu + (U+U_{ab})|\psi|^2 + \frac{\Omega}{2} \\
B_+ &\equiv \frac{(U+U_{ab})}{2}(\psi)^2 \\
A_- &\equiv H_0 - \mu + U|\psi|^2 - \frac{\Omega}{2} \\
B_- &\equiv \frac{(U-U_{ab})}{2}(\psi)^2
\end{aligned} \tag{E.33}$$

just like we got from the time-independent calculation in (6.16).

Appendix F

The symmetry-breaking approach

In this appendix we will calculate the expression (6.60) which is postulated in the main text.

The symmetry breaking approach consists of using the rewritings

$$\begin{aligned} \hat{\Psi}_+(\mathbf{r}) &\approx \psi(\mathbf{r}) + \delta\hat{\psi}_+(\mathbf{r}) \\ \hat{\Psi}_-(\mathbf{r}) &\approx \delta\hat{\psi}_-(\mathbf{r}) \end{aligned} \tag{F.1}$$

instead of the more correct (6.2). In this approach we do not need to introduce the operators $\hat{\Lambda}$, since the definition would become $\hat{\Lambda} \equiv \delta\hat{\psi}$, and nor does we have to introduce the $\mathcal{Q}\circ$-operators as there no longer is a demand for the φ_{i+}-functions to be orthogonal to ψ. When calculating the various operators, we can follow the same method as for the non-symmetry breaking approach and we get for most of the operators the same result as previously, except for the lack of $\mathcal{Q}\circ$-operators and the fact that all sums start form 0. The u and v functions will be found to be the solutions to the simpler version of (6.38)

$$\mathcal{L}(\mathbf{r})\bar{w}_i(\mathbf{r}) = \varepsilon_i\bar{w}_i(\mathbf{r}) \tag{F.2}$$

where

$$\bar{w}_i(\mathbf{r}) \equiv \begin{pmatrix} u_i(\mathbf{r}) \\ v_i^*(\mathbf{r}) \end{pmatrix} \tag{F.3}$$

and

$$\mathcal{L}(\mathbf{r}) \equiv \begin{bmatrix} A(\mathbf{r}) & B(\mathbf{r}) \\ -B^*(\mathbf{r}) & -A(\mathbf{r}) \end{bmatrix} \tag{F.4}$$

since $\mathcal{Q}(\mathbf{r},\mathbf{r}')$ gets replaced with $\delta(\mathbf{r},\mathbf{r}')$ in the symmetry-breaking approach. Insertion gives

$$\begin{aligned} A(\mathbf{r})u_i(\mathbf{r}) + B(\mathbf{r})v_i^*(\mathbf{r}) &= \epsilon_i u_i(\mathbf{r}) \\ B^*(\mathbf{r})u_i(\mathbf{r}) + A(\mathbf{r})v_i^*(\mathbf{r}) &= -\epsilon_i v_i^*(\mathbf{r}) \end{aligned} \tag{F.5}$$

We see that if we switch u and $-v$ we would have another eigenvector[1] with eigenvalue $-\varepsilon$. This means that if $\varepsilon = 0$ a possible solution is $u = -v$. For the plus-mode such a solution actually exists and by inserting the values of A_+ and B_+ from (6.16), we get

$$\left(H_0 - \mu + (U + U_{ab})|\psi|^2 + \frac{\Omega}{2}\right) u_0(\mathbf{r}) - \frac{(U + U_{ab})}{2}(\psi)^2 u_0^*(\mathbf{r}) = 0 \tag{F.6}$$

and from the GPE (5.12) we see that a solution to this is $u_0(\mathbf{r}) = -v_0(\mathbf{r}) = \psi(\mathbf{r})$. Let us denote the eigenvector describing this solution $\bar{w}_0$. Something is, however, wrong with this result. We know that all $\bar{w}$-functions should fulfill (6.31)

$$\delta_{ij} = \int \mathrm{d}\mathbf{r}\Big(u_i^*(\mathbf{r})u_j(\mathbf{r}) - v_i(\mathbf{r})v_j^*(\mathbf{r})\Big) \tag{F.7}$$

and (6.32)

$$0 = \int \mathrm{d}\mathbf{r}\Big(v_i(\mathbf{r})u_j^*(\mathbf{r}) - u_i^*(\mathbf{r})v_j(\mathbf{r})\Big) \tag{F.8}$$

but inserting $\bar{w}_0$ in (F.7) gives $u_0^* \circ u_0 - v_0 \circ v_0^* = u_0 \circ u_0 - u_0 \circ u_0 = 0$, but if we could find another eigenvector with the same eigenvalue, then a superposition of the two might do the trick. From (F.5) we see that any eigenvector $\bar{w}$ with $u = v$ will give the eigenvalue zero, and the same questionable result for insertion into (F.7) as the previous solution. Let us name this $u = \zeta$ and then define the superposition, which we will denote $\bar{w}_+$ as

$$\bar{w}_+(\mathbf{r}) \equiv \frac{1}{\sqrt{2}} \begin{pmatrix} \psi(\mathbf{r}) + \zeta(\mathbf{r}) \\ -\psi^*(\mathbf{r}) + \zeta^*(\mathbf{r}) \end{pmatrix} \tag{F.9}$$

Requiring that $\bar{w}_+$ obeys (F.7) is equivalent to requiring that

$$\int \mathrm{d}\mathbf{r}\Big(\zeta(\mathbf{r})\psi^*(\mathbf{r}) + \psi(\mathbf{r})\zeta^*(\mathbf{r})\Big) = 1 \tag{F.10}$$

So now we can identify a possible value of ζ to $\zeta(\mathbf{r}) = \frac{d\psi(\mathbf{r})}{dN}$, since

$$\int \mathrm{d}\mathbf{r}\left(\frac{d\psi(\mathbf{r})}{dN}\psi^*(\mathbf{r}) + \psi(\mathbf{r})\frac{d\psi^*(\mathbf{r})}{dN}\right) = \frac{d}{dN}\int \mathrm{d}\mathbf{r}\psi(\mathbf{r})\psi^*(\mathbf{r}) = \frac{dN}{dN} = 1 \tag{F.11}$$

This implies that

$$\bar{w}_+(\mathbf{r}) = \frac{1}{\sqrt{2}} \begin{pmatrix} \psi(\mathbf{r}) + \frac{d\psi(\mathbf{r})}{dN} \\ -\psi^*(\mathbf{r}) + \frac{d\psi^*(\mathbf{r})}{dN} \end{pmatrix} \tag{F.12}$$

[1] We could argue that such an eigenvector can not fulfil (F.7) $u'^* \circ u' - v' \circ v'^* = 1$ which we require, but it could if we allow for complex eigenvectors and instead define $u' = iv$ and $v' = iu$, where such a phase shift always is allowed in an eigenvalue equation. This is related to the discussion of positive and negative eigenvalues in section 5.7.

We must also test (F.7) between $\bar{w}_+$ and $\bar{w}_{i\neq 0+}$, and in order to do this it is convenient to regard the expression

$$\int \mathrm{d}\mathbf{r}\left(\bar{w}_i^\dagger \mathcal{M}\bar{w}_j - \left(\bar{w}_j^\dagger \mathcal{M}\bar{w}_i\right)^*\right) \;=\; 0 \tag{F.13}$$

which can be seen to be true from the fact that $\mathcal{M}$ is Hermitian. If $\bar{w}_i$ and $\bar{w}_j$ both are eigenvectors to $\mathcal{L} \equiv \sigma_z\mathcal{M}$, we can rewrite (F.13) to

$$(\varepsilon_j - \varepsilon_i^*)\int \mathrm{d}\mathbf{r}\left(u_i^*(\mathbf{r})u_j(\mathbf{r}) - v_i(\mathbf{r})v_j^*(\mathbf{r})\right) = 0 \tag{F.14}$$

which is equivalent to (F.7) (assuming the eigenvalues to be non-degenerate). This implies that $\bar{w}_0$ obeys (F.7) with another state, even though it does not obey it with itself.

We want to insert $\bar{w}_j = \bar{w}_+$, but in order to do that, we must first calculate $\mathcal{M}\bar{w}_+$, by inserting the concrete expressions for $\mathcal{M}$ and $\bar{w}_+$:

$$\mathcal{M}\bar{w}_+ = \frac{1}{\sqrt{2}}\begin{pmatrix} \hat{A}\psi - B\psi^* + \hat{A}\frac{d\psi}{dN} + B\frac{d\psi^*}{dN} \\ -\hat{A}\psi^* + B^*\psi + \hat{A}\frac{d\psi^*}{dN} + B^*\frac{d\psi}{dN} \end{pmatrix} \tag{F.15}$$

Because of (5.12) the two first terms in each component are seen to be 0, and in order to handle the last two terms we regard the derivative of the GPE (5.12):

$$\begin{aligned} & \frac{d}{dN}\left(H_0\psi + \frac{U+U_{ab}}{2}\psi^*\psi\psi + \frac{\Omega}{2}\psi\right) = \frac{d}{dN}\left(\mu\psi\right) \\ \Leftrightarrow\;\; & H_0\frac{d\psi}{dN} + \left(U+U_{ab}\right)|\psi|^2\frac{d\psi}{dN} + \frac{U+U_{ab}}{2}(\psi)^2\frac{d\psi^*}{dN} + \frac{\Omega}{2}\frac{d\psi}{dN} = \mu\frac{d\psi}{dN} + \frac{d\mu}{dN}\psi \\ \Leftrightarrow\;\; & \hat{A}\frac{d\psi}{dN} + B\frac{d\psi^*}{dN} = \frac{d\mu}{dN}\psi \end{aligned} \tag{F.16}$$

which implies

$$\mathcal{M}\bar{w}_+ = \frac{1}{\sqrt{2}}\begin{pmatrix} \frac{d\mu}{dN}\psi(\mathbf{r}) \\ \frac{d\mu}{dN}\psi^*(\mathbf{r}) \end{pmatrix} = \frac{1}{\sqrt{2}}\frac{d\mu}{dN}\sigma_z\bar{w}_0 \tag{F.17}$$

We thereby see that $\bar{w}_+$ is not an eigenvector to $\mathcal{M}$, and not to $\mathcal{L} = \sigma_z\mathcal{M}$ either, shoving that the ζ-eigenvector is not an eigenvector at all. But (F.13) holds anyway, so we can insert $\bar{w}_j = \bar{w}_+$ in (F.13) and get

$$\begin{aligned} 0 \;&=\; \int \mathrm{d}\mathbf{r}\left(\bar{w}_i^\dagger\mathcal{M}\bar{w}_+ - \left(\bar{w}_+^\dagger\mathcal{M}\bar{w}_i\right)^*\right) \\ &=\; \int \mathrm{d}\mathbf{r}\left(\bar{w}_i^\dagger\frac{1}{\sqrt{2}}\frac{d\mu}{dN}\sigma_z\bar{w}_0 - \left(\bar{w}_+^\dagger\varepsilon_i\sigma_z\bar{w}_i\right)^*\right) \\ &=\; \frac{1}{\sqrt{2}}\frac{d\mu}{dN}\int \mathrm{d}\mathbf{r}\left(u_i^*u_0 - v_iv_0^*\right) - \varepsilon_i\int \mathrm{d}\mathbf{r}\left(u_+^*u_i - v_+v_i^*\right) \Rightarrow \\ 0 \;&=\; \int \mathrm{d}\mathbf{r}\left(u_+^*u_i - v_+v_i^*\right) \end{aligned} \tag{F.18}$$

where the facts that $\bar{w}_0$ fulfils (F.7), and that $\varepsilon_i \neq 0$ have been used. This means that $\bar{w}_+$ fulfils (F.7) with another state, in addition to doing it alone. All states fulfil (F.8) with themselves, and in order to investigate (F.8) for $\bar{w}_+$ and a $\bar{w}_{i\neq 0+}$, we will regard the quantity

$$\int \mathrm{d}\mathbf{r} \left(\bar{y}_+^\dagger \mathcal{M} \bar{w}_i - \left(\bar{w}_i^\dagger \mathcal{M} \bar{y}_+ \right)^* \right) \;=\; 0 \tag{F.19}$$

where

$$\bar{y}_i \;\equiv\; \begin{pmatrix} v_i \\ u_i^* \end{pmatrix} \tag{F.20}$$

which implies

$$\bar{y}_+ \;\equiv\; \frac{1}{\sqrt{2}} \begin{pmatrix} -\psi(\mathbf{r}) + \frac{d\psi(\mathbf{r})}{dN} \\ \psi^*(\mathbf{r}) + \frac{d\psi^*(\mathbf{r})}{dN} \end{pmatrix} \tag{F.21}$$

On the exact same way as for $\bar{w}_+$ we can calculate that $\mathcal{M}\bar{y}_+ = \frac{1}{\sqrt{2}} \frac{d\mu}{dN} \sigma_z \bar{w}_0$, where (5.12) and (F.16) have been inserted. Inserting this into (F.19) gives

$$\begin{aligned} 0 \;&=\; \int \mathrm{d}\mathbf{r} \left(\bar{y}_+^\dagger \mathcal{M} \bar{w}_i - \left(\bar{w}_i^\dagger \mathcal{M} \bar{y}_+ \right)^* \right) \\ &=\; \int \mathrm{d}\mathbf{r} \left(\bar{y}_+^\dagger \varepsilon_i \sigma_z \bar{w}_i - \left(\bar{w}_i^\dagger \frac{1}{\sqrt{2}} \frac{d\mu}{dN} \sigma_z \bar{w}_0 \right)^* \right) \\ &=\; \varepsilon_i \int \mathrm{d}\mathbf{r} \left(v_+^* u_i - u_+ v_i^* \right) - \frac{1}{\sqrt{2}} \frac{d\mu}{dN} \int \mathrm{d}\mathbf{r} \left(u_i^* u_0 - v_i v_0^* \right) \Rightarrow \\ 0 \;&=\; \int \mathrm{d}\mathbf{r} \left(v_+ u_i^* - u_+^* v_i \right) \end{aligned} \tag{F.22}$$

where the fact that $\bar{w}_0$ and $\bar{w}_i$ fulfil (F.7) together, have be used. This shows that $\bar{w}_+$ and $\bar{w}_{i\neq 0}$ together fulfil (F.8).

Summarizing: $\bar{w}_+$ fulfils all that is expected of a $\bar{w}$-state, except being an eigenstate to $\mathcal{L}$. This means that different states fulfil (F.7), (F.8) and (F.2). But (F.7) and (F.8) were derived from the commutation relations which are fundamental, so therefore we have to discard (F.2).

Let us try to calculate $\int \mathrm{d}\mathbf{r} \bar{\Lambda}_+^\dagger \mathcal{M} \bar{\Lambda}_+$, where

$$\bar{\Lambda}_+ \equiv \begin{pmatrix} \delta\hat{\psi}_+ \\ \delta\hat{\psi}_+^\dagger \end{pmatrix} \tag{F.23}$$

with a $\delta\hat{\psi}_+$ that includes the $\bar{w}_+$-state so that

$$\delta\hat{\psi}_+ = u_+ \hat{\alpha}_0 + v_+ \hat{\alpha}_0^\dagger + \sum_{i>0} \left(u_{i+} \hat{\alpha}_{i+} + v_{i+} \hat{\alpha}_{i+}^\dagger \right) \tag{F.24}$$

This gives

$$\begin{aligned}
\int \mathrm{d}\mathbf{r}\bar{\Lambda}_+^\dagger \mathcal{M}_+ \bar{\Lambda}_+ &= \int \mathrm{d}\mathbf{r}\left(\delta\hat{\psi}_+^\dagger A_+ \delta\hat{\psi}_+ + \delta\hat{\psi}_+^\dagger B_+ \delta\hat{\psi}_+^\dagger + \delta\hat{\psi}_+ B_+^* \delta\hat{\psi}_+ + \delta\hat{\psi}_+ A_+ \delta\hat{\psi}^\dagger\right) \\
&= \sum_{ij}\left(\left(\int \mathrm{d}\mathbf{r}\,\bar{y}_i \mathcal{M}_+ \bar{w}_j\right)\hat{\alpha}_i\hat{\alpha}_j + \left(\int \mathrm{d}\mathbf{r}\,\bar{w}_i^\dagger \mathcal{M}_+ \bar{w}_j\right)\hat{\alpha}_i^\dagger\hat{\alpha}_j + \text{h.c.}\right) \\
&= \frac{1}{\sqrt{2}}\frac{d\mu}{dN}\left(\left(\int \mathrm{d}\mathbf{r}\,\bar{y}_+\sigma_z\bar{w}_0\right)\hat{\alpha}_0\hat{\alpha}_0 + \left(\int \mathrm{d}\mathbf{r}\,\bar{w}_+^\dagger\sigma_z\bar{w}_0\right)\hat{\alpha}_0^\dagger\hat{\alpha}_0 + \text{h.c.}\right) \\
&\quad + \sum_{j\neq 0}\varepsilon_j\left(\left(\int \mathrm{d}\mathbf{r}\,\bar{y}_+\sigma_z\bar{w}_j\right)\hat{\alpha}_0\hat{\alpha}_j + \left(\int \mathrm{d}\mathbf{r}\,\bar{w}_+^\dagger\sigma_z\bar{w}_j\right)\hat{\alpha}_0^\dagger\hat{\alpha}_j + \text{h.c.}\right) \\
&\quad + \frac{1}{\sqrt{2}}\frac{d\mu}{dN}\sum_{i\neq 0}\left(\left(\int \mathrm{d}\mathbf{r}\,\bar{y}_i\sigma_z\bar{w}_0\right)\hat{\alpha}_i\hat{\alpha}_0 + \left(\int \mathrm{d}\mathbf{r}\,\bar{w}_i^\dagger\sigma_z\bar{w}_0\right)\hat{\alpha}_i^\dagger\hat{\alpha}_0 + \text{h.c.}\right) \\
&\quad + \sum_{i,j\neq 0}\varepsilon_j\left(\left(\int \mathrm{d}\mathbf{r}\,\bar{y}_i\sigma_z\bar{w}_j\right)\hat{\alpha}_i\hat{\alpha}_j + \left(\int \mathrm{d}\mathbf{r}\,\bar{w}_i^\dagger\sigma_z\bar{w}_j\right)\hat{\alpha}_i^\dagger\hat{\alpha}_j + \text{h.c.}\right) \\
&= \frac{1}{\sqrt{2}}\frac{d\mu}{dN}\frac{1}{\sqrt{2}}\left(\hat{\alpha}_0\hat{\alpha}_0 + \hat{\alpha}_0\hat{\alpha}_0^\dagger + \hat{\alpha}_0^\dagger\hat{\alpha}_0 + \hat{\alpha}_0^\dagger\hat{\alpha}_0^\dagger\right) + \sum_{i,j\neq 0}\varepsilon_j\delta_{ij}\left(\hat{\alpha}_i\hat{\alpha}_j^\dagger + \hat{\alpha}_i^\dagger\hat{\alpha}_j\right) \\
&= \frac{d\mu}{dN}\hat{Q}^2 + \sum_{i\neq 0}\varepsilon_i\left(\hat{\alpha}_i\hat{\alpha}_i^\dagger + \hat{\alpha}_i^\dagger\hat{\alpha}_i\right) \qquad \text{(F.25)}
\end{aligned}$$

As part of the calculation (F.7) and (F.8) have been inserted where they hold (that is between $\bar{w}_i$ and $\bar{w}_j$, between $\bar{w}_i$ and $\bar{w}_+$, and between $\bar{w}_i$ and $\bar{w}_0$) and

$$\begin{aligned}
\hat{Q} &\equiv \frac{1}{\sqrt{2}}(\hat{\alpha}_0 + \hat{\alpha}_0^\dagger) \\
\hat{P} &\equiv \frac{1}{i\sqrt{2}}(\hat{\alpha}_0 - \hat{\alpha}_0^\dagger) \qquad \text{(F.26)}
\end{aligned}$$

have been defined. If we insert (F.25) in (6.13), and use the commutation relation for the $\hat{\alpha}_i$s the result is

$$\hat{\mathcal{H}} = \hat{\mathcal{H}}_0 + \frac{1}{2}\frac{d\mu}{dN}\hat{Q}^2 + \sum_{i>0}\varepsilon_{i+}\left(\hat{\alpha}_{i+}^\dagger\hat{\alpha}_{i+}\right) + \sum_i \varepsilon_{i-}\left(\hat{\alpha}_{i-}^\dagger\hat{\alpha}_{i-}\right) \qquad \text{(F.27)}$$

which is identical to (6.60), the result which we had set out to derive.

Appendix G

The source code

This appendix shows the source code to the program that have been used to produce the data plotted in figs. 7.11 and 7.12. Most of the data shown in the "results"-section and in the "further results"-appendix could have been made using this program by varying the initial parameters.

```
  % prog10:   % This means that this program is the tenth version.

N = 1000;     % The particle number.

  % First we calculate the F-function for the two-mode approximation.
Gchi = 1;
Gstor = 50;

for(j = 1:Gstor)
    Gomegaer(j) = 1*10^(-5) * 10^(j/5);
end               % Only positive values of (-Omega) are needed
                  % to produce the F-functions.
list = 1:(N+1);
lizt = 1:N;

GMx = sparse(list,list,(N/2-list+1));              % See (B.10)
GMz = sparse([lizt,(lizt+1)], [(lizt+1),lizt],     % and (B.12).
    0.5*sqrt([lizt,lizt].*(N+1-[lizt,lizt])));
GMz2 = GMz*GMz;
Genhedsmat = sparse(list,list,1);

for(j = 1:Gstor)

    GOmega = - Gomegaer(j);
```

```
    GOper = Gchi*GMz2 + GOmega*GMx + N*abs(GOmega)*Genhedsmat;
          % The operator defined by (3.33).

    [Gt, Gw] = eigs(GOper,1,'sm');   % Diagonalizaton.
    Gen(j) = Gw;

    GJx(j) = Gt'*GMx*Gt;
    GJz2(j) = Gt'*GMz2*Gt;
    Gxi2(j) = (GJz2(j) - GJz(j)^2)*N/(GJx(j)*GJx(j));
          % The results for the two-mode case.
end
    % At this point the calculation of the F-function is finished.


    % Here we begin the central calculation.

antr = 200;
maxr = 10;           % Variables related the precision on the r-axis.
dr = maxr/antr;

antt = 30000;
maxt = 3;            % Variables related the precision on the t-axis.
dt = maxt/antt;

antl = 30;           % Number of l-modes incuded.

Ter = 0.049;         % The temprature(s).

stort = size(Ter);
stort = stort(2);    % This gives 1, since there only is one T.

ser = [0.01, 0.1, 0.3, 0.6, 1, 3];     % The sums s.

stors = size(ser);
stors = stors(2);    % The number of s-values.

fer = [0, 0.1, 0.3, 0.5, 0.7, 0.9];    % The fractions f.

storf = size(fer);
storf = storf(2);    % The number of f-values.

omegaer = [-0.00010, -0.00008, -0.00006, -0.00004, -0.00002, 0, 0.00001,
  0.00002, 0.00003, 0.00006, 0.0001, 0.00015, 0.00025, 0.0004, 0.0006,
```

```
  0.001, 0.0015, 0.0025, 0.004, 0.006, 0.008, 0.01, 0.02, 0.03, 0.06,
  0.08, 0.1, 0.2, 0.3, 1, 10];     % The values of (- Omega).

stor = size(omegaer);
stor = stor(2);

rud=(1:antr)';
r = dr*rud;                % The r-axis.
rud = rud - 1;
rmat = repmat(r,1,antr);

G = 4*pi*dr*( (r*r') .* eye(antr) );
  % Integration matrix corresponding to the o-operator.

  % Some of the output will be stored in these variables (see later).
eudp = zeros(stor,antr,antl,stors,storf,stort);
budp = zeros(stor,antr,antl,stors,storf,stort);
%uudp = zeros(stor,antr,antr,antl,stors,storf,stort);
%vudp = zeros(stor,antr,antr,antl,stors,storf,stort);
nudp = zeros(stor,antr,antl,stors,storf,stort);
Nudp = zeros(stor,antr,antl,stors,storf,stort);
eudm = zeros(stor,antr,antl,stors,storf,stort);
budm = zeros(stor,antr,antl,stors,storf,stort);
%uudm = zeros(stor,antr,antr,antl,stors,storf,stort);
%vudm = zeros(stor,antr,antr,antl,stors,storf,stort);
nudm = zeros(stor,antr,antl,stors,storf,stort);
Nudm = zeros(stor,antr,antl,stors,storf,stort);

d2dr2 = -2*eye(antr);
for j = 1:(antr-1)
    d2dr2(j+1,j) = 1;
    d2dr2(j,j+1) = 1;      % The d2/dr2-matrix. See (6.69).
end
d2dr2 = d2dr2/(dr*dr);

antn = 40;  % The number of times we will allow N and Nst to update.

fprintf('\n Hello prog10\n\n');
    % This tells us that the loop-part of the program starts.

fil = fopen('output102.txt', 'w');
    % This creates a text-file to store the output.
fprintf(fil, '\n\r  Output from prog10\n\r\n\r');
```

```
for(s = 1:stors)

for(f = 1:storf)     % Loops for different s and f.

    Uer(s,f) = ser(s)/(fer(f) + 1);
    Uaber(s,f) = (ser(s)*fer(f))/(fer(f) + 1);
    U = Uer(s,f);
    Uab = Uaber(s,f);
       % The values of U and Uab corresponing to the values of s and f.

for(b = 1:stort)

    kT = Ter(b);         % The temperature.

    fprintf(fil, '\n\r\n\r kT: %f, U: %f ,  Uab: %f ,  N: %d ,  antr: %d ,
    maxr: %d ,  antl: %d ,  antt: %d ,  maxt: %d\n\r\n\r\n\r', kT, U, Uab,
    N, antr, maxr, antl, antt, maxt);
    fprintf(fil, '%s\t\t%s\t\t%s\t\t%s\t\t%s\t\t%s\t\t%s\t\t%s\n\r\n\r',
    '-Omega', 'lambda', 'Jx', 'Jz2', 'xi2', 'mu', 'Nst', 'Nat');
         %  This writes in the text-file.

for(x = 1:stor)

  Omega = -omegaer(x);    % The value of omega.

  Nst(x,s,f,b) = 0.5*N;   % A first guess of N_0 is N/2.
  Natgl = 2*N;
  Nstgl = N;

  % Nst(x,s,f,b) = N;
  % This should have been used if the zero-temperature
  % form of the program was used.

  for(y = 1:antn)         % This loop updates N and N_0.

    % Calculation of psi.

    upsi = exp(-r.*r/2).*r;
    upsi = upsi*sqrt(Nst(x,s,f,b)) / sqrt( 4*pi*dr*upsi'*upsi );
      % A first guess of psi. The gaussian result for U=0.

    for j=1:antt   % This loop is the Runge-Kutta part
```

```
                % of the complex-time algorithm.

  k1 = 0.5*d2dr2*upsi - 0.5*r.*r.*upsi - 0.5*(U + Uab)*
  ( ( (upsi.*transpose(upsi')).(r.*r) ) .* upsi);

  k2 = 0.5*d2dr2*(upsi+0.5*k1*dt) - 0.5*r.*r.*(upsi+0.5*k1*dt) -
  0.5*(U + Uab)*( ( ((upsi+0.5*k1*dt).*transpose((upsi+0.5*k1*dt)'))
  ./(r.*r) ) .* (upsi+0.5*k1*dt));

  k3 = 0.5*d2dr2*(upsi+0.5*k2*dt) - 0.5*r.*r.*(upsi+0.5*k2*dt) -
  0.5*(U + Uab)*( ( ((upsi+0.5*k2*dt).*transpose((upsi+0.5*k2*dt)'))
  ./(r.*r) ) .* (upsi+0.5*k2*dt));

  k4 = 0.5*d2dr2*(upsi+k3*dt) - 0.5*r.*r.*(upsi+k3*dt) -
  0.5*(U + Uab)*( ( ((upsi+k3*dt).*transpose((upsi+k3*dt)'))
  ./(r.*r) ) .* (upsi+k3*dt));

  upsi = upsi + (dt/6)*(k1 + 2*k2 + 2*k3 + k4);

  upsi = upsi*sqrt(Nst(x,s,f,b)) / sqrt( 4*pi*dr*upsi'*upsi );

end   % End of Runge-Kutta part.

psi = upsi ./ r;
varphi = psi/sqrt(Nst(x,s,f,b));
   % End of calculation of psi.


   Jx(x,s,f,b) = Nst(x,s,f,b)/2;
   Nat(x,s,f,b) = Nst(x,s,f,b); % The major part of the J-operators.
   Jz2(x,s,f,b) = Nst(x,s,f,b)/4;

   lhs = -0.5*d2dr2*upsi + 0.5*r.*r.*upsi + (Omega/2)*upsi +
   0.5*(U + Uab)*( ( (upsi.*transpose(upsi')).(r.*r) ) .* upsi);
   % Left hand side of the GPE.

   mu(x,s,f,b) = sum(lhs)/(sum(upsi));  % Calculation of mu.


   % Calculation of end-state.

   Qr = eye(antr)*(G^(-1)) - (varphi*varphi');  % The Q-operator.
   Qd = eye(antr)*(G^(-1));
```

```
  for L=1:antl  %One calculation for each L-state (L = l+1).

    delap = -0.5*d2dr2.*rmat'./rmat + 0.5*L*(L-1)*eye(antr)./(r*r') +
    0.5*(r*r').*eye(antr) + (U + Uab)*(psi*psi').*eye(antr) +
    (Omega/2)*eye(antr) - mu(x,s,f,b)*eye(antr);  % This is A+.

    delbp = 0.5*(U + Uab) * (psi*transpose(psi)).*eye(antr);  % B+.

    delam = -0.5*d2dr2.*rmat'./rmat + 0.5*L*(L-1)*eye(antr)./(r*r') +
    0.5*(r*r').*eye(antr) + U*(psi*psi').*eye(antr) -
    (Omega/2)*eye(antr) - mu(x,s,f,b)*eye(antr); % This is A-.

    delbm = 0.5*(U - Uab) * (psi*transpose(psi)).*eye(antr);  % B-.

    if(L == 1)
      Q = Qr;
    else          % Q-operators
      Q = Qd;
    end           % Stricly speaking the Q-operator is Q*G.

    delapq = Q*G*delap*Q*G;
    delbpq = Q*G*delbp*Q'*G;   % The L+ matrix.
    delcpq = -Q'*G*delbp'*Q*G;
    deldpq = -Q'*G*delap*Q'*G;

    delamq = delam;
    delbmq = delbm;            % The L- matrix.
    delcmq = -delbm';
    deldmq = -delam;

    Lmatp = [delapq, delbpq; delcpq, deldpq];
    Lmatm = [delamq, delbmq; delcmq, deldmq];
        % The L-matrices

    % A little jump...

[tilstandep, energierp] = eig(Lmatp); % Diagonalizes the matrix.
[tilstandem, energierm] = eig(Lmatm);

energierp = real(diag(energierp));             % Finds u, v and e.
uernep = real(tilstandep(1:antr, 1:2*antr));
vernep = real(tilstandep((antr+1):2*antr, 1:2*antr));
```

```
  energierm = real(diag(energierm));
  uernem = real(tilstandem(1:antr, 1:2*antr));
  vernem = real(tilstandem((antr+1):2*antr, 1:2*antr));

  [yp, indexp] = sort(energierp);    % Sorts the energies
  indp = indexp((antr+1):2*antr);    % and pics the positive ones.
  [ym, indexm] = sort(energierm);
  indm = indexm((antr+1):2*antr);

  energip = energierp(indp);
  up = uernep(:,indp);
  vp = vernep(:,indp);            % The sorted energies, us and vs.
  energim = energierm(indm);
  um = uernem(:,indm);
  vm = vernem(:,indm);

normp = diag( up'*G*Q*G*up - vp'*G*Q*G*vp ); % Normalization of u and v
normm = diag( um'*G*um - vm'*G*vm );         % using int dr (uu-vv) = 1.

  for om=1:antr
      if normp(om) < 0
          buf = up(:,om);
          up(:,om) = vp(:,om);
          vp(:,om) = buf;
          normp(om) = -normp(om);
      end
      if normm(om) < 0                % More normalization.
          buf = um(:,om);
          um(:,om) = vm(:,om);
          vm(:,om) = buf;
          normm(om) = -normm(om);
      end
  end

  up = up./sqrt(repmat(normp',antr,1));
  vp = vp./sqrt(repmat(normp',antr,1));
  um = um./sqrt(repmat(normm',antr,1));  % Even more normalization.
  vm = vm./sqrt(repmat(normm',antr,1));

  tegnp = sign(up(1,:));
  tegnp = repmat(tegnp,antr,1);
  tegnm = sign(um(1,:));
  tegnm = repmat(tegnm,antr,1);
```

```
  up = up.*tegnp;
  vp = vp.*tegnp;
  um = um.*tegnm;    % u starts as positive, and v as negative.
  vm = vm.*tegnm;

  eudp(x,:,L,s,f,b) = energip; % Stores the variables for output.
  eudm(x,:,L,s,f,b) = energim;

% uudp(x,:,:,L,s,f,b) = up;
% uudm(x,:,:,L,s,f,b) = um;

% vudp(x,:,:,L,s,f,b) = vp;
% vudm(x,:,:,L,s,f,b) = vm;

  nudp(x,:,L,s,f,b) = diag(vp'*G*Q*G*vp);
  nudm(x,:,L,s,f,b) = diag(vm'*G*vm);    % The contribution to N.

  Nudp(x,:,L,s,f,b) = nudp(x,:,L,s,f,b)*(2*L-1);
  Nudm(x,:,L,s,f,b) = nudm(x,:,L,s,f,b)*(2*L-1);
       % All m-states taken into account.

  nbidp = 1./(exp(energip/kT)-1);  % The expectation values <aa>
  nbidm = 1./(exp(energim/kT)-1);  % using Bose-Einstein distribution.

  budp(x,:,L,s,f,b) = nbidp;
  budm(x,:,L,s,f,b) = nbidm;

  if(L == 1)
    for j = 1:antr
      up(j,1) = 0;    % The first-order part of Jz2.
      vp(j,1) = 0;
      Jz2(x,s,f,b) = Jz2(x,s,f,b) + (Nst(x,s,f,b)/4)*(nbidm(j)+1)*
        ( (varphi'*G*um(:,j))*(varphi'*G*vm(:,j)) + 2*(vm(:,j)'*G*varphi)*
        (varphi'*G*vm(:,j)) + (vm(:,j)'*G*varphi)*(um(:,j)'*G*varphi) );

      Jz2(x,s,f,b) = Jz2(x,s,f,b) + (Nst(x,s,f,b)/4)*nbidm(j)*
       ( (varphi'*G*vm(:,j))*(varphi'*G*um(:,j)) + 2*(um(:,j)'*G*varphi)*
       (varphi'*G*um(:,j)) + (um(:,j)'*G*varphi)*(vm(:,j)'*G*varphi) );
    end
  end

  for j = 1:antr %Calculation of the expectation values of the operators.
```

```
  Jx(x,s,f,b) = Jx(x,s,f,b) + 0.5*(2*L-1)*( vp(:,j)'*G*Q*G*vp(:,j)*
    (nbidp(j) + 1) + up(:,j)'*G*Q*G*up(:,j)*nbidp(j)
    - vm(:,j)'*G*vm(:,j)*(nbidm(j) + 1) - um(:,j)'*G*um(:,j)*nbidm(j) );

  Nat(x,s,f,b) = Nat(x,s,f,b) + (2*L-1)*( vp(:,j)'*G*Q*G*vp(:,j)*
    (nbidp(j) + 1) + up(:,j)'*G*Q*G*up(:,j)*nbidp(j) +
    vm(:,j)'*G*vm(:,j)*(nbidm(j) + 1) + um(:,j)'*G*um(:,j)*nbidm(j) );

  Jz2(x,s,f,b) = Jz2(x,s,f,b) + 0.25*(2*L-1)*( vp(:,j)'*G*Q*G*vp(:,j)*
    (nbidp(j) + 1) + up(:,j)'*G*Q*G*up(:,j)*nbidp(j) + vm(:,j)'*G*vm(:,j)*
    (nbidm(j) + 1) + um(:,j)'*G*um(:,j)*nbidm(j) );
end

end   % End of L-loop.

fprintf('Here: %d %d %d %d %f %f\n', s, f, b, x, y,
Nat(x,s,f,b), Nst(x,s,f,b));
  % prints 'you are here'.

if(Jx(x,s,f,b) > (0.5*N - 2) && Jx(x,s,f,b) < (0.5*N + 1))
  npre = 0.05;
else
  npre = 0.5; % The value of the precetion of the determination of N.
end

if( Nat(x,s,f,b) < (N+npre) && Nat(x,s,f,b) > (N-npre) )
  break;    % Update algorithm for Nst.
else
  nstbuf = Nst(x,s,f,b);
  if( Nat(x,s,f,b) > N || Nat(x,s,f,b) < 0 )
      if( Natgl > N || Natgl < 0 )
          Nst(x,s,f,b) = Nst(x,s,f,b) - 0.5*(Nstgl - Nst(x,s,f,b));
      else
          Nst(x,s,f,b) = 0.5*(Nst(x,s,f,b) + Nstgl);
      end
  else
      if( Natgl > N || Natgl < 0)
          Nst(x,s,f,b) = 0.5*(Nst(x,s,f,b) + Nstgl);
      else
          Nst(x,s,f,b) = Nst(x,s,f,b) + 0.5*(Nst(x,s,f,b) - Nstgl);
      end
  end
  Nstgl = nstbuf;
```

```
      Natgl = Nat(x,s,f,b);
    end
    %  end of update algorithm.

    % For zero temperature this loop is faster,
    % for non-zero T it does not converge:
  %  if( Nat(x,s,f) < (N+npre) & Nat(x,s,f) > (N-npre) )
  %    break;
  %  else
  %    Nst(x,s,f) = N*Nst(x,s,f)/Nat(x,s,f);
  %  end

    if( y == antn )
     fprintf('\n  Beware!!\n\n');
                % Error statement, if the Nst update loop has
                % not converged after antn rounds.
    end
    end     % End of N-loop

    xi2(x,s,f,b) = Jz2(x,s,f,b)*Nat(x,s,f,b)/(Jx(x,s,f,b)*Jx(x,s,f,b));
      % Calculation of squeezing.

    fprintf(fil, '%f\t%f\t%f\t%f\t%f\t%f\t%f\n\r\n\r', omegaer(x),
    Jx(x,s,f,b), Jz2(x,s,f,b), xi2(x,s,f,b), mu(x,s,f,b),
    Nst(x,s,f,b), Nat(x,s,f,b));
       % Prints to the text-file.

end    % End of omega-loop.
end    % End of T-loop.
end    % End of f-loop.
end    % End of s-loop.

fclose(fil);   % Closes the text-file.

clear GMx;
clear GMz;     % Removes the large variables
clear GMz2;    % that are not used as output.
clear GOper;
clear Genhedsmat;
clear Lmatm;
clear Lmatp;
clear Nudm;
clear Nudp;
```

```
clear delam;
clear delamq;
clear delap;
clear delapq;
clear delbm;
clear delbmq;
clear delbp;
clear delbpq;
clear delcmq;
clear delcpq;
clear deldmp;
clear deldpq;
clear list;
clear lizt;
clear eudm;
clear eudp;
clear nudm;
clear nudp;
clear tegnm;
clear tegnp;
clear tilstandem;
clear tilstandep;
clear uernem;
clear uernep;
clear um;
clear up;
clear vernem;
clear vernep;
clear vm;
clear vp;
clear ym;
clear yp;
clear Gt;
clear budm;
clear budp;

save data10.mat -v7.3   % Saves the results as a
                        % matlab data file.
% End of program
```

Appendix H

Numerical precision

When doing the numerical simulations in this thesis, some precision parameters had to be chosen. These parameters are denoted **antt**, **maxt**, **antr**, **maxr**, **antl**, and **npre**. The values used for most of the simulations in this thesis are

antt	30000
maxt	3
antr	200
maxr	10
antl	30
npre	0.5

antt and **maxt** are used in the imaginary time algorithm described in the vicinity of (4.29). In that algorithm we need to solve the time-dependent GPE, with the time t replaced with an imaginary time $\tau \equiv it$. This is done numerically, and the solution is produced using a fourth order Runge-Kutta algorithm. In this algorithm the τ-axis needs to be discretized. **antt** is the number of steps in the discretization, and the τ for which the algorithm stops is denoted **maxt**. This means that each of the equidistant steps have the length **dt** = **maxt**/**antt**. In fig. H.1a we see a zoom on one point in a plot of ψ, where each curve corresponds to a certain value of **antt**. We see that the function is close to converging for **antt** = 30000. For **antt** $\lesssim$ 800 the curve does not converge at all, but becomes singular in either $r = 0$ or $r =$ **maxr**. The time it takes for the program to execute scales linearly with **antt**. We can calculate the contribution to the total particle number from the 0_--mode for different values of **antt**. The result is that **antt** = 30000 gives a relative error of 0.00402.

In fig. H.1b $\psi(r)$ is plotted for different values of **maxt**. We see that the result has converged for **maxt** = 3 which is why that value was chosen.

antr and **maxr** are used when solving the GPE. The definitions are similar to the τ-case, **antr** is the number of steps in the discretization of the r-axis, and **maxr** is the maximal r used, which makes the step size **dr** = **maxr**/**antr**. In fig. H.1c we see a zoom on a peak in one of the calculated u-functions for different values of **antr**

showing the effect of changing that variable. We can calculate the contribution to the total particle number from the 0_-mode using various values of **antr**. The value obtained for **antr** = 200 diverges from the correct result by a factor of 0.00004. The time it takes to run the program is approximately proportional to **antr** squared.

In fig. H.1d some of the u_--functions are plotted for different values of k. We see that a larger k makes the function go to zero further out on the r-axis. Fig. H.1d is made using **maxr** > 10, and we see that for a k larger than 20 the u-function has not become zero at $r = 10$. This means that we expect some error on the contributions from the Bogoliubov modes with $k > 20$ when we use **maxr** $= 10$. In fig. H.1e we see the contribution to the total particle number from modes with different k. We see that modes with $k > 20$ gives a small contribution, 0.00301 of the total for the plus-modes and 0.00002 for the minus modes. If the error from using **maxr** $= 10$ is 10% on these modes, the total relative error from **maxr** is 0.00030.

antl is the number of l-modes that we include in the calculation. In fig H.1f we see the contribution to the total particle number from modes with different l. The contribution from modes with $l \geq 30$ is 0.00001 for the plus-modes and 0 from the minus-modes. The time it takes to run the program scales linearly with **antl**.

Finally **npre** is the precision of the number of atoms. The formula in (6.52) uses N_0 and not N, but since the known quantity is N, we need to carry out the calculations a couple of times in order to let N converge to the right number. The loop stops when the difference between the calculated and the correct value of N is less than **npre**. The smaller **npre** is, the smaller the numerical bumps on the $(\Delta J_z)^2$ vs. $\langle \hat{J}_x \rangle$-curves will be. The data plotted in figs. 7.4 and 7.5 are made using **npre** $= 0.05$ all the way through, while the data plotted in figs. 7.11 and 7.12 are produced using **npre** $= 0.05$ on the rightmost part of the curves, but **npre** $= 0.5$ for most of the data. The difference can be seen. If the numerical error from **npre** is **npre**$/N$, the total relative error it is 0.0005. The time it takes to execute the program goes logarithmically with $N/$**npre**.

This means that the relative errors from the variables **antt**, **maxt**, **antr**, **maxr**, **antl**, and **npre** are 0.00402, 0, 0.00004, 0.00030, 0.00001, and 0.00050 respectively. If we assume the errors to be independent, we can calculate[1] the total relative error on the expectation value on one of the $\hat{J}$-operators to be 0.00406 where the vast majority of the error stems from the **antt**-variable. If the uncertainties on $(\Delta J_z)^2$ and $\langle \hat{J}_x \rangle$ are assumed independent, this gives the relative uncertainty on a measurement of the squeezing parameter to be 0.00908. The conclusion I derive from this is that the calculated values of $\langle \hat{J} \rangle$ are correct within a margin of error of 0.5% while the calculated squeezings ξ^2 are correct within a margin of error of 1%.

[1] The relative errors found in this section are relative errors on different quantities. Sometimes on the contribution to the total particle number from one Bogoliubov-mode, sometimes on the contribution from all the modes, and sometimes on the particle number itself. This calculation assumes the uncertainties to be uncertainties on measurements of one of the operators involved in our calculations, which is why the error-calculation done here should be seen as an estimate only.

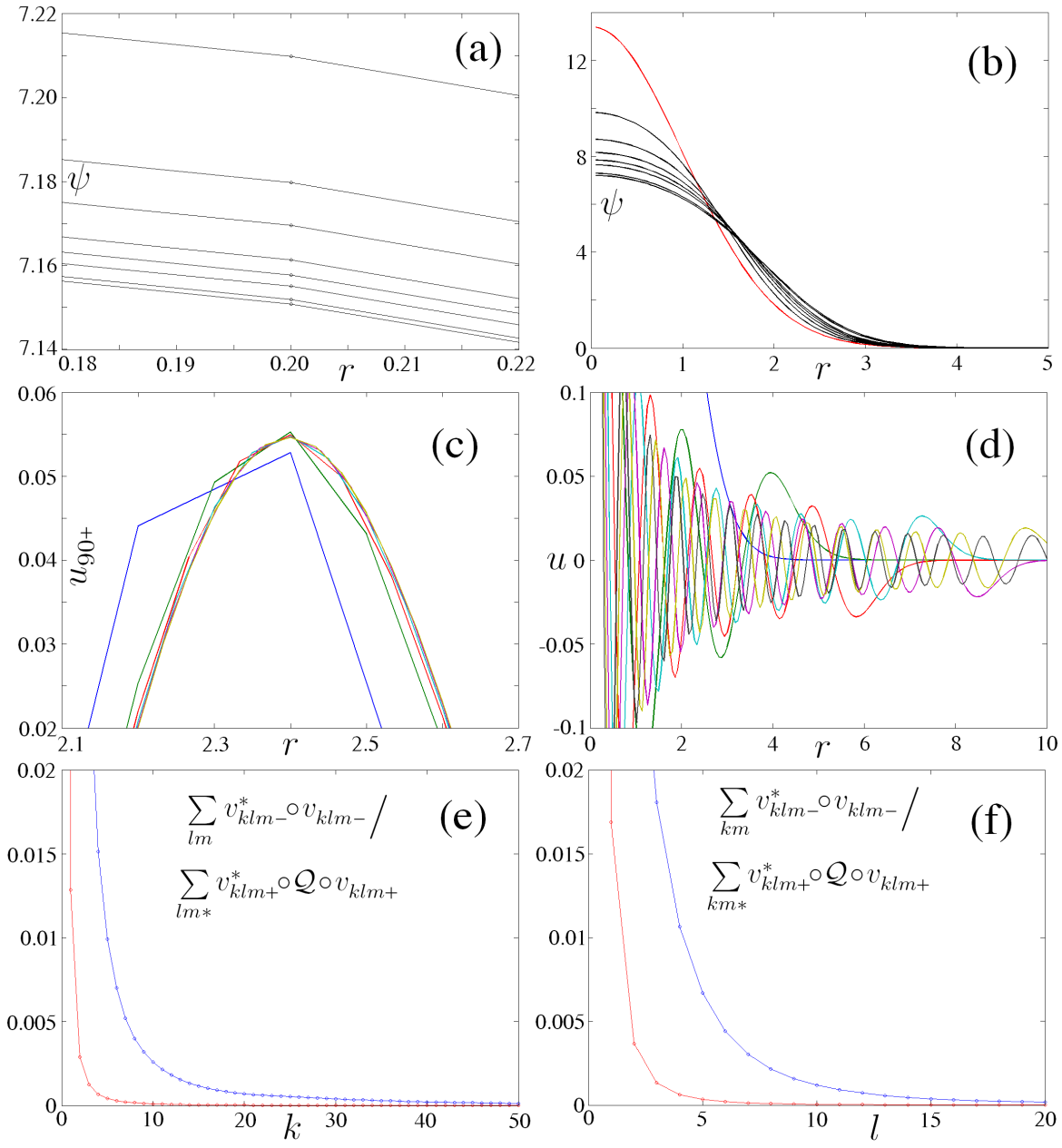

Figure H.1: (a) shows a zoom on a part of ψ for different values of **antt**. The values are 1000, 2000, 3000, 5000, 7000, 10000, 20000, and 30000 from above. (b) shows $\psi(r)$ for different values of **maxt** for a fixed **dt**. The red curve shows the initial curve corresponding to **maxt** $= 0$, and the black curves correspond to **maxt** $= 0.1$, 0.2, 0.3, 0.4, 0.5, 1, 2, and 3 respectively, counted from above at $r = 0$. The curves for 2 and 3 are indistinguishable. (c) shows a zoom on a peak of the u_{90+}-function for different **antr**. Blue, green, red, cyan, violet and brass corresponds to **antr** $= 50$, 100, 150, 200, 250, and 300 respectively. (d) shows the u_{k0-}-function for different values of k, blue, green, red, cyan, violet, brass and black correspond to $k = 0$, 4, 9, 14, 19, 24 and 29 respectively. (e) and (f) show the contribution to the total particle number for different k and l respectively. Blue corresponds to the contribution from plus-modes and red corresponds to the contribution from minus-modes.

Appendix I

Further results

In this appendix some results that did not fit in the main text is shown, with a minimum of discussion.

Fig. I.1 is a detailed plot of various parameters for a single set of U, U_{ab}, $\mathcal{T}$ and N. Fig. I.2 shows the contributions to the total particle number for different Bogoliubov modes. Figs. I.3 and I.4 shows the results of a simulation for varying s and $\mathcal{T}$. Figs. I.5, I.6, I.7, I.8, I.9, I.10, I.11, and I.12 shows the results of varying s and f for temperatures different from the one used in figs. 7.11 and 7.12.

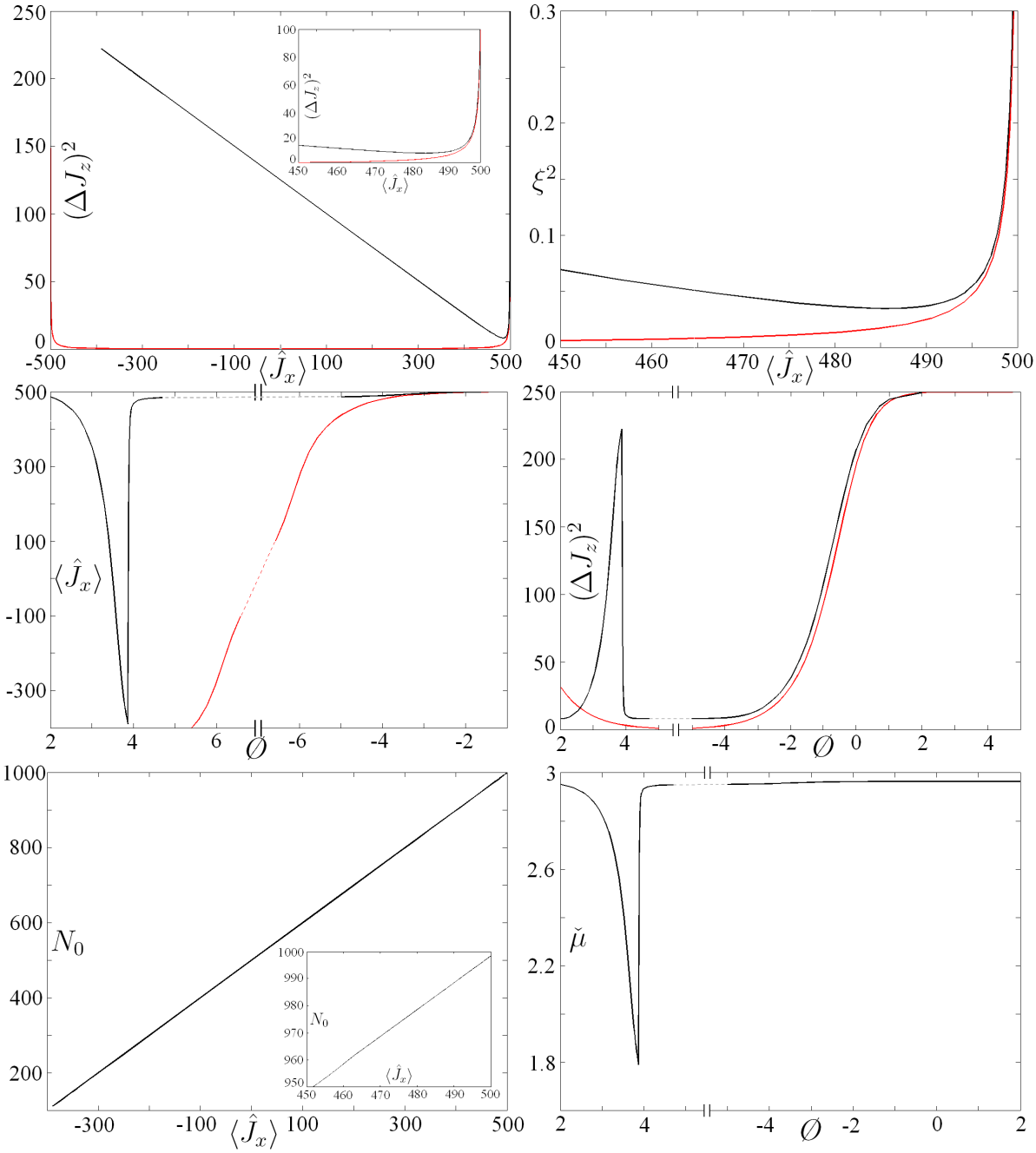

Figure I.1: The results of an implementation of the main theory, shown in further detail than what is presented in the "results"-chapter. The plot is made for atoms with $U = 0.06$, $U_{ab} = 0.04$ and $\mathcal{T} = 0$. The red curves show the results for the F-functions as comparison. The Ø on some of the axis denotes $-\log_{10}(\Omega)$ on the left hand side of the graphs, and $\log_{10}(-\Omega)$ on the right hand side. The large peaks for a positive Ω on some of the graphs shows the break-down of the theory since $N \approx N_0$ is false for these values of Ω. The fact that $\langle \hat{J}_x \rangle = 0$ corresponds to a positive Ω is discussed in section 7.1.

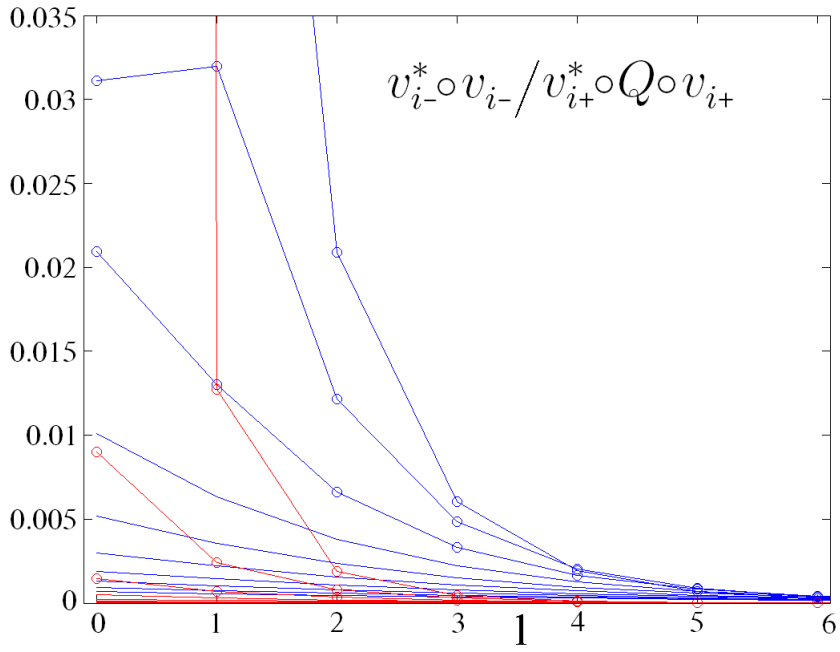

Figure I.2: The contributions to the total particle number, coming from the various Bogoliubov modes at zero temperature. As we can see from (6.52) the contribution is $v^*_{klm+} \circ \mathcal{Q} \circ v_{klm+}$ from the plus-modes and $v^*_{klm-} \circ v_{klm-}$ from the minus-modes. This figure shows the contribution from a single m-mode. If we want to calculate the total contribution for a given pair of k and l, the values in this figure should be multiplied with $(2l+1)$ in order to take all the m-modes into account. The figure shows curves for values of k ranging from 0 to 9 starting from above. The points on the curves for k=0, 1, and 2 are marked with $\circ$-symbols, and the l quantum number is shown on the horizontal axis. The blue curves show the plus-modes and the red curves show the minus-modes. We see that the zoom is made so that δN_{01+} and δN_{00-} are outside the range, the values being $\delta N_{01+} = 0.0923$ and $\delta N_{00-} = 14.291$. The jump between δN_{10+} and δN_{11+} may be explained by the position-independent model presented in the main text, since the value of A_+ could be smaller for $l = 1$ than for $l = 0$ if Ω had some negative value.

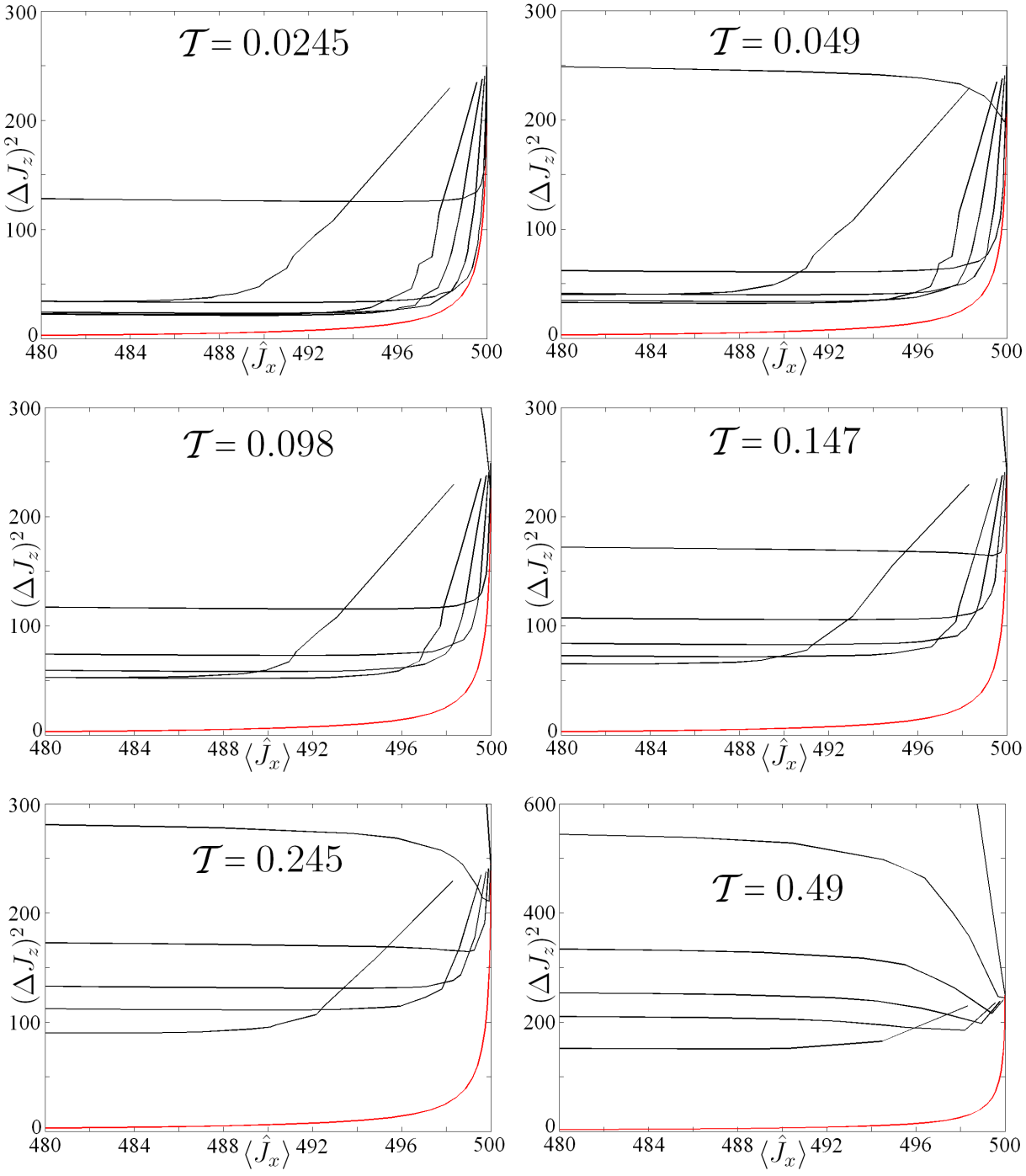

Figure I.3: The $(\Delta J_z)^2$ vs. $\langle \hat{J}_x \rangle$-curves for different temperatures and different values of s. Each subfigure is made for a fixed value of $\mathcal{T}$ while each curve corresponds to a specific value of s. The values are $s = 0.01$, 0.1, 0.3, 0.6, 1, and 3 from the right. The plots are made for $f = \frac{2}{3}$.

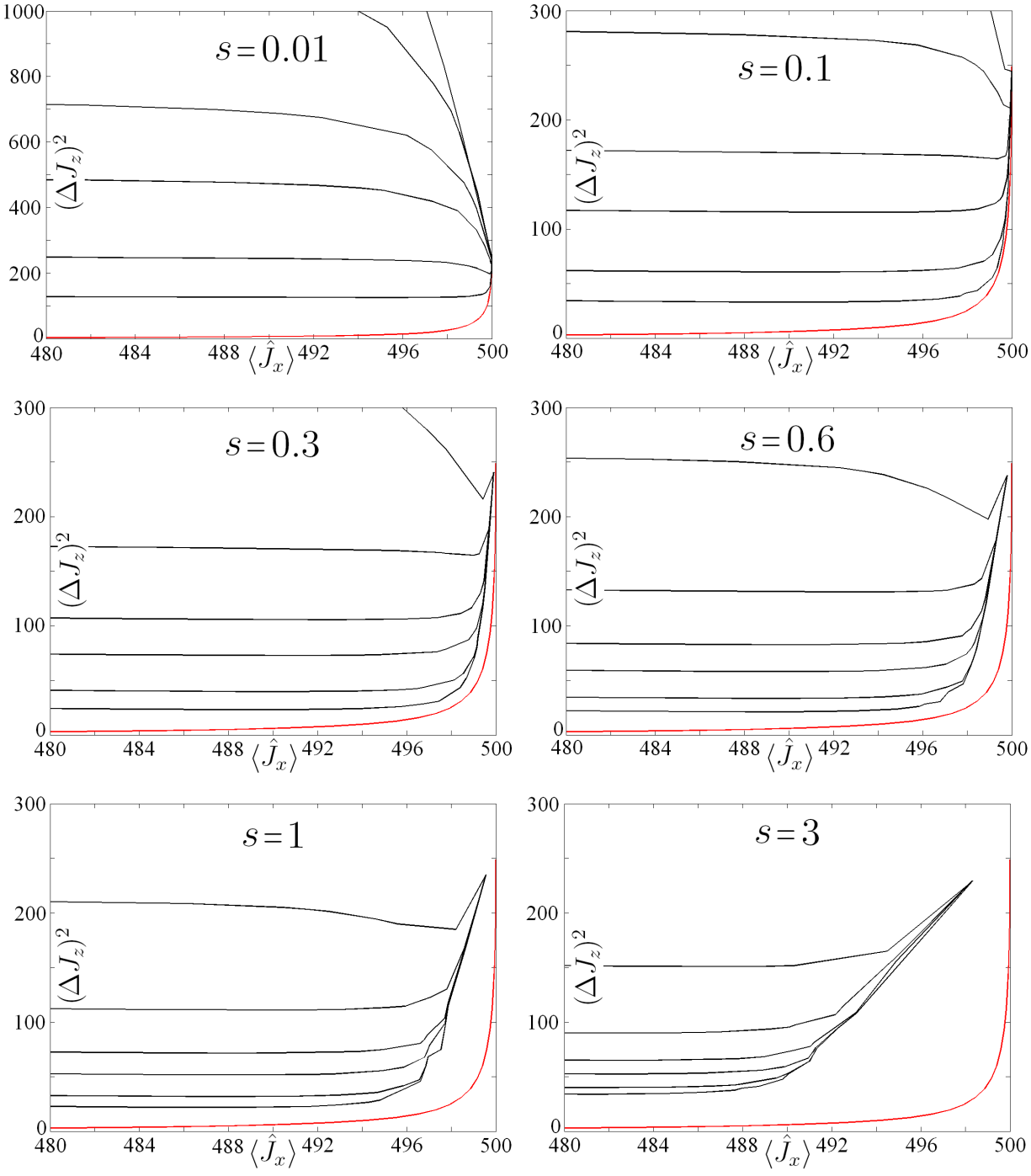

Figure I.4: The $(\Delta J_z)^2$ vs. $\langle \hat{J}_x \rangle$-curves for different temperatures and different values of s. Each subfigure is made for a fixed value of s while each curve corresponds to a specific value of $\mathcal{T}$. The values are $\mathcal{T} = 0.0245$, 0.049, 0.098, 0.147, 0.245, and 0.49 from below. The plots are made for $f = \frac{2}{3}$.

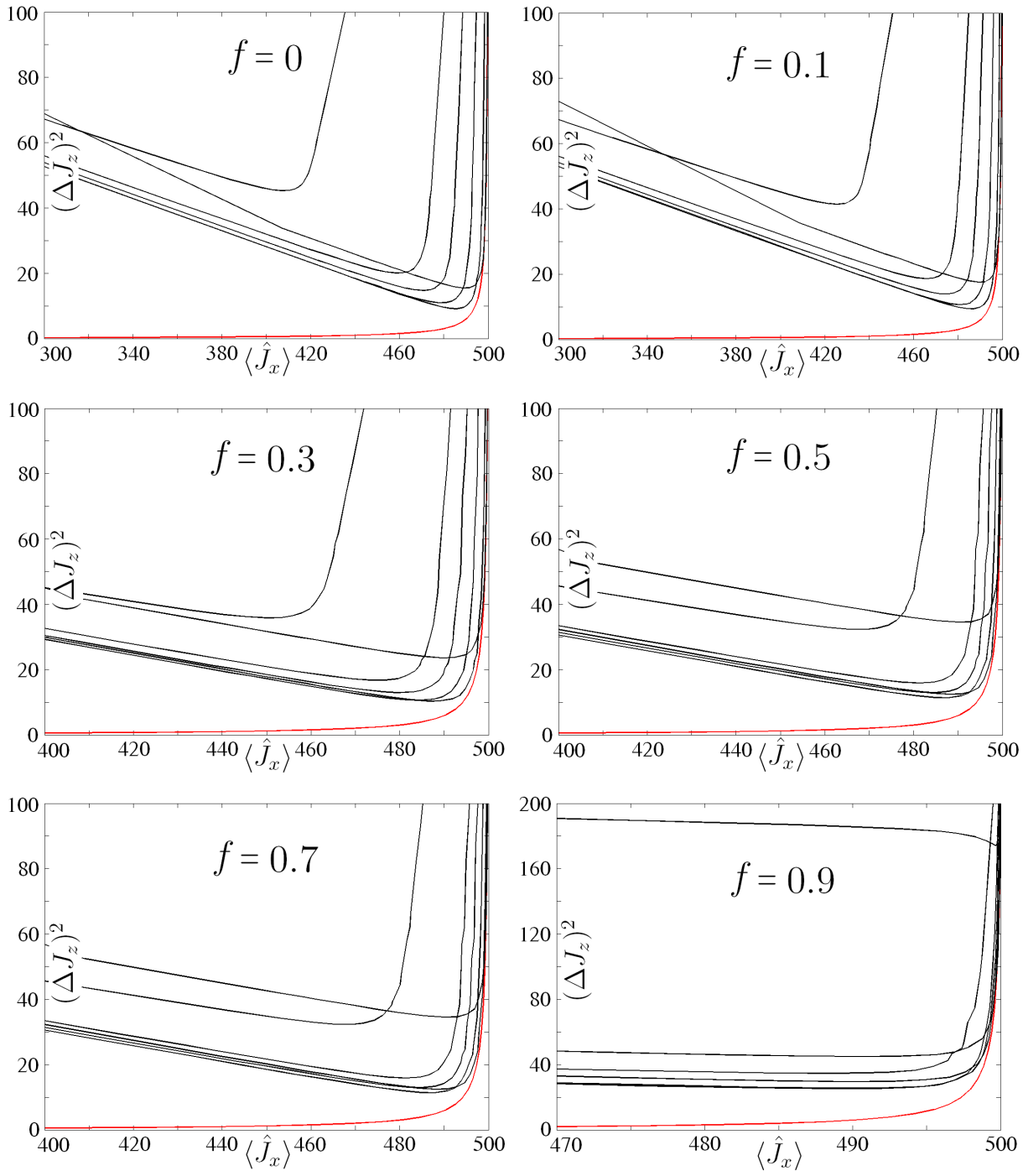

Figure I.5: The $(\Delta J_z)^2$ vs. $\langle \hat{J}_x \rangle$-curves for different values of s and f. Each subfigure is made for a fixed value of f while each curve corresponds to a specific value of s. The values are $s = 0.01$, 0.1, 0.3, 0.6, 1, and 3 from the right. The plots are made for $\mathcal{T} = 0.0098$, differing from the value used in fig. 7.11 in the main text.

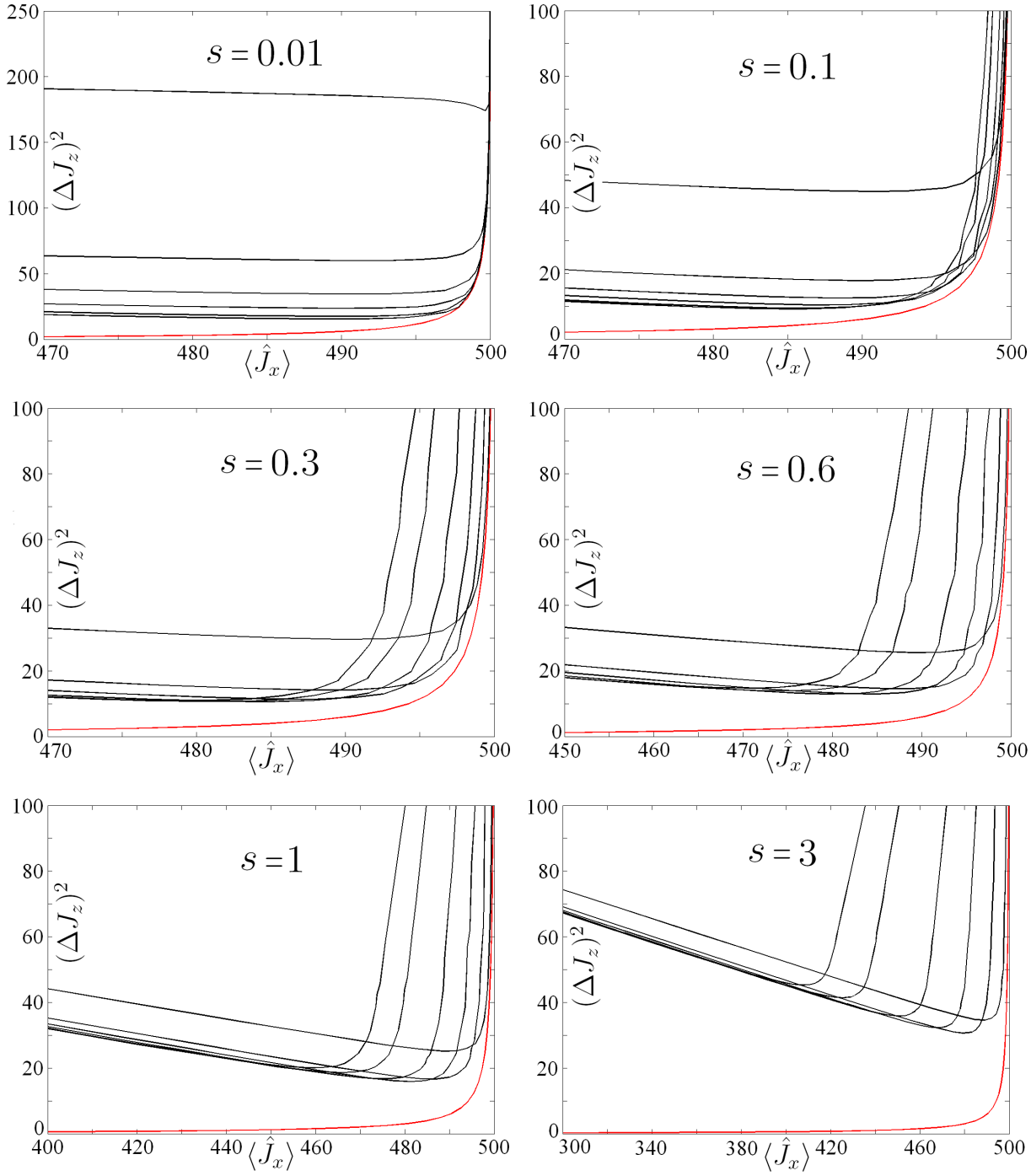

Figure I.6: The $(\Delta J_z)^2$ vs. $\langle \hat{J}_x \rangle$-curves for different values of s and f. Each subfigure is made for a fixed value of s while each curve corresponds to a specific value of f. The values are $f = 0$, 0.1, 0.3, 0.5, 0.7, and 0.9 from the left. The plots are made for $\mathcal{T} = 0.0098$, differing from the value used in fig. 7.12 in the main text.

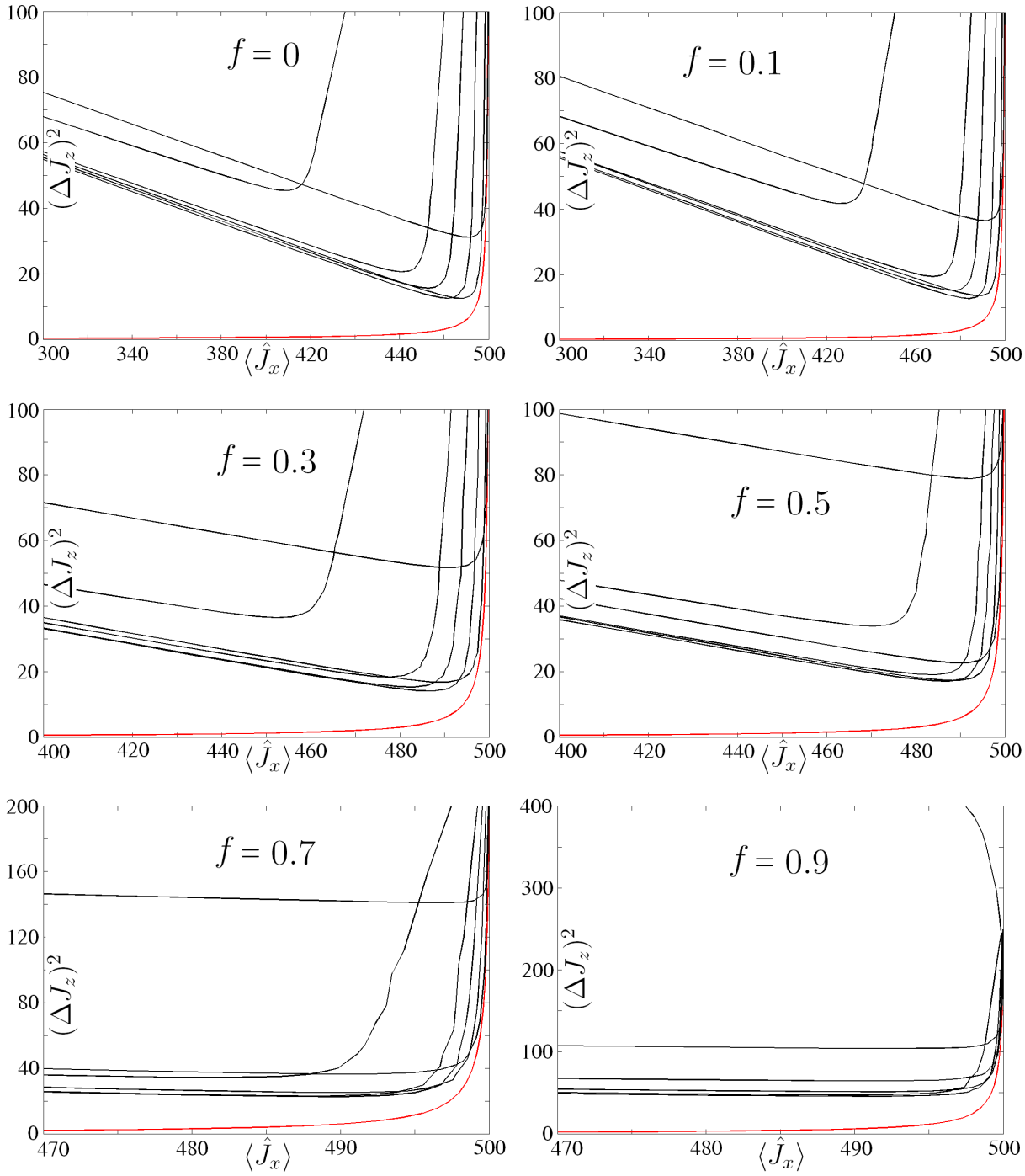

Figure I.7: The $(\Delta J_z)^2$ vs. $\langle \hat{J}_x \rangle$-curves for different values of s and f. Each subfigure is made for a fixed value of f while each curve corresponds to a specific value of s. The values are $s = 0.01$, 0.1, 0.3, 0.6, 1, and 3 from the right. The plots are made for $\mathcal{T} = 0.0245$, differing from the value used in fig. 7.11 in the main text.

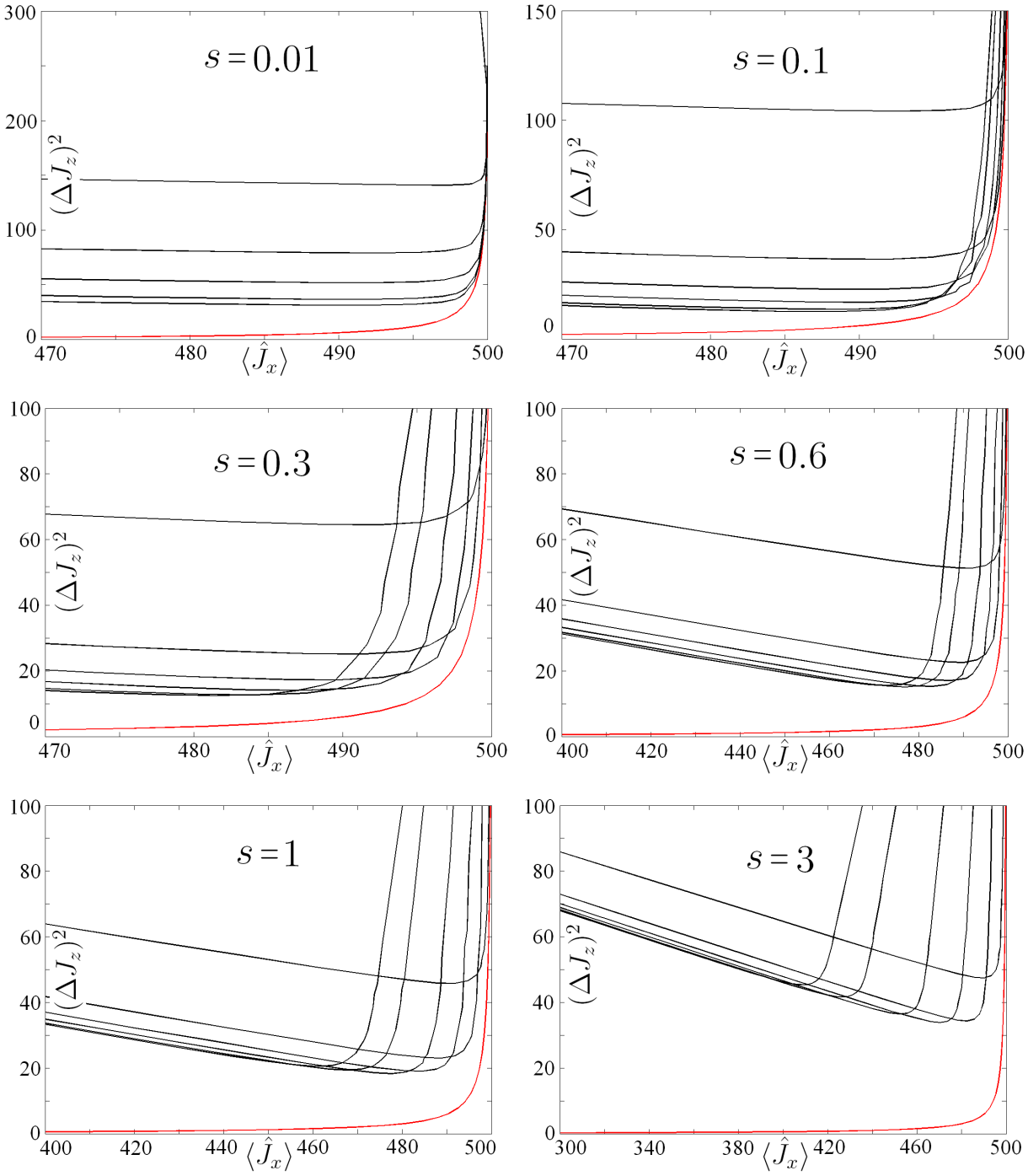

Figure I.8: The $(\Delta J_z)^2$ vs. $\langle \hat{J}_x \rangle$-curves for different values of s and f. Each subfigure is made for a fixed value of s while each curve corresponds to a specific value of f. The values are $f = 0$, 0.1, 0.3, 0.5, 0.7, and 0.9 from the left. The plots are made for $\mathcal{T} = 0.0245$, differing from the value used in fig. 7.12 in the main text.

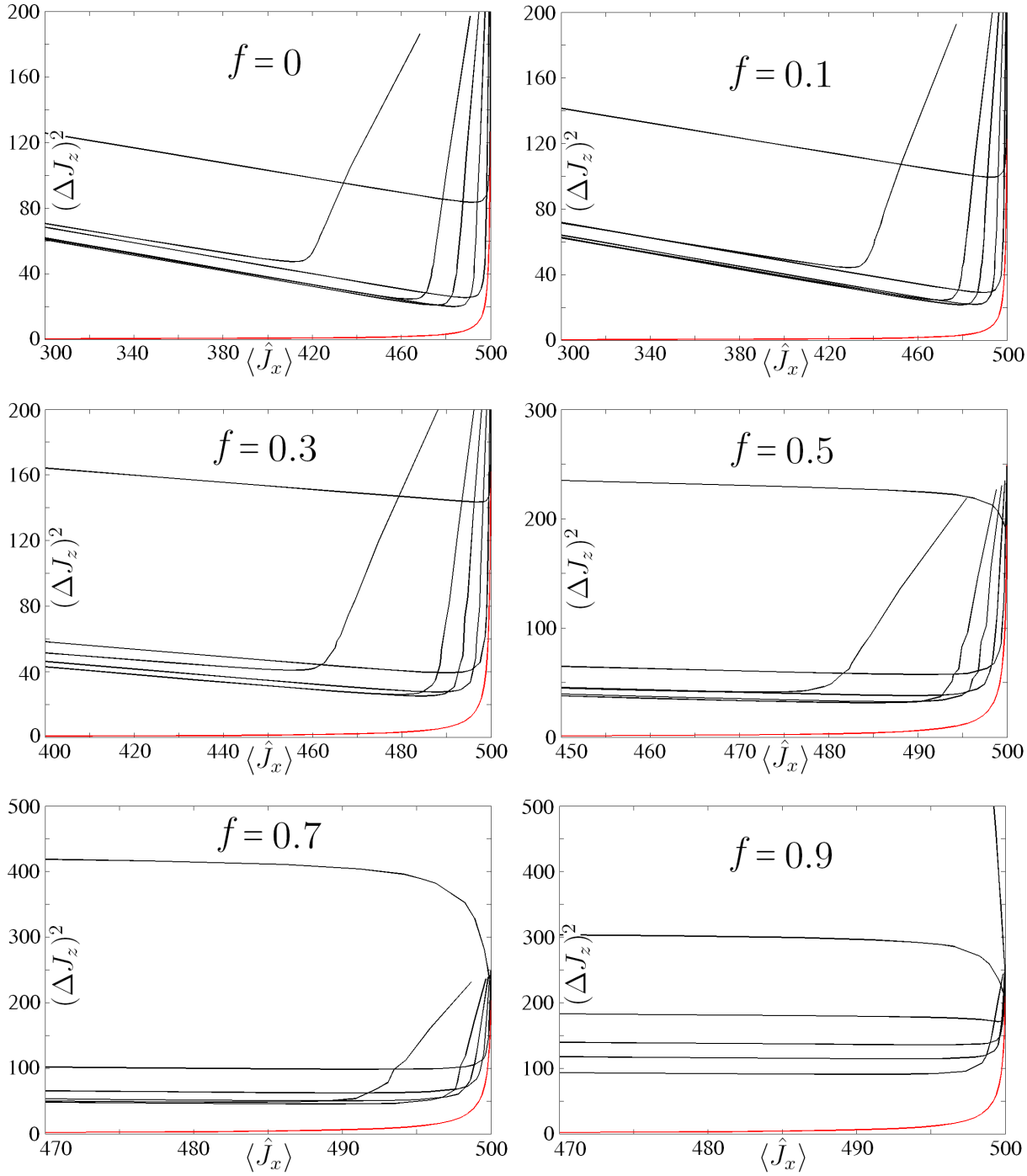

Figure I.9: The $(\Delta J_z)^2$ vs. $\langle \hat{J}_x \rangle$-curves for different values of s and f. Each subfigure is made for a fixed value of f while each curve corresponds to a specific value of s. The values are $s = 0.01$, 0.1, 0.3, 0.6, 1, and 3 from the right. The plots are made for $\mathcal{T} = 0.0735$, differing from the value used in fig. 7.11 in the main text.

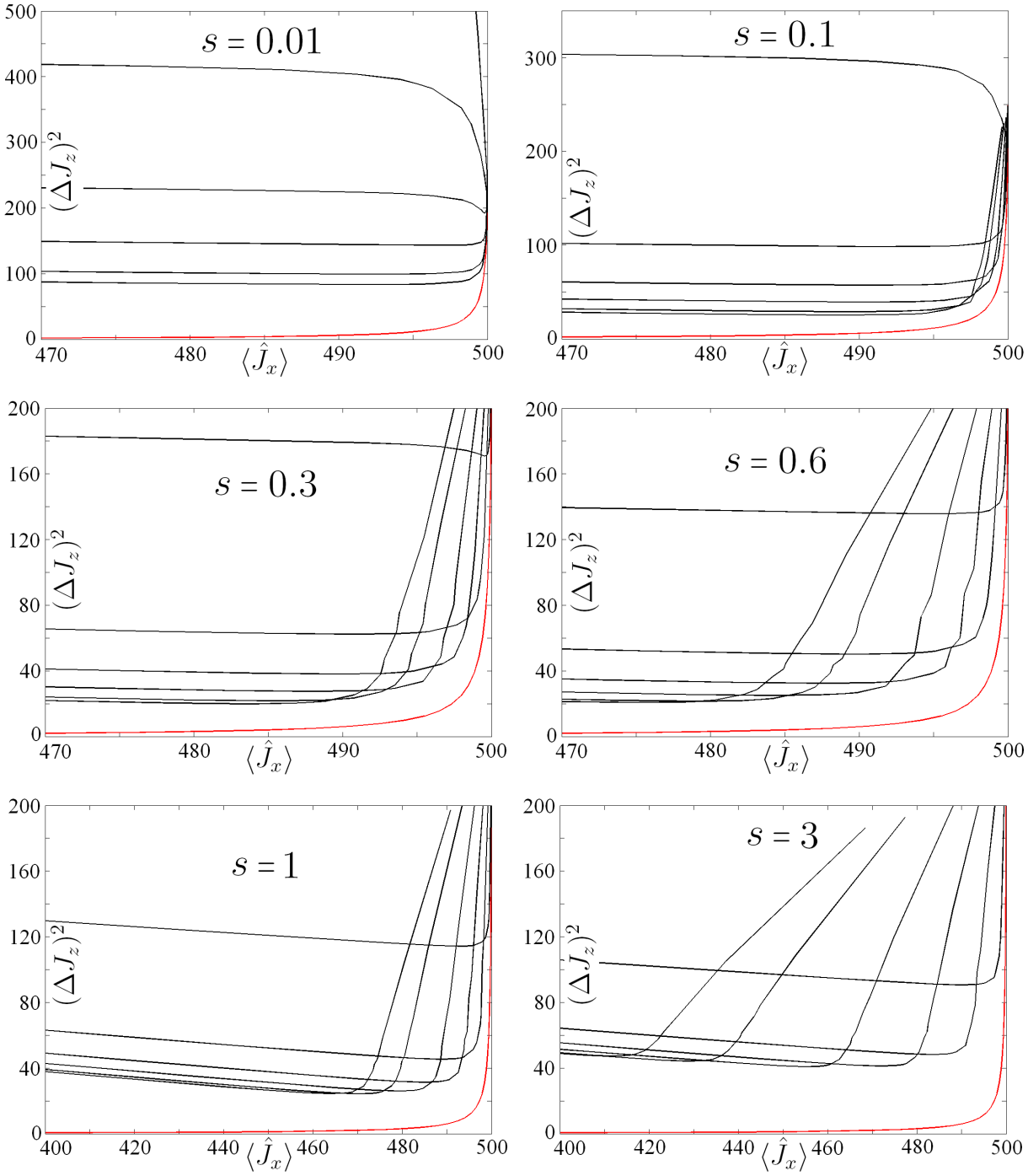

Figure I.10: The $(\Delta J_z)^2$ vs. $\langle \hat{J}_x \rangle$-curves for different values of s and f. Each subfigure is made for a fixed value of s while each curve corresponds to a specific value of f. The values are $f = 0$, 0.1, 0.3, 0.5, 0.7, and 0.9 from the left. The plots are made for $\mathcal{T} = 0.0735$, differing from the value used in fig. 7.12 in the main text.

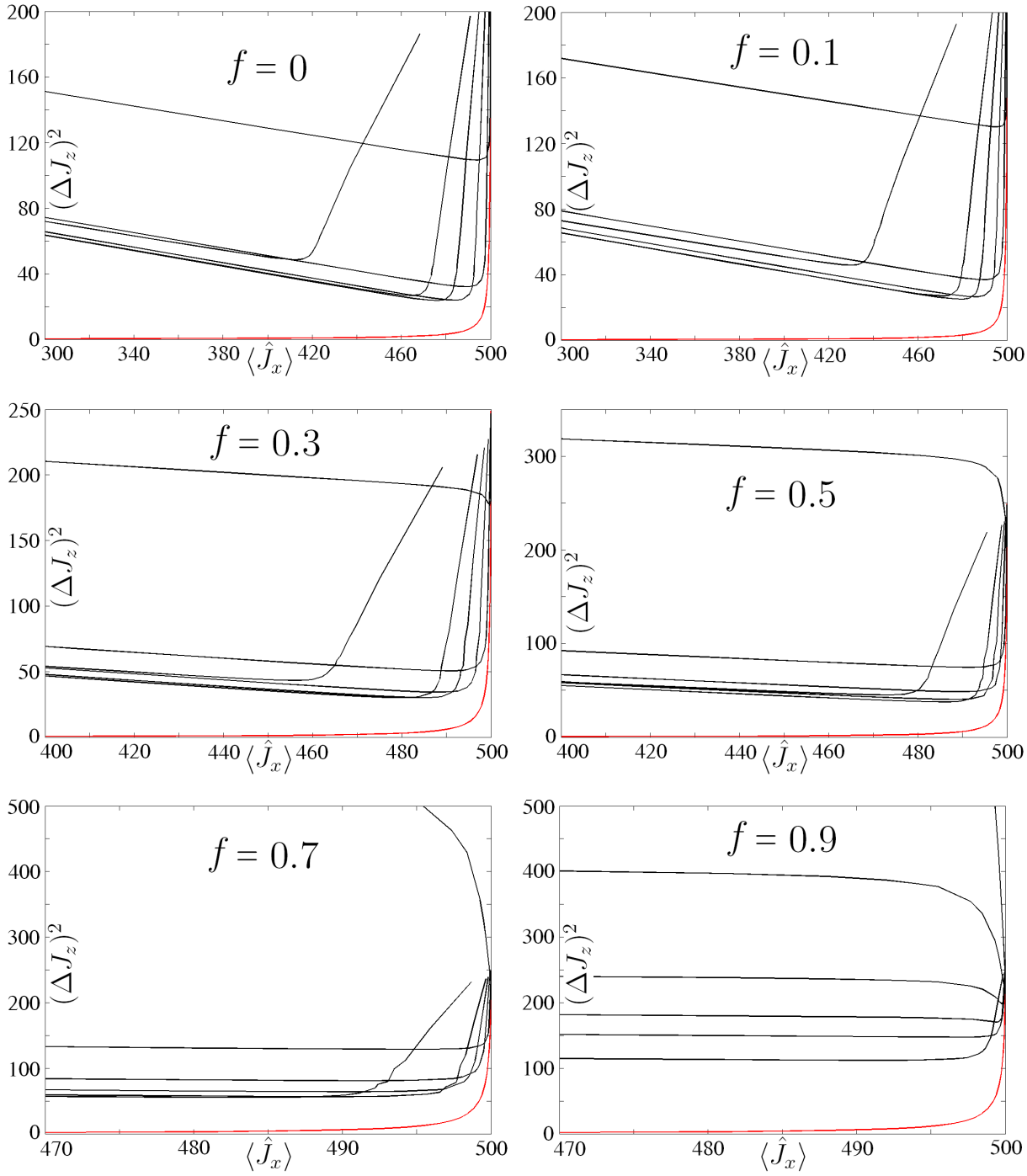

Figure I.11: The $(\Delta J_z)^2$ vs. $\langle \hat{J}_x \rangle$-curves for different values of s and f. Each subfigure is made for a fixed value of f while each curve corresponds to a specific value of s. The values are $s = 0.01$, 0.1, 0.3, 0.6, 1, and 3 from the right. The plots are made for $\mathcal{T} = 0.098$, differing from the value used in fig. 7.11 in the main text.

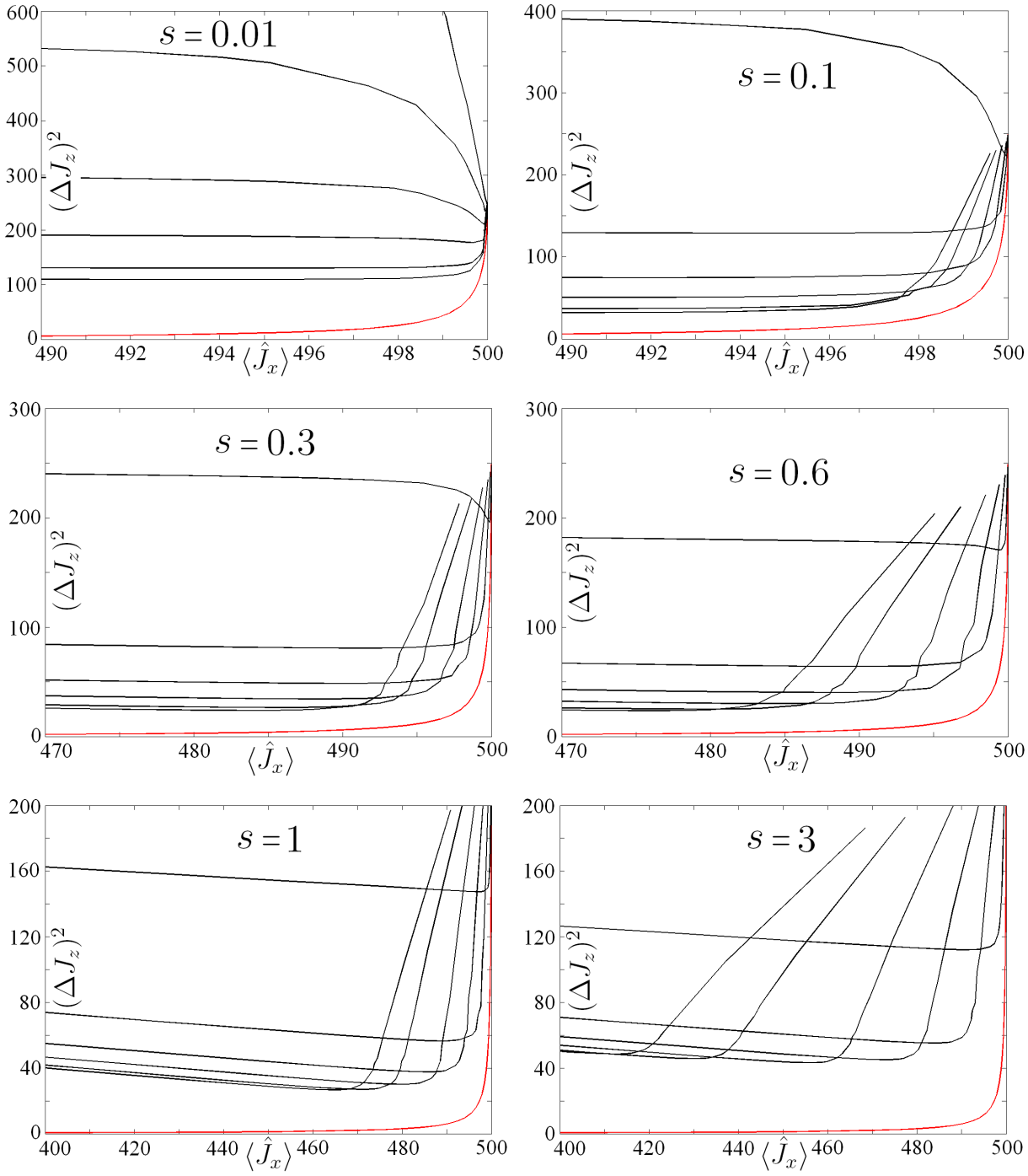

Figure I.12: The $(\Delta J_z)^2$ vs. $\langle \hat{J}_x \rangle$-curves for different values of s and f. Each subfigure is made for a fixed value of s while each curve corresponds to a specific value of f. The values are $f = 0, 0.1, 0.3, 0.5, 0.7$, and 0.9 from the left. The plots are made for $\mathcal{T} = 0.098$, differing from the value used in fig. 7.12 in the main text.

Appendix J

Figures in higher resolution

In this appendix some of the figures from chapter 7 are shown in higher resolution.

Fig. J.1 is equivalent to the $f = 0.5$ subfigure in fig. 7.4.
Fig. J.2 is equivalent to the $s = 0.6$ subfigure in fig. 7.5.
Fig. J.3 is equivalent to fig. 7.8.
Fig. J.4 is equivalent to fig. 7.9a.
Fig. J.5 is equivalent to fig. 7.9b.
Fig. J.6 is equivalent to the $f = 0.5$ subfigure in fig. 7.11.
Fig. J.7 is equivalent to the $s = 0.6$ subfigure in fig. 7.12.
Fig. J.8 is equivalent to fig. 7.13a.
Fig. J.9 is equivalent to fig. 7.13b.

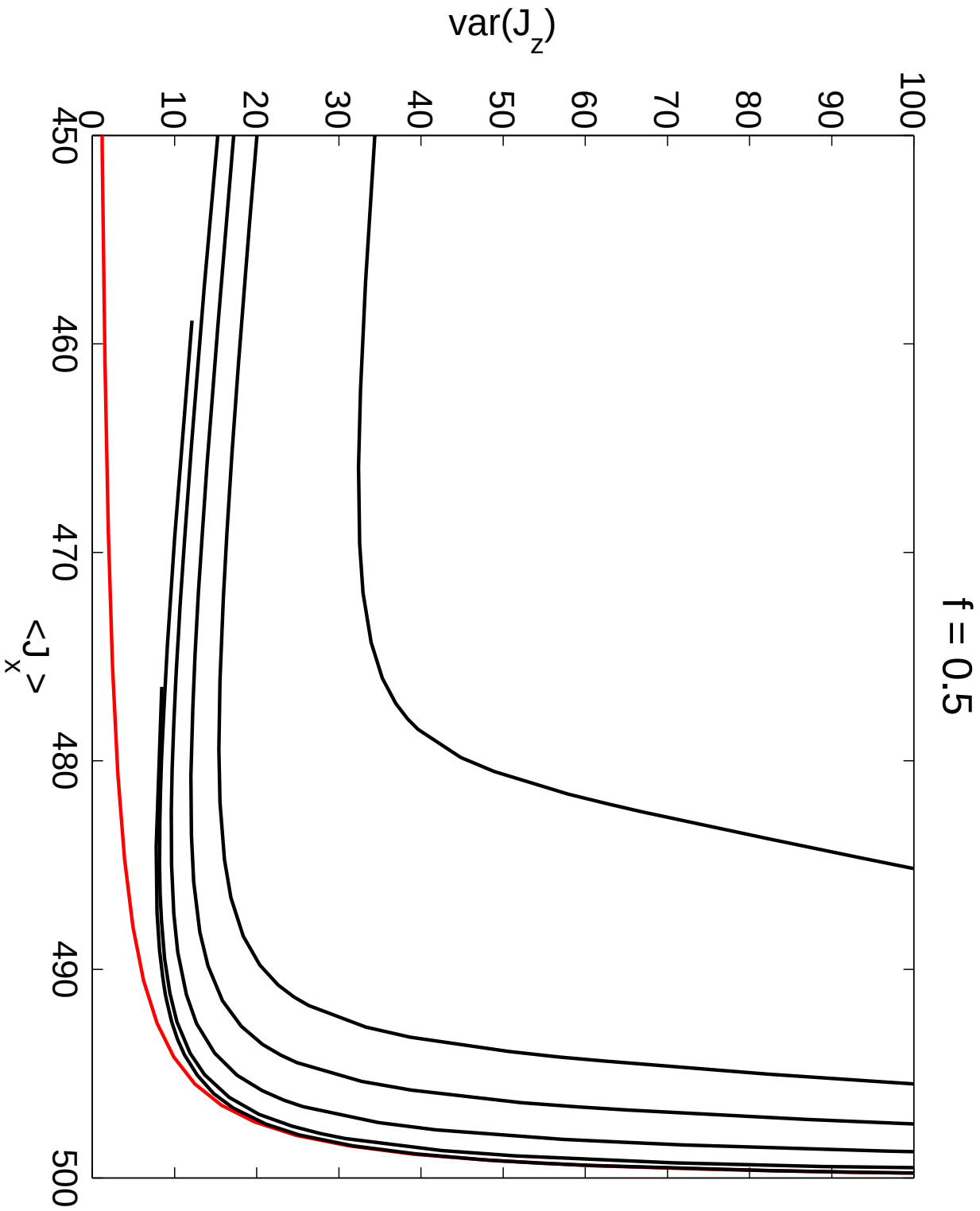

Figure J.1: The $f = 0.5$ subfigure in fig. 7.4 in higher resolution. The temperature is zero and the values of s are 0.01, 0.1, 0.3, 0.6, 1, and 3 from below of the $(\Delta J_z)^2$-axis.

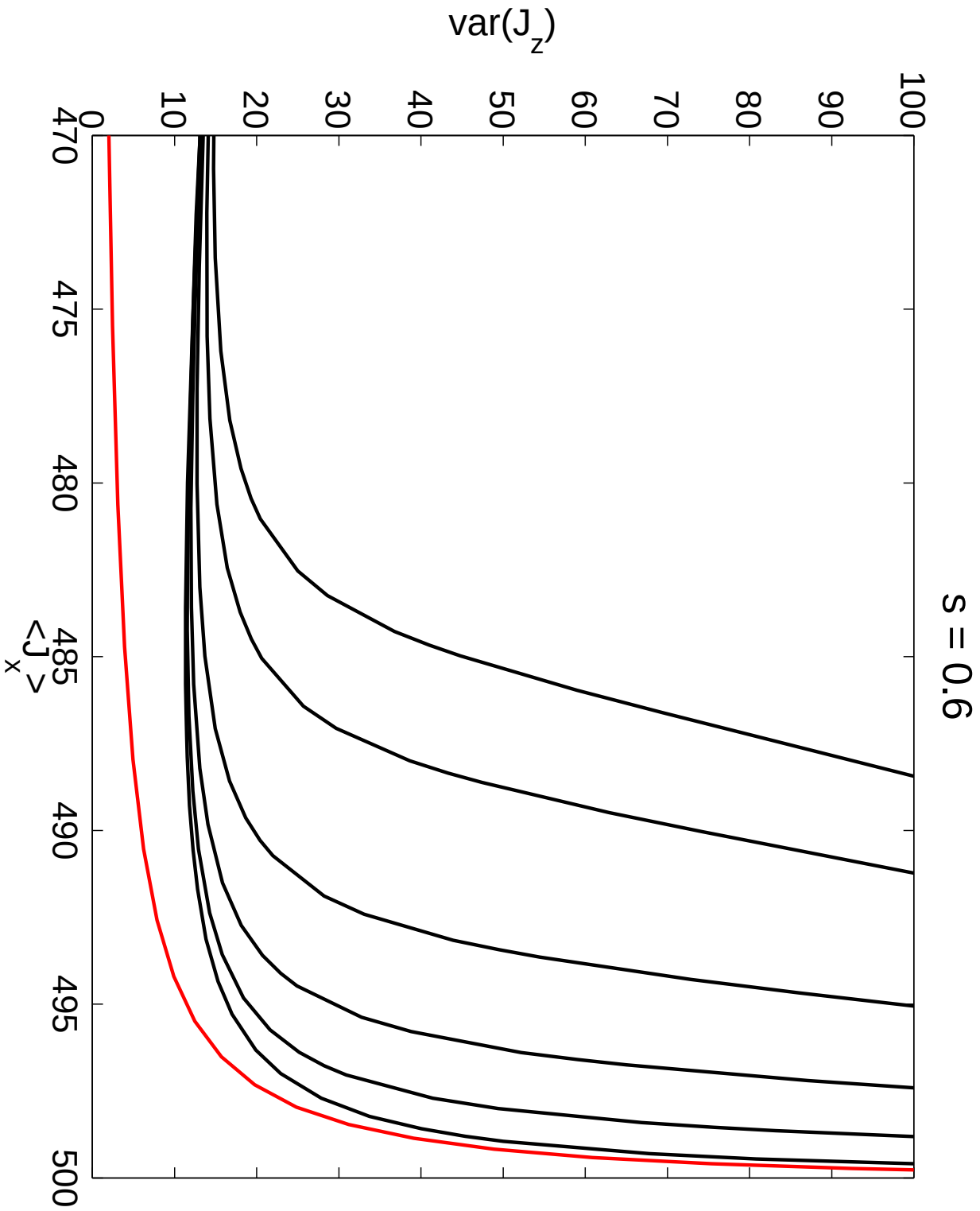

Figure J.2: The $s = 0.6$ subfigure in fig. 7.5 in higher resolution. The temperature is zero and the values of f are 0, 0.1, 0.3, 0.5, 0.7, and 0.9 from above of the $(\Delta J_z)^2$-axis.

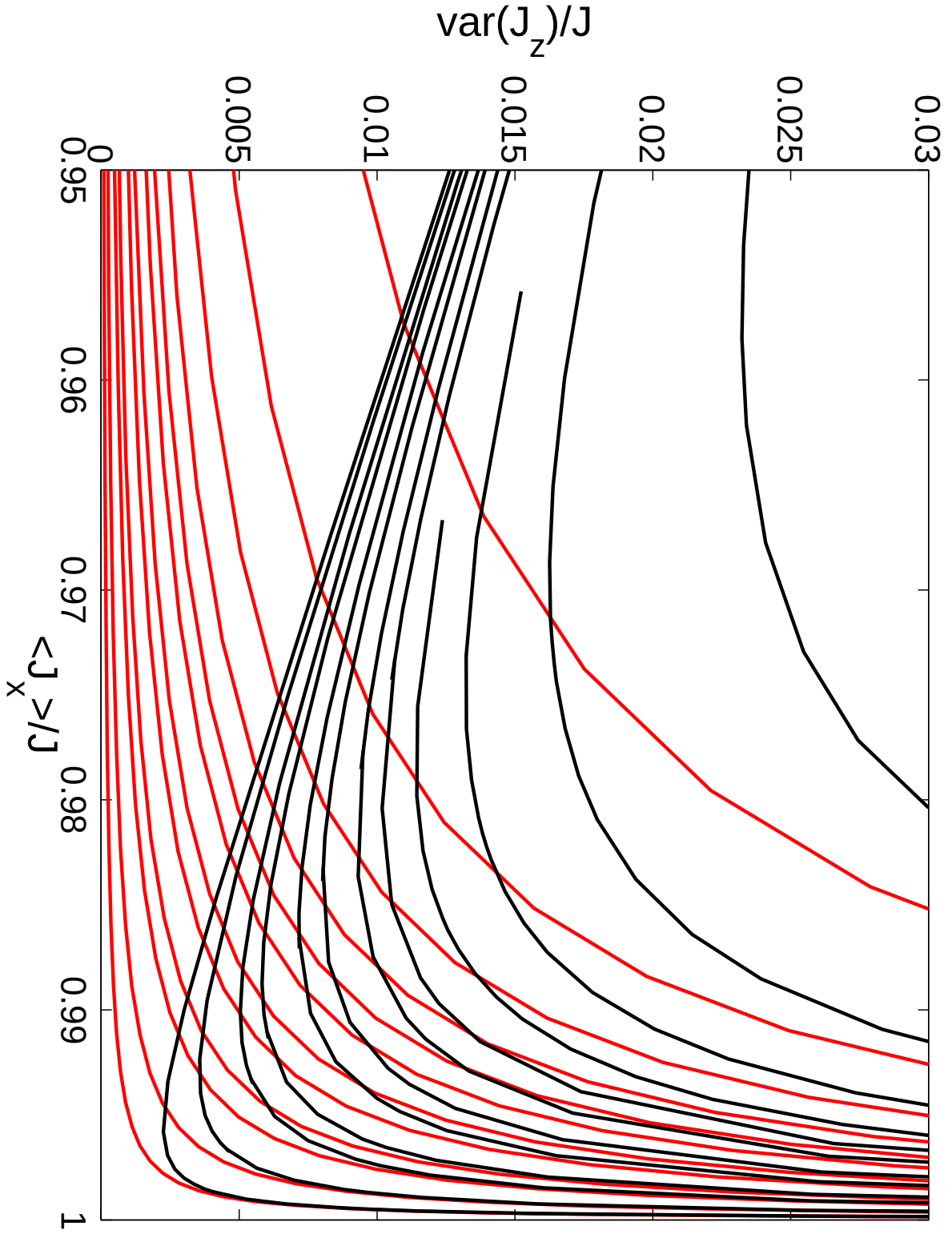

Figure J.3: Fig. 7.8 in higher resolution. The values of N are 500, 1000, 1500, 2000, 2500, 3000, 4000, 5000, 7500, 10000, 20000, and 50000 from above of the $(\Delta J_z)^2$-axis.

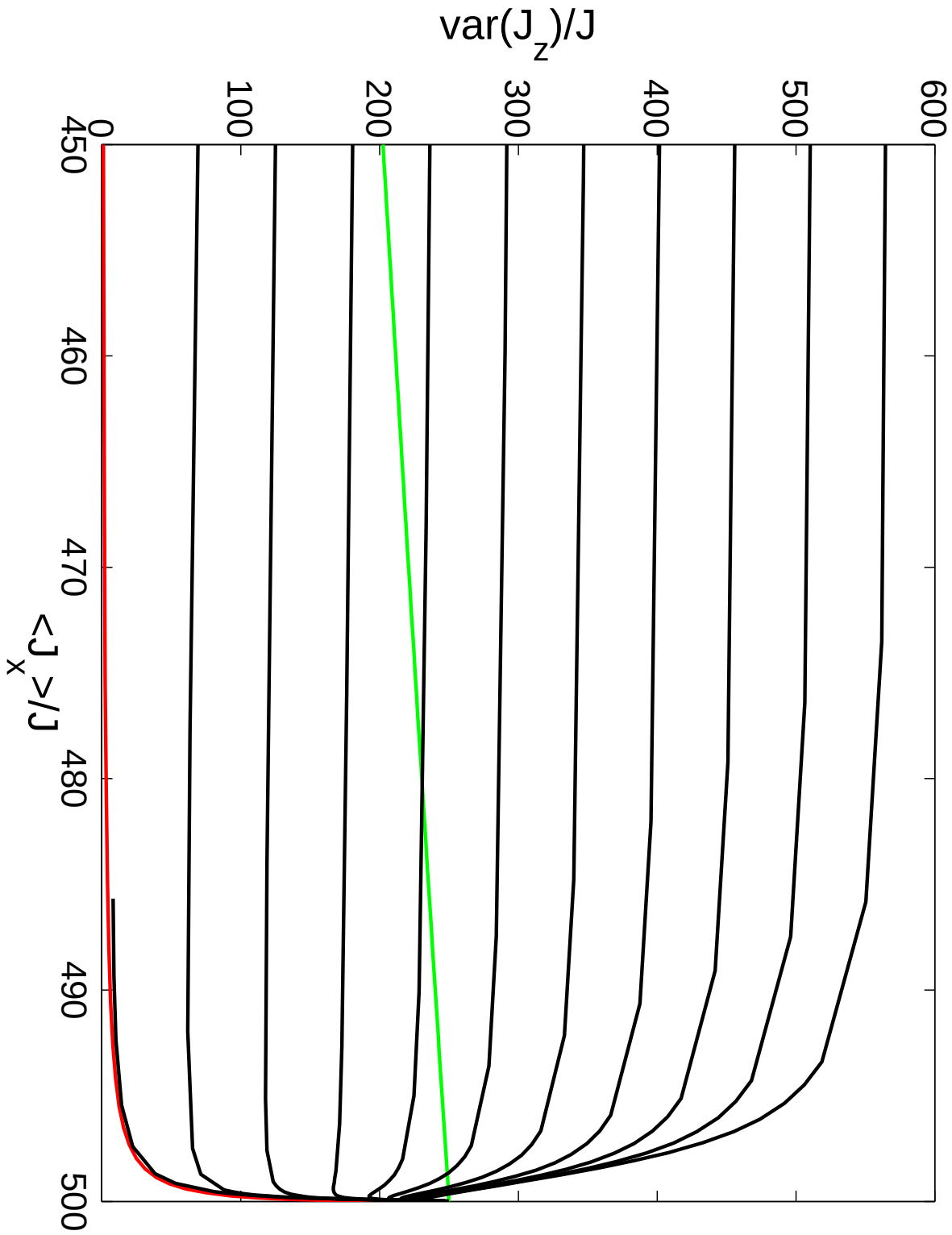

Figure J.4: Fig. 7.9a in higher resolution. The temperatures go from 0 to 0.49 with an interval of 0.049 from below of the $(\Delta J_z)^2$-axis.

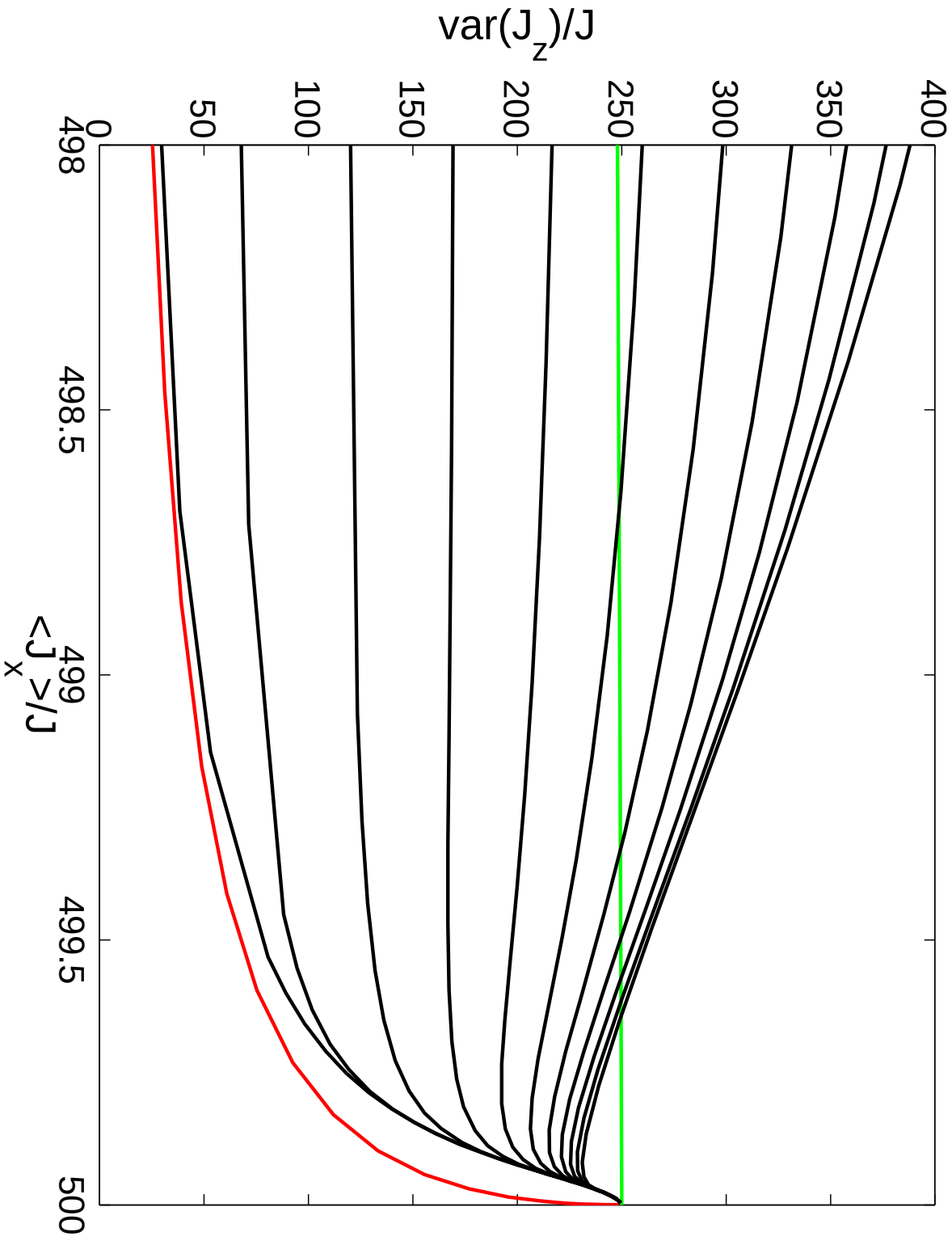

Figure J.5: Fig. 7.9b in higher resolution. The temperatures go from 0 to 0.49 with an interval of 0.049 from below of the $(\Delta J_z)^2$-axis.

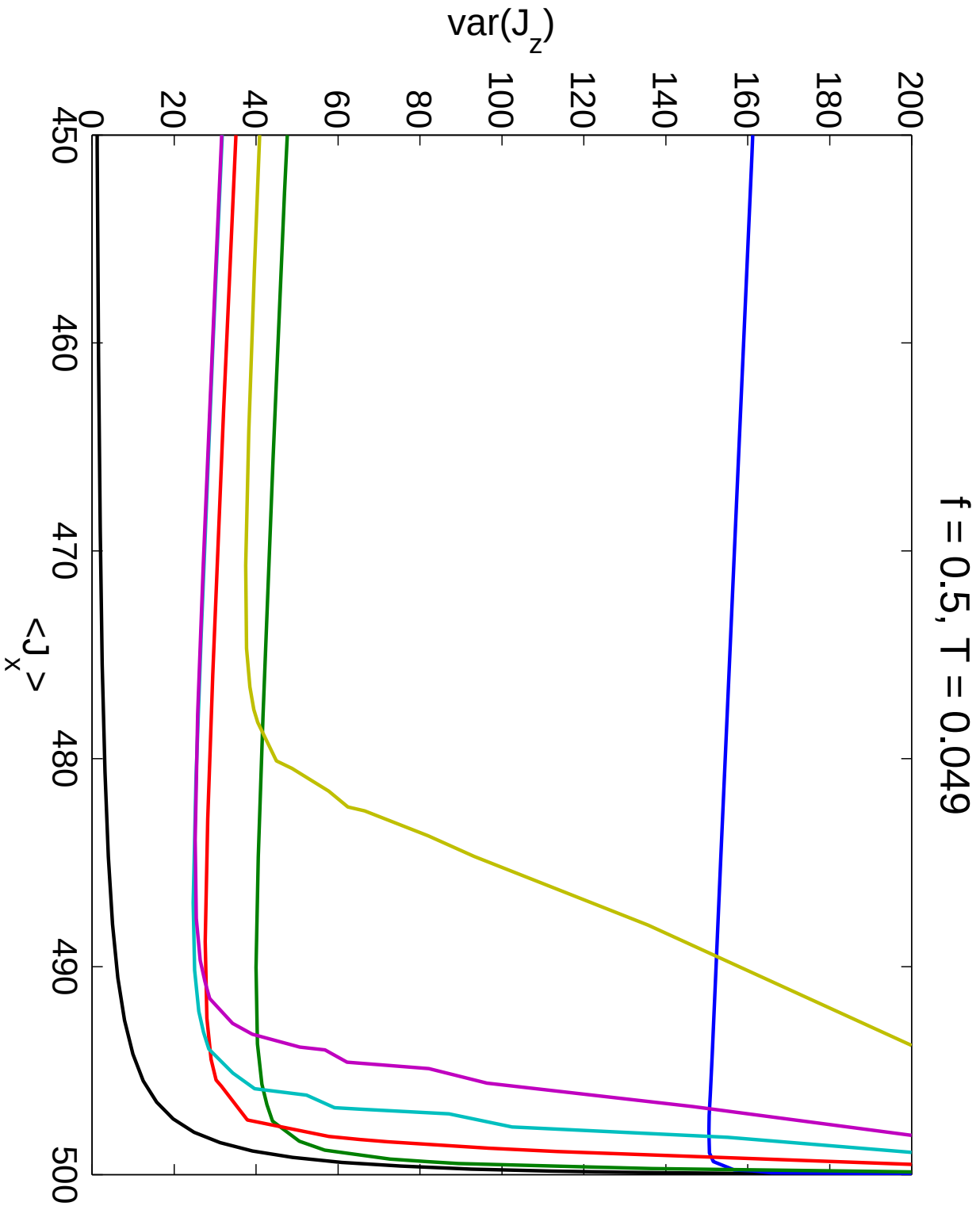

Figure J.6: The $f = 0.5$ subfigure in fig. 7.11 in higher resolution. The temperature is $\mathcal{T} = 0.049$ and the values of s are 0.01, 0.1, 0.3, 0.6, 1, and 3 from the right of the $\langle \hat{J}_x \rangle$-axis.

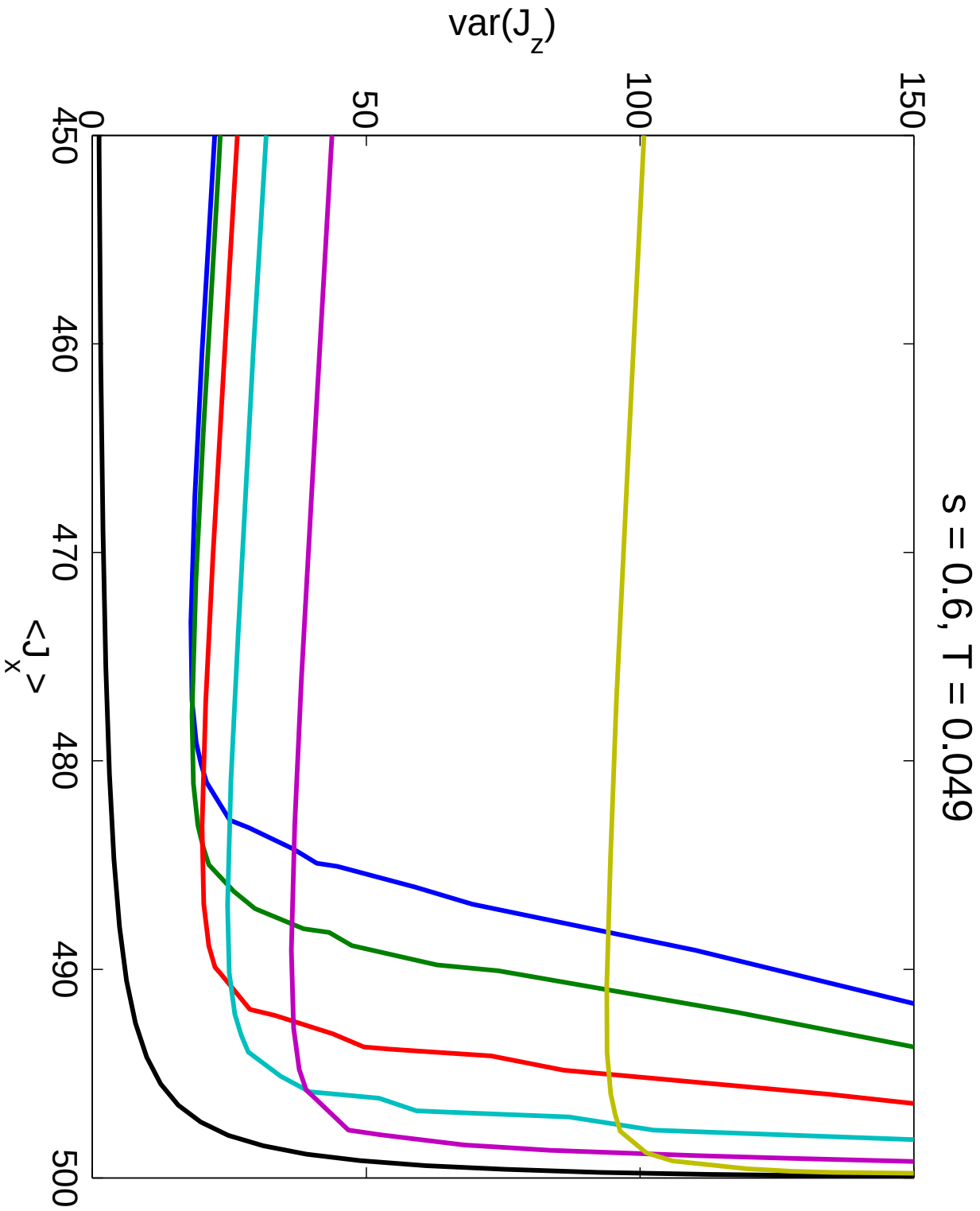

Figure J.7: The $s = 0.6$ subfigure in fig. 7.12 in higher resolution. The temperature is $\mathcal{T} = 0.049$ and the values of f are 0, 0.1, 0.3, 0.5, 0.7, and 0.9 from the left of the $\langle \hat{J}_x \rangle$-axis.

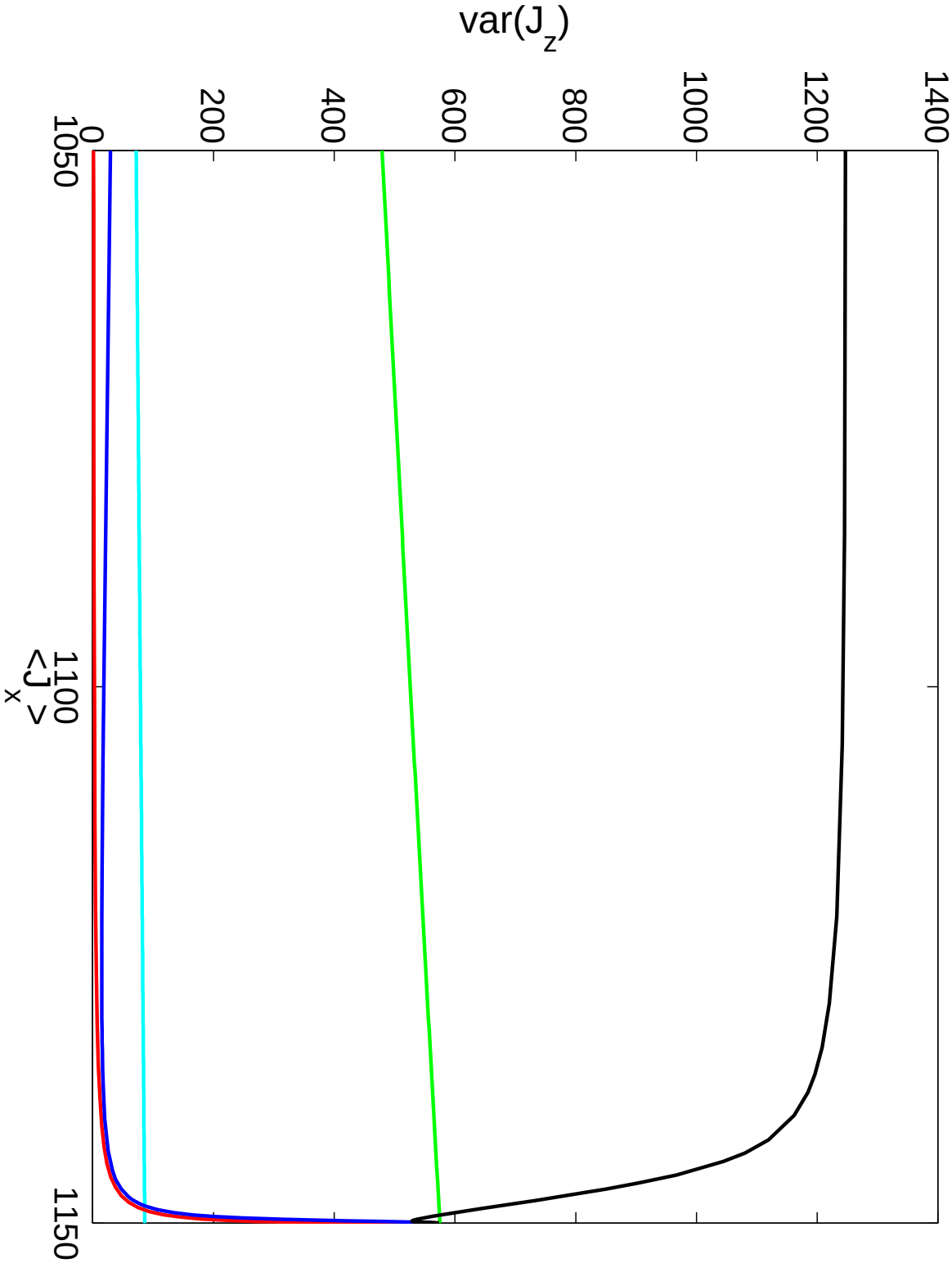

Figure J.8: Fig. 7.13a in higher resolution. The black curve corresponds to $\mathcal{T} = 0.49$ and the blue curve corresponds to $\mathcal{T} = 0$. The red curve is the F-function, and the green and cyan curves corresponds to $\xi^2 = 1$ and $\xi^2 = 0.15$ respectively.

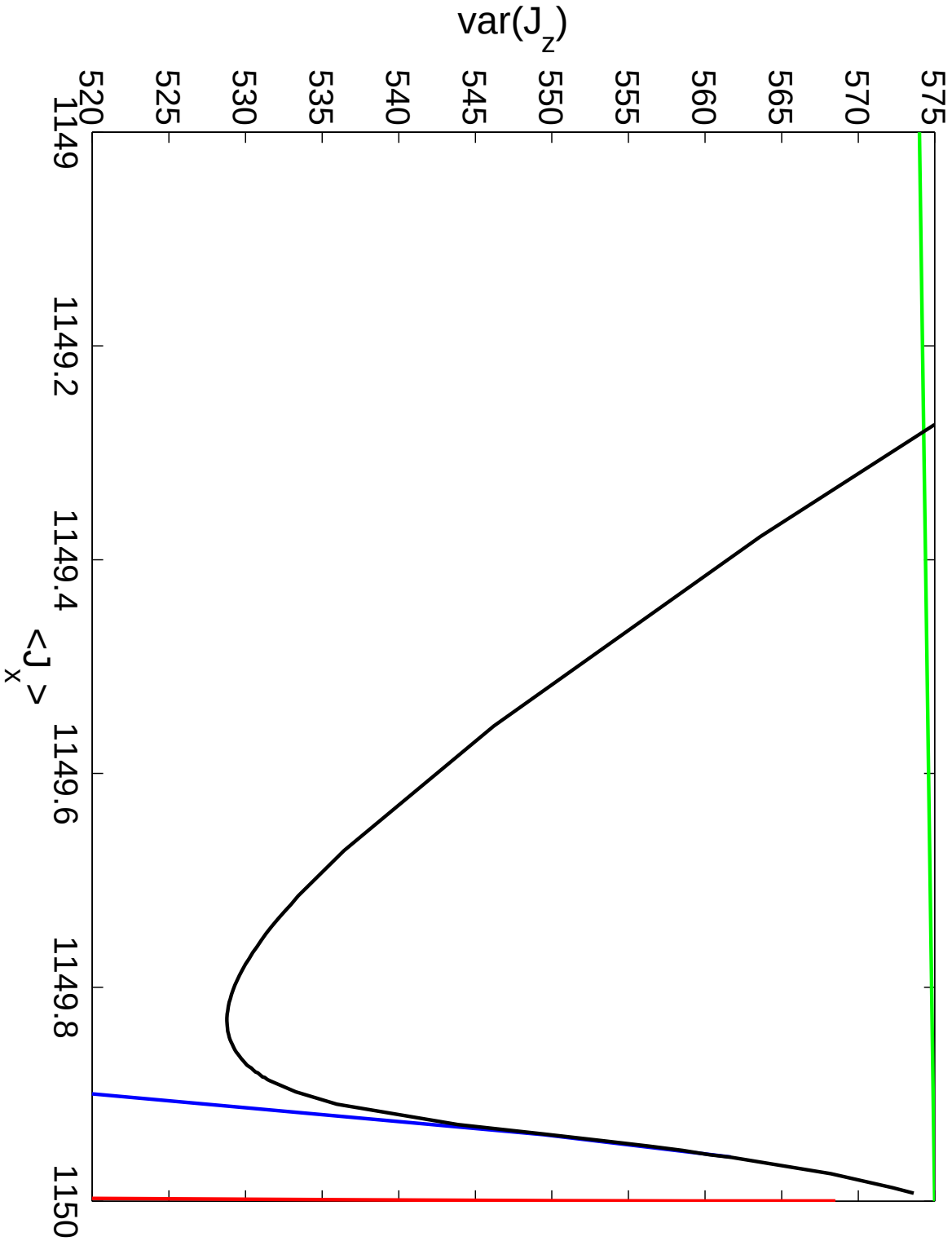

Figure J.9: Fig. 7.13b in higher resolution. The black curve corresponds to $\mathcal{T} = 0.49$ and the blue curve corresponds to $\mathcal{T} = 0$. The red curve is the F-function, and the green curve correspond to $\xi^2 = 1$.

Appendix K

Bibliography

[1] "Many-particle entanglement with Bose-Einstein condensates" A. Sørensen, L.-M. Duan, J. I. Cirac, and P. Zoller "Nature" **409**, 63-66 (2001).

[2] "Squeezed atomic states and projection noise in spectroscopy" D. J. Wineland, J. J. Bollinger, W. M. Itano, and D. J. Heintzen "Physical review A" **50**, 67-88 (1994).

[3] "Entanglement and Extreme Spin Squeezing" Anders S. Sørensen and Klaus Mølmer "Physical Review letters" **86**, 4431-4434 (2001).

[4] "Bogoliubov theory of entanglement in a Bose-Einstein condensate" Anders Søndberg Sørensen "Physical review A" **65**, 043610 (2002).

[5] "Particle-number-conserving Bogoliubov method which demonstrates the validity of the time-dependent Gross-Pitaevskii equation for a highly condensed Bose gas" C. W. Gardiner "Physical review A" **58**, 775-778 (1997).

[6] "Low-temperature Bose-Einstein condensates in time-dependent traps: Beyond the U(1) symmetry-breaking approach" Y. Castin and R. Dum "Physical review A" **57**, 3008-3021 (1998).

[7] "Squeezed spin states" Masahiro Kitagawa and Masahito Ueda "Physical review A" **47**, 5138-5143 (1993).

[8] "Wigner functions, squeezing properties, and slow decoherence of a mesoscopic superposition of two-level atoms" M. G. Benedict and A. Czirják "Physical review A" **60**, 4034-4044 (1999).

[9] "Relation between atomic coherent-state representation, state multipoles, and generalized phase-space distributions" G. S. Agarwal "Physical review A" **24**, 2889-2896 (1981).

[10] "Quantum entanglement" Ryszard Horodecki, Pawel Horodecki, Michal Horodecki, and Karol Horodecki "Reviews of Modern Physics" **81**, 865-942 (2009).

[11] "Binary mixtures of Bose-Einstein condensates: Phase dynamics and spatial dynamics" A. Sinatra and Y. Castin "The European Physical Journal D" **8**, 319-332 (2000).

[12] "Atomic clocks use quantum timekeeping" Zeeya Merali "http://www.nature.com/news/2010/100331/full/news.2010.163.html" (2010).

[13] "Nonlinear atom interferometer surpasses classical precision limit" C. Gross, T. Zibold, E. Nicklas, J. Estève, and M. K. Oberthaler "Nature" **464**, 1165-1169 (2010).

[14] "Atom-chip-based generation of entanglement for quantum metrology" Max F. Riedel, Pascal Böhi, Yun Li, Theodor W. Hänch, Alice Sinatra, and Philipp Treutlein "Nature" **464**, 1170-1173 (2010).

[15] "Squeezing and Entanglement in a Bose-Einstein condensate" J. Estéve, C. Gross, A. Weller, S. Giovanazzi, and M. K. Oberthaler "Nature" **455**, 1216-1219 (2008).

[16] "Squeezing of Atomic Quantum Projection Noise" Patric J. Windpassinger, Daniel Oblak, Ulrich B. Hoff, Anne Louchet, Jürgen Appel, Niels Kjærgaard and Eugene S. Polzik "Journal of Modern Optics" **56**, 1993-1998 (2009).

[17] "NIST's Second 'Quantum Logic Clock' based on Aluminum Ion is Now World's Most Precise Clock" Laura Ost "http://www.nist.gov/physlab/div849/logicclock_020410.cfm" (2010).

[18] "Optical Clock with Ultracold Neutral Atoms" G. Wilpers, T. Binnewies, C. Degenhardt, U. Sterr, J. Helmcke, and F. Riehle "Physical Review Letters" **89**, 230801 (2002).

[19] "Spin-squeezing in a bimodal condensate: spatial dynamics and particle losses" Yun Li, P. Treutlein, J. Reichel, and A. Sinatra "The European Physical Journal B" **68**, 365-381 (2009).

[20] "Can Quantum-Mechanical Description of Physical Reality Be Considered Complete?" A. Einstein, B. Podolsky and N. Rosen "Physical Review" **47**, 777-780 (1935).

[a] "Bose-Einstein Condensation in Dilute Gases" second edition. C. J. Pethick and H. Smith (2008). Publisher: "Cambridge University Press". ISBN: 978-0-521-84651-6.

[b] "Modern Quantum Mechanics" revised edition. J. J. Sakurai (1994). Publisher: "Adison-Wesley Publishing Company". ISBN: 0-201-53929-2.

[c] "An introduction to Error Analysis" second edition. John R. Taylor (1997). Publisher: "University Science Books, Sausalito, California". ISBN: 0-935702-75-X.

[d] "Introductory Quantum Optics" C. C. Gerry and P. L. Knight (2006). Publisher: "Cambridge University Press". ISBN: 0-521-52735-X.

[e] "Many-Body Quantum Theory in Condensed Matter Physics" Henrik Bruus and Karsten Flensberg (2007). Publisher: "Oxford University Press". ISBN: 978-0-19-856633-5.

[f] "Mathematical Methods for Physics and Engineering" second edition. K. F. Riley, M. P. Hobson, and S. J. Bence (2005). Publisher: "Cambridge University Press". ISBN: 0-521-89067-5.